



USE OF NDT EQUIPMENT FOR CONSTRUCTION QUALITY CONTROL OF HOT MIX ASPHALT PAVEMENTS

Research Report 574

Prepared by:

Manuel Celaya, MSCE
Soheil Nazarian, PhD, PE
Manuel Zea, BSCE
Vivek Tandon, PhD, PE
Center for Transportation Infrastructure Systems
The University of Texas at El Paso
El Paso, TX 79968-0516
(915) 747-6925

August 2006

Prepared for:

Arizona Department of Transportation
205 South 17th Ave.
Mail Drop 614E
Phoenix, AZ 85007-3212
in cooperation with
U.S. Department of Transportation
Federal Highway Administration

The contents of this report reflect the view of the authors, who are responsible for the facts and the accuracy of the data presented herein. The contents do not necessarily reflect the official views or policies of the Arizona Department of Transportation or the Federal Highway Administration. This report does not constitute a standard, specification, or regulation.

Technical Report Documentation Page

1. Report No. FHWA-AZ-2006-574		2. Government Accession No.		3. Recipient's Catalog No.	
4. Title and Subtitle Use of NDT Equipment for Construction Quality Control of Hot Mix Asphalt Pavements				5. Report Date August 2006	
				6. Performing Organization Code	
7. Author Manuel Celaya, Soheil Nazarian, Manuel Zea, and Vivek Tandon				8. Performing Organization Report No. Research Report	
9. Performing Organization Name and Address Center for Transportation Infrastructure Systems The University of Texas at El Paso El Paso, Texas 79968-0516				10. Work Unit No.	
				11. Contract or Grant No. SPR-PL-1(61)ITEM 574	
12. Sponsoring Agency Name and Address Arizona Department of Transportation 205 South 17th Ave. Mail Drop 614E Phoenix, AZ 85007-3212				13. Type of Report & Period Covered Technical Report July, 2005 – July, 2006	
				14. Sponsoring Agency Code	
15. Supplementary Notes Research Performed in Cooperation with ADOT and FHWA					
16. Abstract <p>The focus of the study has been to evaluate the utility of seismic methods in the quality management of the hot mix asphalt layers. Procedures are presented to measure the target field moduli of hot mix asphalt (HMA) with laboratory seismic methods, conduct field tests with the Portable Seismic Pavement Analyzer (PSPA) in the field, validate the results in the laboratory with seismic tests on extracted cores and determine the design modulus from measured values.</p> <p>This report contains the results of an effort to address the issues related to the implementation of the recommended methods and devices in the day-to-day operation of the pavement community (in general) and pavements managed by the Arizona Department of Transportation (ADOT). Ten sites throughout Arizona with different pavement conditions and structures were tested between August and December 2005. The results are summarized in this report.</p> <p>Based on the results presented, the combination of the lab and field seismic methods is a viable tool for the quality management of HMA layers and can be easily implemented by ADOT. In addition, performing the simplified seismic laboratory and field tests along with more traditional tests may result in a database that can be used to smoothly unify the design procedures with pavement evaluation.</p>					
17. Key Words Pavement Design, Modulus, Nondestructive Testing, Flexible Pavements, Resilient Modulus, Quality Control, Seismic Methods			18. Distribution Statement No restrictions. This document is available to the public through the National Technical Information Service, 5285 Port Royal Road, Springfield, Virginia 22161		23. Registrant's Seal
19. Security Classification Unclassified	20. Security Classification Unclassified	21. No. of Pages 165	22. Price		

SI* (MODERN METRIC) CONVERSION FACTORS

APPROXIMATE CONVERSIONS TO SI UNITS				APPROXIMATE CONVERSIONS FROM SI UNITS			
Symbol	When You Know	Multiply By	To Find	Symbol	When You Know	Multiply By	To Find
<u>LENGTH</u>							
in	inches	25.4	millimeters	mm	millimeters	0.039	inches
ft	feet	0.305	meters	m	meters	3.28	feet
yd	yards	0.914	meters	m	meters	1.09	yards
mi	miles	1.61	kilometers	km	kilometers	0.621	miles
<u>AREA</u>							
in ²	square inches	645.2	square millimeters	mm ²	Square millimeters	0.0016	square inches
ft ²	square feet	0.093	square meters	m ²	Square meters	10.764	square feet
yd ²	square yards	0.836	square meters	m ²	Square meters	1.195	square yards
ac	acres	0.405	hectares	ha	hectares	2.47	acres
mi ²	square miles	2.59	square kilometers	km ²	Square kilometers	0.386	square miles
<u>VOLUME</u>							
fl oz	fluid ounces	29.57	milliliters	mL	milliliters	0.034	fluid ounces
gal	gallons	3.785	liters	L	liters	0.264	gallons
ft ³	cubic feet	0.028	cubic meters	m ³	Cubic meters	35.315	cubic feet
yd ³	cubic yards	0.765	cubic meters	m ³	Cubic meters	1.308	cubic yards
NOTE: Volumes greater than 1000L shall be shown in m ³ .							
<u>MASS</u>							
oz	ounces	28.35	grams	g	grams	0.035	ounces
lb	pounds	0.454	kilograms	kg	kilograms	2.205	pounds
T	short tons (2000lb)	0.907	megagrams (or "metric ton")	mg (or "t")	megagrams (or "metric ton")	1.102	short tons (2000lb)
<u>TEMPERATURE (exact)</u>							
°F	Fahrenheit temperature	5(F-32)/9 or (F-32)/1.8	Celsius temperature	°C	Celsius temperature	1.8C + 32	Fahrenheit temperature
<u>ILLUMINATION</u>							
fc	foot candles	10.76	lux	lx	lux	0.0929	foot-candles
fl	foot-Lamberts	3.426	candela/m ²	cd/m ²	candela/m ²	0.2919	foot-Lamberts
<u>FORCE AND PRESSURE OR STRESS</u>							
lbf	poundforce	4.45	newtons	N	newtons	0.225	poundforce
lbf/in ²	poundforce per square inch	6.89	kilopascals	kPa	kilopascals	0.145	poundforce per square inch

SI is the symbol for the International System of Units. Appropriate rounding should be made to comply with Section 4 of ASTM E380

TABLE OF CONTENTS

EXECUTIVE SUMMARY	1
I. INTRODUCTION	3
Objectives	3
Organization.....	4
II. BACKGROUND	5
Traditional Methods for Measuring HMA Modulus	6
Diametral Resilient Modulus	6
Dynamic Modulus Tests	7
Free-free Resonant Column Tests.....	8
Ultrasonic Tests	8
Falling Weight Deflectometer (FWD).....	9
Seismic Field Methods.....	10
Empirical Models.....	10
Impact of Temperature and Frequency	12
III. PORTABLE SEISMIC PAVEMENT ANALYZER	15
IV. SEISMIC METHODOLOGY FOR QUALITY MANAGEMENT OF HOT ASPHALT	21
Step 1: Selecting Suitable Materials and Mix for a Given Project	21
Step 2: Determining a Target Modulus for the Mix	22
Step 3: Characterizing the Variation in Modulus with Temperature.....	23
Step 4: Determining Modulus of Material for Structural Design	24
Step 5: Field Quality Tests.....	25
V. EXAMPLE IMPLEMENTATION OF QUALITY MANAGEMENT IN ARIZONA	27
Step 1: Selecting Suitable Materials and Mix for a Given Project	27
Step 2: Determining a Target Modulus for the Mix	27
Step 3: Characterizing the Variation in Modulus with Temperature.....	28
Step 4: Determining Modulus of Material for Structural Design	29
Step 5: Field Quality Tests.....	30
Validation of Results.....	33
VI. PRESENTATION OF RESULTS	39
Description of Sites Investigated	39
Description of Sites.....	39
General Results	41
Step 1: Selecting Suitable Materials and Mix for Each Project.....	41
Step 2: Determining a Target Modulus for Each Mix	41
Step 3: Characterizing the Variation in Modulus with Temperature.....	44
Step 4: Determining Modulus of Each Mix for Structural Design	46
Step 5: Field Quality Tests.....	48
Validation.....	53
VII. SUMMARY, CONCLUSIONS AND RECOMMENDATIONS	57
REFERENCES	60

APPENDIX A. DYNAMIC MODULUS TEST	63
Test Procedure and Calculations for Dynamic Modulus Test	64
Time-Temperature Relationship	65
APPENDIX B. INTRODUCTION TO WAVE PROPAGATION THEORY	69
Seismic Body Waves	69
Seismic Surface Waves.....	69
Seismic Wave Velocities	71
Elastic Constants.....	72
APPENDIX C. VARIATION IN MODULUS WITH AIR VOIDS FOR ALL SITES	73
APPENDIX D. VARIATION IN MODULUS WITH TEMPERATURE	
FOR ALL SITES.....	78
APPENDIX E. MASTER CURVES FOR ALL SITES.....	82
APPENDIX F. GRADATION RESULTS	87
APPENDIX G. CONTOUR MAPS.....	97
APPENDIX H. MODULUS CONTROL CHARTS	107
APPENDIX I. CUMULATIVE DISTRIBUTION CHARTS	116
APPENDIX J. VALIDATION OF RESULTS	125
APPENDIX K. PAY FACTOR CALCULATIONS	129
APPENDIX L. VARIATION IN LAB SEISMIC MODULUS	
WITH AIR VOIDS	134
APPENDIX M. MONTE CARLO SIMULATION RESULTS	139
APPENDIX N. PHOTO ALBUM.....	144

LIST OF TABLES

Table 2.1 – Summary of Material Models	11
Table 5.1 – Job Mix Formula from Project.....	27
Table 5.2 – Comparison of Moduli from PSPA and Lab Tests on Cores.....	34
Table 5.3 – Comparison of Air Voids for Cores Extracted at the Site	35
Table 5.4 – Variation in Constituents of Mix from Field Samples.....	36
Table 5.5 – Gradation Results for Selected Cores from the Site	37
Table 5.6 – Gradation Results for Loose Materials Sampled at Site	37
Table 6.1 – Job Mix Formula from All Sites	42
Table 6.2 – Variation in Seismic Modulus with Air Voids for Lab Specimens	43
Table 6.3 – Variation in Seismic Modulus with Temperature for Lab Specimens at Placement Air Voids	44
Table 6.4 – Master Curve Parameters for All Sites	47
Table 6.5 – Design Modulus and Modulus Ratios for All Sites	48
Table 6.6 – Average Gradations, AC Content and Air Voids at Sites.....	49
Table 6.7 – Comparison of As-Built and Target Moduli.....	51
Table 6.8 – Variation in Core Seismic Modulus with Air Voids.....	54
Table 6.9 – Variation in Mix Constituents for All Sites	55
Table F.1 – Comparison of Air Voids for Cores Extracted at Site 1	87
Table F.2 – Gradation Results for Selected Cores from Site 1	87
Table F.3 – Gradation Results for Loose Materials Sampled at Site 1	87
Table F.4 – Comparison of Air Voids for Cores Extracted at Site 2.....	88
Table F.5 – Gradation Results for Selected Cores from Site 2.....	88
Table F.6 – Gradation Results for Loose Materials Sampled at Site 2.....	88
Table F.7 – Comparison of Air Voids for Cores Extracted at Site 3.....	89
Table F.8 – Gradation Results for Selected Cores from Site 3.....	89
Table F.9 – Gradation Results for Loose Materials Sampled at Site 3.....	89
Table F.10 – Comparison of Air Voids for Cores Extracted at Site 4.....	90
Table F.11 – Gradation Results for Selected Cores from Site 4.....	90
Table F.12 – Gradation Results for Loose Materials Sampled at Site 4.....	90
Table F.13 – Comparison of Air Voids for Cores Extracted at Site 5.....	91
Table F.14 – Gradation Results for Selected Cores from Site 5.....	91
Table F.15 – Gradation Results for Loose Materials Sampled at Site 5.....	91
Table F.16 – Comparison of Air Voids for Cores Extracted at Site 6.....	92
Table F.17 – Gradation Results for Selected Cores from Site 6.....	92
Table F.18 – Gradation Results for Loose Materials Sampled at Site 6.....	92
Table F.19 – Comparison of Air Voids for Cores Extracted at Site 7	93
Table F.20 – Gradation Results for Selected Cores from Site 7	93
Table F.21 – Gradation Results for Loose Materials Sampled at Site 7.....	93
Table F.22 – Comparison of Air Voids for Cores Extracted at Site 8.....	94
Table F.23 – Gradation Results for Selected Cores from Site 8.....	94

Table F.24 – Gradation Results for Loose Materials Sampled at Site 8.....	94
Table F.25 – Comparison of Air Voids for Cores Extracted at Site 9.....	95
Table F.26 – Gradation Results for Selected Cores from Site 9.....	95
Table F.27 – Gradation Results for Loose Materials Sampled at Site 9.....	95
Table F.28 – Comparison of Air Voids for Cores Extracted at Site 10.....	96
Table F.29 – Gradation Results for Selected Cores from Site 10.....	96
Table F.30 – Gradation Results for Loose Materials Sampled at Site 10.....	96
Table J.1 – Comparison of Moduli from PSPA and Lab Tests on Cores Extracted from Same Locations on Site 1.....	125
Table J.2 – Comparison of Moduli from PSPA and Lab Tests on Cores Extracted from Same Locations on Site 2.....	125
Table J.3 – Comparison of Moduli from PSPA and Lab Tests on Cores Extracted from Same Locations on Site 3.....	126
Table J.4 – Comparison of Moduli from PSPA and Lab Tests on Cores Extracted from Same Locations on Site 4.....	126
Table J.5 – Comparison of Moduli from PSPA and Lab Tests on Cores Extracted from Same Locations on Site 5.....	126
Table J.6 – Comparison of Moduli from PSPA and Lab Tests on Cores Extracted from Same Locations on Site 6.....	127
Table J.7 – Comparison of Moduli from PSPA and Lab Tests on Cores Extracted from Same Locations on Site 7.....	127
Table J.8 – Comparison of Moduli from PSPA and Lab Tests on Cores Extracted from Same Locations on Site 8.....	127
Table J.9 – Comparison of Moduli from PSPA and Lab Tests on Cores Extracted from Same Locations on Site 9.....	128
Table J.10 – Comparison of Moduli from PSPA and Lab Tests on Cores Extracted from Same Locations on Site 10.....	128
Table K.1 – Pay Factor Calculations for Buckeye Site	129
Table K.2 – Pay Factor Calculations for Show Low Site.....	129
Table K.3 – Pay Factor Calculations for Holbrook Site	130
Table K.4 – Pay Factor Calculations for Burro Creek Site.....	130
Table K.5 – Pay Factor Calculations for Cordes JCT Site	131
Table K.6 – Pay Factor Calculations for Roosevelt Site	131
Table K.7 – Pay Factor Calculations for Safford Site	132
Table K.8 – Pay Factor Calculations for Holbrook (B) Site.....	132
Table K.9 – Pay Factor Calculations for Payson Site.....	133
Table K.10 – Pay Factor Calculations for Tucson Site.....	133

LIST OF FIGURES

Figure 2.1 – Three Layer Pavement Model	5
Figure 2.2 – Diametral Resilient Modulus Test.....	6
Figure 2.3 – Dynamic Modulus Test Setup	7
Figure 2.4 – Typical Master Curve from Dynamic and Seismic Modulus Test Results	7
Figure 2.5 – Ultrasonic Test Device for AC Specimens.....	9
Figure 2.6 – Schematic of Falling Weight Deflectometer	9
Figure 2.7 – Variation in AC Modulus with Frequency and Temperature	12
Figure 2.8 – Frequency Dependency of AC Modulus	13
Figure 3.1 – Portable Seismic Pavement Analyzer.....	14
Figure 3.2 – Typical Time Records from the Portable Seismic Pavement Analyzer	14
Figure 3.3 – Schematic of Ultra Sonic Surface Wave Method.....	16
Figure 3.4 – Typical Dispersion Curve Obtained from Time Records in Figure 3.2	17
Figure 3.5 – Typical Phase Spectra Obtained from Time Records in Figure 3.2	17
Figure 3.6 – Typical Time Records as Demonstrated by PSPA Software.....	18
Figure 3.7 – Typical Interpreted Results as Demonstrated by PSPA Software.....	19
Figure 4.1 – Process of Determining Ideal Target Modulus.....	22
Figure 4.2 – Process of Characterizing Variation in Modulus with Temperature	23
Figure 4.3 – Master Curve Concept for Defining Design Modulus	24
Figure 4.4 – Process of Field Testing for HMA Materials	25
Figure 5.1 – Variation in Seismic Modulus with Air Voids from Laboratory Testing	28
Figure 5.2 – Variations in Seismic Modulus with Temperature at	29
Figure 5.3 – Master Curve for Estimating Design Modulus.....	29
Figure 5.4 – Typical Marking of Sites	30
Figure 5.5 – Contour Plots of Variations in Design Modulus with PSPA along Site.....	31
Figure 5.6 – Modulus Control Charts from Site	32
Figure 5.7 – Distribution of Equivalent Design Moduli along Site.....	33
Figure 5.8 – Comparison of Moduli from PSPA and Lab Tests on Cores	34
Figure 5.9 – Variation in Design Modulus with Air Voids at Core Locations.....	35
Figure 5.10 – Distribution of Moduli due to Change in Gradation and Asphalt Content of Mixes during Paving	36
Figure 6.1 – Location of Sites Tested	39
Figure 6.2 – Variations in Modulus with Temperature (Slopes) for Lab Specimens at Design and In-place Air Voids.....	45
Figure 6.3 – Master Curves for Specimens Prepared at Design Air Voids	46
Figure 6.4 – Master Curves for Specimens Prepared at Placement Air Voids	46
Figure 6.5 – Comparisons of Target and As-Built Binder Contents at Arizona Sites	49
Figure 6.6 – Comparisons of Target and As-Built Air Voids at Arizona Sites	50
Figure 6.7 – Cumulative Distributions of Moduli	51
Figure 6.8 – Cumulative Distribution of Ratios of As-Built and Target Moduli from all Arizona Tests	52
Figure 6.9 – Comparison of Moduli from PSPA and Lab Tests on Cores	53

Figure A.1 – Variations in Stress and Strain with Time for Different Materials due to a Sinusoidal Load.....	63
Figure A.2 – Sketch of Dynamic Modulus Test Setup.....	65
Figure A.3 – Typical Dynamic Modulus versus Frequency Plot at Different Temperatures.....	67
Figure A.4 – Typical Log Shift Factor versus Temperature Plot.....	67
Figure A.5 – Shifted Dynamic Modulus Curve.....	68
Figure A.6 – Typical Master Curve with Curve Fitting.....	68
Figure B.1 – Description of Different Waves.....	70
Figure C.1 – Variation in Modulus with Air Voids for Buckeye (Site 1).....	73
Figure C.2 – Variation in Modulus with Air Voids for Show Low (Site 2).....	73
Figure C.3 – Variation in Modulus with Air Voids for Holbrook (Site 3).....	74
Figure C.4 – Variation in Modulus with Air Voids for Burro Creek (Site 4).....	74
Figure C.5 – Variation in Modulus with Air Voids for Cordes JCT (Site 5).....	75
Figure C.6 – Variation in Modulus with Air Voids for Roosevelt (Site 6).....	75
Figure C.7 – Variation in Modulus with Air Voids for Safford (Site 7).....	76
Figure C.8 – Variation in Modulus with Air Voids for Holbrook B (Site 8).....	76
Figure C.9 – Variation in Modulus with Air Voids for Payson (Site 9).....	77
Figure C.10 – Variation in Modulus with Air Voids for Tucson (Site 10).....	77
Figure D.1 – Variation in Modulus with Temperature for Buckeye (Site 1).....	78
Figure D.2 – Variation in Modulus with Temperature for Show Low (Site 2).....	78
Figure D.3 – Variation in Modulus with Temperature for Holbrook (Site 3).....	79
Figure D.4 – Variation in Modulus with Temperature for Burro Creek (Site 4).....	79
Figure D.5 – Variation in Modulus with Temperature for Cordes JCT (Site 5).....	79
Figure D.6 – Variation in Modulus with Temperature for Roosevelt (Site 6).....	80
Figure D.7 – Variation in Modulus with Temperature for Safford (Site 7).....	80
Figure D.8 – Variation in Modulus with Temperature for Holbrook B (Site 9).....	80
Figure D.9 – Variation in Modulus with Temperature for Payson (Site 9).....	81
Figure D.10 – Variation in Modulus with Temperature for Tucson (Site 10).....	81
Figure E.1 – Master Curves for Buckeye Mix (Site 1).....	82
Figure E.2 – Master Curves for Show Low Mix (Site 2).....	82
Figure E.3 – Master Curves for Holbrook Mix (Site 3).....	83
Figure E.4 – Master Curves for Burro Creek Mix (Site 4).....	83
Figure E.5 – Master Curves for Cordes JCT Mix (Site 5).....	84
Figure E.6 – Master Curves for Roosevelt Mix (Site 6).....	84
Figure E.7 – Master Curves for Safford Mix (Site 7).....	85
Figure E.8 – Master Curves for Holbrook B Mix (Site 8).....	85
Figure E.9 – Master Curves for Payson Mix (Site 9).....	86
Figure E.10 – Master Curves for Tucson Mix (Site 10).....	86

Figure G.1 – Contour Plots of Variation in Design Modulus with PSPA for Buckeye (Site 1).....	97
Figure G.2 – Contour Plots of Variation in Normalized Modulus (PSPA/Target Modulus) for Buckeye (Site 1).....	98
Figure G.3 – Contour Plots of Variation in Design Modulus with PSPA (a) and Normalized Modulus (b) for Show Low (Site 2).....	99
Figure G.4 – Contour Plots of Variation in Design Modulus with PSPA (a) and Normalized Modulus (b) for Holbrook (Site 3).....	100
Figure G.5 – Contour Plots of Variation in Design Modulus with PSPA (a) and Normalized Modulus (b) for Burro Creek (Site 4).....	101
Figure G.6 – Contour Plots of Variation in Design Modulus with PSPA (a) and Normalized Modulus (b) for Cordes JCT (Site 5).....	102
Figure G.7 – Contour Plots of Variation in Design Modulus with PSPA (a) and Normalized Modulus (b) for Roosevelt (Site 6).....	103
Figure G.8 – Contour Plots of Variation in Design Modulus with PSPA (a) and Normalized Modulus (b) for Safford (Site 7).....	104
Figure G.9 – Contour Plots of Variation in Design Modulus with PSPA (a) and Normalized Modulus (b) for Holbrook B (Site 8).....	105
Figure G.10 – Contour Plots of Variation in Design Modulus with PSPA (a) and Normalized Modulus (b) for Tucson (Site 10).....	106
Figure H.1 – Modulus Control Charts from Buckeye (Site 1).....	107
Figure H.2 – Modulus Control Charts from Show Low (Site 2).....	108
Figure H.3 – Modulus Control Charts from Holbrook (Site 3).....	109
Figure H.4 – Modulus Control Charts from Burro Creek (Site 4).....	110
Figure H.5 – Modulus Control Charts from Cordes JCT (Site 5).....	111
Figure H.6 – Modulus Control Charts from Roosevelt (Site 6).....	112
Figure H.7 – Modulus Control Charts from Safford (Site 7).....	113
Figure H.8 – Modulus Control Charts from Holbrook B (Site 8).....	114
Figure H.9 – Modulus Control Charts from Tucson (Site 10).....	115
Figure I.1 – Distribution of Design Moduli for Buckeye (Site 1).....	116
Figure I.2 – Distribution of Normalized Moduli (PSPA/Target Modulus) for Buckeye (Site 1).....	116
Figure I.3 – Distribution of Design Moduli for Show Low (Site 2).....	117
Figure I.4 – Distribution of Normalized Moduli (PSPA/Target Modulus) for Show Low (Site 2).....	117
Figure I.5 – Distribution of Design Moduli for Holbrook (Site 3).....	118
Figure I.6 – Distribution of Normalized Moduli (PSPA/Target Modulus) for Holbrook (Site 3).....	118
Figure I.7 – Distribution of Design Moduli for Burro Creek (Site 4).....	119
Figure I.8 – Distribution of Normalized Moduli (PSPA/Target Modulus) for Burro Creek (Site 4).....	119
Figure I.9 – Distribution of Design Moduli for Cordes JCT (Site 5).....	120
Figure I.10 – Distribution of Normalized Moduli (PSPA/Target Modulus) for Cordes JCT (Site 5).....	120

Figure I.11 – Distribution of Design Moduli for Roosevelt (Site 6)	121
Figure I.12 – Distribution of Normalized Moduli (PSPA/Target Modulus) for Roosevelt (Site 6)	121
Figure I.13 – Distribution of Design Moduli for Safford (Site 7)	122
Figure I.14 – Distribution of Normalized Moduli (PSPA/Target Modulus) for Safford (Site 7)	122
Figure I.15 – Distribution of Design Moduli for Holbrook B (Site 8)	123
Figure I.16 – Distribution of Normalized Moduli (PSPA/Target Modulus) for Holbrook B (Site 8)	123
Figure I.17 – Distribution of Design Moduli for Tucson (Site 10).....	124
Figure I.18 – Distribution of Normalized Moduli (PSPA/Target Modulus) for Tucson (Site 10)	124
Figure L.1 – Variation in Lab Seismic Modulus with Air Voids at Core Locations from Buckeye (Site 1).....	134
Figure L.2 – Variation in Lab Seismic Modulus with Air Voids at Core Locations from Show Low (Site 2)	134
Figure L.3 – Variation in Lab Seismic Modulus with Air Voids at Core Locations from Holbrook (Site 3).....	135
Figure L.4 – Variation in Lab Seismic Modulus with Air Voids at Core Locations from Burro Creek (Site 4).....	135
Figure L.5 – Variation in Lab Seismic Modulus with Air Voids at Core Locations from Cordes JCT (Site 5).....	136
Figure L.6 – Variation in Lab Seismic Modulus with Air Voids at Core Locations from Roosevelt (Site 6).....	136
Figure L.7 – Variation in Lab Seismic Modulus with Air Voids at Core Locations from Safford (Site 7).....	137
Figure L.8 – Variation in Lab Seismic Modulus with Air Voids at Core Locations from Holbrook (Site 8).....	137
Figure L.9 – Variation in Lab Seismic Modulus with Air Voids at Core Locations from Payson (Site 9)	138
Figure L.10 – Variation in Lab Seismic Modulus with Air Voids at Core Locations from Tucson (Site 10)	138
Figure M.1 – Distribution of Moduli due to Change in Gradation and Asphalt Content of Mixes for Buckeye (Site 1).....	139
Figure M.2 – Distribution of Moduli due to Change in Gradation and Asphalt Content of Mixes for Show Low (Site 2).....	139
Figure M.3 – Distribution of Moduli due to Change in Gradation and Asphalt Content of Mixes for Holbrook (Site 3)	140
Figure M.4 – Distribution of Moduli due to Change in Gradation and Asphalt Content of Mixes for Burro Creek (Site 4).....	140
Figure M.5 – Distribution of Moduli due to Change in Gradation and Asphalt Content of Mixes for Cordes JCT (Site 5)	141
Figure M.6 – Distribution of Moduli due to Change in Gradation and Asphalt Content of Mixes for Roosevelt (Site 6).....	141

Figure M.7 – Distribution of Moduli due to Change in Gradation and Asphalt Content of Mixes for Safford (Site 7).....	142
Figure M.8 – Distribution of Moduli due to Change in Gradation and Asphalt Content of Mixes for Holbrook B (Site 8)	142
Figure M.9 – Distribution of Moduli due to Change in Gradation and Asphalt Content of Mixes for Payson (Site 9).....	143
Figure M.10 – Distribution of Moduli due to Change in Gradation and Asphalt Content of Mixes for Tucson (Site 10).....	143
Figure N.1 – View of Site 1	144
Figure N.2 – ADOT Personnel Collection Loose Samples on Site 1	144
Figure N.3 – Surface Temperature at Time of Collection on Site 1	145
Figure N.4 – PSPA Collecting Information on Site 1.....	145
Figure N.5 – PSPA Collecting on Core Location at Site 1.....	145
Figure N.6 – View of Site 2.....	146
Figure N.7 – Detail of Site 2.....	146
Figure N.8 – PSPA Collecting on Site 2.....	146
Figure N.9 – View of Site 3.....	147
Figure N.10 – PSPA Testing on Core Location at Site 3.....	147
Figure N.11 – Construction Operations at Site 3.....	147
Figure N.12 – View of Site 4.....	148
Figure N.13 – PSPA Collecting on Core Location of Site 4	148
Figure N.14 – Segregated Area on Site 4	148
Figure N.15 – PSPA Testing at Site 5.....	149
Figure N.16 – PSPA Collecting Data on Core Location of Site 5.....	149
Figure N.17 – View of Site 6.....	149
Figure N.18 – PSPA Testing on Site 6	150
Figure N.19 – PSPA Collecting Data on Core Location of Site 6.....	150
Figure N.20 – View of Site 7	150
Figure N.21 – PSPA Testing on Core Location of Site 7	151
Figure N.22 – View of Site 8.....	151
Figure N.23 – PSPA Testing on Core Location of Site 8	151
Figure N.24 – View of Site 9.....	152
Figure N.25 – Nuclear Density Gage Testing on Site 9	152
Figure N.26 – Coring at Site 9.....	152
Figure N.27 – Pavement Construction of Site 10	153
Figure N.28 – ADOT Staff Gathering Loose Samples on Site 10.....	153
Figure N.29 – PSPA Testing on Core Location of Site 10.....	153

Acknowledgements

The authors would like to give their sincere appreciation to Christ Dimitroplos for managing this project. We would also like to thank the constructive advice from the Project Advisory Team, especially Chad Auker, David Burbank, and Scott Weinland. Their hard work and ever-present support and arranging of the logistics for the field tests made the execution of this project much easier than expected.

We would also like to thank the hard working people from the four ADOT districts that generously offered their time to sample and prepare cores for us. They are too numerous to name.

EXECUTIVE SUMMARY

State highway agencies, such as the Arizona Department of Transportation (ADOT), have implemented quality control/quality assurance programs to improve the quality of placed hot-mix asphalt (HMA) pavements. The quality of the HMA is assessed through field inspection, and testing of pavement cores (for density and thickness) and loose materials (for binder content and gradation).

One of the primary parameters considered in the design of flexible pavements is the modulus of the HMA layer. Unfortunately, current quality management programs do not provide any information about the modulus of the layer. To successfully implement a mechanistic pavement design procedure or to develop realistic performance based specifications, a method of monitoring the modulus of placed HMA is needed. Simple performance tests, such as the dynamic modulus tests, on specimens prepared from material retrieved during construction has been advocated for quality control. These test procedures are time consuming, the costs of acquiring the equipment are high, and well-trained laboratory staff is needed. Moreover, these tests are conducted on laboratory-prepared specimens that are not representative of the as-placed HMA.

New devices and procedures overcome some of the shortcomings indicated above. These procedures allow rapid data collection and interpretation in the lab and in the field. The focus of the study has been on measuring the modulus of HMA with two nondestructive devices: an ultrasonic device for testing HMA cores and briquettes, and a Portable Seismic Pavement Analyzer (PSPA) for testing the newly-constructed HMA layer.

The major advantage of seismic methods is that similar results are anticipated from the field and laboratory tests as long as the material is tested under comparable conditions. This unique feature of seismic methods in material characterization is particularly significant for implementing performance-based specifications.

This report contains the results of an effort to address the issues related to the implementation of the recommended seismic methods and devices in the day-to-day operation of ADOT. The major issues addressed are the utility of the methods, means of relating the measured parameters to the design moduli, and relating the parameters to performance of the pavement

The outcomes from this project exhibit that the proposed equipment and methodologies strike a balance between laboratory and field testing. Performing the simplified laboratory and field tests along with more traditional tests may result in a database that can be used to smoothly unify the design procedures and construction quality control.

I. INTRODUCTION

Quality assurance-quality control (QA/QC) of hot mix asphalt (HMA) projects is mostly oriented to the constructability and durability of the materials through process control. Typical QA/QC consists of ensuring the proper gradation, adequate asphalt content, adequate voids-in-mineral aggregates (VMA), and finally the desired in-place density of the finished mat (hot mix asphalt layer). Even though this process control is vital to the success of a project, it does not provide all the information necessary to ensure a high-quality product. Existing practices need to be supplemented with methods that will provide continuity between the design, construction, and laboratory testing, so that performance-based specifications can be implemented.

Several interrelated parameters have to be considered in a comprehensive QA/QC protocol. First, major parameters considered in the process need to be correlated to the parameters used in the design (modulus of HMA in this case). Based on the selected design parameters, pre-construction laboratory tests need to be carried out to determine the suitability of a material in terms of modulus. Adequate target moduli should be established based on the results of the laboratory tests. The last step involves the quality control during construction, ensuring that the target moduli have been achieved. In this project, seismic methods are presented to demonstrate the usefulness of these techniques to overcome some of these concerns.

A quality control device should have four major features to be effective in practical use. First, it should measure fundamental properties of materials (i.e., it should not be an index test). Second, the device should be sensitive enough to the parameter of interest so that poor and high quality materials can be readily delineated. Third, the measurements should be accurate enough so that they can provide feedback to the pavement designer and the laboratory personnel. Fourth, the device should be precise enough so that it can be readily used in the QA/QC process.

The focus of this project is to demonstrate the utility of the Portable Seismic Pavement Analyzer (PSPA) for in-situ modulus measurement of the HMA. The PSPA allows rapid data collection and interpretation. Procedures have been presented to measure the moduli of HMA with PSPA, calibrate and validate the results with simplified laboratory tests on extracted cores or lab-prepared specimens, and as a side issue, determine the design modulus from the measured values.

OBJECTIVES

The goal is to develop a pilot construction HMA quality management program for ADOT based on seismic moduli. The equipment and protocols discussed here were developed primarily through funding from the Texas Department of Transportation (Nazarian et al. 2004). This quality management program is similar to the one that the Texas Department of Transportation is considering for implementation.

The primary objective of this project is to demonstrate the utility of seismic field test protocols and equipment, which in a rational manner, combine the results from laboratory and field tests with those used for quality control during construction. A series of simplified seismic laboratory tests that are compatible with the field tests have been recommended. All these tests have several features in common. They can be performed rapidly (less than three minutes), they are inexpensive and their data reduction processes are simple and almost instantaneous. The major advantage of seismic methods is that similar results are anticipated from the field and laboratory tests as long as the material is tested under comparable conditions.

These types of tests are one of the major components needed to develop a mechanistic pavement design and performance-based construction specifications. A gradual transition from the existing specifications to performance-based specifications may be necessary. Performing the simplified laboratory and field tests on pavement materials will allow us to develop a database that can be used to smoothly unify the design procedures and construction quality control. Moreover, PSPA may be used to monitor the condition of highway projects at any time after construction for quality control, acceptance or management of such projects.

ORGANIZATION

The report consists of seven chapters and several appendixes. A brief description of the background information is included in Chapter 2. The field seismic test setup is discussed in Chapter 3. The overall test protocols are summarized in Chapter 4. A comprehensive example of implementing the process is included in Chapter 5. Chapter 6 is dedicated to test results and analysis from ten sites. Summary, conclusions and the future work plan are described in Chapter 7.

II. BACKGROUND

Current mechanistic-empirical flexible pavement design procedures are based on modeling a pavement system as an elastic multi-layered and/or viscoelastic system. The remaining life of flexible pavements is mainly based on predicting the strains or stresses at the interfaces of different layers. For instance, for a three-layer pavement composed of an HMA layer, a base course, and a subgrade layer (Figure 2.1), the two main strains considered are the tensile strain at the bottom of the HMA layer and the compressive strain on top of the subgrade.

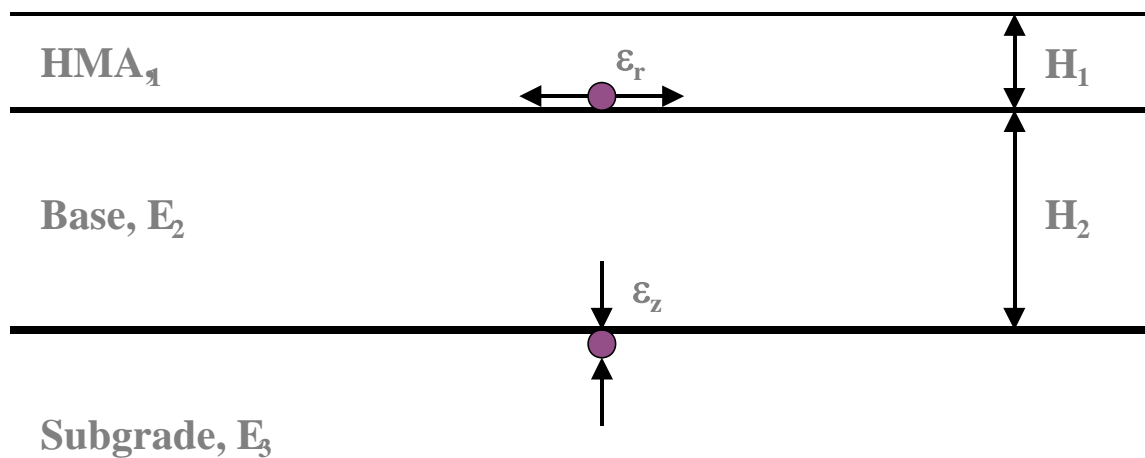


Figure 2.1 – Three Layer Pavement Model

The fatigue cracking of a thin HMA layer is mainly due to the tensile strain at the bottom of the HMA layer and to the modulus of the HMA layer (Finn et al. 1977). The subgrade rutting is a function of the compressive strain on top of the subgrade (Shook et al. 1982). The strains developed within a pavement system are strongly related to the moduli of different layers. As a result, moduli of all layers should be accurately determined.

The general form for most distress models, which are used to estimate the fatigue damage and the rutting failure, may be expressed as Equations 2.1 and 2.2 (Ayres and Witzczak 1998)

$$N_F = K_1 (\epsilon_t)^{K_2} (E_{HMA})^{K_3} \quad (2.1)$$

$$N_R = K_4 (\epsilon_c)^{K_5} \quad (2.2)$$

where N_F is the number of equivalent single axle loads (ESAL), ϵ_t is the tensile strain at the bottom of the HMA layer, and E_{HMA} is the modulus of the HMA layer. Therefore, one of the most important parameters in a mechanistic design procedure is the strains and the modulus of the HMA layer.

TRADITIONAL METHODS FOR MEASURING HMA MODULUS

Daniel and Kim (1998) defined several field and laboratory tests for determining HMA moduli. These tests range from modeling the viscoelastic behavior of HMA to indirect (nomograph based) methods. The most common laboratory tests are the resilient modulus, creep, dynamic modulus, free-free resonant column, and ultrasonic wave velocity tests. The main field tests are the falling weight deflectometer (FWD) and wave propagation (or seismic) tests. The most common and practical test methods are reviewed in this section.

Diametral Resilient Modulus

The diametral resilient modulus is perhaps the only practical traditional method for measuring the modulus of field cores. A picture of the test setup used is shown in Figure 2.2. A cyclic compressive load, P , is applied to the specimen vertically along one diameter. This compressive load induces tensile stresses along the diameter of the specimen in line with the load. These tensile stresses cause horizontal deformation of the specimen, ΔH . The resilient modulus of the specimen, E_{RT} is calculated from

$$E_{RT} = P (\nu + 0.27) / t \quad (2.3)$$

where t = core thickness and ν = Poisson's ratio.

There is a strong consensus amongst pavement engineers that this testing procedure is rather time-consuming and results are not very repeatable (Shah 1993, 7-16). The estimated repeatability of the test is about 15% to 20%, depending on the sophistication of the test system, and the quality of the specimens.

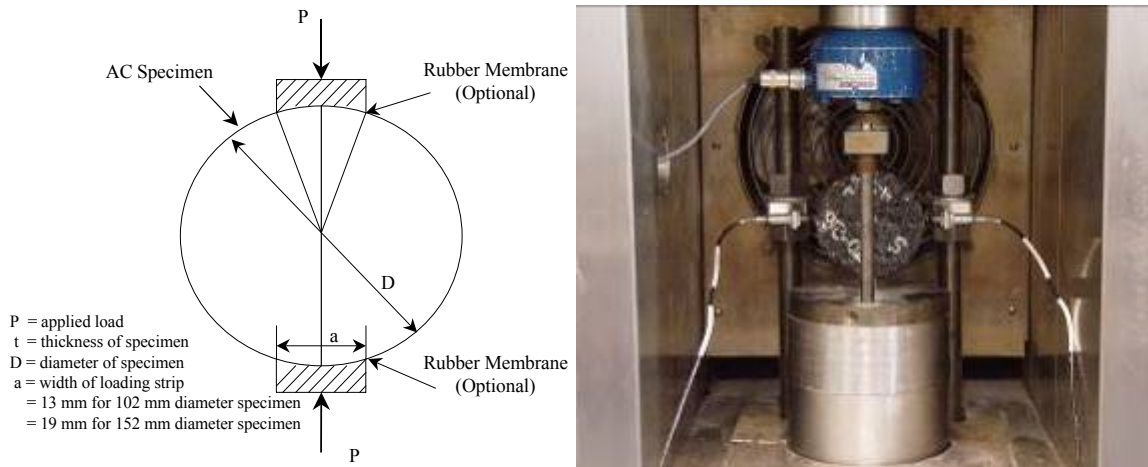


Figure 2.2 – Diametral Resilient Modulus Test

Dynamic Modulus Tests

Since the dynamic modulus tests were utilized in this study, they are described in detail in Appendix A. The schematic of the test set up is shown in Figure 2.3. In the dynamic modulus test, stresses and strains under sinusoidal loading are measured. Assuming that the material behaves linearly viscoelastic, the dynamic modulus is determined. By varying the frequency and temperature over a wide range, a “master curve” can be developed. A typical master curve, as shown in Figure 2.4, can be used to estimate the modulus of the HMA at any loading frequency or temperature.

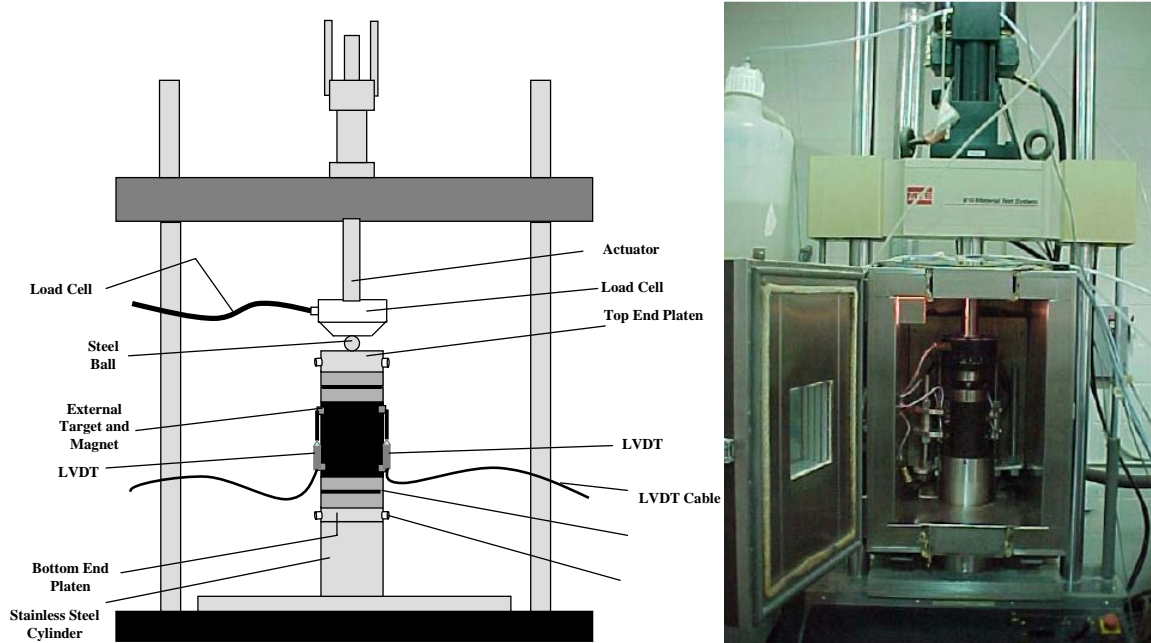


Figure 2.3 – Dynamic Modulus Test Setup

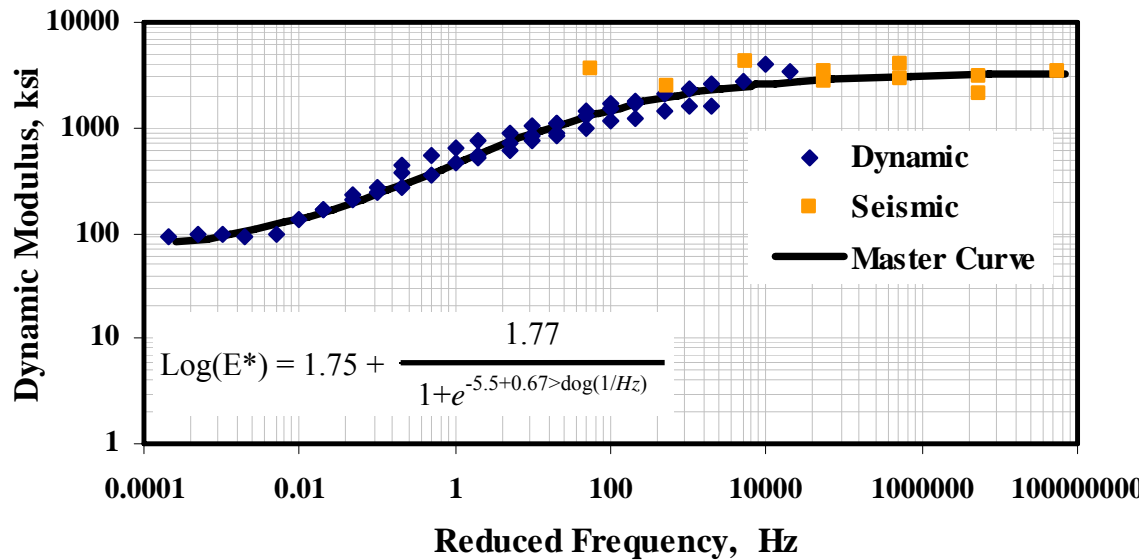


Figure 2.4 – Typical Master Curve from Dynamic and Seismic Modulus Test Results

Since the dynamic modulus tests are comprehensive and time-consuming, they are not suitable for testing a large number of specimens. Even under the simplified version of the test provided by the National Cooperative Highway Research Program (NCHRP), not more than a few specimens can be tested in one day. Based on an extensive study by Tandon et al. (2006), the variability of the tests is less than 5% on synthetic specimens and more than 15% on actual briquettes.

The dynamic modulus test is a fundamental test that provides comprehensive insight into the behavior of the materials. One of the limitations of the method as a quality management tool is that the length of the specimen has to be at least 6 in. Since most HMA layers are constructed in lifts of about 2 to 3 in., a specimen from loose materials has to be compacted for testing. As indicated by Tashman et al. (2001), the internal structure of the specimens prepared with a compactor may be different than those in the field, resulting in different moduli (typically greater on lab specimens).

Free-free Resonant Column Tests

In the free-free resonant column test (a.k.a. impact resonance test), the specimen is impacted with a hammer, and the resonant frequency associated with the standing waves within the specimen is measured (Nazarian et al. 2004; Kim and Kweon 2006). The resonant frequency along with the length of the specimen can be used to determine the modulus (ASTM C215).

For this test to be effective, a specimen with a length-to-diameter ratio from 1.5 to 2 is required. As such, these tests cannot be conducted on cores retrieved from the field.

Ultrasonic Tests

The ultrasonic setup used in this study is shown in Figure 2.5. The elastic modulus of a specimen is measured using a device (marketed as a V-meter) containing a pulse generator and a timing circuit, coupled with piezoelectric transmitter. Special removable epoxy coupling caps are used on both transducers to ensure full contact between the transducers and a specimen. To secure the specimen between the transducers, a loading plate is placed on top of it, and a spring-supporting system is placed underneath the transmitting transducer. The compression wave (P-wave) receiving transducer is placed on top of the specimen, on the opposite end from the transmitter. The timing circuit digitally displays the time needed for a wave to travel through, t_v . The modulus, M_v , is then calculated using

$$M_v = \frac{WH}{(\pi R^2 t_v^2)}, \quad (2.4)$$

where W, R and H are the mass, radius, and height of the specimen. The size of the sensors used with the test device is large relative to the wave travel path. The modulus

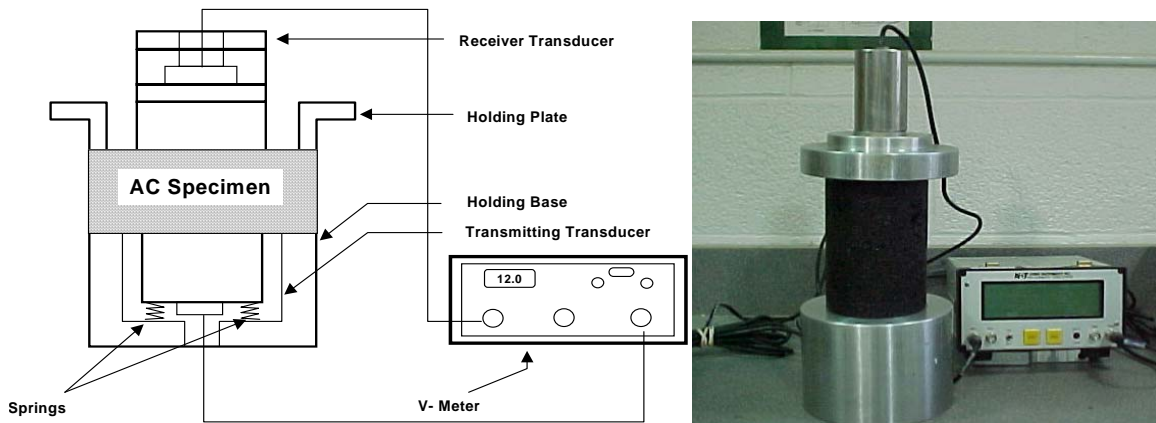


Figure 2.5 – Ultrasonic Test Device for AC Specimens

measured with the V-meter, M_v , is the so-called constraint modulus. The constraint modulus, M_v can then be converted to Young's modulus, E_v through a theoretically-correct relationship in the form of

$$E_v = M_v \frac{(1 + \nu)(1 - 2\nu)}{(1 - \nu)} \quad (2.5)$$

where ν is Poisson's ratio. Tandon et al. (2006) estimated that the uncertainty in the measurements is about 2%.

Falling Weight Deflectometer (FWD)

The FWD measures the response (surface deflections) of a pavement from an applied impulse load. A schematic of a FWD is shown in Figure 2.6. The impulse load is created by dropping a weight from predetermined heights. The deflections at the surface of the pavement are measured through seven geophones, which are automatically lowered onto the pavement.

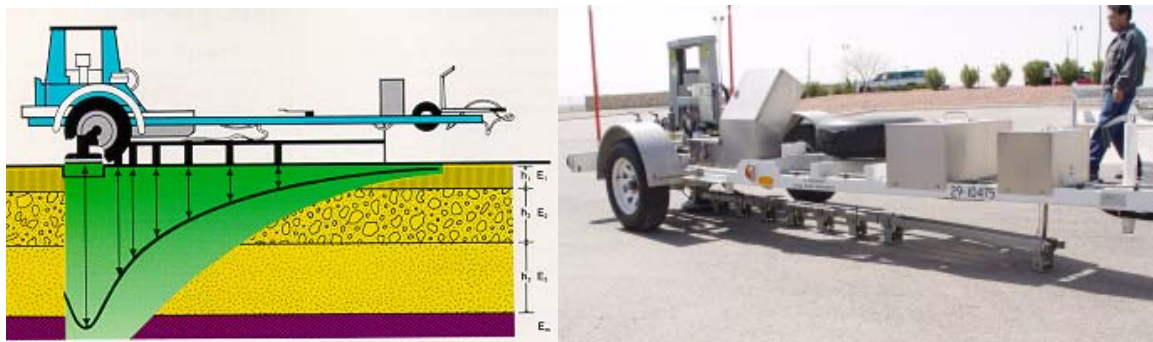


Figure 2.6 – Schematic of Falling Weight Deflectometer

To analyze the measured load and deflections, the pavement is modeled as a multi-layered linear elastic system. The measured deflections are compared to predicted deflections generated with a computer program that performs a linear elastic analysis. The modulus of each layer is obtained when the measured and predicted deflections compare well. The analysis is mainly conducted by comparing the measured and predicted deflections until they compare well, which is known as deflection basin-fitting.

The main advantages to the FWD are that tests are conducted in the field and that the method is practical for daily use. However, several combinations of moduli and layer thickness may generate predicted deflections that match measured deflections. Furthermore, many studies have shown that with the current configuration of the receivers in the FWD it may be difficult to accurately determine the modulus of the top layer in the pavement.

Seismic Field Methods

The seismic methods are based on generating and detecting stress waves in the pavement. Several automated devices are available for this purpose. The Portable Seismic Pavement Analyzer (PSPA) is one of them. The seismic methodology is described in the next chapter.

Empirical Models

A number of empirical models for estimating the dynamic modulus of the HMA from the volumetric properties of the mixes have been suggested. These models can be used in the absence of laboratory testing with an understanding that they are approximate in nature. A series of popular models, known as the “Witczak” models, have been proposed for this purpose. These models are summarized in Table 2.1. The latest Witczak model is in the form of (Witczak et al. 2003):

$$\begin{aligned} \log |E_{AC}| = & -1.249937 + 0.029232 P_{200} - 0.001767 (P_{200})^2 \\ & + 0.002841 P_4 - 0.058097 V_a - 0.808808 \frac{V_{beff}}{(V_{beff} + V_a)} \\ & + \frac{[3.871977 - 0.0021 P_4 + 0.003958 P_{38} - 0.000017 (P_{38})^2 + 0.00547 P_{34}]}{1 + e^{(-0.603313 - 0.31335 \log(f) - 0.393532 \log(\eta))}} \end{aligned} \quad (2.6)$$

where E_{AC} is the dynamic modulus of the asphalt concrete (AC) mix (in 10^5 psi), η is the bitumen viscosity (in 10^6 poise), f is the load frequency (in Hz), V_v is the percent air voids in the mix by volume, P_{ac} is the percent effective bitumen content by volume, and P_{200} is the percent passing No. 200 sieve by total aggregate weight. The “Witczak” model is part of the new mechanistic-empirical design guide being developed by the National Cooperative Highway Research Program. A new model called the Hirsch Model (Christiansen et al. 2003) has also been proposed. This model is provided in Table 2.1.

Table 2.1 – Summary of Material Models

<p>Witzak 1982 Model (Asphalt Institute, 1982).</p>	$\log E_{AC} = 5.553833 + 0.028829 \frac{P_{200}}{f^{0.17033}} - 0.03476 V_v$ $+ 0.070377 \eta + 0.000005 t_p^{(1.3+0.49825 \log f)} P_{ac}^{0.5} -$ $0.00189 t_p^{(1.3+0.49825 \log f)} \frac{P_{ac}^{0.5}}{f^{1.1}} + 0.931757 f^{-0.02774} + \epsilon$ <p>E_{AC} = dynamic modulus of AC mix (in psi), η = bitumen viscosity (in 10^6 poise) at 70°F, f = load frequency (in Hz), V_v = percent air voids in the mix by volume, P_{ac} = percent effective bitumen content by volume, and P_{200} = percent passing No. 200 sieve by total aggregate weight.</p>
<p>Witzak 1995 Model (Andrei et al., 1999)</p>	$\log E_{AC} = -0.261 + 0.008225 P_{200} - 0.00000101 (P_{200})^2$ $+ 0.00196 P_4 - 0.03157 V_a - 0.415 \frac{V_{beff}}{(V_{beff} + V_a)}$ $+ \frac{[1.87 + 0.002808 P_4 + 0.00000404 P_{38} - 0.0001786 (P_{38})^2 + 0.0164 P_{34}]}{1 + e^{(-0.716 \log(f) - 0.7425 \log(\eta))}}$ <p>E_{AC} = dynamic modulus of AC mix (in 10^5 psi), η = bitumen viscosity (in 10^6 poise) at 70°F, f = load frequency (in Hz), V_a = percent air voids in the mix by volume, V_{beff} = percent effective bitumen content by volume, and P_{200} = percent passing No. 200 sieve by total aggregate weight, P_4 = cumulative percent retained No. 4 sieve by total aggregate weight, P_{34} = cumulative percent retained No. 3/4 sieve by total aggregate weight, and P_{38} = cumulative percent retained No. 3/8 sieve by total aggregate weight.</p>
<p>Witzak 2000 Model (NCHRP, 2004)</p>	$\log E_{AC} = -1.249937 + 0.029232 P_{200} - 0.001767 (P_{200})^2$ $+ 0.002841 P_4 - 0.058097 V_a - 0.808808 \frac{V_{beff}}{(V_{beff} + V_a)}$ $+ \frac{[3.871977 - 0.0021 P_4 + 0.003958 P_{38} - 0.000017 (P_{38})^2 + 0.00547 P_{34}]}{1 + e^{(-0.603313 - 0.31335 \log(f) - 0.393532 \log(\eta))}}$
<p>Hirsch Model (Christiansen, et al., 2003)</p>	$ E^* _{mix} = P_c \left[4,200,000 \left(1 - \frac{VMA}{100} \right) + 3 G^* _{binder} \left(\frac{VFA \times VMA}{10,000} \right) \right] + \frac{1 - P_c}{\left[\frac{1 - \frac{VMA}{100}}{4,200,000} + \frac{VMA}{3VFA G^* _{binder}} \right]}$ $P_c = \frac{\left(20 + \frac{VFA \times 3 G^* _{binder}}{VMA} \right)^{0.58}}{650 + \left(\frac{VFA \times 3 G^* _{binder}}{VMA} \right)^{0.58}}$ <p>VMA = Voids in mineral aggregates (%), VFA = Voids filled with asphalt (%), and $G^* _{binder}$ = shear complex modulus of binder (psi)</p>

Impact of Temperature and Frequency

Several parameters affect the dynamic modulus of HMA. The most important parameters are the rate of the loading (i.e., frequency of loading), temperature, and air void content.

The typical frequency range at which HMA moduli measured with seismic methods is about 10 kHz to 25 kHz; whereas, the actual traffic load has a dominant frequency of about 10 to 30 Hz. Aouad et al. (1993) clearly demonstrated the importance of considering the impact of frequency on modulus. Typically, the modulus measured with seismic methods should be reduced by a factor of about 3 to 15 depending on the temperature, as shown in Figure 2.7. Daniel and Kim (1998) and Kim and Lee (1995) used the results from several laboratory and field tests (such as FWD, ultrasonic, uniaxial sweep, and creep) to show the frequency dependence of modulus. The results from Daniel and Kim are shown in Figure 2.8. Again, the frequency dependence is temperature related.

The HMA modulus is strongly dependent on temperature. Von Quintus and Kilingsworth (1998) demonstrated the importance of temperature gradient within a pavement section. Aouad et al. (1993), Li and Nazarian (1994) and several other investigators have studied the variation in modulus with temperature.

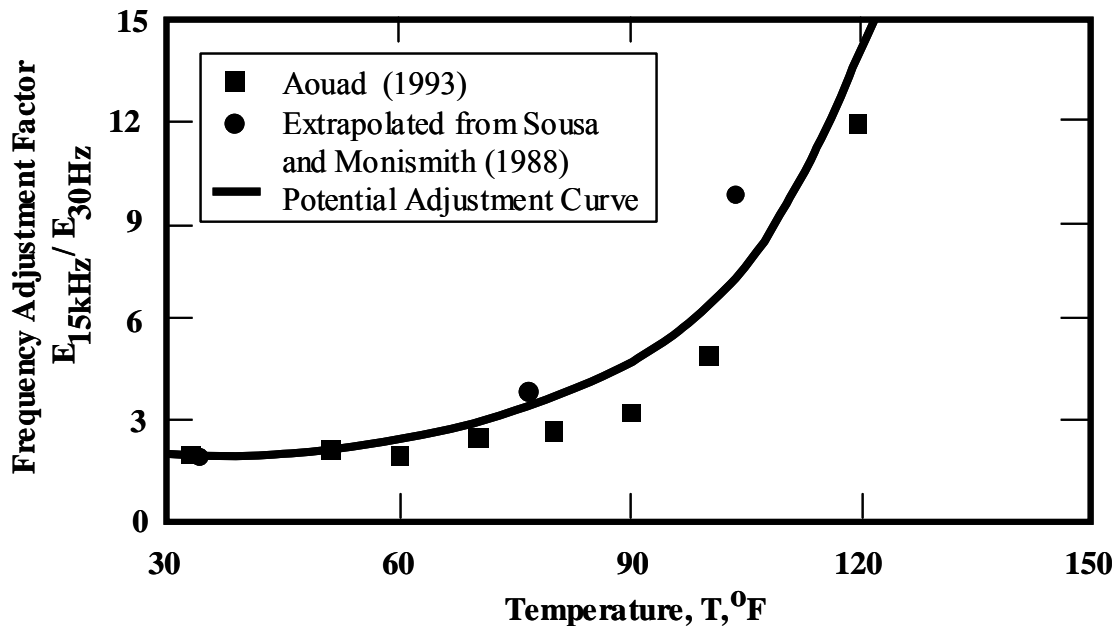


Figure 2.7 – Variation in AC Modulus with Frequency and Temperature (from Aouad et al. 1993)

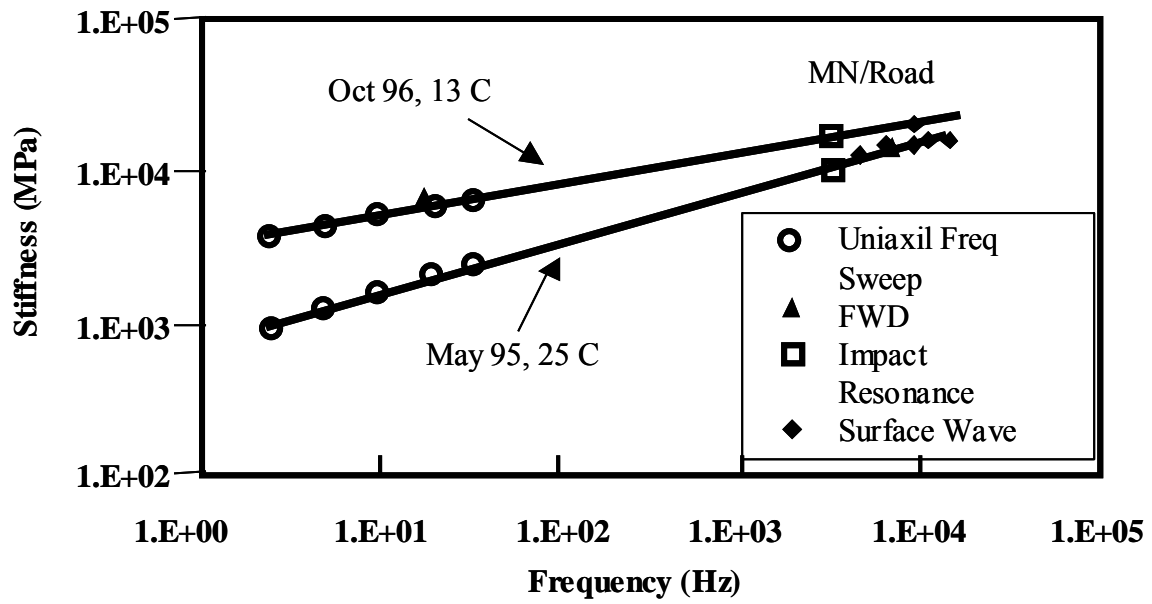


Figure 2.8 – Frequency Dependency of AC Modulus (from Daniel and Kim 1998)

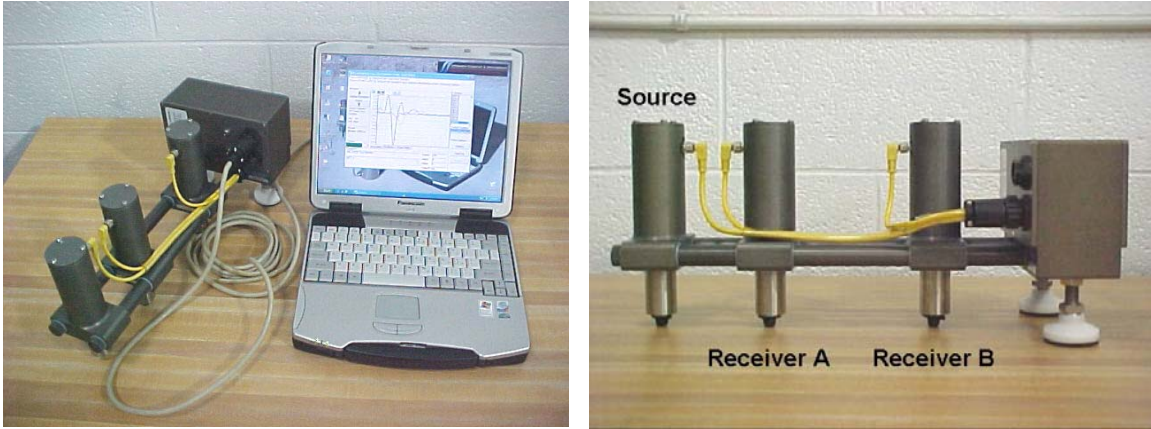


Figure 3.1 – Portable Seismic Pavement Analyzer

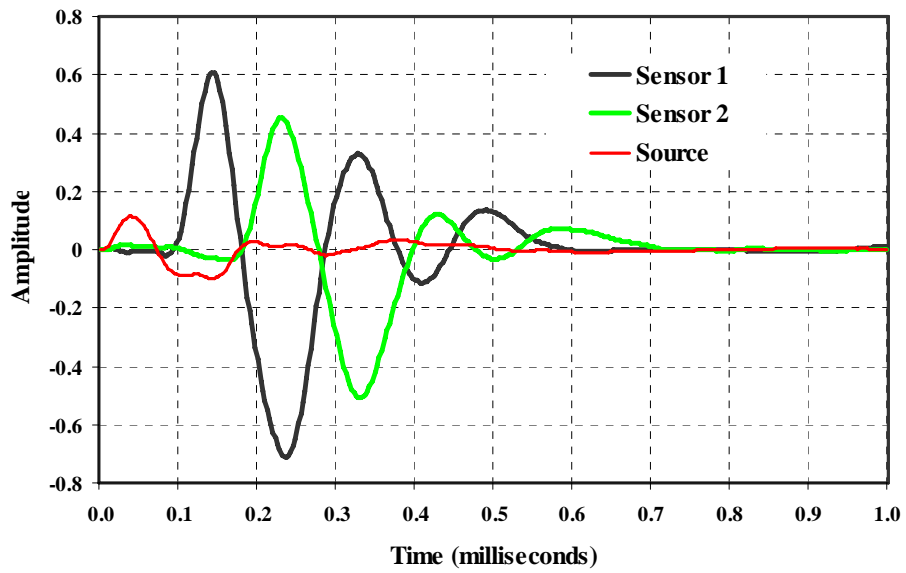


Figure 3.2 – Typical Time Records from the Portable Seismic Pavement Analyzer

III. PORTABLE SEISMIC PAVEMENT ANALYZER

The Portable Seismic Pavement Analyzer (PSPA) measures the average modulus of the ex-posed surface layers within a few seconds in the field. The operating principle of the PSPA is based on generating and detecting stress waves in a layer. The Ultrasonic Surface Wave (USW) interpretation method is used to determine the modulus of the material. Description of the measurement and implementation techniques is the subject of the next few pages.

The PSPA, as shown in Figure 3.1, consists of two transducers (accelerometers in this case) and a source packaged into a hand-portable system. The source package is also equipped with a transducer for consistency in triggering. The device is operable from a computer tethered to the hand-carried transducer unit through a cable that carries operational com-mands to the PSPA and returns the measured signals to the computer.

To collect data with the PSPA, the technician initiates the testing sequence through the computer. All the other data acquisition tasks are handled automatically by the computer. The source, which is a computer-controlled solenoid, is activated four to six times. Pre-recording impacts of the source are used to adjust the amplifiers in a manner that optimizes the dynamic range of the electronics. The outputs of the three transducers from the final three impacts are saved and averaged for more reliability. Typical voltage outputs of the three accelerometers are shown in Figure 3.2. In any seismic method, the goal is to deter-mine the velocity of propagation of waves within a material. These records are used to determine the velocity of propagation of waves in the HMA layer.

A short primer on wave propagation theory and propagation velocity is included in Appendix B. Three common types of seismic waves are compression waves, shear waves and surface (Rayleigh) waves. Surface waves contain about two-thirds of the seismic energy making them the easiest to measure. For this reason, Rayleigh wave velocity is used in the PSPA.

For pavement engineering, the interest is to determine the modulus, not the velocity of propagation. Young's modulus, E , and Rayleigh wave velocity, V_R , are theoretically related through:

$$E = 2(1 + \nu) \rho [V_R(1.13 - 0.16\nu)]^2 \quad (3.1)$$

where ν is Poisson's ratio, and ρ is the density of the material.

The next question is how to determine the propagation velocity from waveforms such as those shown in Figure 3.2. In the most general term, the velocity of wave propagation, V , can be determined by obtaining the travel time of waves, Δt , and receiver spacing, ΔX , from:

$$V = \frac{\Delta X}{\Delta t} \quad (3.2)$$

Several techniques are available for obtaining the travel time, Δt . The Ultrasonic Surface Wave (USW) method (Nazarian et al. 1993) is the one utilized in the PSPA for this purpose. In the USW method, the variation in the phase velocity with wavelength is

measured. A plot of the phase velocity vs. wavelength is called a dispersion curve. At wavelengths less than or equal to the thickness of the uppermost layer, the travel time (and as such velocity of propagation) of surface waves is independent of wavelength, as sketched in Figure 3.3. Therefore, if one simply generates high-frequency (short-wavelength) waves and if one assumes that the properties of the uppermost layer are uniform, the phase velocity of the upper layer can be determined. The wavelength at which the phase velocity, i.e. phase velocity of individual frequency components, is no longer constant is closely related to the thickness of the top layer (NCHRP 1996).

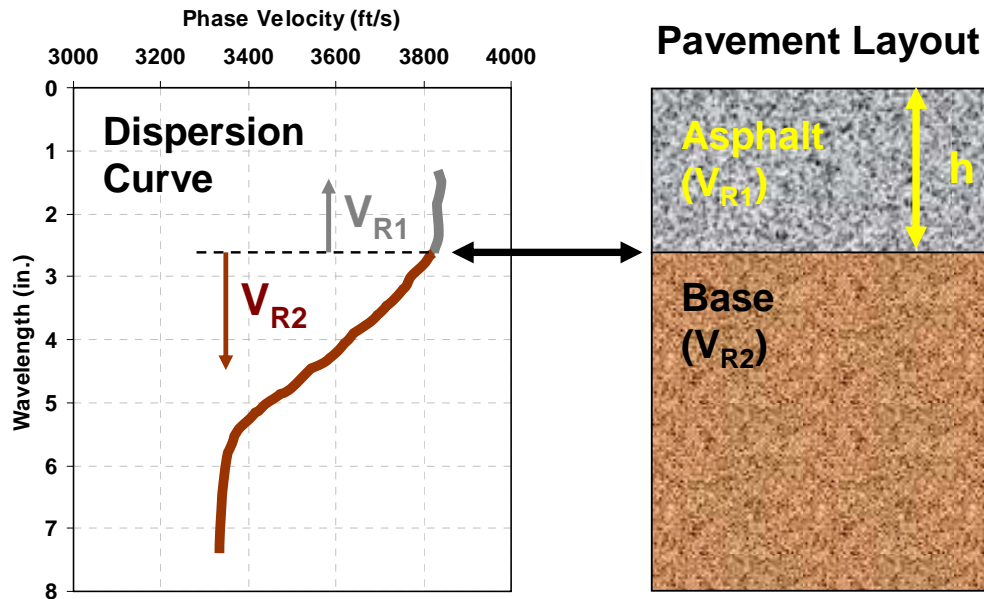


Figure 3.3 – Schematic of Ultra Sonic Surface Wave Method

An actual dispersion curve from the time record shown in Figure 3.2 is included in Figure 3.4a. As approximated by the solid line, the phase velocity (labeled as velocity in the soft-ware) is reasonably constant for the first 3 in. below which the phase velocity tends towards lower values with depth. Comparing this figure with the idealized one in Figure 3.3, the average phase velocity is about 4200 fps and the approximate thickness is about 3 in. To obtain the average modulus, the dispersion curve from a wavelength of about 1 in. to slightly less than the nominal thickness of the layer is used.

For practical inspection of dispersion curve in the field (see Figure 3.4b), the velocities in Figure 3.4a are converted to moduli using Equation 3.1, while the wavelength is simply relabeled as depth. In that manner, the operator of the PSPA can get a qualitative feel for the variation in modulus with depth.

The dispersion curve shown in Figure 3.4 is developed from the phase spectra shown in Figure 3.5. The phase spectrum can be considered as an intermediate step between the time records shown in Figure 3.3 and the dispersion curve shown in Figure 3.4 (Nazarian and Desai. 1993). This step makes the determination of the velocity with wavelength much easier. The phase spectrum is determined by conducting Fourier transform and spectral analysis on the time records from the two sensors.

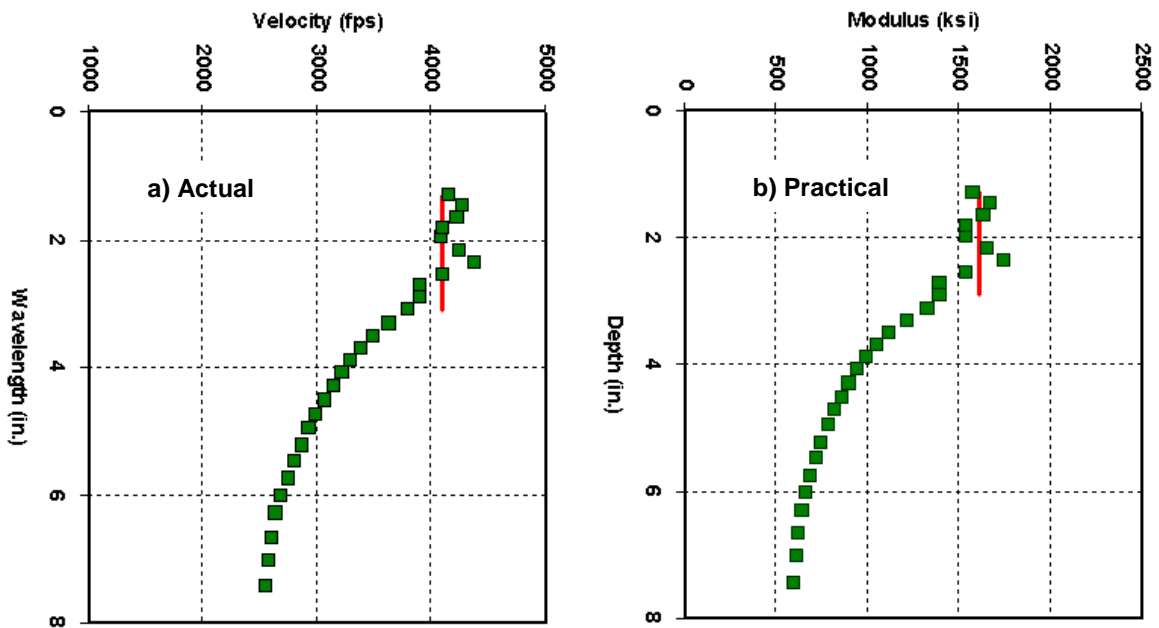


Figure 3.4 – Typical Dispersion Curve Obtained from Time Records in Figure 3.2

Two phase spectra are shown, one measured from the time records, and the other that represents the best estimation of the phase when the effect of other waves are removed. The second one is used to compute the dispersion curve as described above and detailed in Nazarian and Desai (1993).

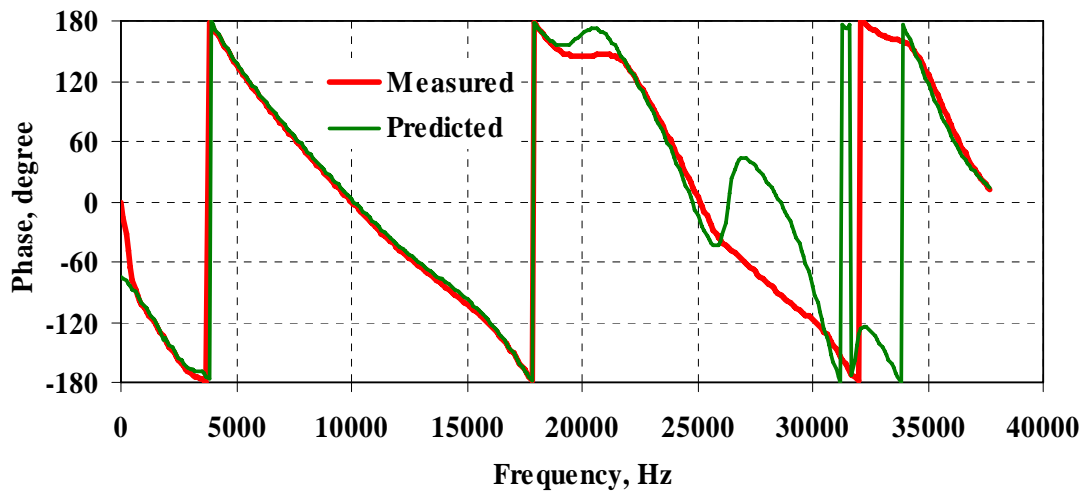


Figure 3.5 – Typical Phase Spectra Obtained from Time Records in Figure 3.2

The software that operates and reduces the PSPA data is called the Spa Manager. The screens of the software that can be used in the field during data collection are shown next.

A typical waveform screen from the Spa Manager at one point is shown in Figure 3.6. Three time records are shown in the figure. The red record is the time history of the sensor placed in the source, with the amplitude heavily attenuated. This record is useful to the advanced user for ensuring that the source is functioning properly. The black record depicts the time history as recorded by the sensor closer to the source (near receiver), and the green record is the time history from the far sensor. The black and green receiver records are used in the determination of the modulus with the USW method. Both records demonstrate the typical arrival of the surface wave energy as depicted by an initial almost zero-amplitude record followed by a full sine-wave cycle in the left hand of the records. These full-sine waves are followed by a region of virtually zero amplitude as depicted in the right hand side of the graph. On the left side of the figure, under the “Results” section, the modulus obtained for this section (i.e. 1090 ksi) is presented as soon as the data collection is completed.

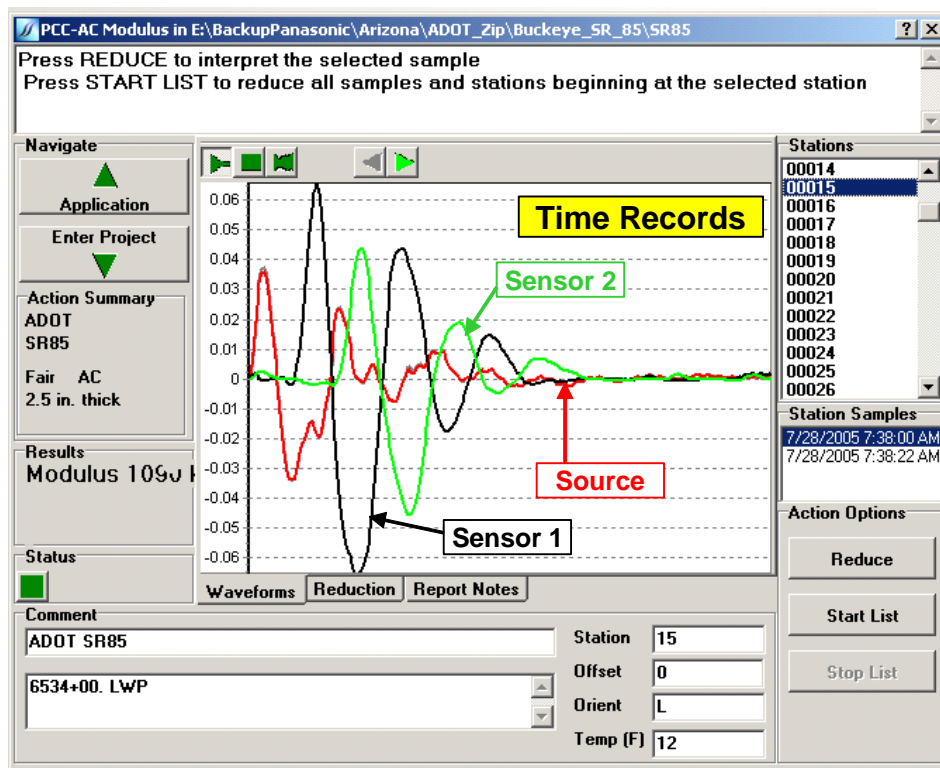


Figure 3.6 – Typical Time Records as Demonstrated by PSPA Software

In the next step, the operator has the option of viewing the reduced data, as shown in Figure 3.7. Several items can be inspected in the figure. The graph at the bottom is the phase spectrum as discussed above. This curve should represent a saw-tooth pattern (Nazarian et al. 2004). The green record is the measured phase spectrum and the red one is the best fit to the data by the software. The two curves follow one another quite well.

The upper graph labeled “Dispersion Curve is a representation of the variation in modulus (horizontal axis) with wavelength (vertical axis). The dispersion curve, which is directly calculated from the phase spectrum, is represented by green dots. The red vertical solid line

in this graph corresponds to the range of thickness along which the average modulus is calculated. This average value is the number shown in the “Results” section (i.e., 1090 ksi, where 1 ksi = 1000 lbs. force per square inch). The shortest thickness is controlled by the spacing between the receivers, the top aggregate size of the mixture and the shortest wavelengths measured by the PSPA at this transducer spacing. The longest thickness is input by the user as a nominal value. In this case the nominal thickness and the actual thickness of the layer coincide quite well, as the measured dispersion curve is uniform up to a thickness of 2.5 in. beyond which the curve breaks towards lower moduli.

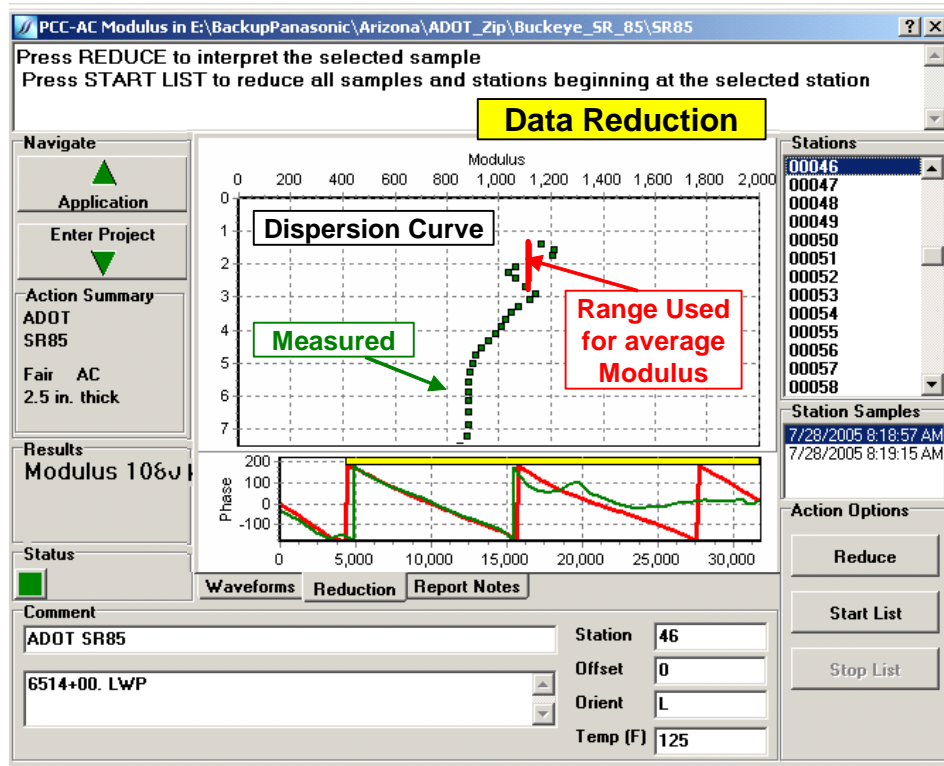


Figure 3.7 – Typical Interpreted Results as Demonstrated by the Portable Seismic Pavement Analyzer Software

Because the temperature varies from location to location, it is measured at each point with a laser temperature gun to adjust the AC moduli to 77 °F. The relationship suggested by Li and Nazarian (1994) can be used for adjusting the modulus of AC to a reference temperature of 77 °F (25 °C) in the absence of mix-specific modulus-temperature relationship. That relationship is in the form of

$$E_{77^{\circ}} = E_t / (1.60 - 0.0078 t) \quad (3.3)$$

where E_{77} and E_t are the moduli at 77 °F and measured temperature (in Fahrenheit). However, the modulus-temperature relationship established for a given mix can be utilized for more accurate results. The process of developing a mix-specific relationship is discussed in the next chapter.

IV. SEISMIC METHODOLOGY FOR QUALITY MANAGEMENT OF HOT ASPHALT

The goal of any highway agency is to construct a durable longer lasting layer of HMA. Another recent goal of most highway agencies is to shift from the prescriptive (method-based) specifications to performance-based specifications. To achieve these two goals, the following three inter-related activities have to be performed adequately and in harmony:

1. The pavement engineer should verify that the thickness and modulus of the layer are adequate, so that structural failure would not happen.
2. The laboratory engineer should select material and mix (job mix formula) that can provide durable pavement with adequate modulus.
3. The construction and lab engineers should perform lab and field tests to ensure that the layer is adequately constructed and the material delivered is as designed in the laboratory so that the mat is durable.

Since these three items are inter-related, a close coordination among the pavement engineer, lab engineer, and construction engineer is necessary. This means that the modulus assumed for the HMA by the pavement engineer should be verified by the lab engineer during mix design and by the resident engineer during construction. Under the current specifications of almost all highway agencies, the modulus is hardly ever measured in the laboratory during mix selection or on the completed mat during construction. The proposed quality management protocol will provide a convenient process by which the three bullet items above can be harmonized.

The proposed quality management procedure consists of the following five steps.

1. Selecting suitable materials and mix for a given project.
2. Determining a target modulus for the mix.
3. Characterizing the variation in modulus with temperature.
4. Determining modulus of material for structural design.
5. Field quality tests (measuring field moduli and comparing them with the target modulus).

Each step is described below.

Step 1: Selecting Suitable Materials and Mix for a Given Project

The process of volumetric design of an HMA, from the simplest (Marshall method) to the most sophisticated (Strategic Highway Research Program method), ensures a constructible and durable material. The durability of a material cannot be directly included in the structural design of a pavement, even though durability definitely does impact performance. The characteristics of a durable material depend on the collective experience of a large and diverse group of scientists and practitioners. Each highway agency's specifications clearly define how to obtain a durable HMA material by considering parameters such as angularity of the aggregates, the hardness of aggregates, percent allowable fines, the type of binder, and the degree and method of compaction. This practice should be continued to ensure a durable mix. Current ADOT specifications, such as Items 416 and 417 (ADOT 2000) are appropriate for this purpose. In addition, to tie the structural design of a mix to the laboratory mix selection, the modulus of the HMA has to be measured. Methods to measure the modulus of the mix are described in the next steps.

Step 2: Determining a Target Modulus for the Mix

After the material is selected and the job mix formula is ascertained, the next step is to determine its target modulus. The modulus can be related to one of the primary construction parameters such as the compaction effort (i.e., air voids). This activity can be carried out in conjunction with the determination of the job mix formula. The following steps are involved in this activity:

- Prepare four or five specimens from the JMF with different air voids. This can be achieved by controlling the number of gyrations used for compaction or by controlling the height of the specimen. The range of air voids from as low as 2% to as high as 12% is recommended.
- Measure the air voids and the modulus of each specimen at about 75°F. The ultrasonic device shown in Figure 2.5 is recommended to measure the seismic modulus of each specimen in less than one minute. The current ADOT Test Method 424a (similar to AASHTO T-269) can be used to measure the air voids.
- Develop a plot of seismic modulus vs. air voids. An example is shown in Figure 4.1.
- Select the modulus corresponding to the target air voids at placement (typically 7-8%). Ideally, this is the target modulus for field quality control. However, because of the differences in the nature of field and laboratory compaction, this ideal modulus should be multiplied by an adjustment factor. This adjusted modulus is used by the construction engineer for field quality control as described in Step 5.

As an example, a seismic modulus of about 1523 ksi is selected as the field target modulus for the mix shown in Figure 4.1; as such, the seismic moduli measured in the field should be equal to or greater than 1523 ksi¹.

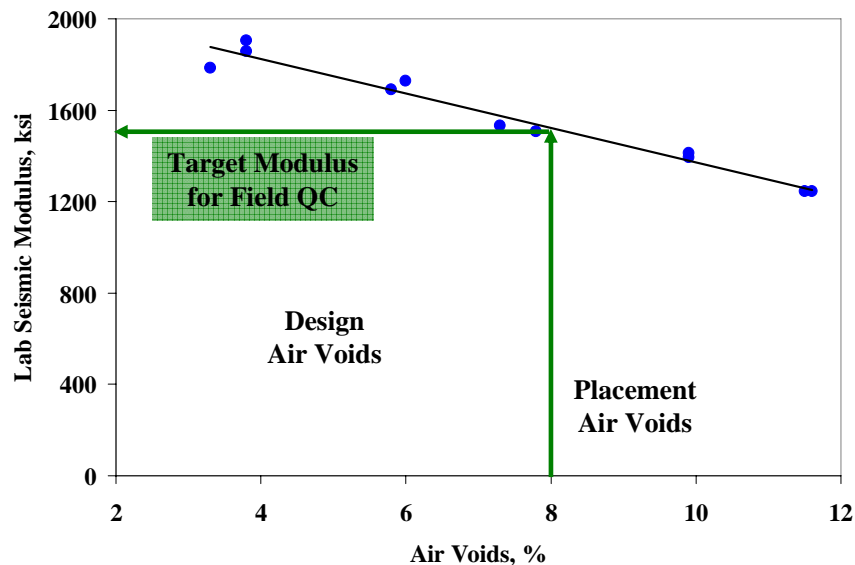


Figure 4.1 – Process of Determining Ideal Target Modulus

1. an adjustment factor of 1 is used in this report. However, based on this study, an adjustment factor of 0.85 is recommended. The justification is provided in Chapter 6.

Step 3: Characterizing the Variation in Modulus with Temperature

The modulus of a layer varies with temperature of the mat. It is difficult to know the temperature of the mat during field quality control, since it is a function of the ambient temperature and the time of day that the tests are performed. The following steps can be followed to relate modulus to temperature:

- Prepare a specimen at the target placement air voids. Since the lab tests are nondestructive, the same specimen used in Step 2 can be used in this step.
- Place the specimen in a temperature-control chamber. Vary the temperature at least four times and allow the specimen to equilibrate to the desired temperature. The suitable temperature range can be determined based on the guidelines set forward by SHRP for selecting the regional air temperature extremes to determine the appropriate performance grade (PG) binder².
- Measure the seismic modulus of the specimens at each temperature with the ultrasonic device.
- Develop a plot of seismic modulus vs. temperature. An example is shown in Figure 4.2. Determine the slope of the best-fit relationship between modulus and temperature. The slope of the best-fit line is used to adjust the field modulus to a uniform design temperature (75°F in this study).

For example, a slope of 9.63 ksi/°F is obtained for the mix shown in Figure 4.2.

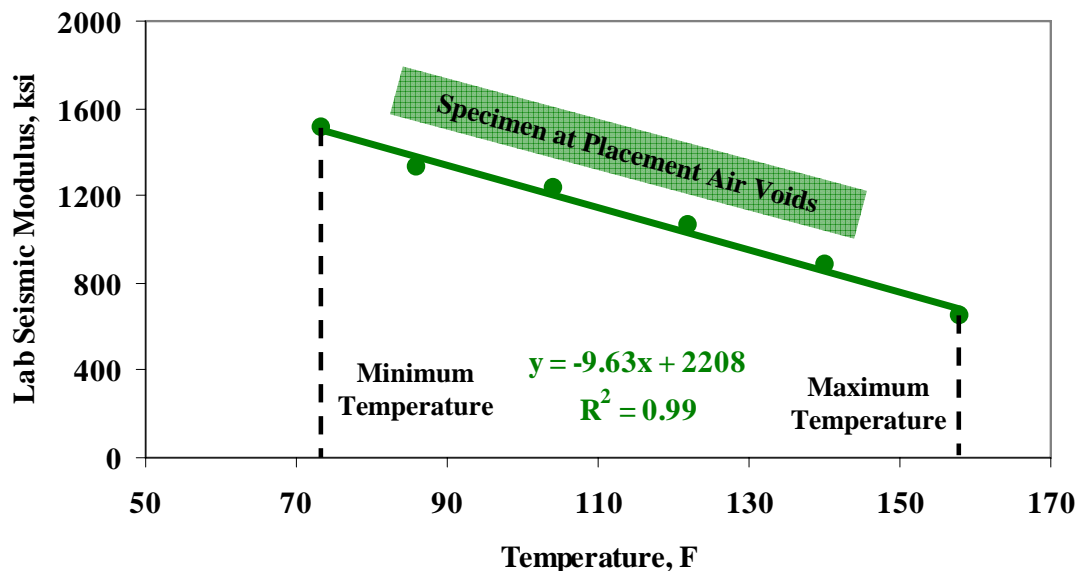


Figure 4.2 – Process of Characterizing Variation in Modulus with Temperature

2. The short-term exposure of the specimen to high temperatures (up to 160°F) does not seem to cause any degradation (such as slumping) to the specimen. However, it would be advisable to check the dimensions of the specimens to ensure that the specimen has not slumped.

Step 4: Determining Modulus of Material for Structural Design

Moduli obtained with seismic measurements are low-strain, high-strain rate values. Vehicular traffic causes high strain deformation at low strain rates. Because of these differences, the pavement community has been concerned with how to implement seismic moduli in the design. This concern has been resolved by implementing the master curve concept, which tracks the modulus over a wide frequency and temperature range.

Tandon et al. (2006) and Kim and Kweon (2006) have shown that the seismic modulus and the master curve from dynamic modulus can be combined together. A typical master curve from a specimen with combined results from both the ultrasonic and dynamic modulus tests is shown in Figure 4.3. The moduli from the two tests complement one another in defining one master curve. As such, the results of the combined seismic / dynamic modulus tests can be used with confidence in the structural design.

Once the master curve is established, the design modulus can be readily determined from the design vehicular speed and the design temperature as recommended in any mechanistic-empirical design guide. If the modulus assumed by the designer and the one obtained from this analysis **significantly differ**, either an alternative material should be used, or the layer thickness should be adjusted. **That way**, the design and material selection can be harmonized.

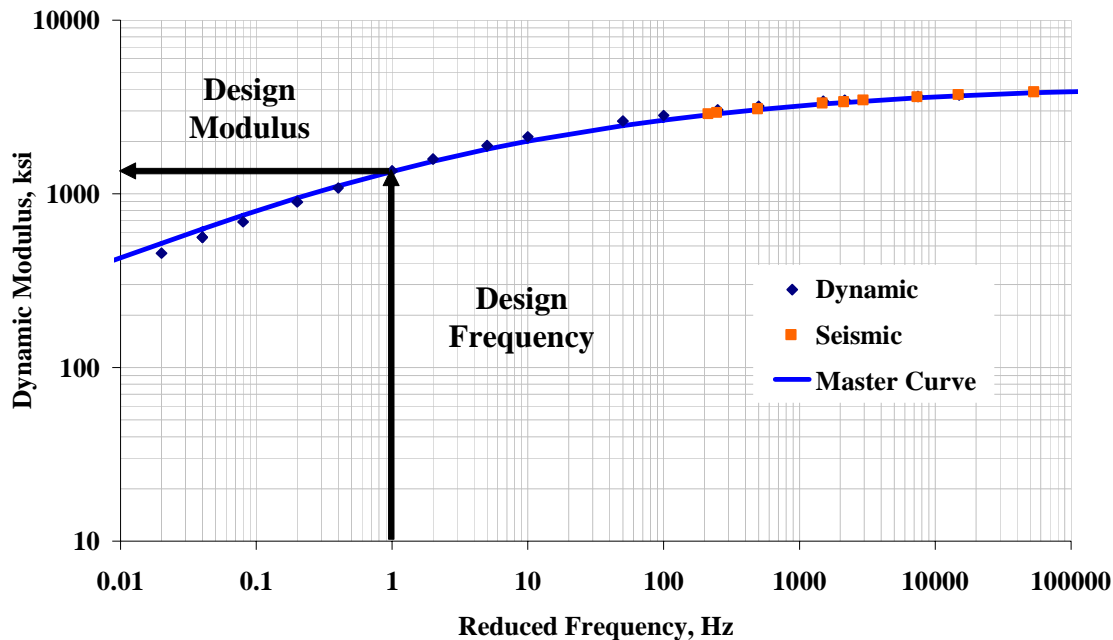


Figure 4.3 – Master Curve Concept for Defining Design Modulus

The ratio of moduli at 10 Hz (typical of an FWD) and 10 kHz (typical for the seismic method) from the master curve is 2.1:1 for the example shown in Figure 4.3. One concern raised is that the dynamic modulus tests are not routinely performed. In the absence of mix-specific dynamic modulus test results, empirical relationships presented in Chapter 2 can be used.

Based on this discussion, the development of the master curve is desirable but optional. Practically speaking, the design modulus obtained in Step 2 from the seismic modulus vs. air

voids plot can be divided by a factor obtained by dividing the moduli at 10 Hz (typical of an FWD) and 10 kHz (typical for seismic) from the empirical relationships to obtain the modulus used in the structural design, if the dynamic modulus tests are not performed on the mix.

Step 5: Field Quality Tests

Depending on ADOT policies, this step can be conducted by ADOT personnel as a part of their quality assurance program, or can be performed by the contractor as a part of the quality control program. PSPA tests are carried out at regular intervals (for this project every 100 ft) or at any point that the construction inspector suspects segregation, lack of compaction or any other construction related anomalies. An example of seismic moduli adjusted to a temperature of 75°F at one site is shown in Figure 4.4a.

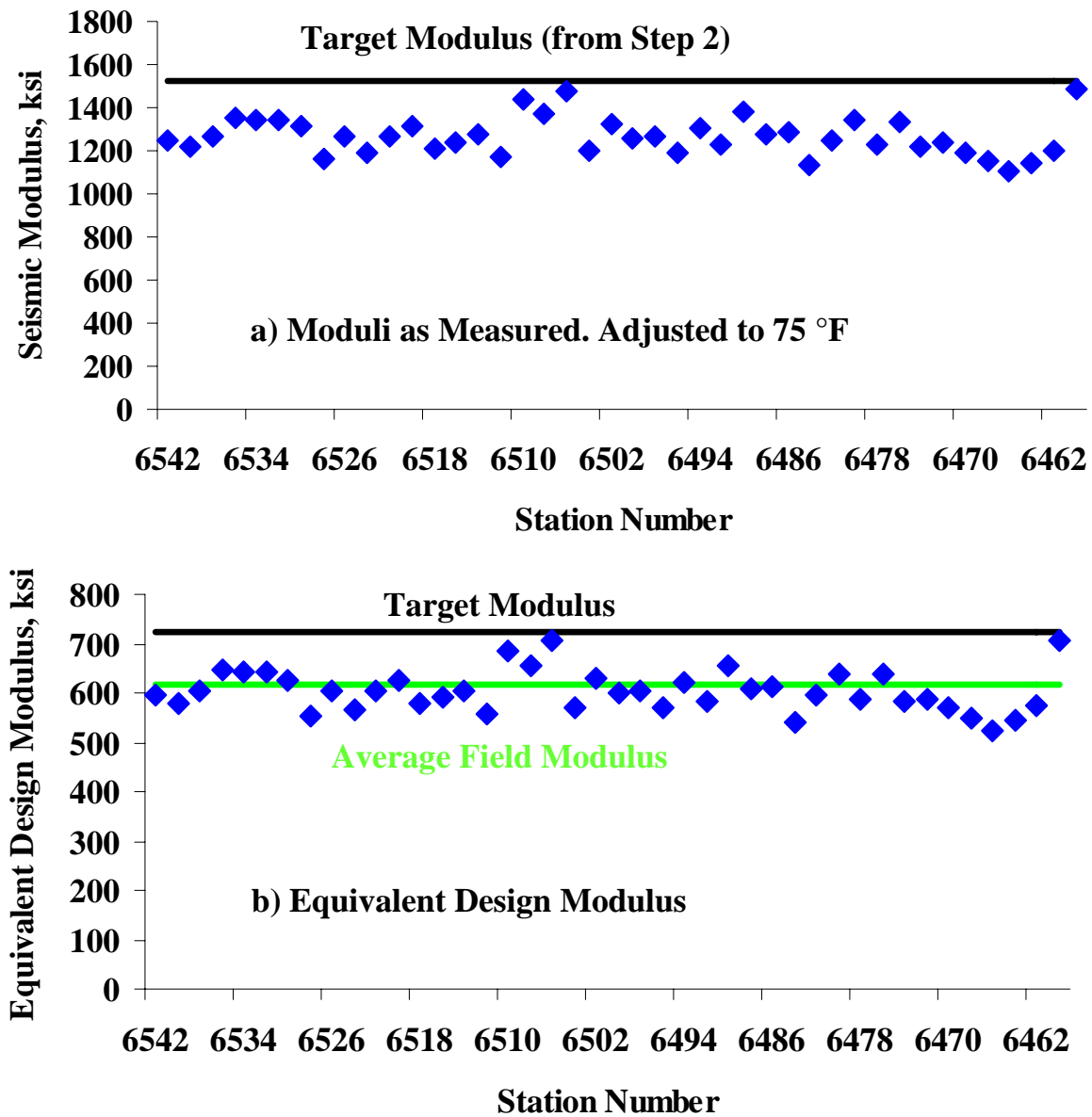


Figure 4.4 – Process of Field Testing for HMA Materials

Alternatively, the field and lab seismic moduli shown in Figure 4.4a can be converted to equivalent design modulus as discussed in Step 4 (see Figure 4.4b)³. The field moduli should be equal to or greater than the target seismic modulus determined in Step 2. In this case, moduli usually fall below the target value of 725 ksi. As reflected in Figure 4.4b, the average field equivalent design modulus is about 616 ksi, about 82% of the lab value. This pattern is normally observed due to the compaction efforts associated with laboratory specimens and field mats being different. Laboratory specimens usually yield moduli that are greater than field specimens. This is another reason to rely on the in place modulus rather than lab-prepared specimens. The relationship between field and lab tests will be more rigorously established in Chapter 6.

3. From here on the report is generally based on the equivalent design moduli.

V. EXAMPLE IMPLEMENTATION OF QUALITY MANAGEMENT IN ARIZONA

The five-step quality management procedure was adapted for evaluating the modulus of the HMA. As a review, the steps that were taken are as follows:

1. Selecting suitable materials and mix for a given project.
2. Determining a target modulus for the mix.
3. Characterizing the variation in modulus with temperature.
4. Determining modulus of material for structural design.
5. Field quality tests

A sixth and final step, the validation of the results, was also carried out to ensure the compatibility of field and lab processes. The procedure as applied to one site is discussed in this chapter as an illustrative example.

Step 1: Selecting Suitable Materials and Mix for a Given Project

The job mix formulae for all sites were provided to the UTEP team by ADOT staff. The mix design was either in accordance with Item 416 (Marshall method) or Item 417 (SHRP method) of ADOT specifications (ADOT 2000). The pertinent information for the example site is shown in Table 5.1. For this example, the mix design was according to Item 416. Three 5-gallon containers of the mix were sampled during the paving operation for a variety of lab testing.

Table 5.1 – Job Mix Formula from Project

AC Type	Type of Aggregate	Nominal Aggregate Size	Target Asphalt Content	Design Air Voids	In-place Air Voids	G _{mm}	Compaction Temperature
PG-76-16	Granite	0.75 in.	4.6 %	6.0 %	8%*	2.460	310 °F

* Rounded to the nearest integer

Step 2: Determining a Target Modulus for the Mix

Ten⁴ specimens, each 4 in. in diameter and 6 in. in height, were prepared in the lab with different air voids using materials collected from the site during construction. For both Marshall and SHRP mixes, the specimens were prepared using a Superpave gyratory compactor for uniformity and to be compliant with the specimen requirements for dynamic modulus tests. The ultrasonic device was used to measure the seismic modulus of each specimen in less than one minute. The variation in seismic modulus with air

4. Four specimens are adequate for normal operation

voids for a nominal temperature of 75°F is shown in Figure 5.1. The two parameters are well-related with an R^2 value of 0.96. Based on this figure, a target seismic modulus of 1523 ksi is anticipated at the target placement air voids of 8% shown in Table 5.1.

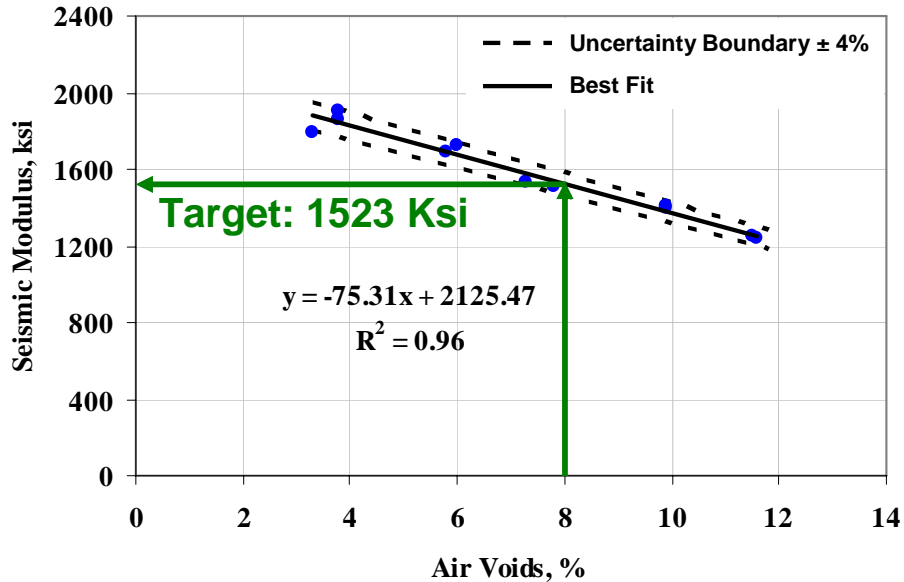


Figure 5.1 – Variation in Seismic Modulus with Air Voids from Laboratory Testing

The 95% confidence interval around the best fit line is also shown in Figure 5.1 assuming that the lab prepared specimens are very similar in terms of gradation, asphalt content, asphalt viscosity. The uncertainty is, therefore, primarily due to the uncertainty in the measurements with the ultrasonic device. Tandon et al. (2006) determined the estimated uncertainty in the measurements as 2%.

Step 3: Characterizing the Variation in Modulus with Temperature

The specimen prepared in Step 2 at the target placement air voids was then tested with the ultrasonic device at a sequence of temperatures ranging from 70°F to about 160°F. Since the lab tests are nondestructive, the same specimen can be tested repeatedly to minimize the variability in the results due to sample preparation. The variation in modulus with temperature for that specimen is shown in Figure 5.2. Once the modulus-temperature relationship is established for a given mix, it can be utilized in all project using similar mixes. The slope of the best-fit relationship in Figure 5.2 can be used to adjust the modulus at the field temperature to a uniform design temperature (75°F in this study).

In this research project, a second specimen prepared at the design air voids was also tested to determine how the change in air voids would impact the slope of modulus-temperature relationship. That information is also shown in Figure 5.2. The slope for the specimen prepared at the design air voids is 10.1 ksi/°F and for the specimen at the placement air voids is 9.6 ksi/°F. The rate of change in modulus with temperature is fairly similar at both air voids. However, at a given temperature, the modulus at the design air voids is naturally greater than the placement air voids. This affirms that testing one specimen at one air voids is reasonable for practical use. Once this relationship is developed for one mix, it can be utilized for all mixes placed with the same source of aggregates and binder type in the same region. As such, this step is not necessary for all projects.

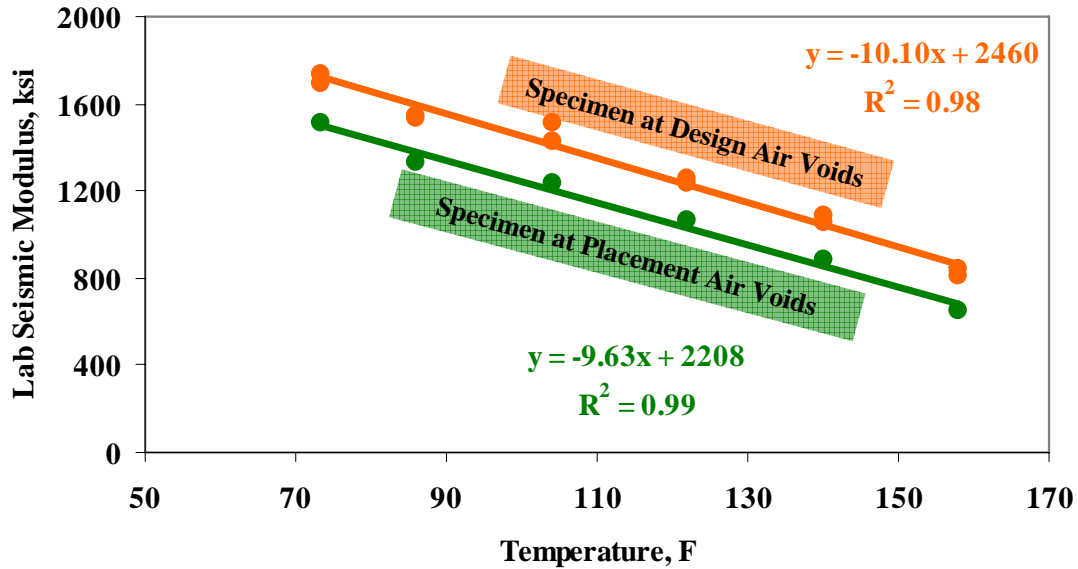


Figure 5.2 – Variations in Seismic Modulus with Temperature at Design and Placement Air Voids

Step 4: Determining Modulus of Material for Structural Design

The most rigorous way of calculating the design modulus is to develop a master curve using dynamic modulus tests based on the recommendations of Witczak et al. (2002). Master curves from two specimens prepared at the design and placement air voids are shown in Figure 5.3. The data from the ultrasonic device and from the dynamic modulus tests are shown separately. The results from the two devices integrate quite well. As shown in Figure 5.3, the moduli at 10 Hz and 10 kHz are 3152 ksi and 1502 ksi, respectively. The ratio of moduli at 10 Hz and 10 KHz from the master curve developed for the placement air voids can be used to adjust the field seismic moduli to the equivalent design modulus. In this case, this ratio is 2.1:1.

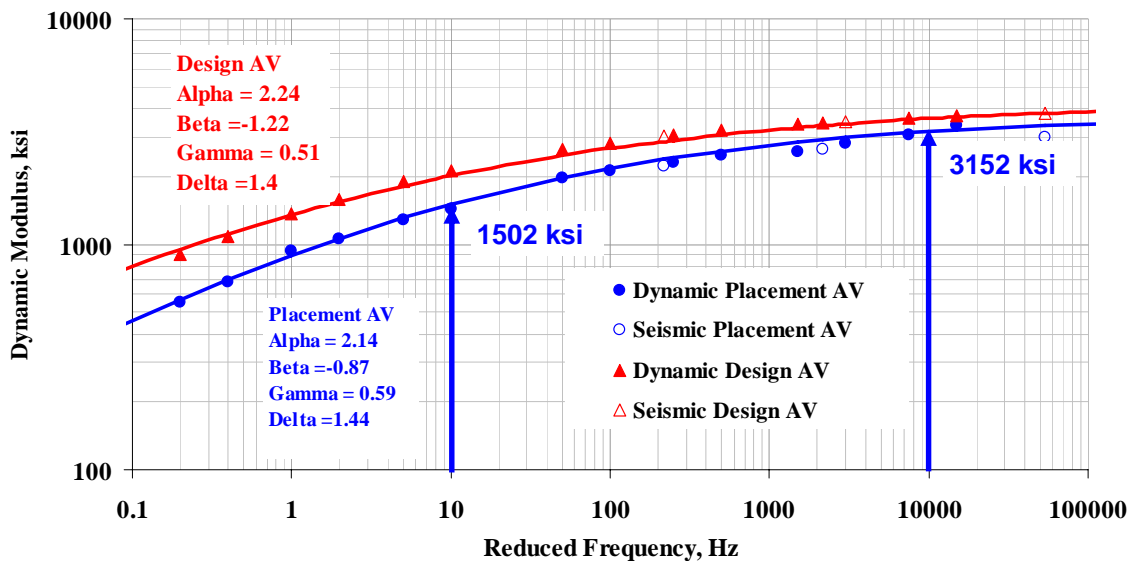


Figure 5.3 – Master Curve for Estimating Design Modulus

If ADOT does not desire to carry out the dynamic modulus tests, simplified relationships developed by Witczak and colleagues can be used. An example of such a relationship is given in Chapter 2.

Step 5: Field Quality Tests

About 45 points divided in 15 stations were tested on the pavement as depicted in Figure 5.4. Of these points, fifteen were located on the left wheel path, fifteen on the right wheel path and fifteen along the midlane of the road. The spacing between two consecutive points was usually 100 ft. Each point was tested with the PSPA to obtain the in place seismic modulus.

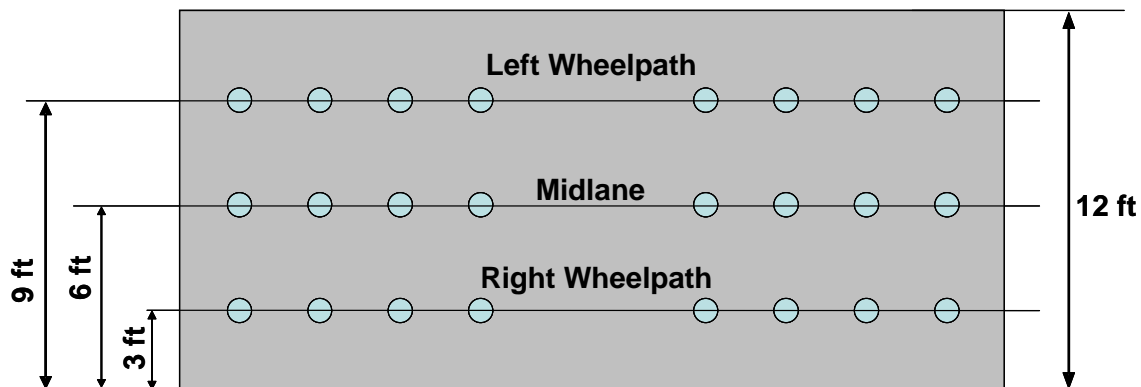


Figure 5.4 – Typical Marking of Sites

Alternatively, the location of the points can be determined based on the principals of random sampling as commonly done for determining the core locations.

The contour maps of the variation in field equivalent design modulus are shown in Figures 5.5. Some variation in the modulus along the mat can be observed. The red areas correspond to lower moduli. In that sense, the areas about Stations 6462 and 6486 are less stiff than the rest of the areas tested.

The modulus control charts associated with each wheel path are shown in Figure 5.6. Also shown in the figure are the target moduli from laboratory testing corresponding to placement air voids of 8%, 10%, and 12% obtained from Figure 5.1 and converted to the equivalent design moduli using Step 4. In this case, the representative design modulus for target air voids of 8% is about 725 ksi (obtained from the seismic modulus of 1523 ksi indicated in Step 2). The moduli usually fall below the target lines. This pattern is normally observed because the compaction efforts associated with laboratory specimens and field mats are different. Laboratory specimens usually yield moduli that are greater than field specimens. This is another reason to rely on the in place modulus rather than lab-prepared specimens.

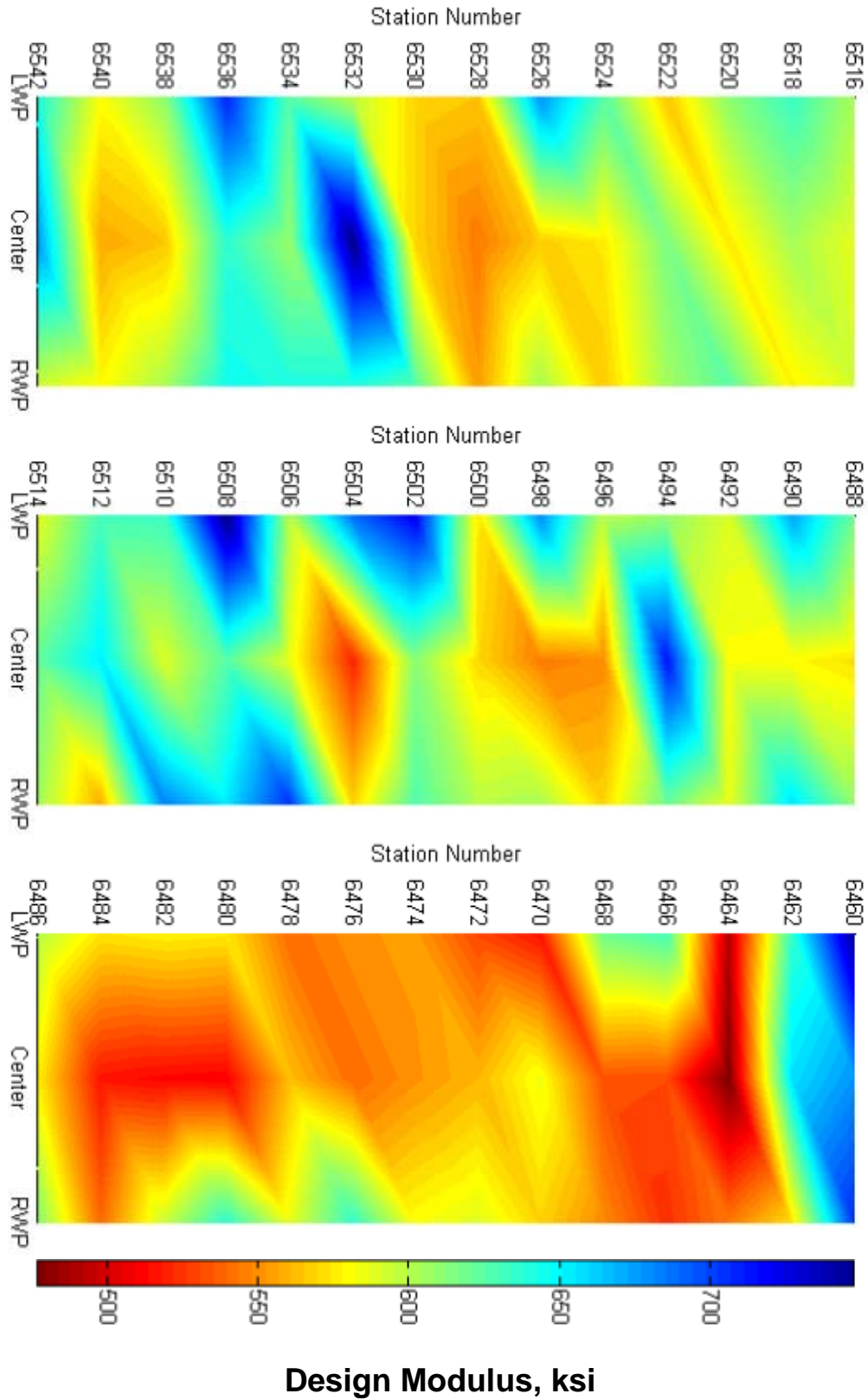


Figure 5.5 – Contour Plots of Variations in Design Modulus with PSPA along Site

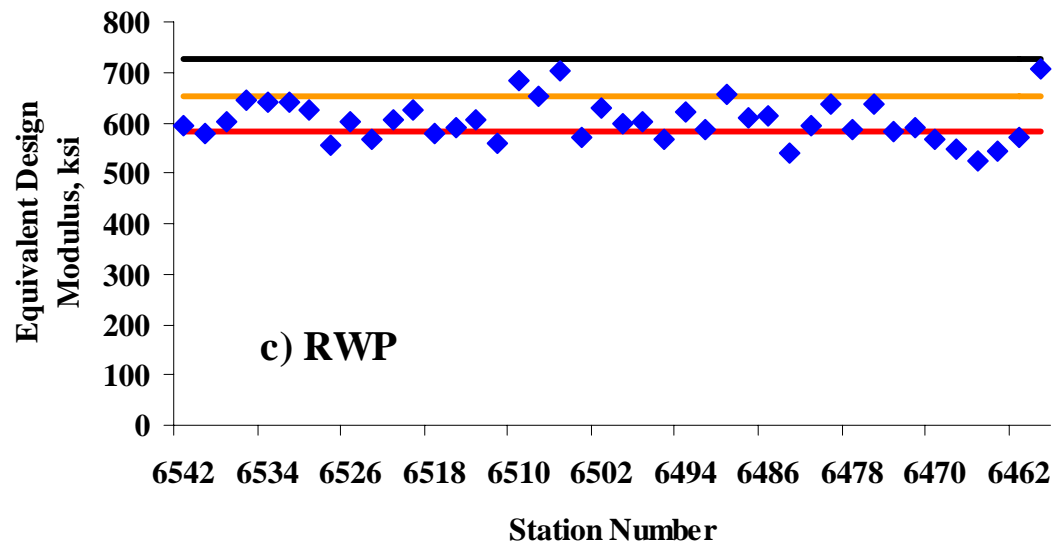
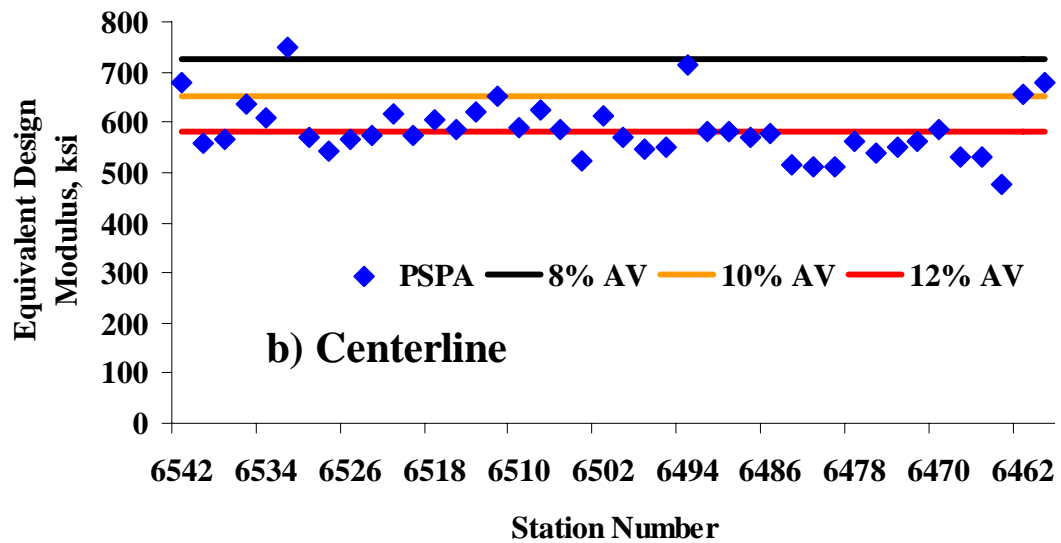
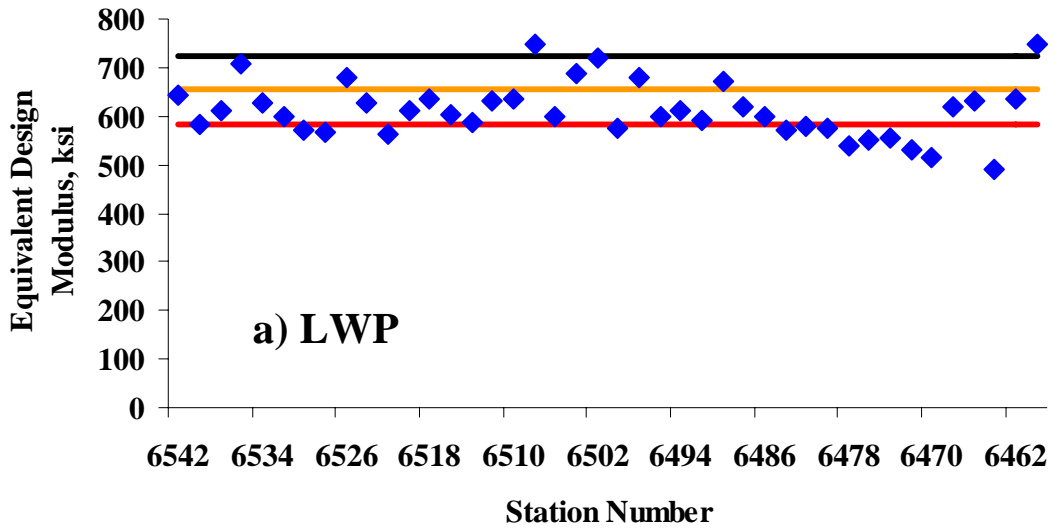


Figure 5.6 – Modulus Control Charts from Site

Finally, the cumulative distribution of design moduli along the site is included in Figure 5.7. On average (corresponding to a cumulative distribution of 50%) the representative modulus for this section of the road at the time of testing is about 595 ksi. Since the target lab modulus is 725 ksi, the field modulus on the average is about 82% of the target modulus for this project. This means that, the compaction effort obtained from the Superpave gyratory compactor does not fully imitate the compaction effort provided by the construction equipment used in the field. If the current acceptance criteria based on density seems reasonable to ADOT, an allowance has to be given to the contractor for this lack of compatibility between the lab and field methods. For this specific example, this allowance is about 82%. A global allowance will be proposed in Chapter 6 based on all sites tested in Arizona.

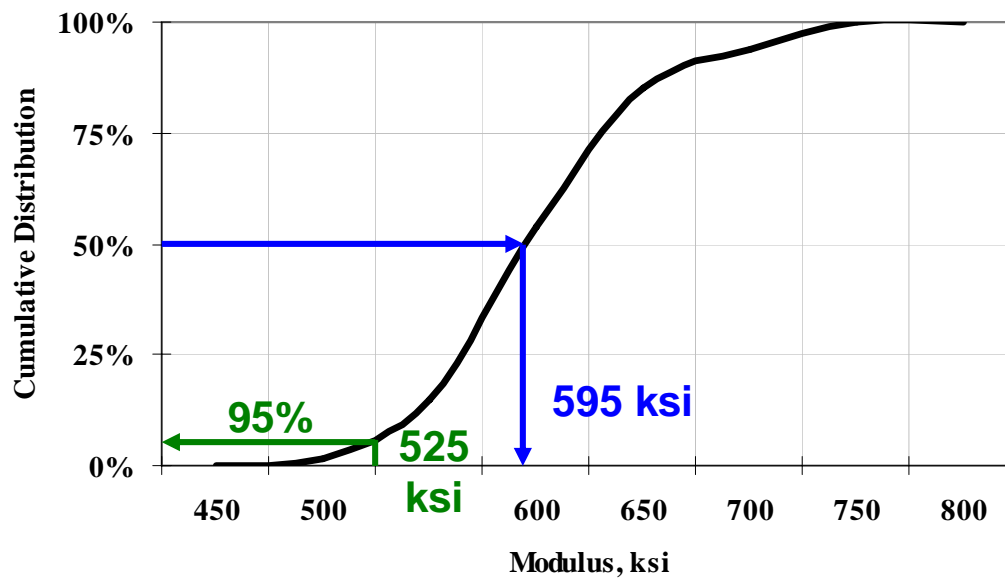


Figure 5.7 – Distribution of Equivalent Design Moduli along Site

Validation of Results

To validate the results, ten additional points were tested with the PSPA and then the pavement was cored for laboratory tests. The core locations were selected at random by ADOT personnel as a part of their routine quality acceptance activity. At each location, an additional core was retrieved and shipped to UTEP.

The equivalent design moduli obtained with the PSPA in the field are compared with the corresponding lab moduli obtained from the ultrasonic testing in Figure 5.8 and Table 5.2. The results are typically within 10% of one another, with a maximum difference of 14% indicating close correspondence between the field PSPA results and lab seismic tests on cores.

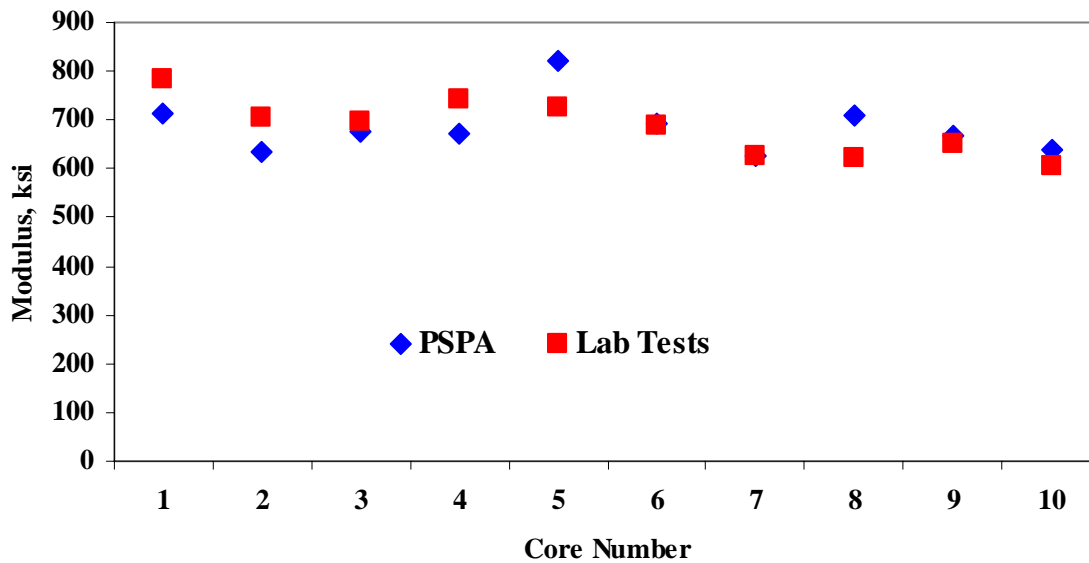


Figure 5.8 – Comparison of Moduli from PSPA and Lab Tests on Cores Extracted from Same Locations

Table 5.2 – Comparison of Moduli from PSPA and Lab Tests on Cores Extracted from Same Locations

Core Number	Modulus, ksi		
	PSPA	Lab Test on Cores	Difference*
1	711	783	9.2%
2	635	704	9.8%
3	675	695	2.9%
4	671	742	9.6%
5	823	724	13.7%
6	693	690	0.4%
7	628	628	0.0%
8	710	620	14.4%
9	667	651	2.6%
10	639	605	5.6%

* Difference = ABS (PSPA Modulus-Lab Modulus)/Lab Modulus

The air voids of the ten cores tested by UTEP were measured using a Corelock device. The air voids obtained from this activity are compared with those reported by ADOT in Table 5.3. For this site, the air voids are fairly close in most cases with an average difference of 0.7% and a maximum difference of about 1.5% in one occasion. The differences can be mainly attributed to the different methods used by the two groups to obtain the air voids.

Table 5.3 – Comparison of Air Voids for Cores Extracted at the Site

Core Number	Air Voids, %		
	ADOT	UTEP	Difference*
1	6.6	6.2	+ 0.4
2	8.4	6.9	+ 1.5
3	7.5	7.0	+ 0.5
4	6.9	6.9	+ 0.0
5	7.7	7.8	- 0.1
6	6.4	7.4	- 1.0
7	7.9	8.8	- 0.9
8	8.5	9.0	- 0.5
9	8.3	7.4	+ 0.9
10	7.4	8.5	- 1.1

* Difference = ADOT Air voids – UTEP Air voids

The seismic moduli from the cores are compared with their corresponding in-place air voids in Figure 5.9. The two parameters correlate reasonably well as judged with a R^2 of 0.75. However, the modulus air voids results from lab-prepared specimens (see Figure 5.1) yield a higher R^2 of 0.96. This pattern is anticipated because of differences in compaction patterns and possible variability in the mix constituents (asphalt content, aggregate gradation, etc.).

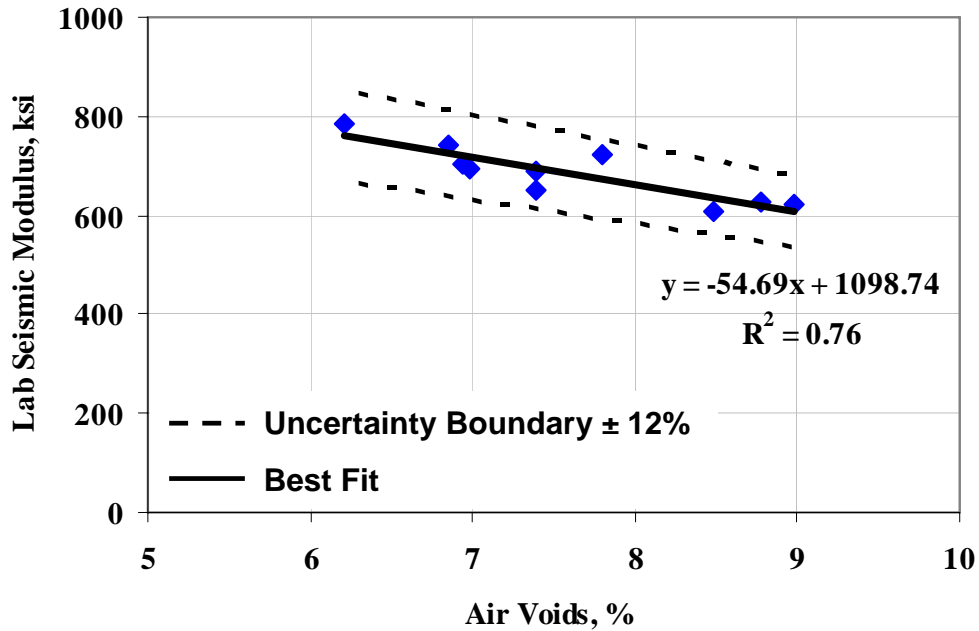


Figure 5.9 – Variation in Design Modulus with Air Voids at Core Locations

A study was carried out to verify the hypothesis that the change in the mix constituents may contribute to the variability in the moduli, and as a result, a weaker correlation between field modulus and air voids. Typical coefficients of variation (cov) in the gradation, asphalt content and asphalt viscosity from this example site are shown in Table 5.4. A Monte Carlo simulation was carried out to simulate 1500 cases where these constituents were randomly varied within their corresponding COV. The set of values obtained for all the parameters was then entered into the 1995 Witczak equation (see Table 2.1) to estimate the modulus. A frequency of 10 kHz and the average air voids from the site were used in the equation. The distribution of modulus from that equation for the 1500 cases is shown in Figure 5.10. The axis is normalized with respect to the modulus obtained using the average values of the constituents. The modulus distribution resembles a normal distribution with a COV of 6%. With a confidence level of 95%, the moduli can vary by 12% just due to the variation in constituents along the project.

Table 5.4 – Variation in Constituents of Mix from Field Samples

Rotational Viscosity (G*/Sinδ), KPa	Asphalt Content, %		Percent Retained on ¾ in. Sieve		Percent Retained on 3/8 in. Sieve		Percent Retained on No. 4 Sieve		Percent Passing No. 200 Sieve	
	Mean	COV	Mean	COV	Mean	COV	Mean	COV	Mean	COV
0.84	4.85	1.6%	2.5	51.6%	23.0	5.0%	39.5	2.5%	4.38	2.2%

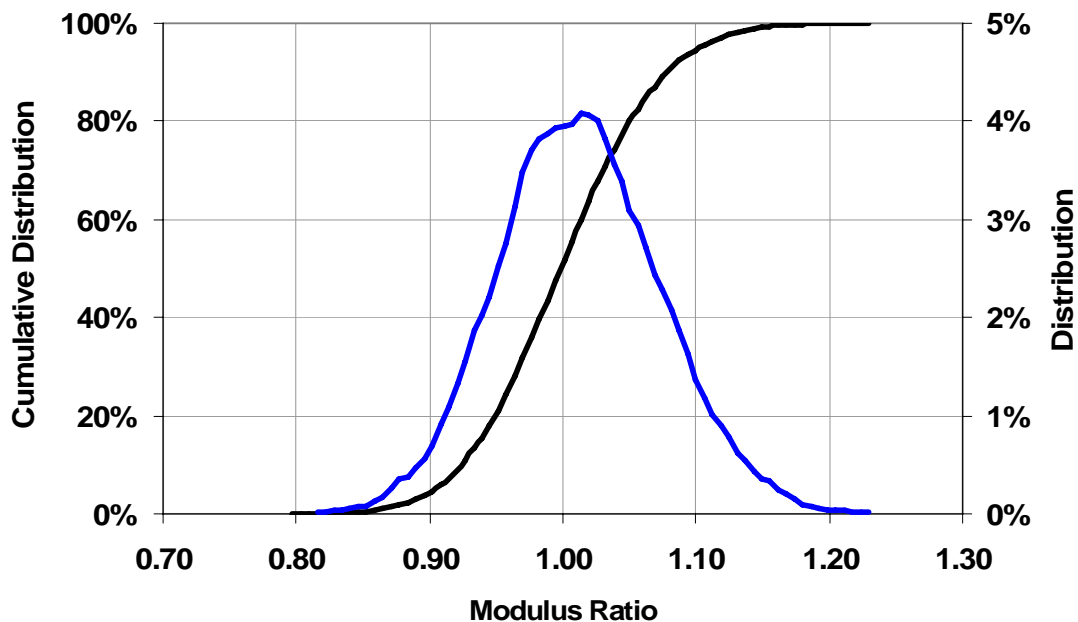


Figure 5.10 – Distribution of Moduli due to Change in Gradation and Asphalt Content of Mixes during Paving

The uncertainty bounds based on this analysis are shown in Figure 5.9. Since all data points fall within the uncertainty bounds, the changes in constituents describe the lower R^2 achieved from the field cores. In this exercise, the uncertainty due to ultrasonic tests was ignored since it is rather small as compared to the uncertainties due to changes in the mix constituents.

In addition, four of the cores were first subjected to the ignition oven to obtain the asphalt content, and the remaining aggregates were sieved for gradation. The results are summarized in Table 5.5. The gradations and AC contents seem to be reasonably close to the specifications.

Finally, to ensure appropriate gradation of the materials at the site, loose materials from two locations sampled during paving were subjected to ignition oven and gradation tests. The results from this exercise are summarized in Table 5.6. The gradations and AC contents obtained by ADOT and UTEP are quite close and within the specifications.

Table 5.5 – Gradation Results for Selected Cores from the Site

Sieve #	% Passing				
	Core 1	Core 2	Core 3	Core 4	Target
3/8"	82	76	75	77	77
8	48	39	43	43	46
40	17	15	16	16	16
200	3.5	2.8	2.9	2.4	4.5
Asphalt Content	4.6%	4.6%	4.9%	5.0%	4.6%

Table 5.6 – Gradation Results for Loose Materials Sampled at Site

Sieve #	% Passing				Target
	Location 1		Location 2		
	UTEP	ADOT	UTEP	ADOT	
3/8"	78	78	80	76	77
8	42	45	41	44	46
40	16	17	16	17	16
200	2.4	4.5	2.4	4.3	4.5
AC Content	5.1%	4.8%	4.8%	4.9%	4.6%

VI. PRESENTATION OF RESULTS

DESCRIPTION OF SITES INVESTIGATED

Ten projects throughout the State of Arizona were subjected to the proposed quality management process. The locations of the sites are shown in Figure 6.1. Tests were carried out between August and December, 2005 on the layers placed the day before. Results from the field and lab tests are reported herein.

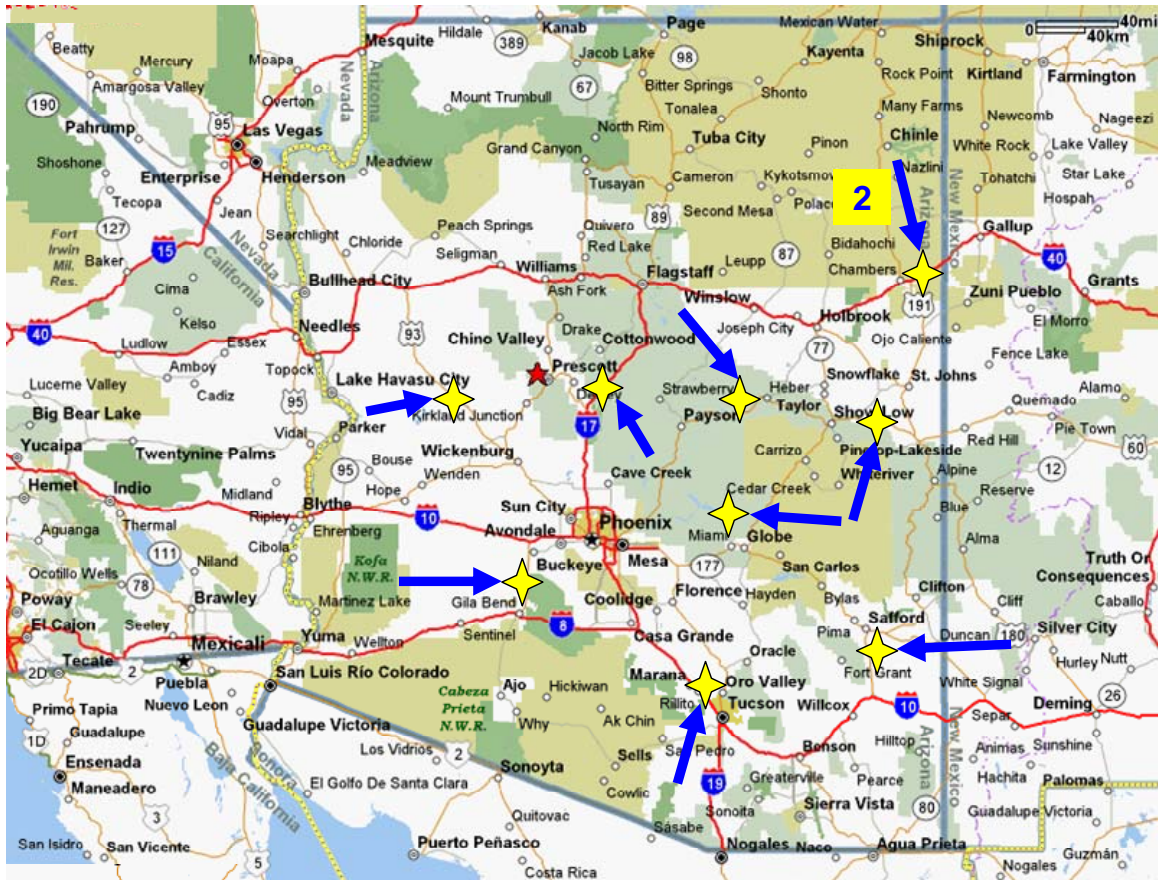


Figure 6.1 – Location of Sites Tested

DESCRIPTION OF SITES

Site 1. Buckeye SR85 (H595506C) was located on SR 85 near Buckeye (about 40 miles southwest of Phoenix) on the northbound section of two new lanes between MP 141.71 and 147.74 (Lot # 16, Station Numbers 6540 to 6640). The top layer was about 2.5 in. thick. Tests were carried out on July 28, 2005.

Site 2. Show Low SR61 (H525001C) was located on SR 61 near Show Low (about 120 miles northeast of Phoenix) on the westbound section of the two existing lanes between Station Numbers 640 to 719 of Lot # 14. The top layer was about 2.5 in. thick. Tests were carried out on August 2, 2005.

Site 3. Holbrook I-40 (H613901C) was located on Interstate 40 about 40 miles east of Holbrook on the eastbound section of the two existing lanes between Station Numbers 2403 to 2418 of Lot # 6. Tests were carried out on September 7, 2005. The top layer at this site was about 5 in. thick.

Site 4. Burro Creek US93 (H549401C) was located on US 93 about 15 miles south of Wikieup near the intersection with Burro Creek on the westbound section of the two existing lanes between Station Numbers 2699 to 2684 of Lot # 53. Tests were carried out on September 9, 2005. The top layer at this site was about 3 in. thick.

Site 5. Cordes JCT I-17 (H584501C) was located on Interstate 17 in the vicinity of Cordes Junction (about 50 miles north of Phoenix) on the northbound section of the two existing lanes between Station Numbers 65+00 to 80+00 of Lot # 3. Tests were carried out on September 8, 2005. The top layer at this site was about 5 in. thick.

Site 6. Roosevelt SR188 (H407601C) was located on SR 188 in the vicinity of Roosevelt (about 10 miles northwest of Globe) on the southbound section of two new lanes between Station Numbers 722+25 and 650+63 of Lot # 22. Tests were carried out on August 4, 2005. The top layer at this site was about 2 in. thick.

Site 7. Safford US191 (H503706C) was located on US 191 in the vicinity of Safford (about 20 miles south of Safford) on the northbound section of two new lanes between Station Numbers 573+00 to 588+00 of Lot # 10. Tests were carried out on September 1, 2005. The top layer at this site was about 2.5 in. thick.

Site 8. Holbrook I-40B (H613901C) was located on Interstate 40 in the vicinity of Holbrook (about 40 miles east of Holbrook) on the westbound section of the two existing lanes between Station Numbers 2520 to 2505 of Lot # 28. Tests were carried out on November 9, 2005. The top layer at this site was about 2.5 in. thick.

Site 9. Payson SR260 (H615101C) was located on SR 260 in the vicinity of Payson (about 15 miles east of Payson) on the southbound section of two new lanes between Station Numbers 1519 to 1561 of Lot # 8. Tests were carried out on November 10, 2005. The top layer at this site was about 2.5 in. thick.

Site 10. Tucson I-10 (H458201C) was located on Interstate 10 about 20 miles north of Tucson on the westbound section of the two existing lanes between Station Numbers 4580 to 4565 of Lot # 69. Tests were carried out on December 14, 2005. The top layer at this site was about 4 in. thick.

GENERAL RESULTS

The proposed quality management process described in Chapter 4 was applied to all ten sites.

Step 1: Selecting Suitable Materials and Mix for Each Project

Table 6.1 contains the JMF for each of the sites as provided by ADOT. Four mixes were developed based on Item 416 (Conventional Volumetric Mix) and six mixes based on Item 417 (SHRP Volumetric Mix) (ADOT 2000). The nominal aggregate size for all mixes was 0.75 in. Four different types of binders were used. The target asphalt contents of the mixes varied between 4.6% and 5.7%. The design air voids varied between 4.5% and 6.1% while the target field air voids varied between 7% and 8%.

Step 2: Determining a Target Modulus for Each Mix

Based on the mix design for each site, several specimens were prepared in the lab with different air voids using materials collected from the sites. The variations in seismic modulus with air voids for a nominal temperature of 75°F were first determined for each mix. The detailed results are included in Appendix C. As demonstrated in Figure 5.1 and Appendix C, a linear relationship can be used to describe the variation in seismic modulus with air voids.

The slopes and intercepts of the seismic modulus-air voids relationships for all sites are summarized in Table 6.2. The two parameters are well correlated, as judged with an average R^2 value of 0.95 from the regression equations.

The slope, which corresponds to the sensitivity of the modulus to change in air voids, is influenced by a number of parameters such as the type and amount of binder, the aggregate gradation and type. For the ten sites, the slope varied from 110 to 46 ksi per percent air voids. The flatter the slope is, the smaller the change in modulus with air voids will be. The global average of the slope for the ten sites in Arizona is 75 ksi per percent air voids, with a coefficient of variation of about 27%.

The intercepts of the lines in Table 6.2 correspond to the modulus at an air void content of zero. These values are basically used to estimate the moduli at any air void content. The target moduli at placement air voids are summarized in Table 6.2 as well. The target moduli varied from 1100 ksi to 1900 ksi. On average, the target modulus is about 1730 ksi with a coefficient of variation of about 16%. These target moduli can be utilized as a guideline for the future projects with similar JMFs.

Table 6.1 – Job Mix Formula from All Sites

Site	Project Number	Design Type*	AC Type	Type of Aggregate	Nominal Aggregate Size	Target Asphalt Content	Design Air Voids	In-place Air Voids	Max. Theoretical Specific Gravity	Compaction Temp
Buckeye	H595506C	416	PG 76-16	Granite	0.75 in.	4.6 %	6.0 %	8%**	2.442	310 °F
Show Low	H525001C	417	PG 64-22	Alluvial	0.75 in.	5.1 %	4.6 %	7%	2.410	295 °F
Holbrook	H613901C	417	PG 64-22	Basalt	0.75 in.	4.9 %	4.5 %	7%	2.564	298 °F
Burro Creek	H549401C	417	PG 76-16	Alluvial	0.75 in.	4.6 %	5.1 %	7%	2.484	310 °F
Cordes JCT	H584501C	416	PG 70-10	Basalt	0.75 in.	5.7 %	5.8 %	8%	2.500	300 °F
Roosevelt	H407601C	417	PG 70-10	Alluvial	0.50 in.	4.7 %	5.0 %	7%	2.492	308 °F
Safford	H503706C	416	PG 64-22	Alluvial	0.75 in.	5.6 %	5.6 %	8%	2.373	295 °F
Holbrook (B)	H613901C	417	PG 64-22	Basalt	0.75 in.	4.9 %	5.1 %	7%	2.566	298 °F
Payson	H615101C	417	PG 64-28	Alluvial	0.75 in.	5.4 %	4.9 %	7%	2.426	290 °F
Tucson	H458201C	416	PG 70-10	Alluvial	0.75 in.	5.2 %	6.1 %	8%	2.413	306 °F

* ADOT. *Standard Specifications for Road and Bridge Construction*. 2000

**Rounded to the nearest integer

Table 6.2 – Variation in Seismic Modulus with Air Voids for Lab Specimens

Site	Slope, ksi/%AV	Intercept, ksi	Modulus at Placement AV, ksi	R²
Buckeye	-75.3	2125	1523	0.96
Show Low	-69.5	2157	1670	0.98
Holbrook	-93.6	2301	1646	0.97
Burro Creek	-46.0	2010	1687	0.95
Cordes JCT	-92.6	2571	1830	0.96
Roosevelt	-68.9	2296	1813	0.95
Safford	-46.1	1511	1143	0.91
Holbrook (B)	-79.3	2540	1985	0.91
Payson	-69.3	2272	1787	0.91
Tucson	-109.6	2904	2027	0.97
Average	-75.0	2269	1732	0.95
Standard Deviation	20.0	372	280	--
Coeff. of Variation	27%	16%	16%	--

Step 3: Characterizing the Variation in Modulus with Temperature

The two specimens prepared at the design air voids and at the target placement air voids were then tested at a sequence of temperatures ranging from 70°F to about 160°F to obtain the variations in modulus with temperature. The results are included in Appendix D and are summarized in Table 6.3. Once again, a linear relationship seems to describe such relationships well. The average R^2 value is about 0.97.

The slope of the best-fit relationship can be used to adjust the modulus measured at the field temperature to a uniform design temperature (75°F in this study). The modulus-temperature slope varies between 7 ksi/°F and 13.5 ksi/°F. For most sites, the average value of 10 ksi/°F seems to be a reasonable value for Arizona.

The intercept in Table 6.3, which corresponds to the modulus at 0°F, is primarily used along with the slope to estimate the modulus at any given temperature. The moduli at the standard temperature of 75°F are also reported in Table 6.3. Naturally, these values are very similar to the target moduli reported in Table 6.2.

Table 6.3 – Variation in Seismic Modulus with Temperature for Lab Specimens at Placement Air Voids

Site	Slope, ksi/°F	Intercept (Modulus at 0°F), ksi	Modulus at 75°F, ksi	R^2
Buckeye	-9.6	2208	1485	0.99
Show Low	-10.9	2420	1601	0.98
Holbrook	-11.1	2507	1675	0.98
Burro Creek	-8.6	2360	1714	0.99
Cordes JCT	-9.7	2565	1835	0.97
Roosevelt	-9.1	2599	1915	0.99
Safford	-7.0	1658	1132	0.98
Holbrook (B)	-11.7	2986	2108	0.88
Payson	-13.5	2885	1869	0.98
Tucson	-10.4	2764	1981	0.96
Average	-10.2	2495	1732	0.97
Standard Deviation	1.8	378	280	--
Coeff. of Variation	18%	15%	16%	--

The modulus-temperature slopes for the specimens prepared at the design air voids are compared with the corresponding slopes for specimens prepared at the placement air voids in Figure 6.2. The two slopes are well correlated. This indicates that the rate of change in modulus with temperature is fairly similar for the two air voids. Practically speaking, it is sufficient to develop the modulus-temperature relationship only at the in-place air voids.

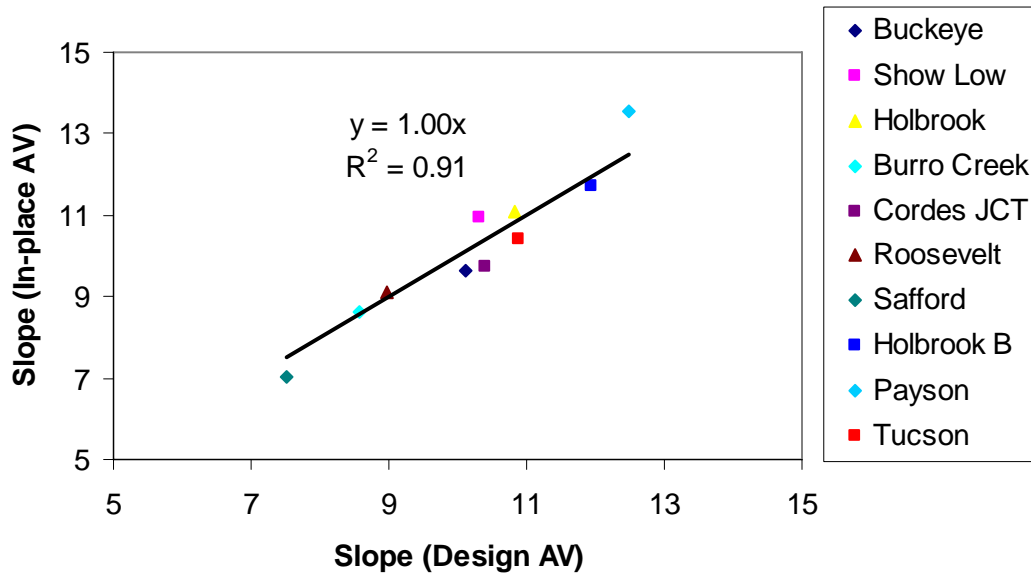


Figure 6.2 – Variations in Modulus with Temperature (Slopes) for Lab Specimens at Design and In-place Air Voids

Step 4: Determining Modulus of Each Mix for Structural Design

The master curves generated for each site at design and placement air voids are shown in Appendix E. The data from the seismic and the dynamic modulus tests integrate quite well in all cases as shown in Figure 5.3 and in Appendix E. Master curves from the ten specimens prepared at the design air voids for all sites are shown in Figure 6.3. Figure 6.4 shows master curves for all sites except the placement air voids. In both cases, the master curves vary significantly for different mixes. The material from Payson site demonstrates the lowest modulus, whereas the materials from Tucson, Burro Creek and Roosevelt are the stiffest.

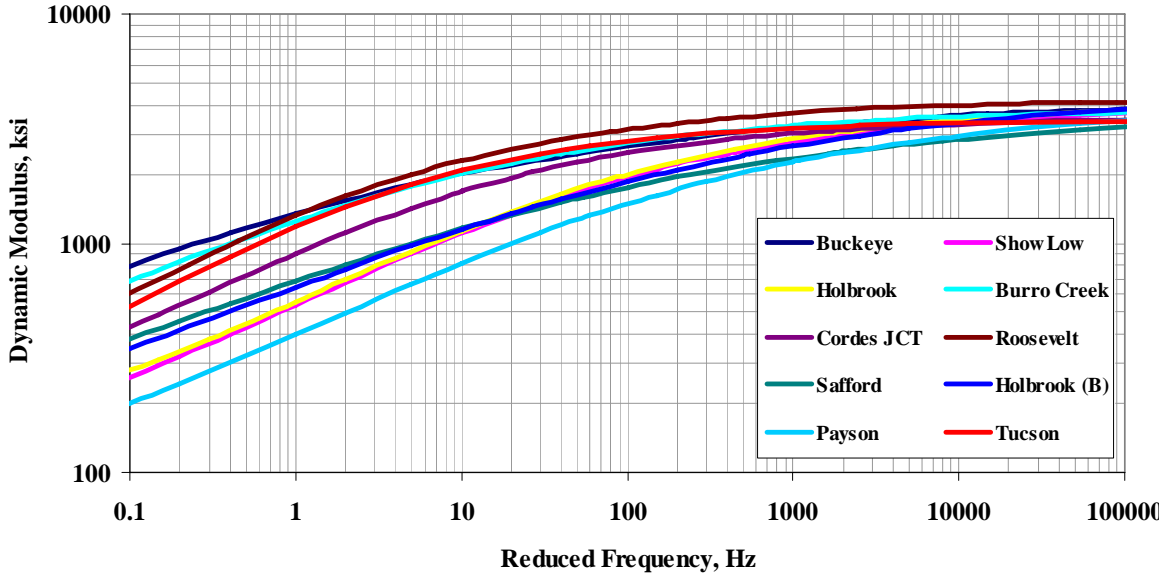


Figure 6.3 – Master Curves for Specimens Prepared at Design Air Voids

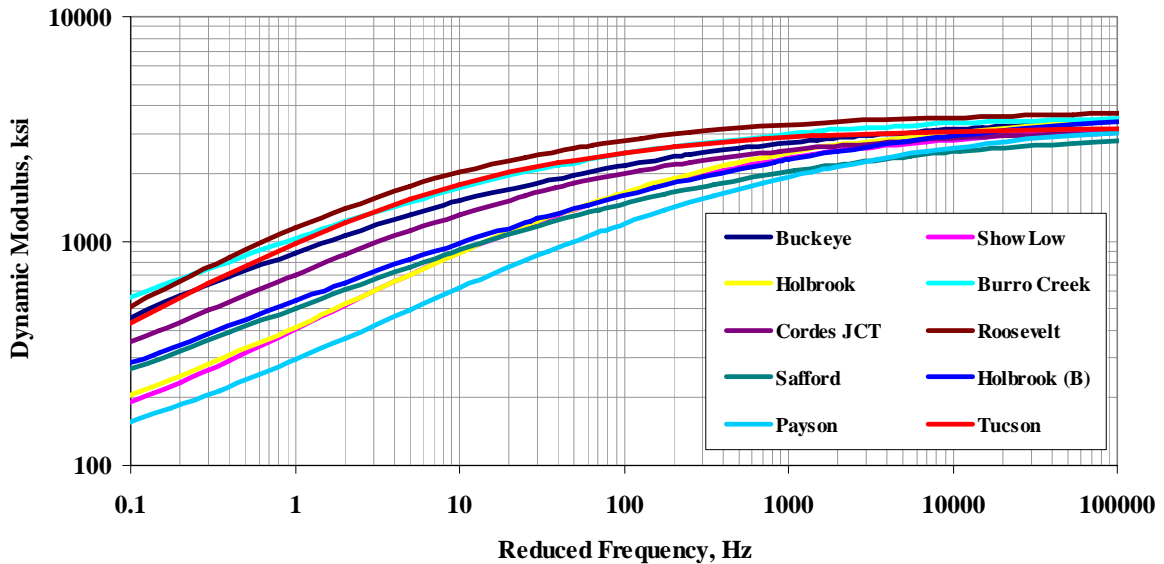


Figure 6.4 – Master Curves for Specimens Prepared at Placement Air Voids

The parameters to generate the master curves are shown on Table 6.4. These values can be used for future projects that utilize the mixes with similar JMF's. Once the master curve is established, the design modulus can be readily determined from the design vehicular speed and the design temperature as recommended in the new Mechanistic-Empirical Design Guide.

Table 6.4 – Master Curve Parameters for All Sites

Site	Master Curve Parameters*							
	Design AV				Placement AV			
	α	β	γ	δ	α	β	γ	δ
Buckeye	2.24	-1.22	0.51	1.40	2.14	-0.87	0.59	1.44
Show Low	1.76	-0.001	0.75	1.85	1.76	0.10	0.80	1.77
Holbrook	1.64	0.13	0.78	1.98	1.76	0.10	0.80	1.77
Burro Creek	1.44	-0.65	0.74	2.15	1.43	-0.45	0.74	2.14
Cordes JCT	1.53	-0.45	0.86	2.02	1.53	-0.30	0.80	1.97
Roosevelt	1.89	-1.00	0.80	1.74	1.94	-1.00	0.80	1.64
Safford	1.83	-0.38	0.56	1.75	1.76	-0.16	0.63	1.75
Holbrook (B)	1.94	-0.20	0.56	1.74	2.05	-0.23	0.54	1.59
Payson	1.92	0.10	0.66	1.69	1.82	0.40	0.71	1.74
Tucson	1.56	-0.85	0.94	1.98	1.66	-0.79	0.90	1.85

$$* \log(E^*) = \delta + \frac{\alpha}{1 + e^{\beta + \gamma \times \log t_r}}$$

Based on the master curves shown in Figure 6.3, the representative moduli that should be used in the structural design of the materials from different sites are shown in Table 6.5. As expected, the mixes with the stiffer binders yield higher moduli.

The adjustment factors from the seismic modulus to design modulus (ratios of the moduli at 10 kHz and 10 Hz) are also shown in Table 6.5. These adjustment factors varied from 1.73 to 3.22. The default adjustment factor of 3.2 recommended by Auoad et al. (2003) seems to correspond to the upper limits of the values obtained for the ADOT mixtures. The adjustment factors reflected in Table 6.5 can be used by ADOT for similar mixes.

For almost all mixes with PG 64 binders, the default value of 3.2 seems to be reasonable in the absence of actual dynamic modulus tests. For the mixes with the PG 70 and higher binders, the adjustment factor seems to be closer to 1.95.

Table 6.5 – Design Modulus and Modulus Ratios for All Sites

Site	Modulus at Design AV, ksi (Frequency 10 Hz)	Moduli Ratios at Placement AV (Frequencies: 10KHz/10Hz)
Buckeye	1347	2.10
Show Low	537	3.22
Holbrook	558	3.22
Burro Creek	1247	1.94
Cordes JCT	900	2.17
Roosevelt	1323	1.76
Safford	686	2.73
Holbrook (B)	640	3.00
Payson	400	4.21
Tucson	1183	1.73

Step 5: Field Quality Tests

The average variations in the gradations, binder contents and air void contents for the ten sites are summarized in Table 6.6. The individual results are summarized in Appendix F. The average gradations measured in the field are quite similar to the specified values for nine sites, indicating a well-executed process control. The gradation from the Burro Creek site seems to deviate with the specified gradation.

The variations in as-built binder contents at different sites are summarized in Figure 6.5. The target binder contents are close to those measured during construction.

The as-built air voids are compared with the target values in Figure 6.6. The as-built air voids at the Cordes Junction site are somewhat higher than the target value, and for the Tucson site are somewhat less than target.

The contour maps of the variations in field seismic modulus with the PSPA converted to equivalent design modulus are shown in Appendix G for each site. Some variation in the modulus along the mats can be observed, with red areas corresponding to lower moduli. Also shown in that appendix are the normalized moduli (the ratio of the as-built measured modulus with PSPA and the target modulus) to demonstrate how much the measured moduli vary from the target values obtained in the lab.

The modulus control charts associated with each wheel path and the midlane are included in Appendix H. The target moduli from laboratory testing corresponding to placement air

voids, 2% above placement air voids and 4% above placement air voids are depicted for each site. For all cases, the moduli usually fall below the target lines.

Table 6.6 – Average Gradations, AC Content and Air Voids at Sites

Site	ADOT Sieve # Results (% Passing)				AC Content (%)	Air Voids (%)
	3/8"	8	40/30	200		
Buckeye	77 (77)	45 (46)	17 (16)	4.4 (4.5)	4.9 (4.6)	7.6 (8)
Show Low	77 (75)	46 (41)	22 (24)	5.2 (5.0)	5.4 (5.1)	7.0 (7)
Holbrook	71 (70)	43 (47)	25 (26)	5.0 (5.0)	4.8 (4.9)	6.3 (7)
Burro Creek	76 (62)	36 (29)	16 (14)	6.1 (5.0)	4.9 (4.6)	6.4 (7)
Cordes JCT	75 (77)	38 (42)	10 (11)	4.9 (5.1)	5.6 (5.7)	9.7 (8)
Roosevelt	72 (74)	32 (34)	19 (18)	4.7 (3.8)	5.1 (4.7)	6.6 (7)
Safford	72 (71)	40 (40)	13 (14)	3.9 (4.4)	5.6 (5.7)	7.9 (8)
Holbrook (B)	73 (68)	32 (33)	17 (17)	4.3 (3.8)	5.1 (4.9)	6.7 (7)
Payson	71 (77)	40 (45)	21 (24)	4.7 (5.1)	5.2 (5.4)	6.5 (7)
Tucson	71 (68)	46 (43)	17 (15)	4.2 (4.1)	5.4 (5.2)	6.7 (8)

Numbers in parentheses correspond to the target values

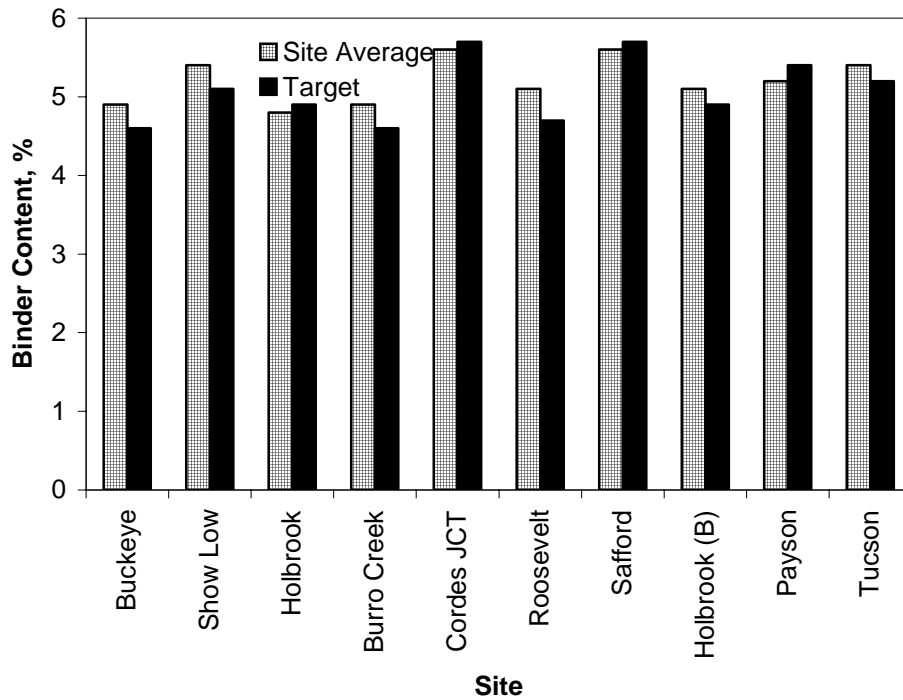


Figure 6.5 – Comparisons of Target and As-Built Binder Contents at Arizona Sites

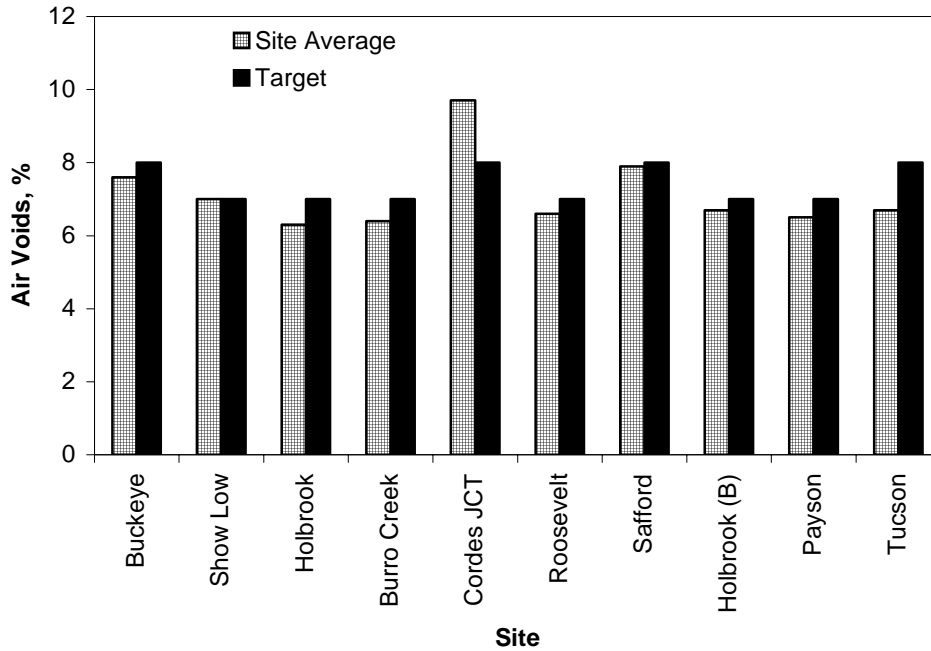


Figure 6.6 – Comparisons of Target and As-Built Air Voids at Arizona Sites

The cumulative distribution of moduli along each site is included in Appendix I. The results are summarized in Figure 6.7. The more vertical the lines are, the more uniform the moduli of the sites would be. In most sites, the distribution of the moduli is reasonably uniform.

The moduli associated with a cumulative distribution of 50% correspond to the average moduli. The average moduli at the ten sites are compared with the target values in Table 6.7. The average moduli are less than the target moduli for all but one site.

The ratio of the as-built and target moduli are also reported in Table 6.7. This pattern is normally observed because the compaction efforts associated with laboratory specimens and field mats are different. Laboratory specimens usually yield moduli that are greater than field specimens. These ratios vary from a low of about 0.7 to a high of 1.06.

The main two reasons for the field moduli being below the target lab moduli are less than desirable construction practices, or the fact that the Superpave gyratory compactor yields lab specimens that are stiffer than those achievable in the field. The contractor should be held accountable for the quality of construction. However, allowance should be provided to the contractor for the inconsistency between the lab and field compaction. To assist ADOT in setting target moduli that provide allowance for the differences between lab and field compaction methods, the ratios of the as-built and target moduli from all sites are

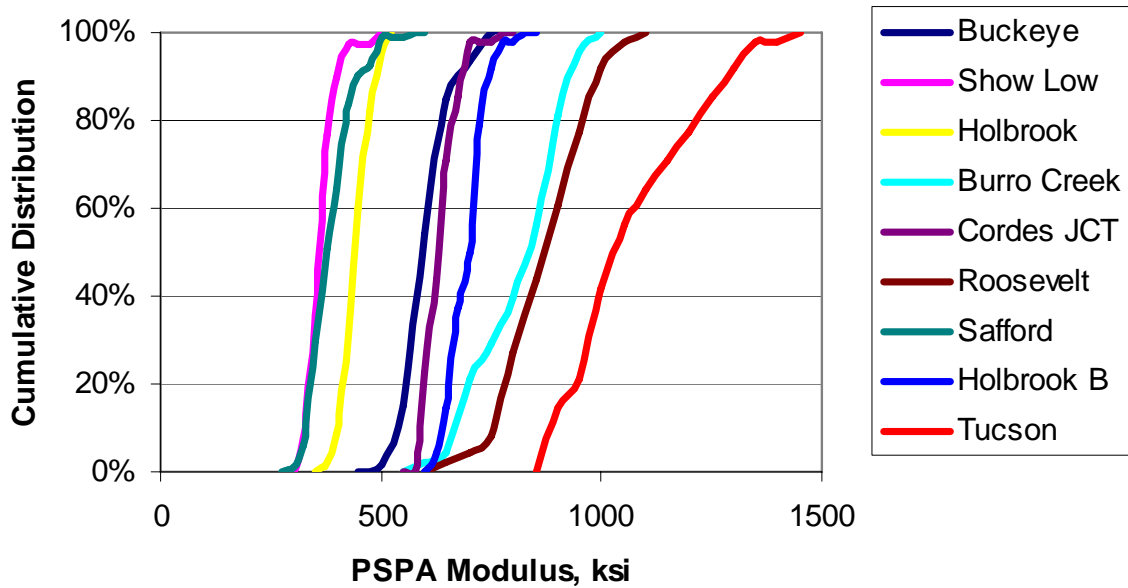


Figure 6.7 – Cumulative Distributions of Moduli

Table 6.7 – Comparison of As-Built and Target Moduli

Site	Average Modulus, ksi	Target Modulus, ksi	Ratio (Avg./Target)	Pay Factor (\$/ton)	
				Mix	Compaction
Buckeye	595	725	0.82	-0.75	-0.25
Show Low	358	518	0.69	1.00	1.00
Holbrook	441	511	0.86	0.25	1.00
Burro Creek	831	870	0.96	-3.00	1.00
Cordes JCT	631	842	0.75	0.25	-1.30
Roosevelt	869	1028	0.85	-3.00	1.00
Safford	375	418	0.90	1.00	0.50
Holbrook (B)	700	662	1.06	1.00	1.00
Payson	N/A*	425	N/A*	-2.00	0.00
Tucson	1028	1171	0.88	1.00	0.50

* Results are not available because the site was opened to traffic before field testing

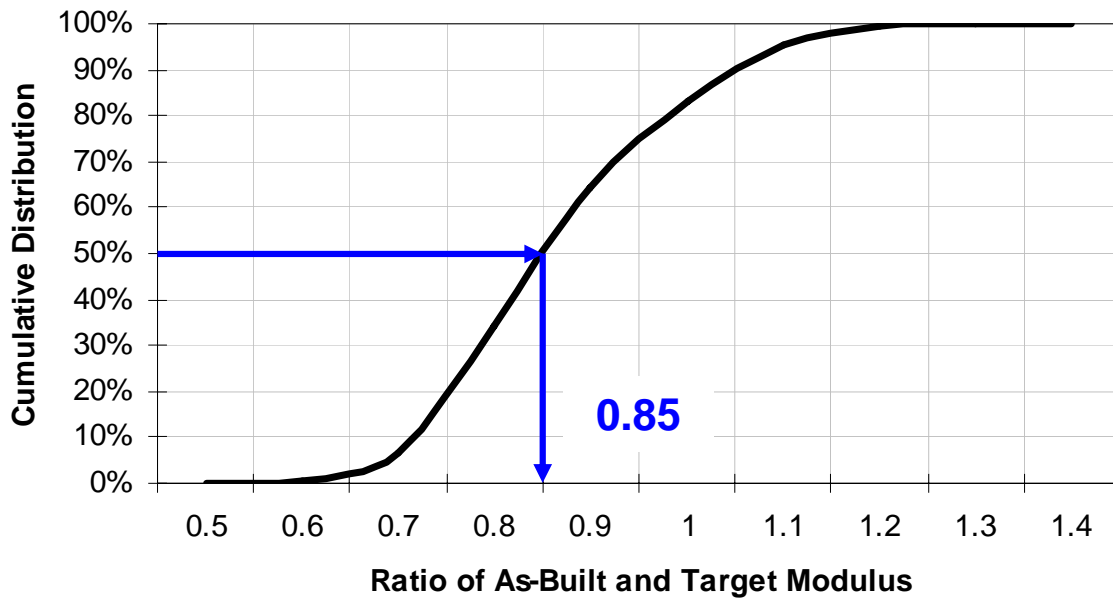


Figure 6.8 – Cumulative Distribution of Ratios of As-Built and Target Moduli from all Arizona Tests

combined in Figure 6.8 for all data points. At a cumulative distribution of 50%, the ratio of 0.85 is obtained. This means that a reasonably achievable level of modulus should be set at 85% of the target modulus obtained from lab tests on specimens prepared at target air voids. With a confidence level of 90%, a value of 75% should be used in the structural design.

The acceptance tests and associated bonuses and penalties associated with the lot for each site tested in this study are included in Appendix J. ADOT imposes two types of pay adjustments, one related to the mix quality and the other related to the construction (compaction) quality.

The mix-related and construction-related pay adjustments are included in Table 6.7 and Appendix K. Since all specimens tested by UTEP were prepared from mixes collected at the site, it is not possible to quantify the impact of the mix-related pay adjustments on the quality of the mix. In an actual project, it would be desirable for ADOT to prepare specimens for Step 2 with the original job mix formula (as opposed to specimens prepared from materials retrieved from the site) to obtain the target modulus for each site. In that manner, the moduli measured in the field with the PSPA would reflect the impact of both the mix-related and construction-related parameters.

As reflected in Table 6.7, two projects incurred construction-related penalties under the current ADOT specifications (Buckeye and Cordes JCT). Under the seismic modulus criterion using 85% of target modulus from Step 2, these projects are also considered sub-standard. Under the seismic criterion a third project (Show Low) is also sub-standard, even

though according to the current ADOT specification that site is eligible for a bonus. The reason for this pattern is not known at this time.

Validation

To validate the results of the PSPA, ten additional points were tested and then cored for laboratory tests at each sites. Detailed results from this activity are included in Appendix J. The moduli obtained with the PSPA in the field are compared with the moduli obtained with a lab ultrasonic device on the cores from all sites in Figure 6.9. The PSPA moduli and lab seismic moduli are reasonably close, since the results are clustered close to the line of equality. The largest difference at one individual point was 18%, with average differences of about 9%.

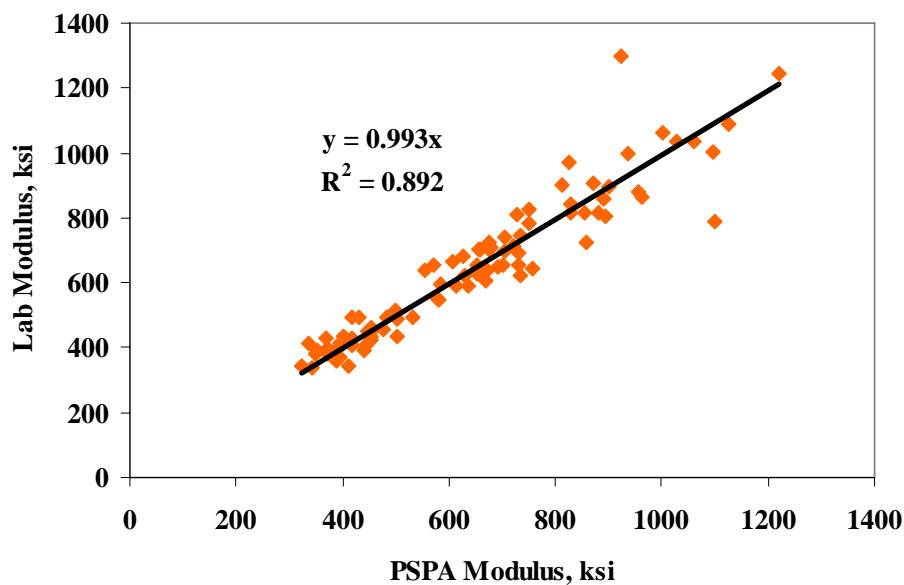


Figure 6.9 – Comparison of Moduli from PSPA and Lab Tests on Cores

The variations in the measured seismic modulus with air voids are presented in Appendix L and summarized in Table 6.8. As for the lab-prepared specimens, a linear relationship was established between the modulus and air voids. As reflected in Table 6.8, the R^2 values of the best-fit lines are typically around 0.8 unlike for the lab-prepared specimens where the R^2 values were greater than 0.9.

Since the same method was used to determine the moduli and air voids, the lower R^2 values relationships can be attributed to the variations in the gradation and asphalt content, which are not as precise as the lab-prepared specimens. The variations in the mix constituents based on the field records are summarized in Table 6.9. The distributions in the moduli from the Monte Carlo simulations are included in Appendix M (see Chapter 5 for process of determining the distributions). The uncertainties associated with the estimated moduli at a level of confidence of 95% are included in Table 6.8. An

average uncertainty of 15% is obtained due to normal variations in the mix constituents. Considering these uncertainties, the relationships between modulus and air voids are reasonable, and the lower R^2 relative to the lab specimens are described.

Table 6.8 – Variation in Core Seismic Modulus with Air Voids

Site	Slope, ksi/%AV	Intercept, ksi	R²	Uncertainty Bound*
Buckeye	-118	2365	0.76	12%
Show Low	-62	1795	0.85	11%
Holbrook	-90	2022	0.78	17%
Burro Creek	-91	2188	0.94	17%
Cordes JCT	-88	2222	0.67	13%
Roosevelt	-61	2060	0.83	12%
Safford	-53	1535	0.90	12%
Holbrook (B)	-125	2880	0.73	16%
Payson	-162	3290	0.84	24%
Tucson	-156	2890	0.76	14%
Average	-101	2325	0.81	15%
Standard Deviation	37	515	--	--
Coeff. of Variation	37%	22%	--	--

* Uncertainty Bound is defined at a level of confidence of 95% from Monte Carlo simulations discussed in Chapter 5

Table 6.9 – Variation in Mix Constituents for All Sites

Site	Rotational Viscosity (G*/Sinδ), KPa	Air Voids, %		Asphalt Content, %		Percent Retained on ¾ in. Sieve		Percent Retained on 3/8 in. Sieve		Percent Retained on No. 4 Sieve		Percent Passing No. 200 Sieve	
		Mean	COV	Mean	COV	Mean	COV	Mean	COV	Mean	COV	Mean	COV
Buckeye	0.84	7.6	9.9%	4.85	1.6%	2.5	51.6%	23.0	5.0%	39.5	2.5%	4.38	2.2%
Show Low	1.34	7.0	10.4%	5.38	3.3%	0.0	0.0%	23.3	10.8%	45.0	27.1%	5.23	2.4%
Holbrook	1.46	6.3	13.0%	4.84	3.6%	0.0	0.0%	29.5	11.2%	43.5	9.8%	4.95	7.6%
Burro Creek	0.94	6.4	11.0%	4.91	8.6%	0.0	0.0%	23.8	18.3%	46.3	2.1%	6.05	2.9%
Cordes JCT	1.27	9.7	9.3%	5.61	2.4%	0.0	0.0%	25.3	8.2%	43.0	7.4%	4.85	14.0%
Roosevelt	1.68	6.6	11.0%	5.09	2.9%	0.0	0.0%	28.3	7.8%	55.0	15.6%	4.68	7.5%
Safford	1.71	7.9	16.8%	5.60	2.0%	0.0	0.0%	28.0	2.9%	52.7	9.2%	3.85	8.6%
Holbrook (B)	1.44	6.7	13.1%	5.12	2.6%	0.0	0.0%	27.5	12.1%	51.0	13.3%	4.33	3.5%
Payson	1.27	6.5	23.2%	5.19	5.0%	0.0	0.0%	28.8	16.9%	42.5	11.0%	4.70	14.4%
Tucson	1.37	6.7	15.3%	5.41	3.4%	4.0	35.4%	28.8	3.3%	43.2	7.2%	4.20	5.8%

The seismic modulus-air voids relationships can also be developed based on the PSPA results. Since the lab and PSPA moduli are quite similar, the field and lab modulus-air field relationships are quite similar with similar R^2 values. For brevity, field relationships are not shown.

The slopes of the relationships vary from 53 to 162 ksi/%AV. On the average, the slope is about 100 ksi/%AV which is greater than 75 ksi/%AV measured in the lab. This indicates that the moduli of field specimens are more sensitive to the variations in air voids as compared to lab-prepared specimens, another indication that the lab and field compacted specimens are different.

VII. SUMMARY, CONCLUSIONS, and RECOMMENDATIONS

SUMMARY

The goal of any highway agency is to construct a layer of HMA that will perform well for a long time. Another recent goal of most highway agencies is to shift from prescriptive (method-based) specifications to the performance-based specifications. To achieve this goal, the following three inter-related activities have to be performed adequately and in harmony:

- The pavement engineer should verify that the thickness and modulus of the layer are adequate, so that structural failure will not happen.
- The laboratory engineer should select material and mix (job mix formula) that can provide durable pavement with adequate modulus.
- The construction and lab engineers should perform lab and field tests to ensure that the construction method is adequate and the material delivered is as designed in the laboratory so that the mat is durable and can yield the proper modulus.
- This report contains a process that provides the results to relate these three items based on seismic methods.

The outcomes from this project exhibit that the proposed equipment and methodologies strike a balance between the existing level of sophistication in the design methodology, laboratory testing and field testing. Performing the simplified laboratory and field tests along with more traditional tests may result in a database that can be used to smoothly unify the design procedures and construction quality control.

The process consists of the following five steps:

1. Selecting suitable materials and mix for a given project.
2. Determining a target modulus for the mix.
3. Characterizing the variation in modulus with temperature.
4. Determining modulus of material for structural design.
5. Field quality tests

CONCLUSIONS

Based on this study, the following specific concluding remarks can be made:

- The target modulus for field quality control can be determined from laboratory tests. Even though it is preferred to perform lab tests to determine the target modulus for each individual mix, typical values for the ten mixtures tested are provided.
- The modulus of HMA is temperature dependent. The variation in modulus with temperature for mixes can be readily developed in the lab. Once again, typical values are presented that can be used to quantify the modulus-dependence of the mixes similar to those studied in this project. Based on the comparison of lab and

- field moduli, a target modulus of 85% of the lab-developed target should be achievable by contractors using the current construction practices.
- A method for combining the results from the dynamic modulus and seismic tests on lab-prepared specimens is presented to determine the structural modulus of the mixes to be used in the structural design of pavement sections.
 - To obtain the structural design modulus, the specimens should be prepared at the in-place air voids. In the absence of lab tests, parameters for estimating the modulus for mixes similar to those used in this project are provided. Based on the state of the practice in Arizona for constructing HMA layers, the modulus for structural design should be 75% of the lab values.
 - The variations in the as-built modulus measured with the PSPA are repeatable and rapid.
 - Based on a validation study, the moduli measured with the PSPA are quite similar to the lab seismic moduli measured from cores extracted at the points where PSPA tests were carried out.
 - Due to the nondestructive nature of PSPA tests, a larger number of tests can be carried out on the finished mat. The larger number of tests will result in more confidence in the quality of the final product.

IMPLEMENTATION RECOMMENDATIONS

The issues related to the implementation of seismic methods and devices in the day-to-day operation of ADOT were studied through comprehensive tests at ten sites. The major issues addressed are the utility of the methods, means of relating the measured parameters to the design moduli and relating the parameters to performance of the pavement. The significance of the process proposed here is that the quality management process can be incorporated in a performance-based specification.

This new method of quality management constitutes a paradigm shift that may require some adjustment to the current institutional practices of ADOT. In the current ADOT quality management method, a number of surrogate parameters (such as the asphalt content, gradation, and air voids) are controlled hoping to achieve an “adequate” but unknown modulus. In the method suggested here, the modulus that the mix can potentially provide is known. Any deviation from this modulus in the field is as a result of construction practices, especially lack of desired density.

The process seems to be ready for shadow specification by ADOT personnel on a larger number of projects so that acceptance criteria can be statistically developed. The following items are recommended for the inclusion in the new specifications:

1. The current methods for developing job mix formula should be carried out as-is to ensure a durable mix.
2. The target field modulus should be determined from lab-prepared specimens using a Superpave gyratory compactor as soon as practical. Given the construction practices of ADOT, a target modulus of 85% of the lab-developed

- target modulus should be specified as the target field modulus to account for inconsistencies between the laboratory and field compaction methods.
3. The structural design modulus of the mix should be determined by either performing combined seismic/dynamic modulus tests on specimens prepared at the in-place air voids in Item 2 (preferred) or using seismic modulus in combination with the Witzak empirical equations. The modulus for structural design should be specified as 75% of the lab modulus to account for inconsistencies between the laboratory and field compaction methods.
 4. PSPA tests should be carried out at a number of points (perhaps 30 points initially) for each lot to evaluate the quality of the mat.

To develop the specifications, a number of institutional issues need to be addressed by ADOT including:

- Setting incentive and disincentive levels based on the field moduli with respect to the target modulus established for the mix.
- Establishing communication between the design engineer and laboratory engineer during mix design to adjust either the mix to provide modulus required by the designer or to adjust the thickness of the layers based on the target modulus to ensure adequate performance.

REFERENCES

- Andrei, D., M. W. Witzczak, and W. Mirza. 1999. *Development of the 2002 Guide for the Design of New and Rehabilitated Pavement Structures. APPENDIX CC-4: Development of a Revised Predictive Model for the Dynamic (Complex) Modulus of Asphalt Mixtures.* NCHRP 1-37A. College Park, MD: University of Maryland, March 1999.
- Aouad, M. F., K. H. Stokoe II, and R. C. Briggs. 1993. Stiffness of Asphalt Concrete Surface Layers from Stress Wave Measurements. *Transportation Research Record* 1384:29-35.
- Arizona Department of Transportation (ADOT). 2000. *Standard Specifications for Road and Bridge Construction.* Phoenix, Ariz.: the Department.
- Asphalt Institute. 1982. *Research and Development of the Asphalt Institute's Thickness Design Manual (MS-1), Ninth Edition.* Research Report No. 82-2. College Park, MD: the Institute, August 1982.
- Ayres M. and M. W. Witzczak. 1998. "AYMA – A mechanistic probabilistic system to evaluate flexible pavement performance." *Proceedings of 77th Annual Meeting of Transportation Research Board*, pp. 11-15. Washington D.C.: the Board, January 1998.
- Chehab, G., Y. R. Kim, R. A. Schapery, M. W. Witzczak, and R. Bonaquist. 2002. "Time-Temperature Superposition Principle for Asphalt Concrete Mixtures with Growing Damage in Tension State." *Journal of Association of Asphalt Paving Technologists* 71:559-593.
- Christensen, D.W.; T. Pellinen, and R. F. Bonaquist. 2003. "Hirsch Model for Estimating the Modulus of Asphalt Concrete." *Journal of the Association of Asphalt Paving Technologists* 72:97-121.
- Daniel, J. S., and Y. R. Kim. 1998 "Relationships among Rate-Dependent Stiffness of Asphalt Concrete Using Laboratory and Field Test Methods." *Transportation Research Record* 1630:3-9.
- Ferry, J. D. 1970. *Viscoelastic Properties of Polymers.* 2nd edition. New York: John Wiley, 1970.
- Finn, F., C. Saraf, R. Kulkarni, K. Nair, W. Smith, and A. Abdullah. 1977. "The Use of Distress Prediction Subsystems for the Design of Pavement Structures." *Proceedings, 4th International Conference on the Structural Design of Asphalt Pavements.* pp. 3-38. Ann Arbor, MI: University of Michigan.

- Kim, Y. R. and Y. C. Lee. 1995. "Interrelationships among Stiffnesses of Asphalt Aggregate Mixtures." *Journal of Association of Asphalt Paving Technologists* 64:575-609.
- Kim, Y. R. and G. Kweon. 2006. "Determination of the Complex Modulus of Asphalt Concrete Using the Impact Resonance Test." *85th Annual Meeting of the Transportation Research Board*. Paper 06-0464. Washington, D.C.: Transportation Research Board.
- Li, Y. and S. Nazarian. 1994. "Evaluation of Aging of Hot-Mix Asphalt Using Wave Propagation Techniques." *Engineering Properties of Asphalt Mixtures And the Relationship to Their Performance*. ASTM STP 1265. pp.166-179. Philadelphia, Pa.: American Society for Testing and Materials.
- Miller, G. F. and H. Pursey. 1955. "On the Partition of Energy between Elastic Waves in a Semi-Infinite Solid." In *Proceedings, International Conference on Microzonation for Safer Construction: Research and Application*. vol. 2, 545-58. Seattle, WA.: Society of Exploration Geophysicists.
- Nazarian, S. and M. Desai. 1993. "Automated Surface Wave Testing: Field Testing," *Journal of Geotechnical Engineering* 119(GT7):1094-112.
- Nazarian, S., D. Yuan, V. Tandon, and M. Arellano. 2004. *Quality Management of Flexible Pavement Layers with Seismic Methods*. Research Report 1735-3. El Paso, TX: Center for Transportation Infrastructure Systems, University of Texas at El Paso.
- National Cooperative Highway Research Program (NCHRP). 1996. *Nondestructive Testing to Determine Material Properties of Pavement Layers*. Interim Report, NCHRP 10-44. Washington, D.C.: the Program.
- National Cooperative Highway Research Program (NCHRP). 2004. *Mechanistic-Empirical Design of New and Rehabilitated Pavement Structures*. NCHRP Project 1-37A Report. Washington, D.C.: the Program.
- Pagen, C. A. 1963. *An Analysis of the Themorheological Response of Bituminous Concrete*. Master of Science Thesis. Columbus, OH: Ohio State University.
- Pellinen, T.K. and M. W. Witczak. 2002. "Stress Dependent Master Curve Construction for Dynamic (Complex) Modulus." *Journal of Association of Asphalt Paving Technologists* 71:281-309.
- Richart, Jr., F.E., R. D. Woods, and J. R. Hall, Jr. 1970. *Vibrations of Soils and Foundations*. Englewood Cliffs, NJ: Prentice-Hall, Inc.
- Shah, K. A. 1993. *Development of a New Laboratory Testing Procedure for Resilient Modulus of Asphalt Concrete*. Master of Science Thesis. Raleigh, NC: North Carolina State University.

Shook, J.F., F.N. Finn, M.W. Witzak, and C.L. Monismith. 1982. "Thickness Design of Asphalt Pavements – The Asphalt Institute Method." *Fifth International Conference on the Structural Design of Asphalt Pavements*. Vol. 1. Ann Arbor, MI: University of Michigan.

Tandon, T., S. Nazarian, and X. Bai. 2006. "Assessment of Relationship between Seismic and Dynamic Modulus of Hot Mix Asphalt Concrete." *International Journal of Road Materials and Pavement Design* (accepted for publication).

Tashman, L., E. Masad, B. Peterson, and H. Saleh. 2001. "Internal Structure Analysis of Asphalt Mixes to Improve the Simulation of Superpave Gyratory Compaction to Field Conditions." *Journal of the Association of Asphalt Paving Technologists* 70:605-645.

Von Quintus, H.L. and B. M. Kilingsworth. 1998. *Analyses Relating to Pavement Material Characterizations and their Effects on Pavement Performance*. Research Report FHWA-RD-97-085. Washington, DC.: Federal Highway Administration.

Witzak M. W., K. Kaloush, T. Pellinen, M. El-Basyouny, and Von Quintus H. 2002. *Simple Performance Test for Superpave Mix Design*. NCHRP Report 465. Washington, DC.: Transportation Research Board.

APPENDIX A. DYNAMIC MODULUS TEST

In the new mechanistic-empirical pavement design guide, fundamental properties of materials are used rather than empirical parameters. The preferred fundamental property for hot-mix asphalt (HMA) is the modulus of the material. The dynamic modulus test is used to characterize the viscoelastic modulus of the HMA. A viscoelastic material is one that exhibits both elastic and viscous characteristics, and stress is related to strain by a function of time in the linear viscoelastic range (Pagen 1963, pp. 26-33). The dynamic modulus testing is performed at various temperatures and frequencies and a master curve is developed for a reference temperature based on the assumption that asphalt concrete is thermo-rheologically simple material (Chehab et al. 2002).

The response of viscoelastic material, such as HMA, due to sinusoidal load application will also be sinusoidal but the response will be out-of-phase with the stress by a certain amount as shown in Figure A.1. A $\phi = 0^\circ$ is indicative of a pure elastic material; a value of $\phi = 90^\circ$ indicates a pure viscous (Newtonian) material. A phase value between 0° and 90° indicates a viscoelastic material.

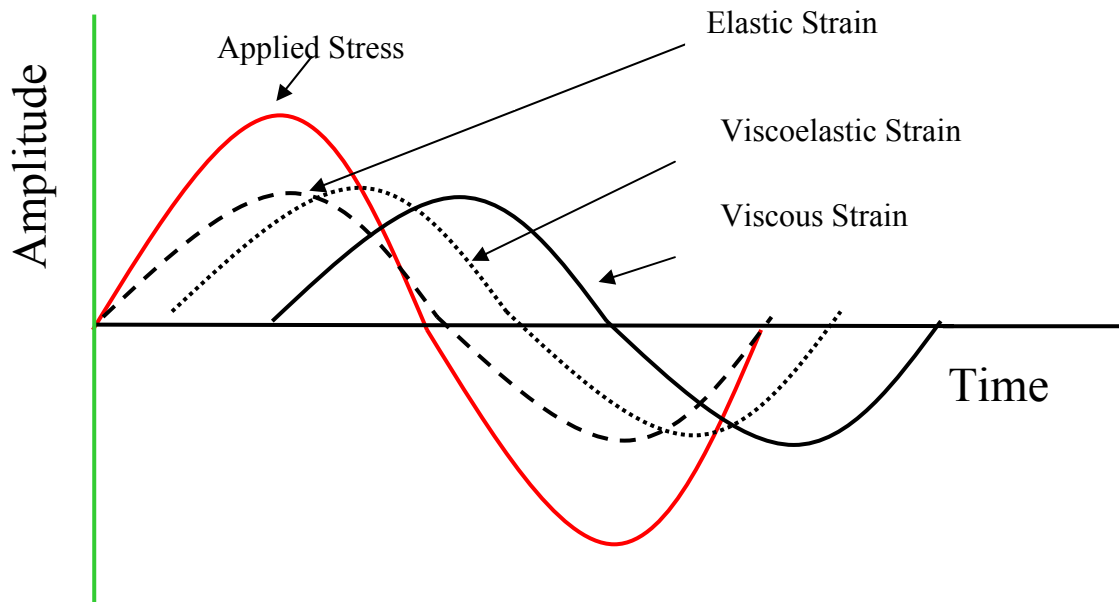


Figure A.1 – Variations in Stress and Strain with Time for Different Materials due to a Sinusoidal Load

For sinusoidal load, the applied stress and observed strain can be denoted by the following equations:

$$\sigma = \sigma_0 \sin \omega t \quad (\text{A-1})$$

and

$$\varepsilon = \varepsilon_0 \sin (\omega t - \phi) \quad (\text{A-2})$$

where:

σ = stress at time t

σ_0 = maximum applied stress

ω = angular velocity $2 \pi f$

f = frequency

ϕ = phase shift between stress and strain

ε = strain at time t

ε_0 = maximum observed strain

The dynamic (complex) modulus of the material, which is the ratio of the applied stress and the measured strain, can be defined as:

$$E^* = E_0 e^{j\phi} \quad (\text{A-3})$$

where E_0 is the ratio of σ_0 and ε_0 , j is the imaginary number and E^* is the dynamic modulus of the material. The absolute value of E^* is equal to E_0 and is termed as dynamic modulus and is typically used in the new mechanistic-empirical pavement design guide.

TEST PROCEDURE AND CALCULATIONS FOR DYNAMIC MODULUS TEST

The dynamic modulus test procedure is described in the test protocols submitted to the NCHRP in Project 1-37, Standard Test Method for Dynamic Modulus of Asphalt Concrete Mixtures (Witczak 2002). Specimens are manufactured by coring and sawing 4 in. (100 mm) diameter by 6 in. (150 mm) high test specimens from the middle portions of 6 in. (150 mm) by 6.5 in. (165 mm) high specimens molded using a Superpave gyratory compactor (SGC). The air void content of the cored and sawed specimens should be $7 \pm 1\%$.

The measurement setup for dynamic modulus (DM) must be rigid enough to withstand the applied cyclic loads. A hydraulic dynamic servo-valve closed-loop system manufactured by the Material and Test System (MTS) Corporation was used in this study. The schematic of the loading subsystem is shown in Figure A.2. The specimen is placed on the bottom end plate, which is tightly attached to a steel base plate through a stainless steel cylinder. To minimize the vibration of the specimen, all components should be precisely machined and custom matched.

Two linear variable differential transformers (LVDT's) are used to measure the deformation of the specimen. The positions of the LVDT's are also shown in Figure A.2. Two targets are fixed on one side of the specimen with a gauge length of 4 in. (102 mm) and two other targets are fixed exactly on the opposite side of the specimen. The strain experienced by the specimen is the average of the deformations on the two opposite sides of the specimen divided by the gauge length.

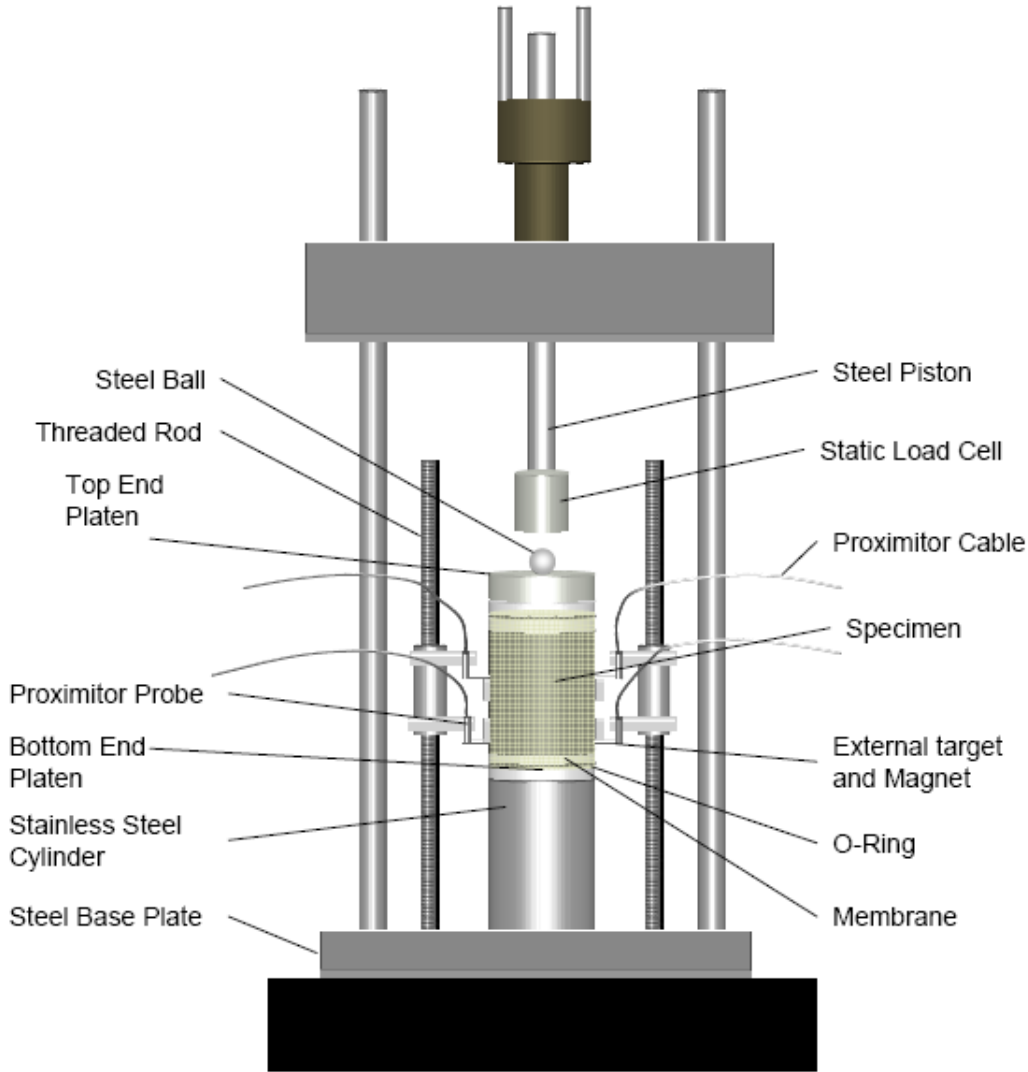


Figure A.2 – Sketch of Dynamic Modulus Test Setup

To measure the dynamic modulus, the test procedure and data reduction process proposed in NCRHP Project 1-37 (Witczak 2002) are adapted. Since that test procedure recommends that the strain within the specimen should be maintained within a range of $50 \mu\epsilon$ to $150 \mu\epsilon$, the applied load is adjusted for every frequency and temperature to achieve the appropriate strain level. A seating load is applied at each loading sequence in a manner that the minimum loads were never less than 5% of the maximum load.

TIME-TEMPERATURE RELATIONSHIP

The response of a viscoelastic material is dependent on the magnitude and period of loading. The temperature at the time of test also has an impact on the response. Testing is performed at various temperatures at similar loading times and a master curve is generated at a reference temperature by using time-temperature shift factors. The master

curve is developed based on the assumption that HMA is a thermo-rheologically simple material.

Ferry (1970) introduced the reduced variable method or viscoelastic corresponding states concept. Ferry found that the viscoelastic material tested at different temperatures exhibited responses which were similar to the responses exhibited when tested at different loading periods. This suggested that there is a relationship between the loading period and the test temperature behavior. The reduced variable method affords a simple function in separating the two main variables of time and temperature in the phenomenological functions representing the viscoelastic behavior.

A typical distribution of dynamic modulus with time and temperature of an HMA mixture is shown in Figure A.3. Each specimen is tested at five temperatures: 14, 40, 73, 100 and 130°F (-10, 4, 23, 38 and 54°C). The specimen is initially subjected to 200 conditioning cycles at 20 Hz at each temperature. After the initial conditioning, the specimen is subjected to 50 loading cycles at 10 Hz and 5 Hz. In the end, the specimen is subjected to 7 loading cycles at frequencies of 10, 5, 2 and 1 Hz. This sequence of testing results in a total of 50 dynamic modulus tests on each specimen. To minimize the potential internal damage to the specimen, tests are performed from the lower to higher temperatures and from the higher to lower frequencies. After each test, the data is analyzed to ensure that the strains are between 50 $\mu\epsilon$ and 150 $\mu\epsilon$ and that the displacements of the opposite sides of the specimen are within 15% of one another. If the difference exceeds 15%, the specimen is discarded and a new specimen is tested. To estimate the dynamic modulus, the average amplitude of the load and the strain over the last six loading cycles are recorded. The dynamic modulus is estimated using the ratio of peak stress and peak strain.

Assuming that the time-temperature superposition principle is valid, the moduli from each temperature are shifted horizontally to produce a master curve at a reference temperature. The typical shift factor plot is shown in Figure A.4. The shifted master curve at 73°F (23°C) is shown in Figure A.5. As expected, the dynamic moduli for the higher temperatures (130°F and 100°F, or 54°C and 38°C) have to be shifted to the left while the moduli for the lower temperatures (40°F and 14°F, or 4°C and -10°C) have to be shifted to the right to generate the master curve. The curve fitting to the master curve (Figure A.6) is done by using a method developed by Pellinen and Witzak (2002). That method consists of fitting a sigmoidal curve described in Equation A-4 to the measured dynamic modulus test data using nonlinear least-squares regression techniques.

$$\text{Log} (E^*) = \delta + \frac{\alpha}{1 + e^{[\beta + \gamma \log(T_r)]}} \quad (\text{A-4})$$

where:

E^* = Dynamic modulus

T_r = Reduced time

δ = Minimum value of dynamic modulus

$\delta + \alpha$ = Maximum value of dynamic modulus

β, γ = Sigmoidal function shape parameter.

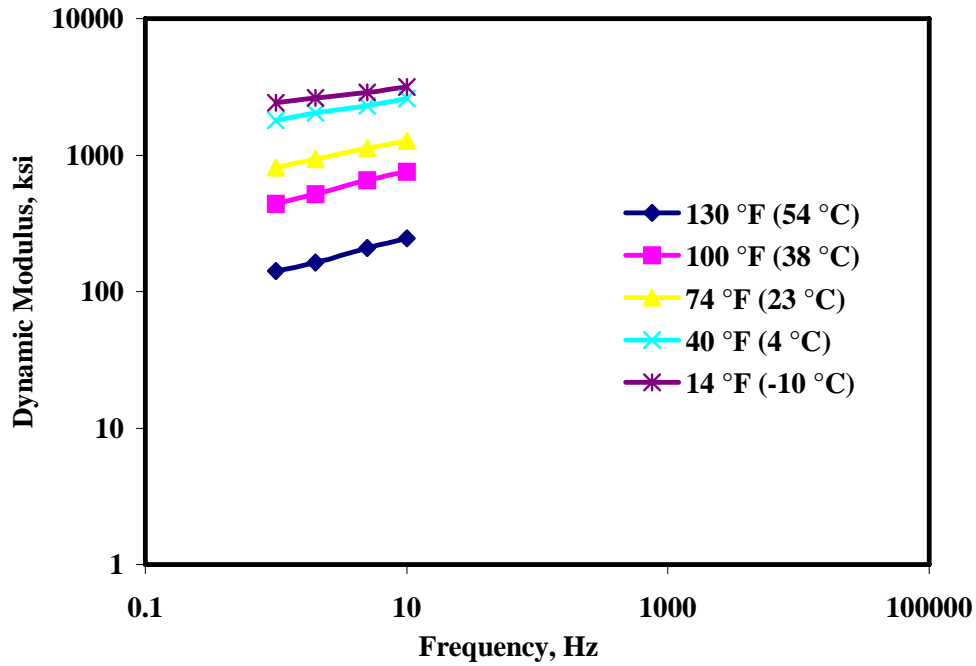


Figure A.3 – Typical Dynamic Modulus versus Frequency Plot at Different Temperatures

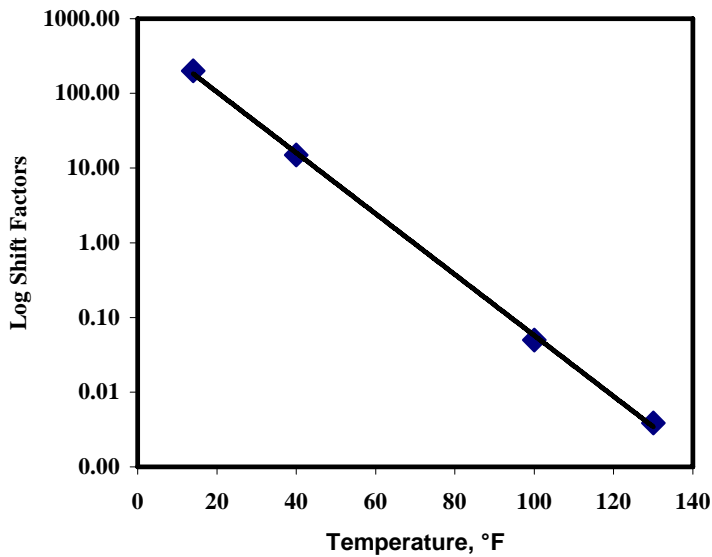


Figure A.4 – Typical Log Shift Factor versus Temperature Plot

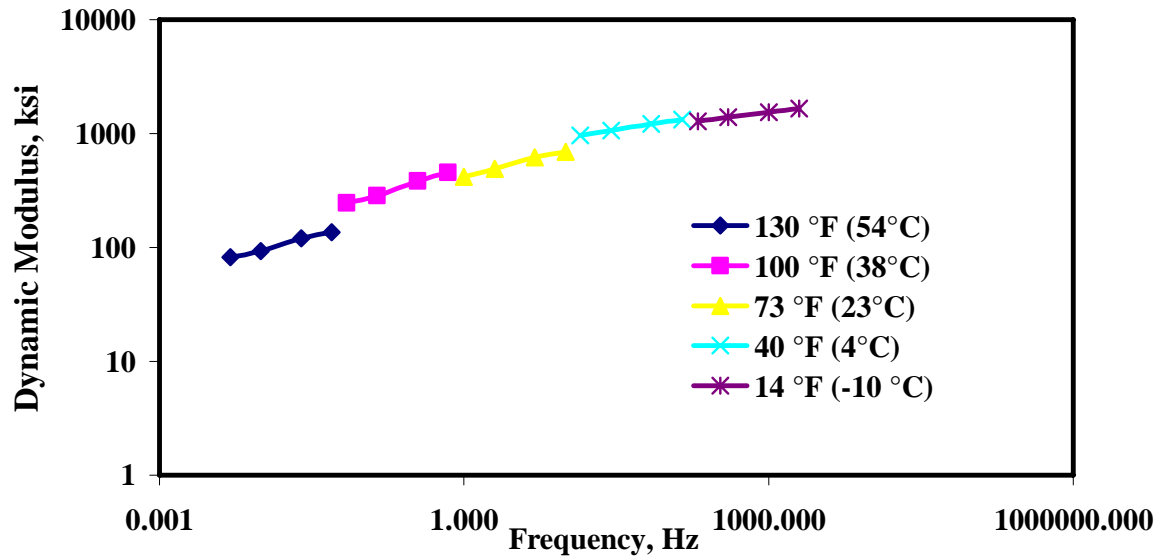


Figure A.5 – Shifted Dynamic Modulus Curve

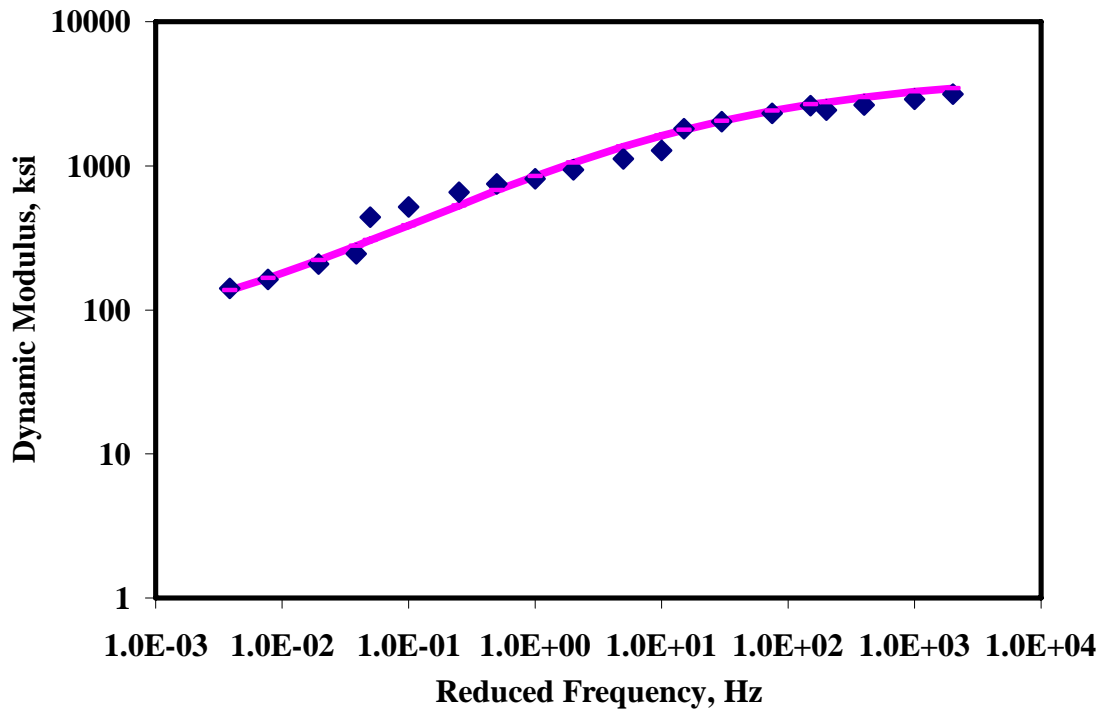


Figure A.6 – Typical Master Curve with Curve Fitting

APPENDIX B. INTRODUCTION TO WAVE PROPAGATION THEORY

This appendix introduces the principle of wave propagation and clarifies the relationships between wave velocities and moduli.

For engineering purposes, profiles of most pavement sections can be reasonably approximated by a layered half-space. With this approximation, the profiles are assumed to be homogeneous and to extend to infinity in two horizontal directions. They are assumed to be heterogeneous in the vertical direction, often modeled by a number of layers with constant properties within each layer. In addition, it is assumed that the material in each layer is elastic and isotropic.

SEISMIC BODY WAVES

Wave motion created by a disturbance within an ideal whole-space can be described by two kinds of waves: compression waves and shear waves. Collectively, these waves are called body waves, as they travel within the body of the medium. Compression and shear waves can be distinguished by the direction of particle motion relative to the direction of wave propagation (see Figure B-1).

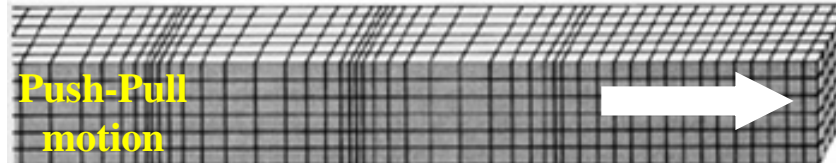
Compression waves (also called dilatational waves, primary waves, or P-waves) exhibit a push-pull motion. As a result, wave propagation and particle motion are in the same direction. Compression waves travel faster than the other types of waves, and therefore appear first in a direct travel-time record.

Shear waves (also called distortional waves, secondary waves, or S-waves) generate a shearing motion, causing particle motion to occur perpendicular to the direction of wave propagation. Shear waves can be polarized. If the directions of propagation and particle motion are contained in a vertical plane, the wave is "vertically polarized." This wave is called an SV-wave. However, if the direction of particle motion is perpendicular to a vertical plane containing the direction of propagation, the wave is "horizontally polarized." This wave is termed a SH-wave. Shear waves travel more slowly than P-waves and thus appear as the second major wave type in a direct travel-time record.

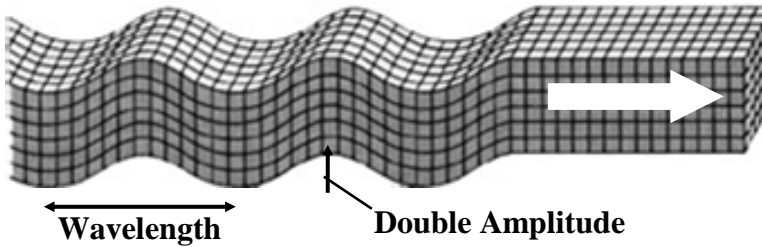
SEISMIC SURFACE WAVES

In a half-space, other types of waves occur in addition to body waves. These waves are called surface waves. Many different types of surface waves have been identified and described. The two major types are Rayleigh waves and Love waves.

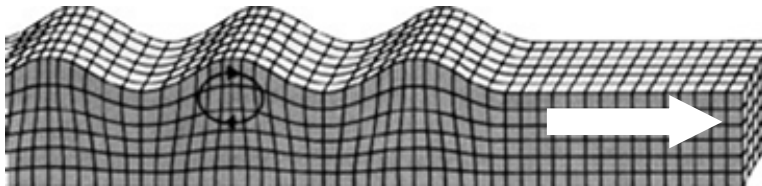
Surface waves propagate near the surface of a half-space. Rayleigh waves (R-waves) propagate at a speed of approximately 90 percent of S-waves. Particle motion associated



Compression Wave Motion



Shear Vertical Wave Motion



Particle motion has both vertical and horizontal components

Rayleigh Wave Motion

Figure B.1 – Description of Different Waves

with R-waves is composed of both vertical and horizontal components, that when combined, form a retrograde ellipse close to the surface. However, with increasing depth, R-wave particle motion changes to a pure vertical and, finally, to a prograde ellipse. The amplitude of motion attenuates quite rapidly with depth. At a depth equal to about 1.5 times the wavelength, the vertical component of the amplitude is about 10 percent of that at the ground surface.

Particle motion associated with Love waves is confined to a horizontal plane and is perpendicular to the direction of wave propagation. This type of surface wave can exist only when low-velocity layers are underlain by higher velocity layers, because the waves are generated by total multiple reflections between the top and bottom surfaces of the low-velocity layer. As such, Love waves are not generated in pavement sections.

The propagation of body waves (shear and compression waves) and surface waves (Rayleigh waves) are away from a vertically vibrating circular source at the surface of a homogeneous, isotropic, elastic half-space. Miller and Pursey (1955) found that approximately 67 percent of the input energy propagates in the form of R-waves. Shear and compression waves carry 26 and 7 percent of the energy, respectively. Compression and shear waves propagate radially outward from the source. R-waves propagate along

a cylindrical wave front near the surface. Although, body waves travel faster than surface waves, body waves attenuate in proportion to $1/r^2$, where r is the distance from the source. Surface wave amplitude decreases in proportion to $1/r^{0.5}$.

SEISMIC WAVE VELOCITIES

Seismic wave velocity is defined as the speed at which a wave advances in the medium. Wave velocity is a direct indication of the stiffness of a material; higher wave velocities are associated with higher stiffness. By employing elastic theory, compression wave velocity can be defined as

$$V_p = [(\lambda + 2G)/\rho]^{0.5} \quad (\text{B.1})$$

where

V_p = compression wave velocity,
 λ = Lamé's constant,
 G = shear modulus, and
 ρ = mass density.

Shear wave velocity, V_s , is equal to

$$V_s = (G/\rho)^{0.5} \quad (\text{B.2})$$

Compression and shear wave velocities are theoretically interrelated by Poisson's ratio

$$V_p/V_s = [(1 - \nu)/(0.5 - \nu)]^{0.5} \quad (\text{B.3})$$

where ν is the Poisson's ratio. For a constant shear wave velocity, compression wave velocity increases with an increase in Poisson's ratio. For a ν of 0.0, the ratio of V_p to V_s is equal to $\sqrt{2}$; for a ν of 0.5 (an incompressible material), this ratio goes to infinity.

For a layer with constant properties, R-wave velocity and shear wave velocity are also related by Poisson's ratio. Although, the ratio of R-wave to S-wave velocities increases as Poisson's ratio increases, the change in this ratio is not significant. For Poisson's ratio of 0.0 and 0.5, this ratio changes from approximately 0.86 to 0.95, respectively. Therefore, it can be assumed that the ratio is equal to 0.90 without introducing an error larger than about 5 percent.

Equation B.3 can be rewritten as

$$\nu = [0.5(V_p/V_s)^2 - 1]/[(V_p/V_s)^2 - 1] \quad (\text{B.4})$$

This equation can then be used to calculate Poisson's ratio once V_s and V_p are known.

ELASTIC CONSTANTS

Propagation velocities per se have limited use in engineering applications. In pavement engineering, Young's moduli of the different layers should be measured. Therefore, calculating the elastic moduli from propagation velocities is important.

Shear wave velocity, V_s , is used to calculate the shear modulus, G , by

$$G = \rho V_s^2 \quad (\text{B.5})$$

in which ρ is the mass density. Mass density is equal to γ_t/g , where γ_t is the total unit weight of the material, and g is gravitational acceleration. If Poisson's ratio (or compression wave velocity) is known, other moduli can be calculated for a given V_s .

Young's and shear moduli are related by

$$E = 2G(1 + \nu) \quad (\text{B.6})$$

or

$$E = 2\rho V_s^2(1 + \nu) \quad (\text{B.7})$$

In a medium where the material is restricted from deformation in two lateral directions, the ratio of axial stress to axial strain is called constrained modulus. Constrained modulus, M , is defined as

$$M = \rho V_p^2 \quad (\text{B.8})$$

or in terms of Young's modulus and Poisson's ratio

$$M = [(1 - \nu)E]/[(1 + \nu)(1 - 2\nu)] \quad (\text{B.9})$$

The Bulk modulus, B , is the ratio of hydrostatic stress to volumetric strain and can be determined by

$$B = M - (4/3)G \quad (\text{B.10})$$

APPENDIX C. VARIATION IN MODULUS WITH AIR VOIDS FOR ALL SITES

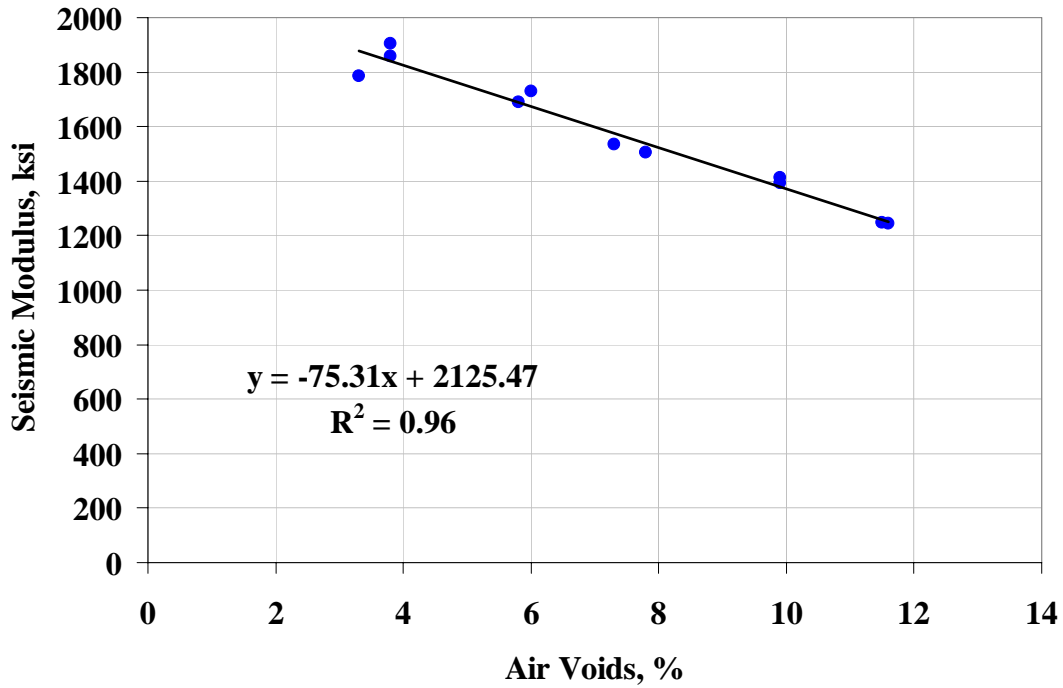


Figure C.1 – Variation in Modulus with Air Voids for Buckeye (Site 1)

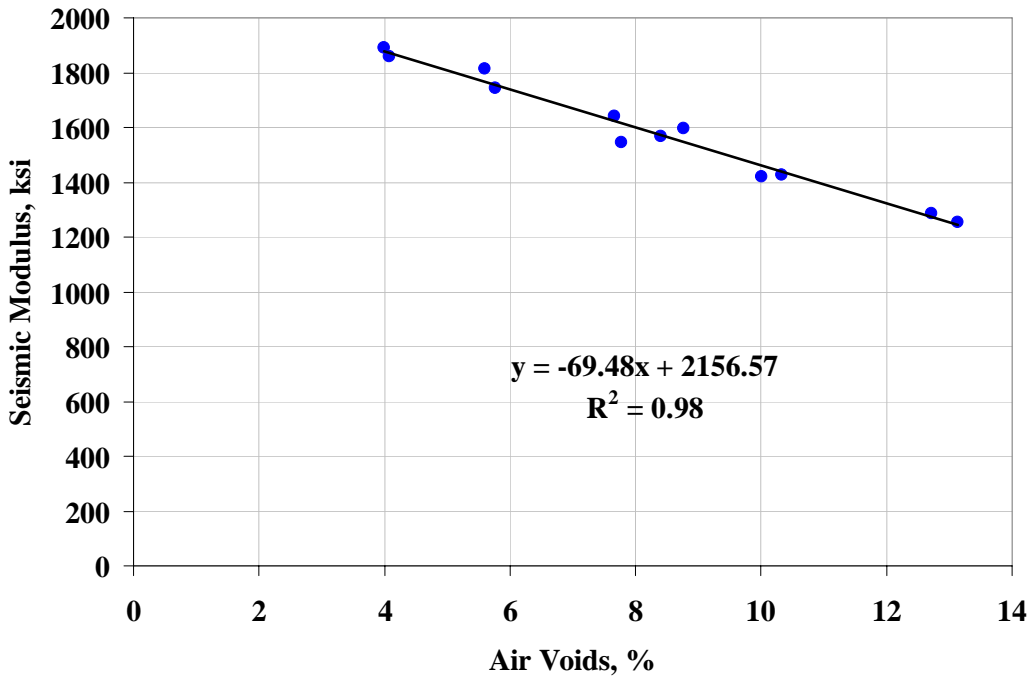


Figure C.2 – Variation in Modulus with Air Voids for Show Low (Site 2)

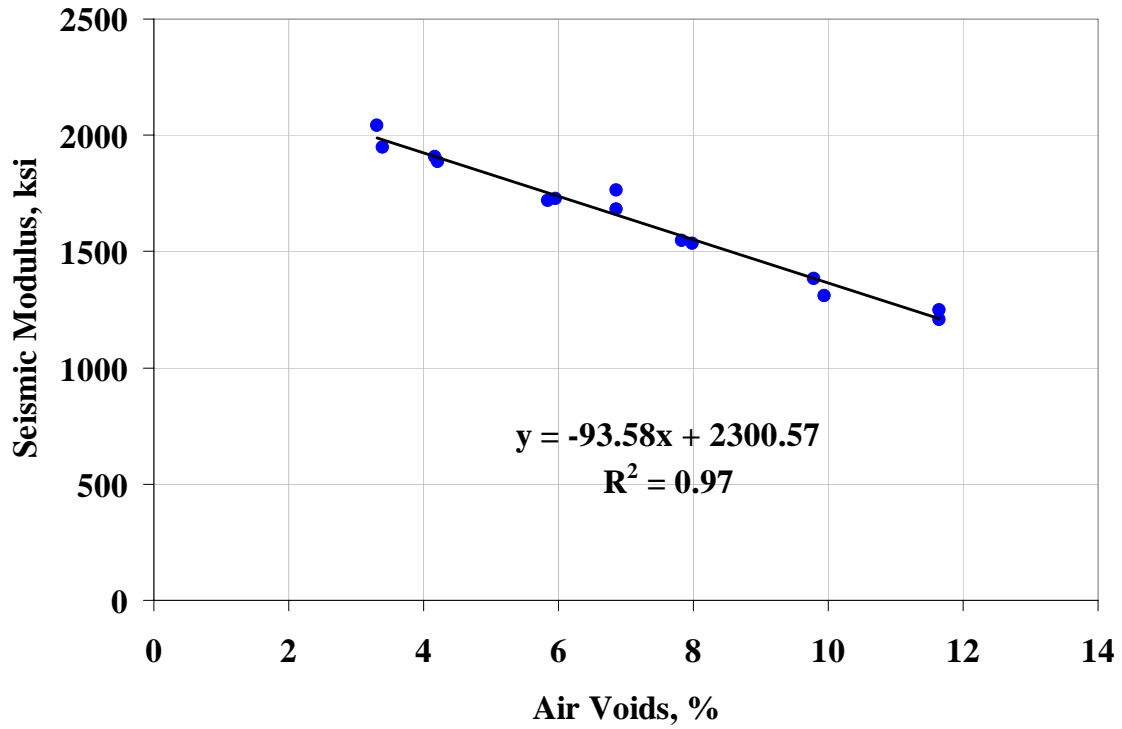


Figure C.3 – Variation in Modulus with Air Voids for Holbrook (Site 3)

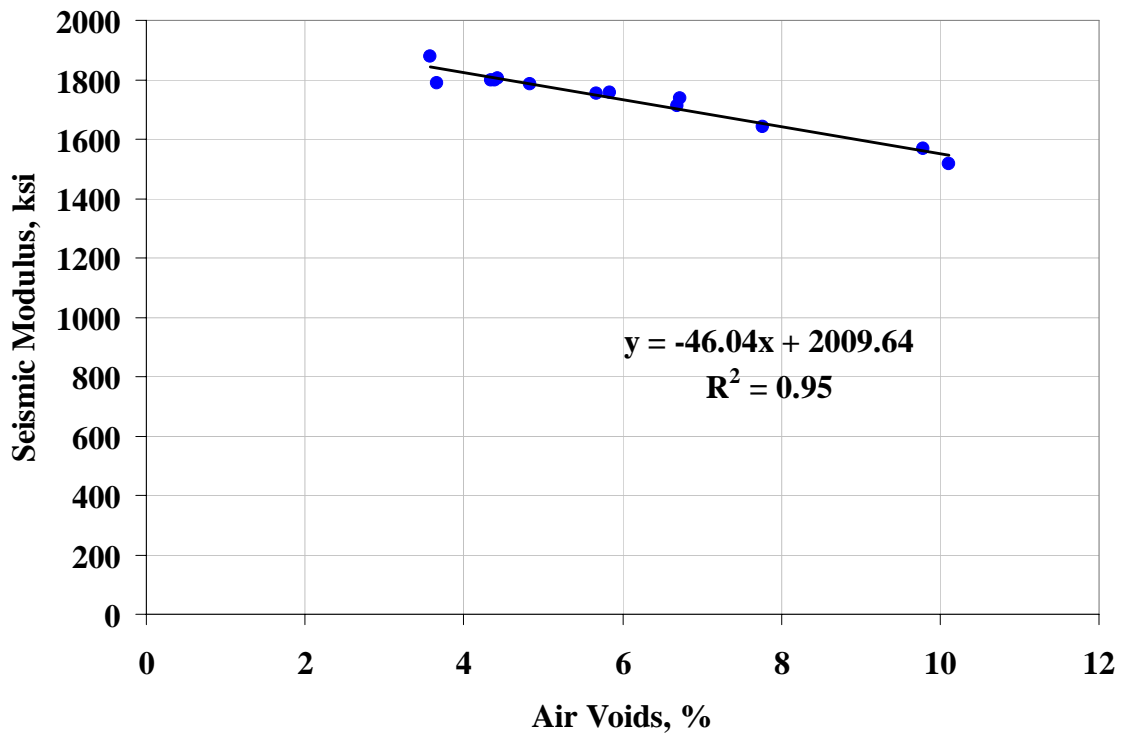


Figure C.4 – Variation in Modulus with Air Voids for Burro Creek (Site 4)

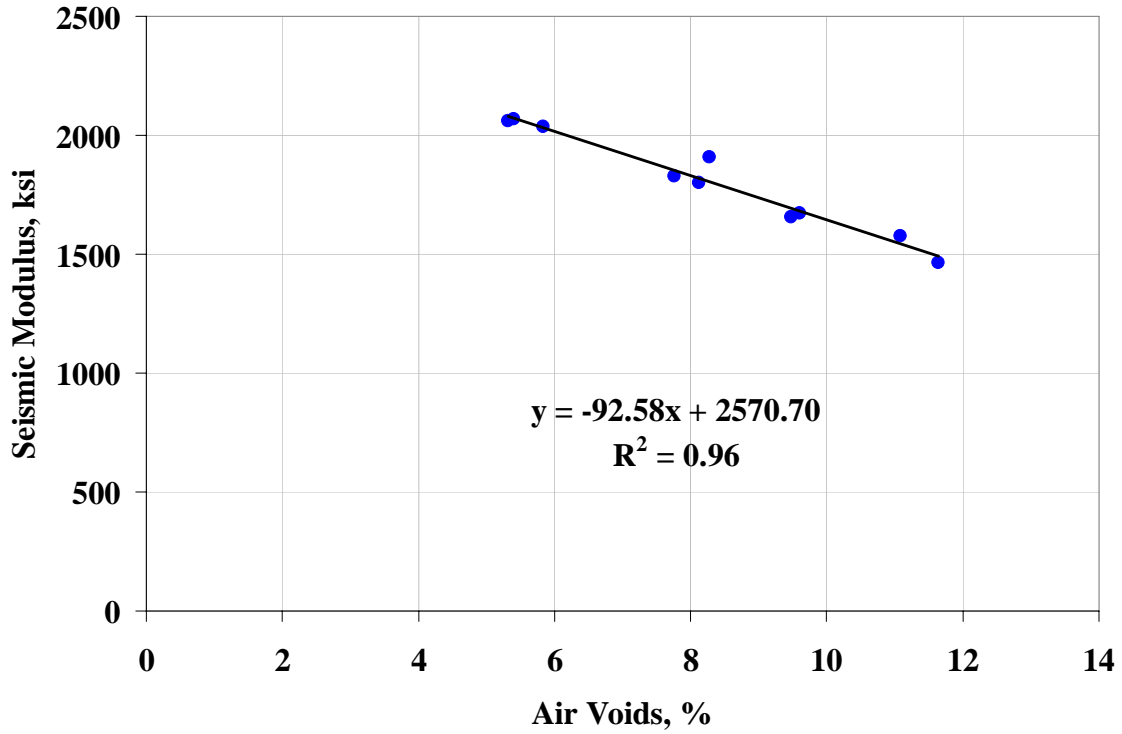


Figure C.5 – Variation in Modulus with Air Voids for Cordes JCT (Site 5)

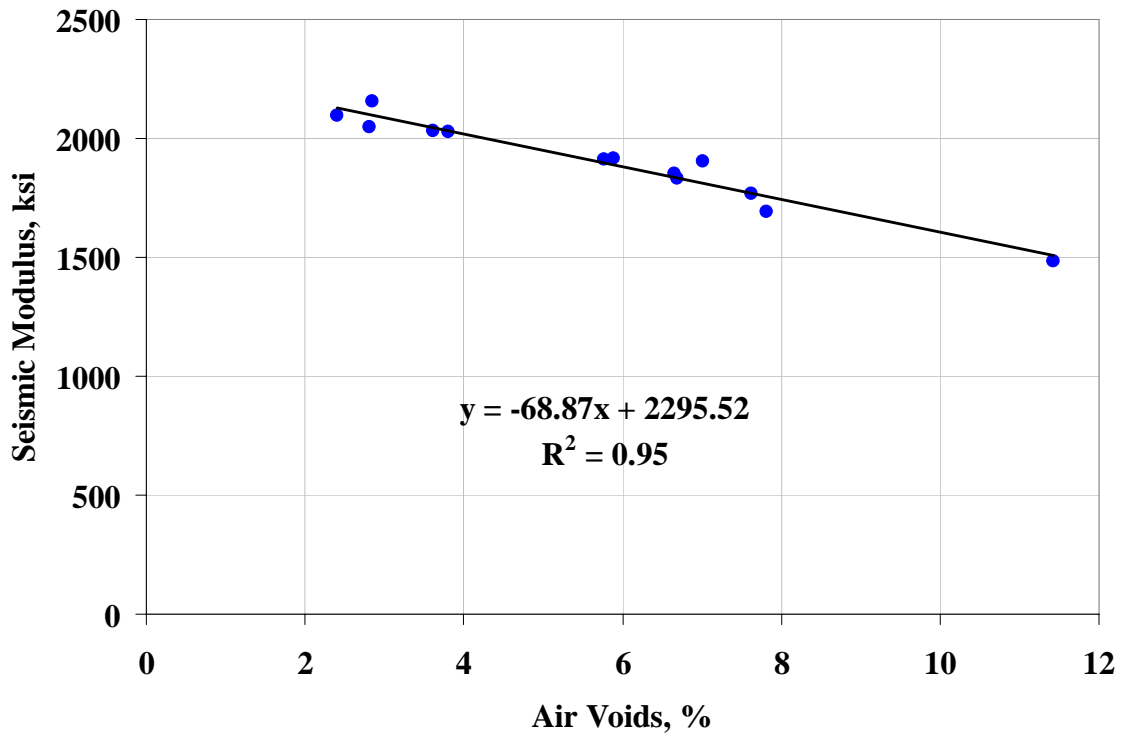


Figure C.6 – Variation in Modulus with Air Voids for Roosevelt (Site 6)

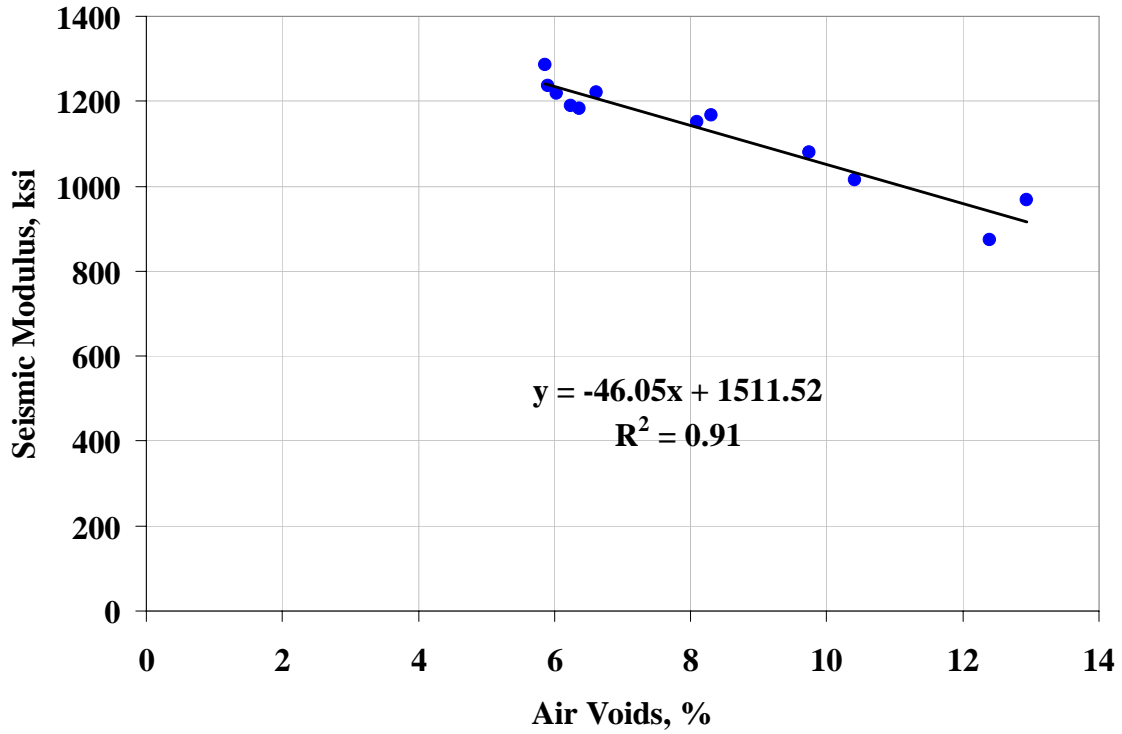


Figure C.7 – Variation in Modulus with Air Voids for Safford (Site 7)

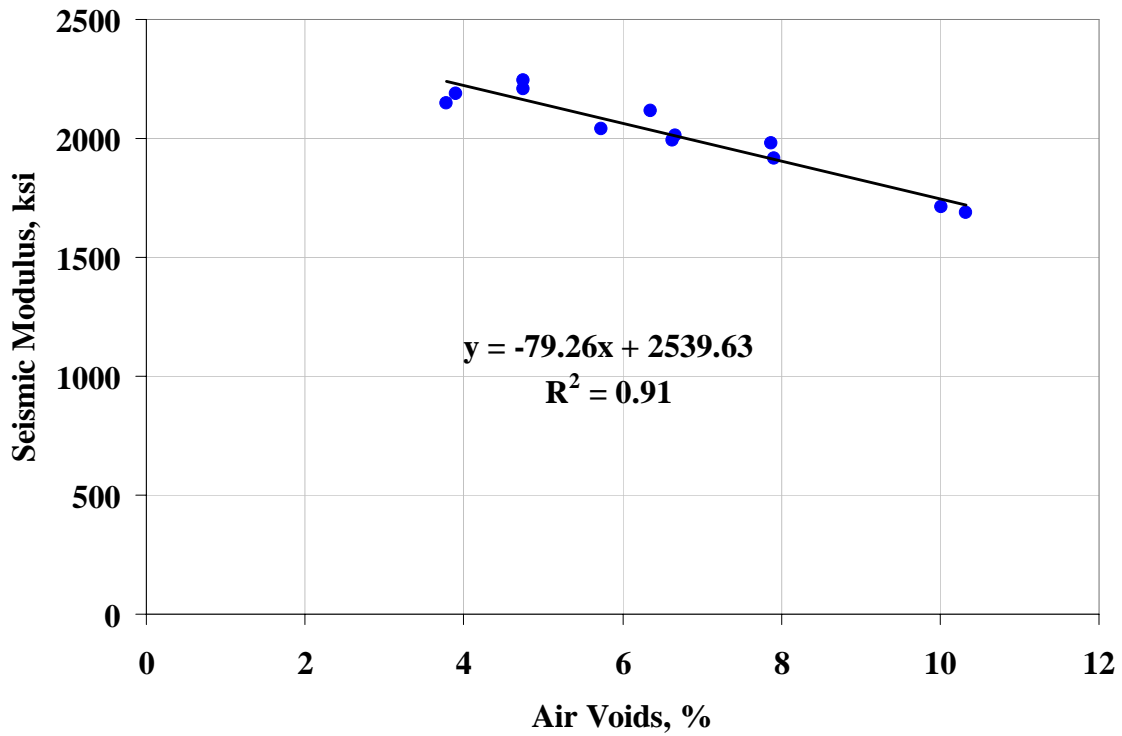


Figure C.8 – Variation in Modulus with Air Voids for Holbrook B (Site 8)

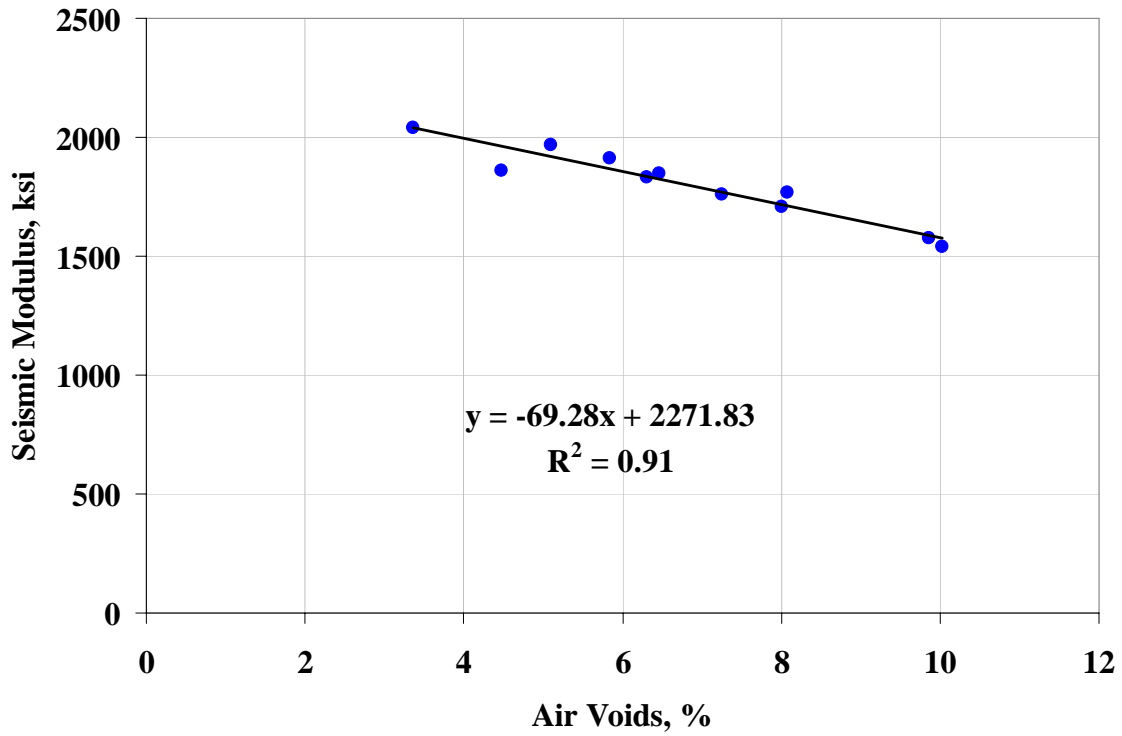


Figure C.9 – Variation in Modulus with Air Voids for Payson (Site 9)

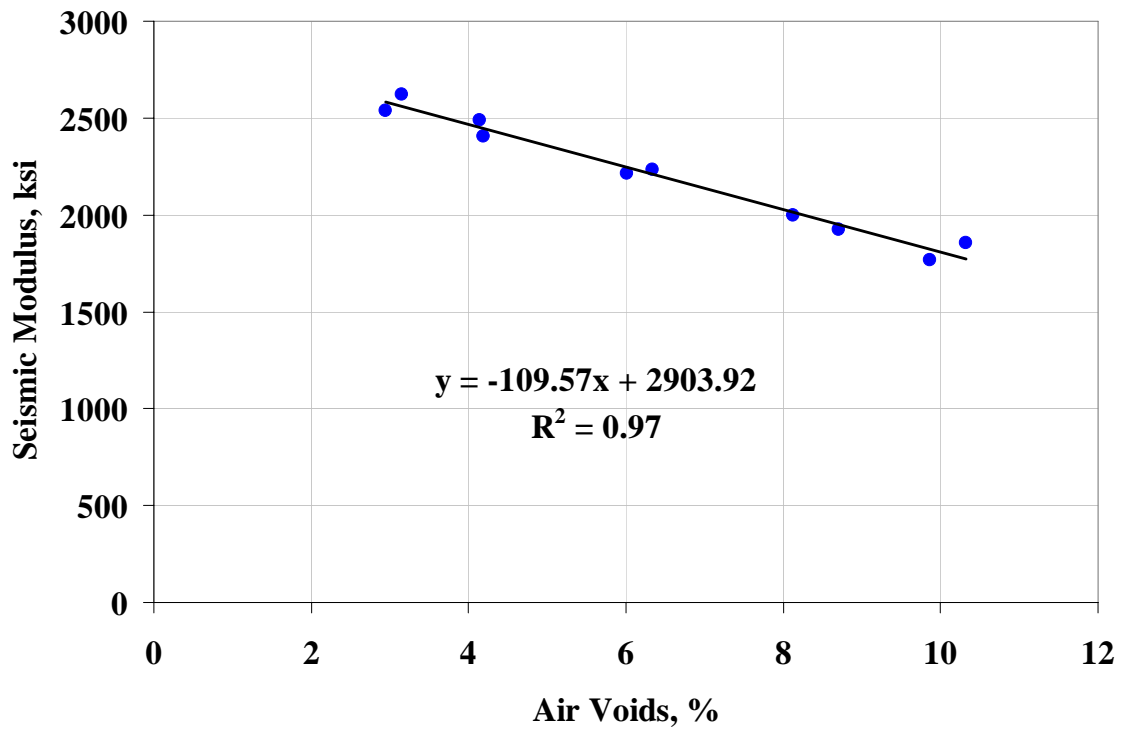


Figure C.10 – Variation in Modulus with Air Voids for Tucson (Site 10)

APPENDIX D. VARIATION IN MODULUS WITH TEMPERATURE FOR ALL SITES

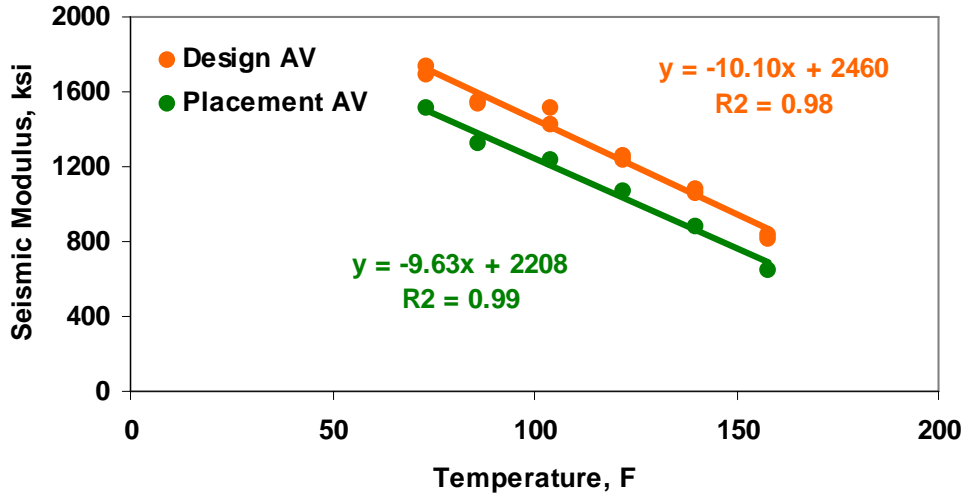


Figure D.1 – Variation in Modulus with Temperature for Buckeye (Site 1)

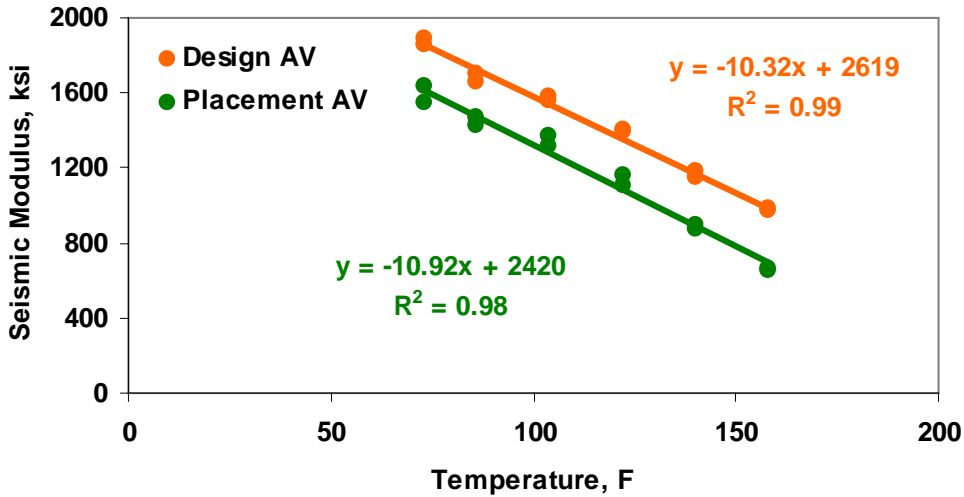


Figure D.2 – Variation in Modulus with Temperature for Show Low (Site 2)

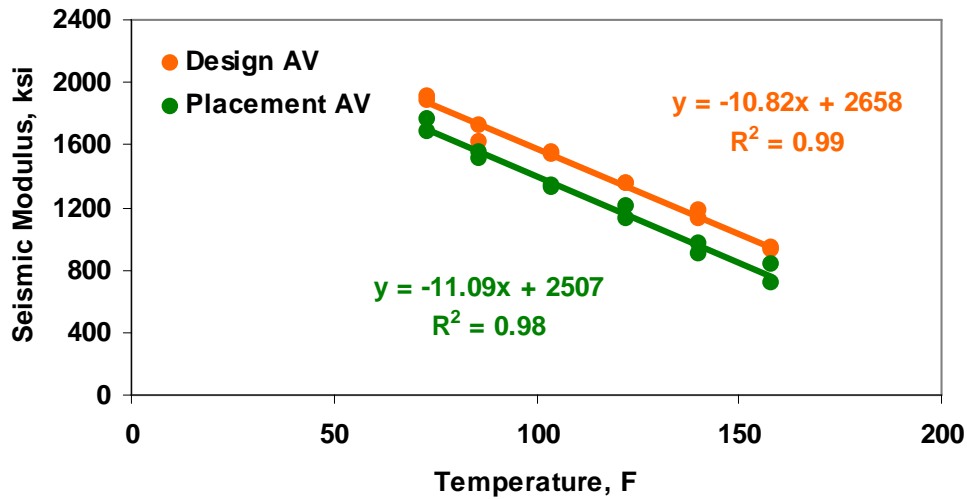


Figure D.3 – Variation in Modulus with Temperature for Holbrook (Site 3)

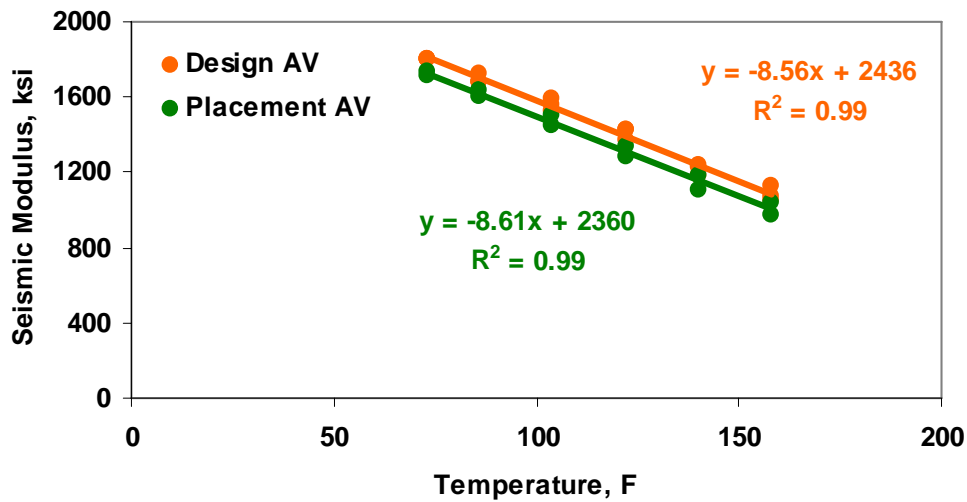


Figure D.4 – Variation in Modulus with Temperature for Burro Creek (Site 4)

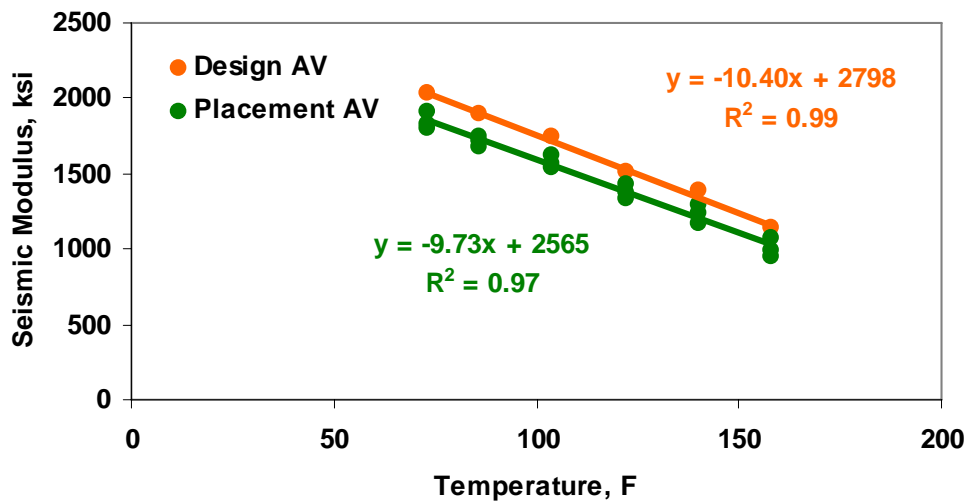


Figure D.5 – Variation in Modulus with Temperature for Cordes JCT (Site 5)

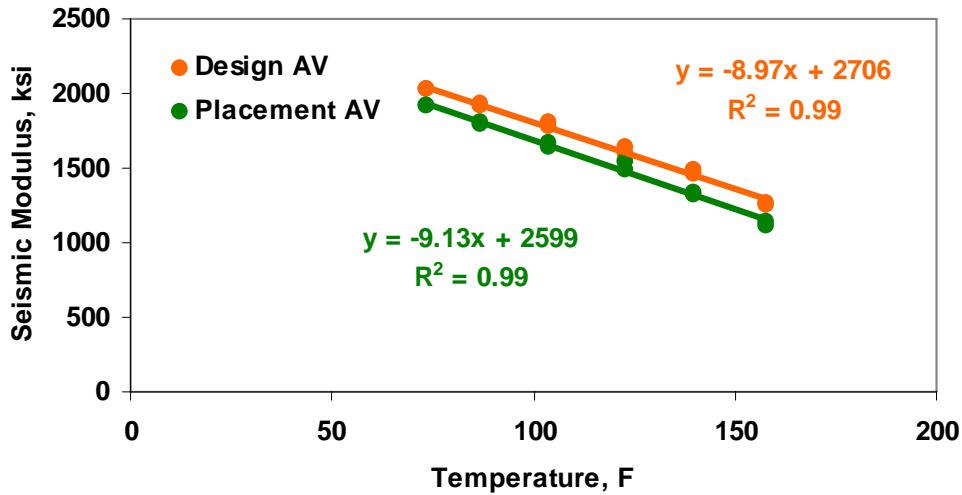


Figure D.6 – Variation in Modulus with Temperature for Roosevelt (Site 6)

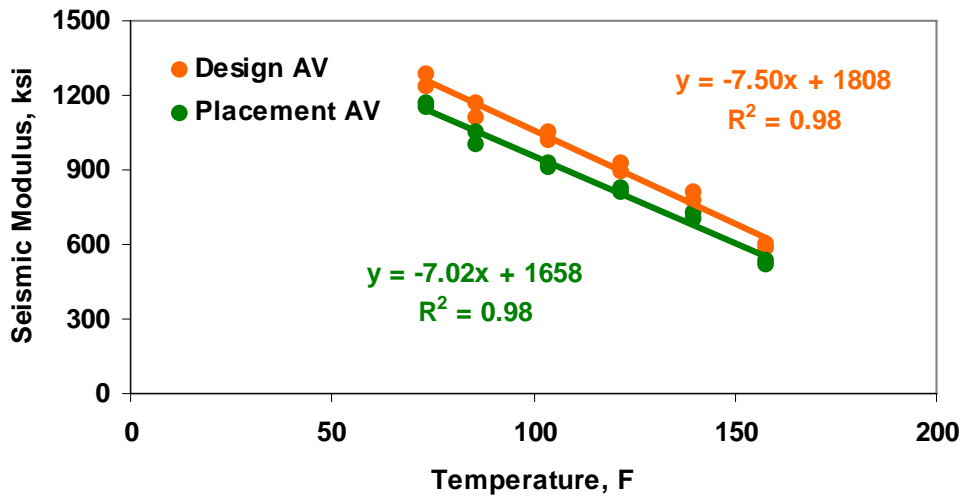


Figure D.7 – Variation in Modulus with Temperature for Safford (Site 7)

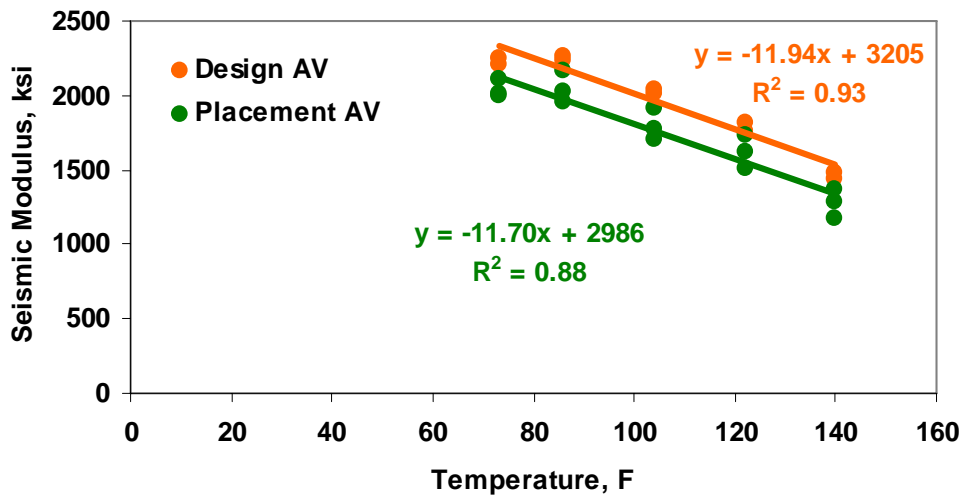


Figure D.8 – Variation in Modulus with Temperature for Holbrook B (Site 9)

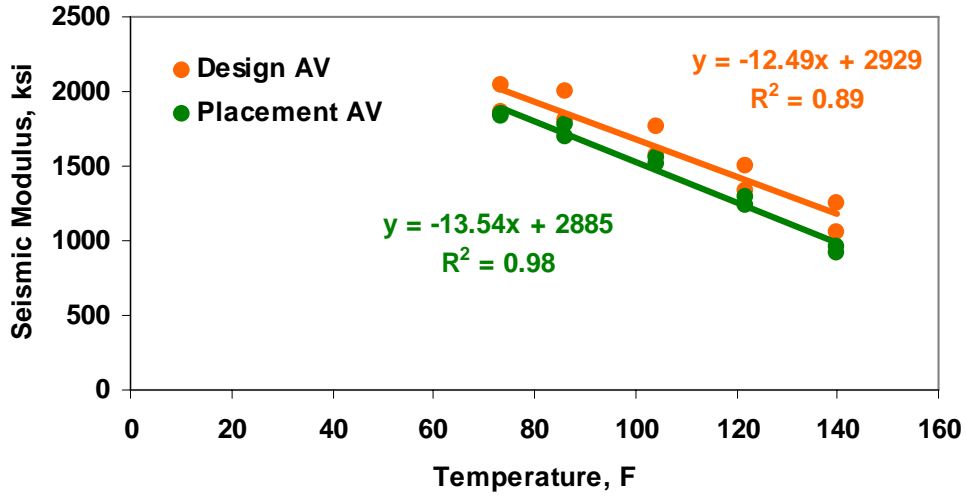


Figure D.9 – Variation in Modulus with Temperature for Payson (Site 9)

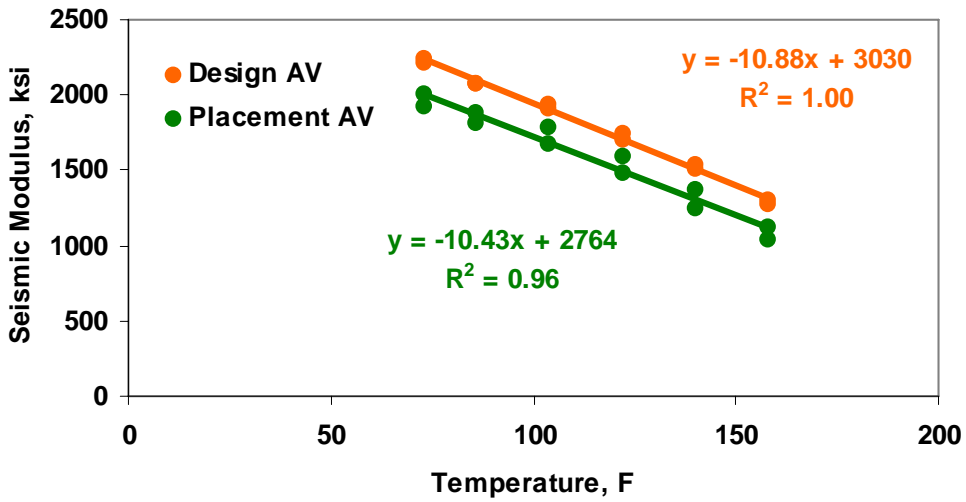


Figure D.10 – Variation in Modulus with Temperature for Tucson (Site 10)

APPENDIX E. MASTER CURVES FOR ALL SITES

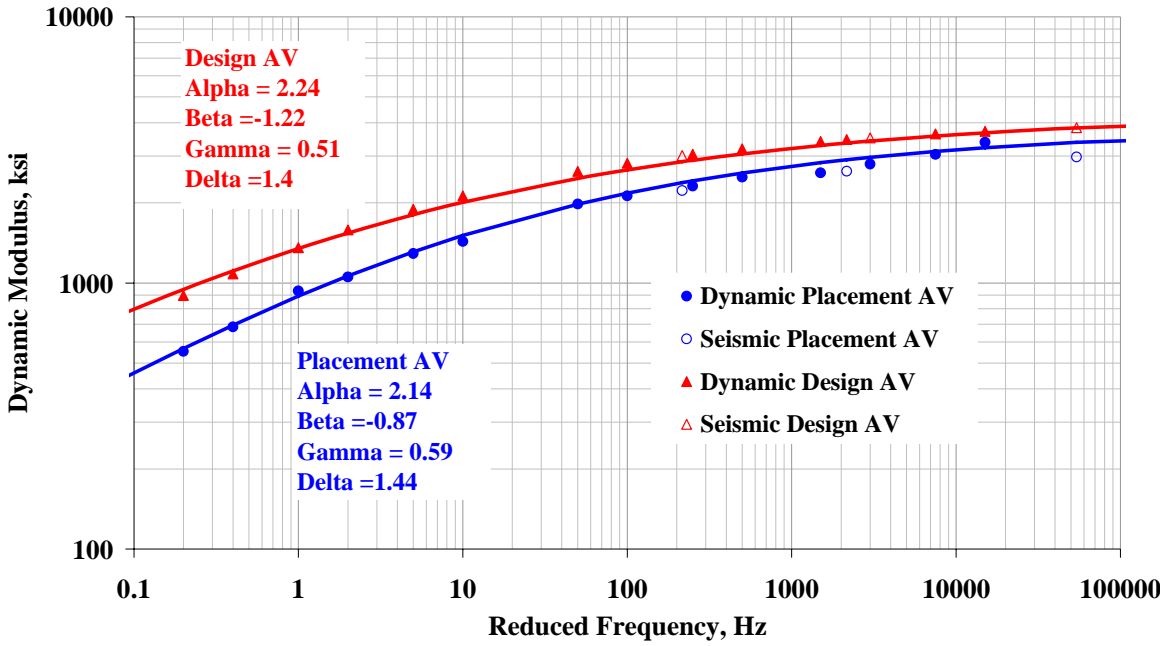


Figure E.1 – Master Curves for Buckeye Mix (Site 1)

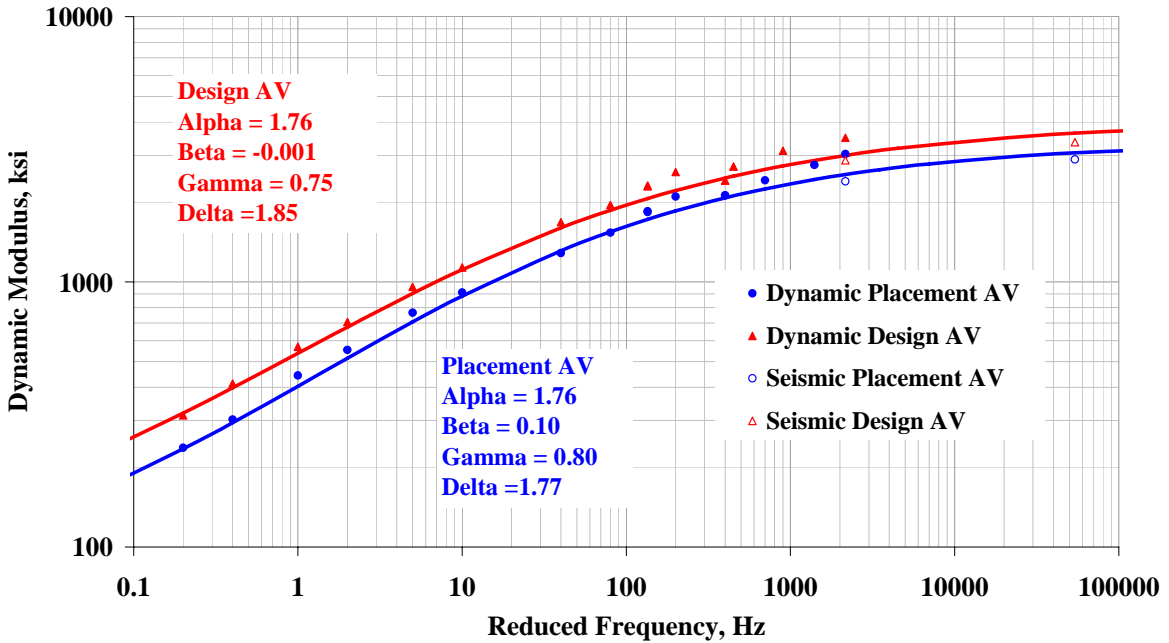


Figure E.2 – Master Curves for Show Low Mix (Site 2)

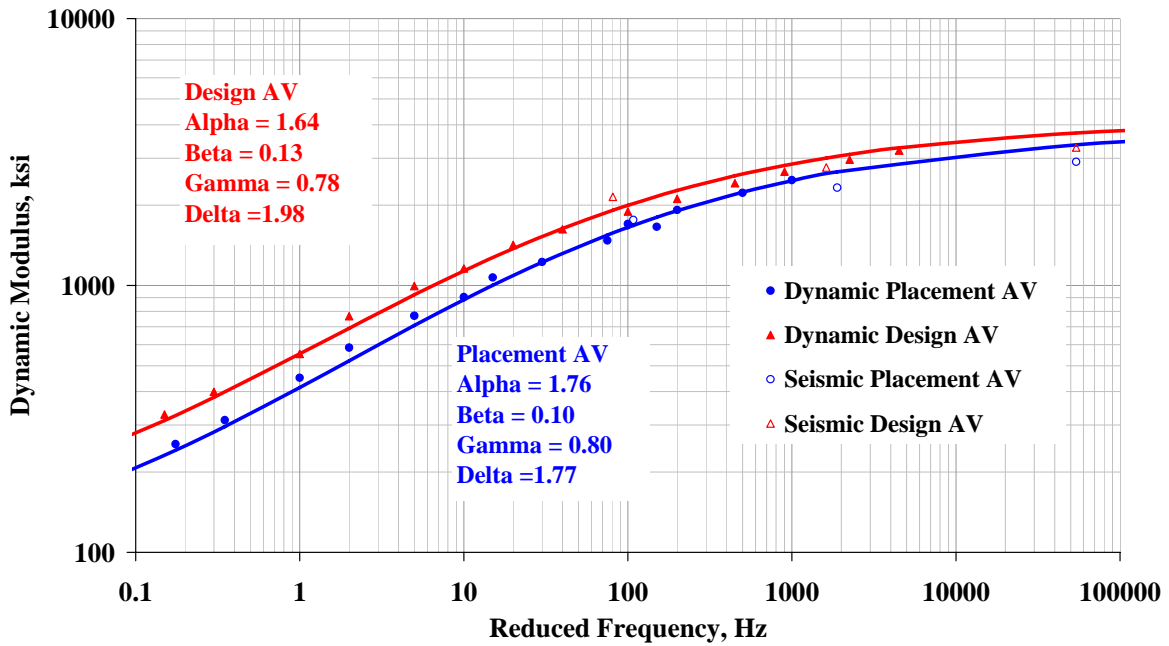


Figure E.3 – Master Curves for Holbrook Mix (Site 3)

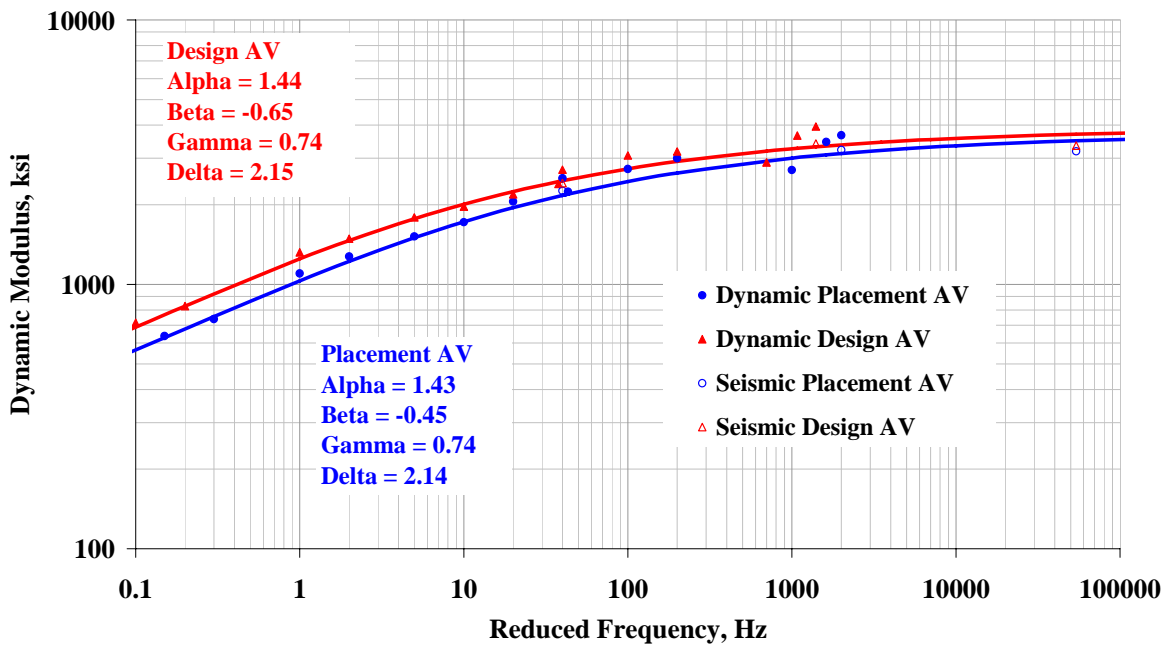


Figure E.4 – Master Curves for Burro Creek Mix (Site 4)

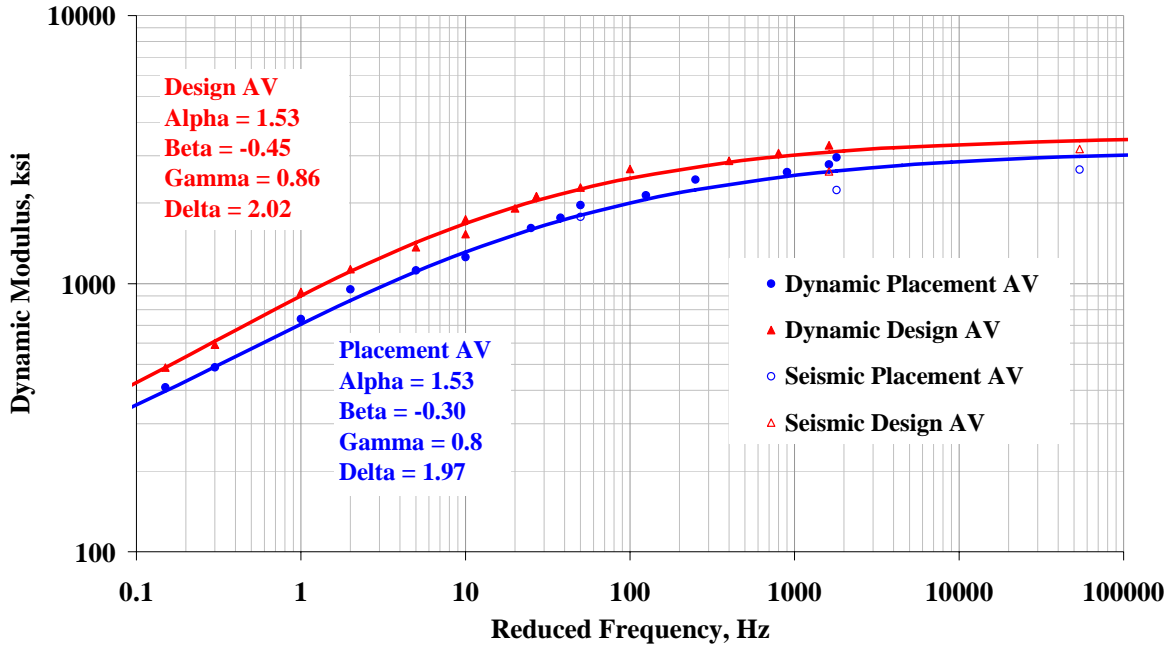


Figure E.5 – Master Curves for Cordes JCT Mix (Site 5)

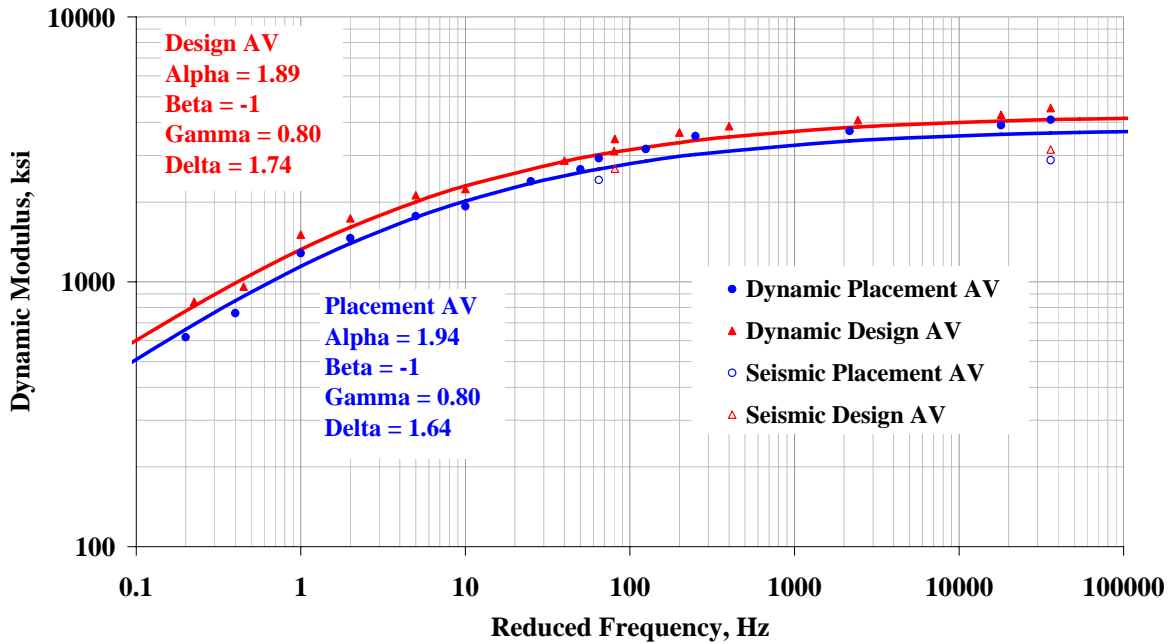


Figure E.6 – Master Curves for Roosevelt Mix (Site 6)

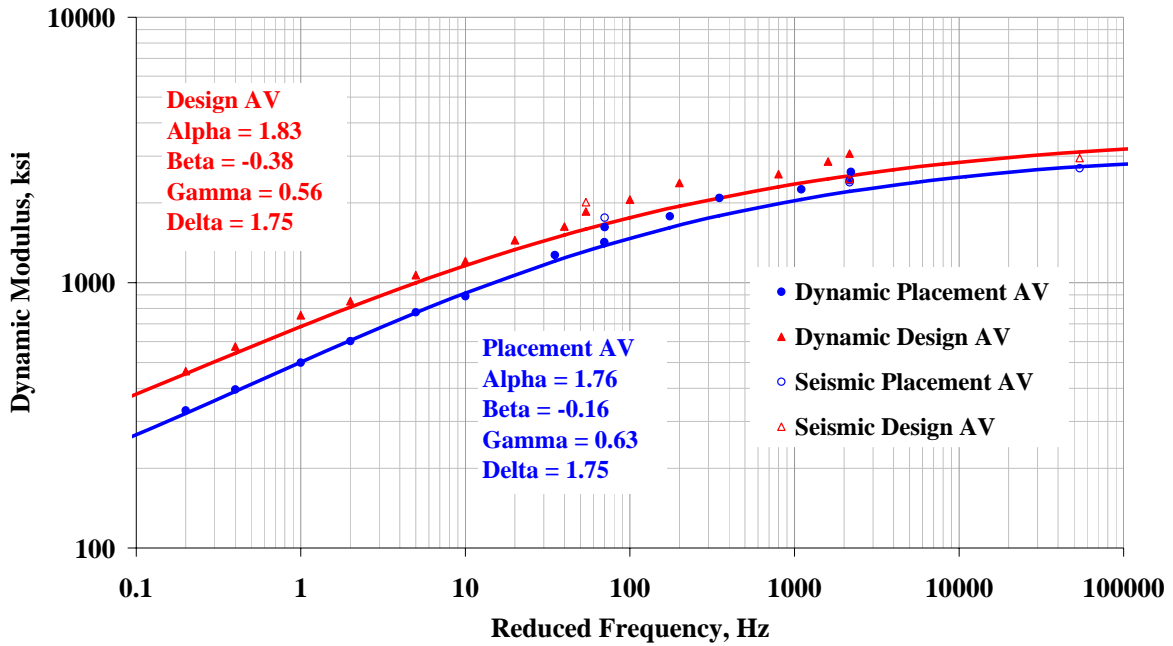


Figure E.7 – Master Curves for Safford Mix (Site 7)

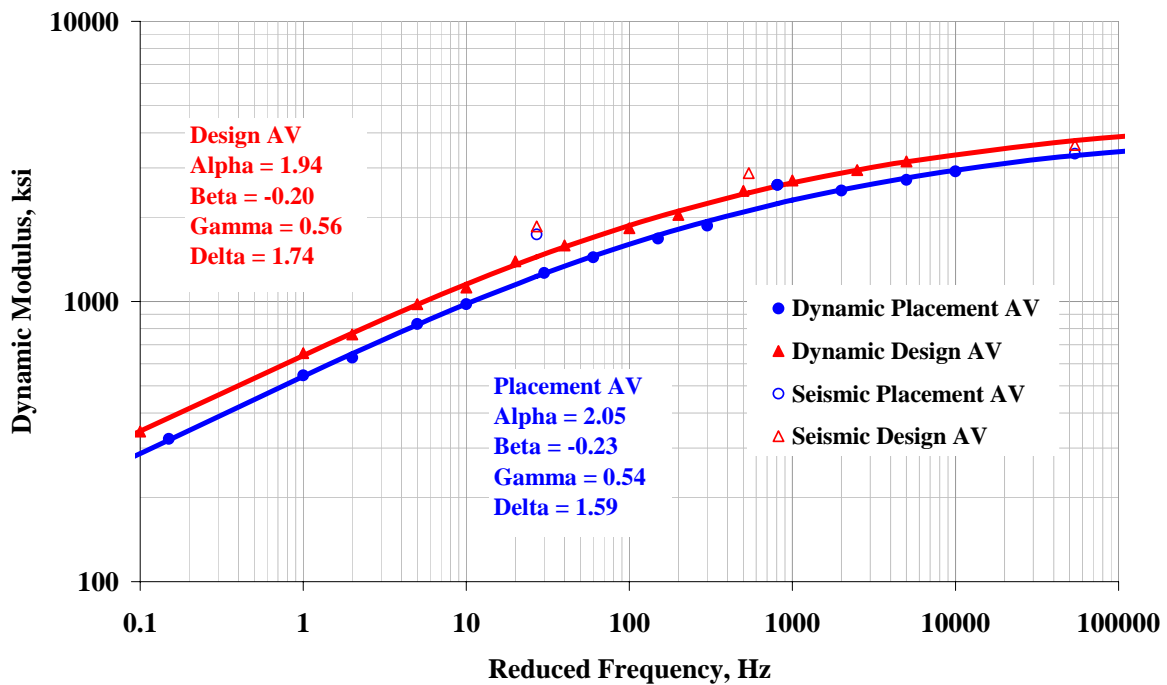


Figure E.8 – Master Curves for Holbrook B Mix (Site 8)

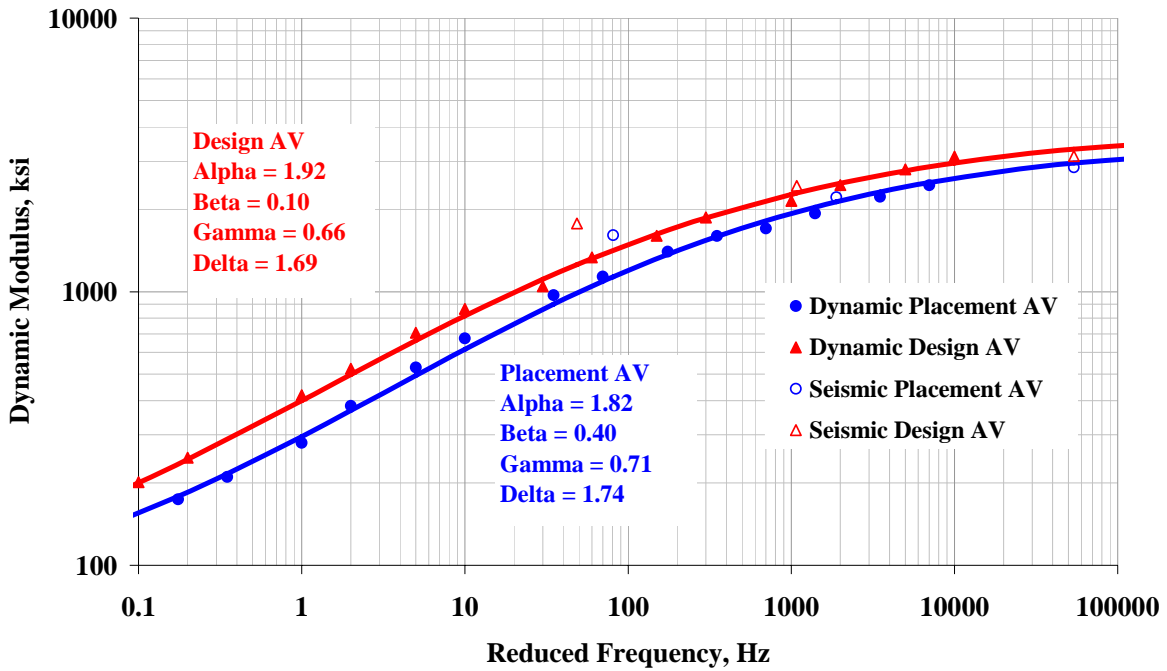


Figure E.9 – Master Curves for Payson Mix (Site 9)

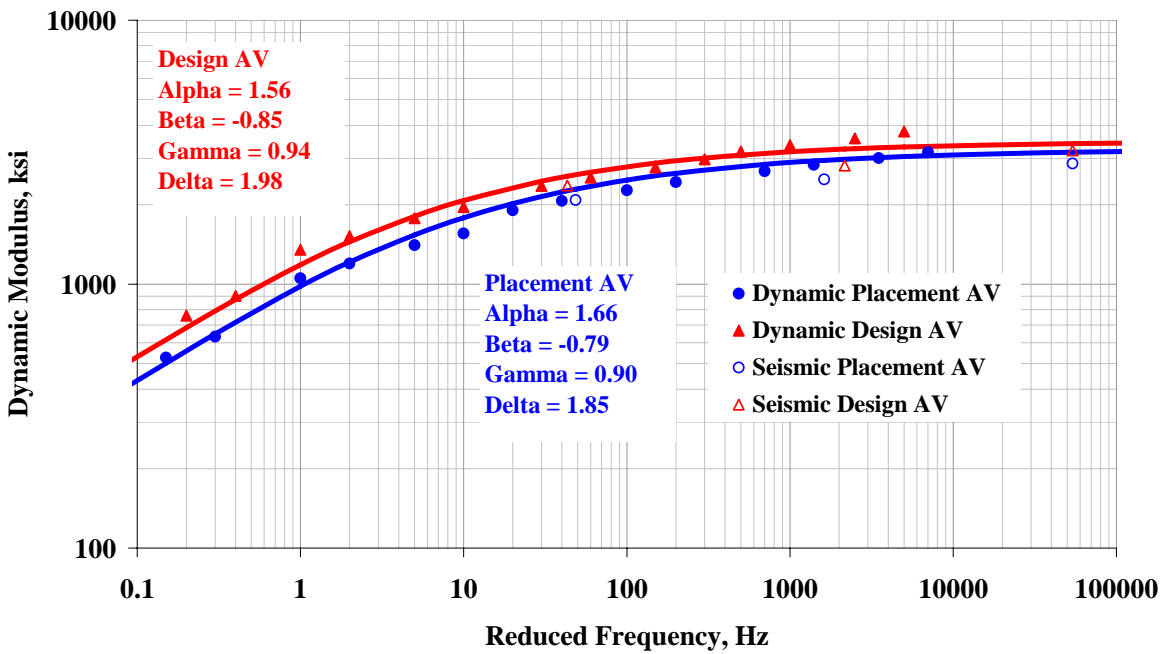


Figure E.10 – Master Curves for Tucson Mix (Site 10)

APPENDIX F. GRADATION RESULTS

Table F.1 – Comparison of Air Voids for Cores Extracted at Site 1

Core Number	Air Voids, %		
	ADOT	UTEP	Difference
1	6.6	6.2	+ 0.4
2	8.4	6.9	+ 1.5
3	7.5	7.0	+ 0.5
4	6.9	6.9	+ 0.0
5	7.7	7.8	- 0.1
6	6.4	7.4	- 1.0
7	7.9	8.8	- 0.9
8	8.5	9.0	- 0.5
9	8.3	7.4	+ 0.9
10	7.4	8.5	- 1.1

Table F.2 – Gradation Results for Selected Cores from Site 1

Sieve #	% Passing				
	Core 1	Core 2	Core 3	Core 4	Target
3/8"	82	76	75	77	77
8	48	39	43	43	46
40	17	15	16	16	16
200	3.5	2.8	2.9	2.4	4.5
Asphalt Content	4.6%	4.6%	4.9%	5.0%	4.6%

Table F.3 – Gradation Results for Loose Materials Sampled at Site 1

Sieve #	% Passing				Target
	Location 2		Location 3		
	UTEP	ADOT	UTEP	ADOT	
3/8"	78	78	80	76	77
8	42	45	41	44	46
40	16	17	16	17	16
200	2.4	4.5	2.4	4.3	4.5
AC Content	5.1%	4.8%	4.8%	4.9%	4.6%

Table F.4 – Comparison of Air Voids for Cores Extracted at Site 2

Core Number	Air Voids, %		
	ADOT	UTEP	Difference
1	7.0	8.0	- 1.0
2	5.9	6.5	- 0.6
3	7.0	7.5	- 0.5
4	6.4	6.7	- 0.3
5	6.9	7.9	- 1.0
6	7.6	8.3	- 0.7
7	7.6	8.6	- 1.0
8	7.6	11.3	- 3.7
9	7.8	7.6	+ 0.2
10	5.8	6.5	- 0.7

Table F.5 – Gradation Results for Selected Cores from Site 2

Sieve #	% Passing				
	Core 1	Core 2	Core 3	Core 4	Target
3/8"	75	73	73	76	75
8	45	40	42	44	41
30	22	20	21	22	24
200	3.9	4.1	3.8	3.9	5.0
Asphalt Content	5.0 %	5.4 %	5.5 %	5.6 %	5.1 %

Table F.6 – Gradation Results for Loose Materials Sampled at Site 2

Sieve #	% Passing				Target
	Location 2		Location 3		
	UTEP	ADOT	UTEP	ADOT	
3/8"	65	74	70	77	75
8	29	44	41	44	41
30	17	21	20	22	24
200	3.3	5.1	3.6	5.4	5.0
AC Content	5.2 %	5.3 %	5.1 %	5.4 %	5.1 %

Table F.7 – Comparison of Air Voids for Cores Extracted at Site 3

Core Number	Air Voids, %		
	ADOT	UTEP	Difference
1	6.9	6.5	+ 0.4
2	8.0	7.7	+ 0.3
3	5.9	5.7	+ 0.2
4	6.8	5.8	+ 1.0
5	5.9	5.6	+ 0.3
6	5.0	4.5	+ 0.5
7	5.9	5.9	0.0
8	6.3	5.8	+ 0.5
9	5.9	5.7	+ 0.2
10	5.9	5.8	+ 0.1

Table F.8 – Gradation Results for Selected Cores from Site 3

Sieve #	% Passing				
	Core 1	Core 2	Core 3	Core 4	Target
3/8"	71	69	72	71	70
8	43	41	43	43	47
30	27	23	25	25	26
200	8.5	3.8	3.8	4.1	5.0
Asphalt Content	5.0	5.1	5.3	5.1	4.9

Table F.9 – Gradation Results for Loose Materials Sampled at Site 3

Sieve #	% Passing				Target
	Location 1		Location 2		
	UTEP	ADOT	UTEP	ADOT	
3/8"	83	70	72	73	70
8	50	41	52	45	47
30	27	24	29	25	26
200	3.0	4.9	4.7	4.7	5.0
AC Content	5.3	4.9	5.4	5.0	4.9

Table F.10 – Comparison of Air Voids for Cores Extracted at Site 4

Core Number	Air Voids, %		
	ADOT	UTEP	Difference
1	6.9	7.0	- 0.1
2	6.5	5.6	+ 0.9
3	7.2	6.4	+ 0.8
4	6.5	7.0	- 0.5
5	5.0	5.0	--
6	6.1	9.9	- 3.8
7	6.6	5.4	+ 1.2
8	5.5	4.5	+ 1.0
9	7.1	6.7	+ 0.4
10	6.1	5.8	+ 0.3

Table F.11 – Gradation Results for Selected Cores from Site 4

Sieve #	% Passing				
	Core 1	Core 2	Core 3	Core 4	Target
3/8"	74	73	75	75	62
8	34	34	39	37	29
30	16	16	17	17	14
200	5.5	5.0	5.4	5.4	5.0
Asphalt Content	4.6 %	4.8 %	5.1 %	5.0 %	4.6 %

Table F.12 – Gradation Results for Loose Materials Sampled at Site 4

Sieve #	% Passing				Target
	Location 1		Location 2		
	UTEP	ADOT	UTEP	ADOT	
3/8"	72	72	74	77	62
8	35	35	37	37	29
30	16	16	17	16	14
200	4.9	6.0	5.0	6.0	5.0
AC Content	4.9 %	4.7 %	5.0 %	5.5 %	4.6 %

Table F.13 – Comparison of Air Voids for Cores Extracted at Site 5

Core Number	Air Voids, %		
	ADOT	UTEP	Difference
1	8.8	8.3	+ 0.5
2	10.1	8.8	+ 1.3
3	9.4	8.8	+ 0.6
4	9.8	9.9	- 0.1
5	10.4	10.1	+ 0.3
6	10.4	9.2	+ 1.2
7	7.9	8.4	- 0.5
8	10.2	9.8	+ 0.4
9	9.0	9.2	- 0.2
10	10.8	7.9	+ 2.9

Table F.14 – Gradation Results for Selected Cores from Site 5

Sieve #	% Passing				
	Core 1	Core 2	Core 3	Core 4	Target
3/8"	78	76	82	--	77
8	42	39	45	--	42
40	11	11	11	--	11
200	4.2	4.2	4.2	--	5.1
Asphalt Content	6.5 %	7.5 %	7.5 %	--	5.7 %

Table F.15 – Gradation Results for Loose Materials Sampled at Site 5

Sieve #	% Passing				Target
	Location 1		Location 2		
	UTEP	ADOT	UTEP	ADOT	
3/8"	79	75	75	75	77
8	41	36	41	40	42
40	11	9	10	11	11
200	4.8	3.9	3.8	5.5	5.1
AC Content	6.9 %	5.6 %	6.9 %	5.8 %	5.7 %

Table F.16 – Comparison of Air Voids for Cores Extracted at Site 6

Core Number	Air Voids, %		
	ADOT	UTEP	Difference
1	7.4	9.8	- 2.4
2	5.6	6.8	- 1.2
3	5.8	5.2	+ 0.6
4	7.4	7.8	- 0.4
5	6.6	7.1	- 0.5
6	7.5	7.9	- 0.4
7	6.6	*	--
8	5.9	*	--
9	7.1	*	--
10	6.1	*	--

* Specimens were not retrieved due to construction traffic blocking the core locations

Table F.17 – Gradation Results for Selected Cores from Site 6

Sieve #	% Passing				
	Core 1	Core 2	Core 3	Core 4	Target
3/8"	70	76	75	--	74
8	29	35	35	--	34
30	18	20	21	--	18
200	3.8	3.6	3.3	--	3.8
Asphalt Content	5.0%	4.9%	4.6%	--	4.7%

Table F.18 – Gradation Results for Loose Materials Sampled at Site 6

Sieve #	% Passing				Target
	Location 2		Location 3		
	UTEP	ADOT	UTEP	ADOT	
3/8"	68	74	72	71	74
8	31	34	41	32	34
30	18	20	21	19	18
200	3.8	4.8	3.1	5.1	3.8
AC Content	5.3%	5.2%	5.1%	5.1%	4.7%

Table F.19 – Comparison of Air Voids for Cores Extracted at Site 7

Core Number	Air Voids, %		
	ADOT	UTEP	Difference
1	9.8	10.2	- 0.4
2	6.6	6.3	+ 0.3
3	6.5	6.3	+ 0.2
4	8.1	7.6	+ 0.5
5	7.6	7.1	+ 0.5
6	7.7	7.3	+ 0.4
7	7.0	6.4	+ 0.6
8	6.5	6.3	+ 0.2
9	9.9	11.6	- 1.7
10	9.2	9.3	- 0.1

Table F.20 – Gradation Results for Selected Cores from Site 7

Sieve #	% Passing				
	Core 1	Core 2	Core 3	Core 4	Target
3/8"	61	72	70	70	71
8	32	37	38	38	40
30	14	14	16	16	14
200	2.6	3.4	3.3	3.3	4.4
Asphalt Content	5.6 %	5.8 %	6.1 %	6.4 %	5.2 %

Table F.21 – Gradation Results for Loose Materials Sampled at Site 7

Sieve #	% Passing				Target
	Location 1		Location 2		
	UTEP	ADOT	UTEP	ADOT	
3/8"	57	71	64	73	71
8	30	40	34	42	40
30	14	12	15	13	14
200	3.0	3.5	3.3	3.8	4.4
AC Content	5.3 %	5.7 %	5.8 %	5.7 %	5.2 %

Table F.22 – Comparison of Air Voids for Cores Extracted at Site 8

Core Number	Air Voids, %		
	ADOT	UTEP	Difference
1	6.2	6.3	- 0.1
2	7.2	6.6	+ 0.6
3	8.9	9.1	- 0.2
4	6.4	6.0	+ 0.4
5	6.2	5.1	+ 1.1
6	6.1	5.8	+ 0.3
7	7.2	6.7	+ 0.5
8	6.5	6.7	- 0.2
9	5.9	5.5	+ 0.4
10	6.7	6.7	0.0

Table F.23 – Gradation Results for Selected Cores from Site 8

Sieve #	% Passing				
	Core 1	Core 2	Core 3	Core 4	Target
3/8"	71	76	74	74	68
8	30	32	32	34	33
30	17	18	16	18	17
200	3.9	4.1	3.8	3.9	3.8
Asphalt Content	5.2 %	5.2 %	5.3 %	5.5 %	4.9 %

Table F.24 – Gradation Results for Loose Materials Sampled at Site 8

Sieve #	% Passing				Target
	Location 1		Location 2		
	UTEP	ADOT	UTEP	ADOT	
3/8"	71	73	75	76	68
8	31	33	43	33	33
30	17	17	23	17	17
200	3.8	4.2	3.1	4.4	3.8
AC Content	5.2 %	5.2 %	5.5 %	5.2 %	4.9 %

Table F.25 – Comparison of Air Voids for Cores Extracted at Site 9

Core Number	Air Voids, %		
	ADOT	UTEP	Difference
1	5.4	6.8	- 1.4
2	8.8	8.8	0.0
3	6.3	7.6	- 1.3
4	8.7	9.5	- 0.8
5	6.9	7.9	- 1.0
6	5.4	6.2	- 0.8
7	8.1	9.1	- 1.0
8	4.9	6.5	- 1.6
9	5.1	6.5	- 0.6
10	5.6	6.9	- 1.3

Table F.26 – Gradation Results for Selected Cores from Site 9

Sieve #	% Passing				
	Core 1	Core 2	Core 3	Core 4	Target
3/8"	78	76	81	82	77
8	44	44	47	45	45
30	23	23	24	23	24
200	3.2	2.9	2.8	3.3	5.1
Asphalt Content	5.6 %	5.5 %	5.7 %	5.7 %	5.4 %

Table F.27 – Gradation Results for Loose Materials Sampled at Site 9

Sieve #	% Passing				Target
	Location 1		Location 2		
	UTEP	ADOT	UTEP	ADOT	
3/8"	75	74	77	70	77
8	42	42	34	39	45
30	22	22	18	21	24
200	2.9	5.2	3.6	4.9	5.1
AC Content	5.3 %	5.3 %	5.4 %	5.1 %	5.4 %

Table F.28 – Comparison of Air Voids for Cores Extracted at Site 10

Core Number	Air Voids, %		
	ADOT	UTEP	Difference
1	6.9	6.7	+ 0.2
2	7.4	6.9	+ 0.5
3	7.8	7.7	+ 0.1
4	7.3	7.5	- 0.2
5	6.2	6.1	- 0.1
6	6.1	4.6	+ 1.5
7	6.7	6.2	+ 0.5
8	6.2	6.5	- 0.3
9	8.2	8.4	- 0.2
10	4.6	3.8	+ 0.8

Table F.29 – Gradation Results for Selected Cores from Site 10

Sieve #	% Passing				
	Core 1	Core 2	Core 3	Core 4	Target
3/8"	71	72	71	64	68
8	44	45	43	38	43
40	16	16	15	14	15
200	1.5	0.8	2.2	1.7	4.1
Asphalt Content	3.7 %	5.6 %	3.5 %	5.1 %	5.2 %

Table F.30 – Gradation Results for Loose Materials Sampled at Site 10

Sieve #	% Passing				Target
	Location 1		Location 2		
	UTEP	ADOT	UTEP	ADOT	
3/8"	69	72	67	70	68
8	44	47	43	45	43
40	17	17	17	16	15
200	3.0	4.4	3.0	4.1	4.1
AC Content	5.1 %	5.2 %	5.3 %	5.4 %	5.2 %

APPENDIX G. CONTOUR MAPS

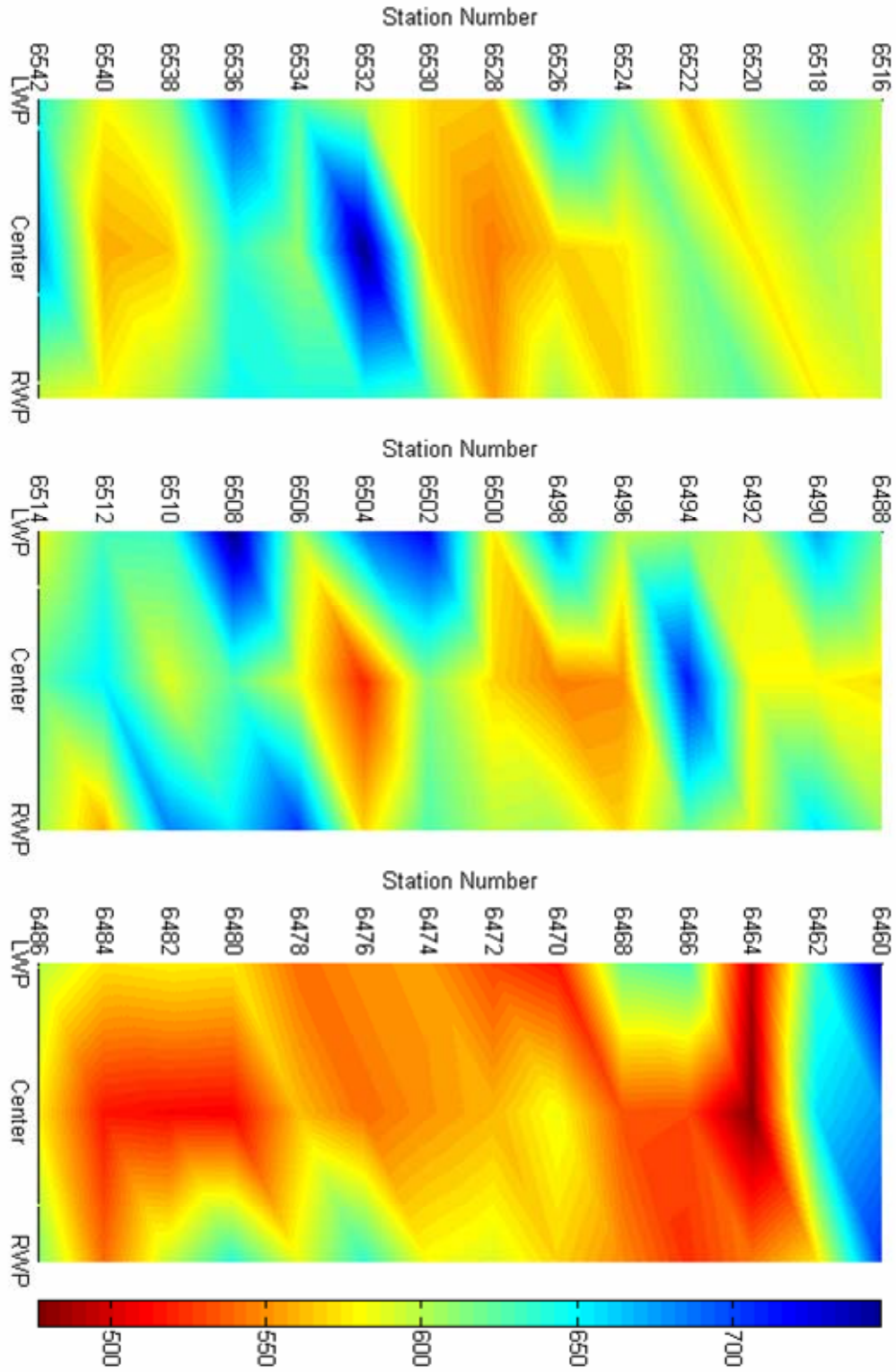


Figure G.1 – Contour Plots of Variation in Design Modulus with PSPA for Buckeye (Site 1)

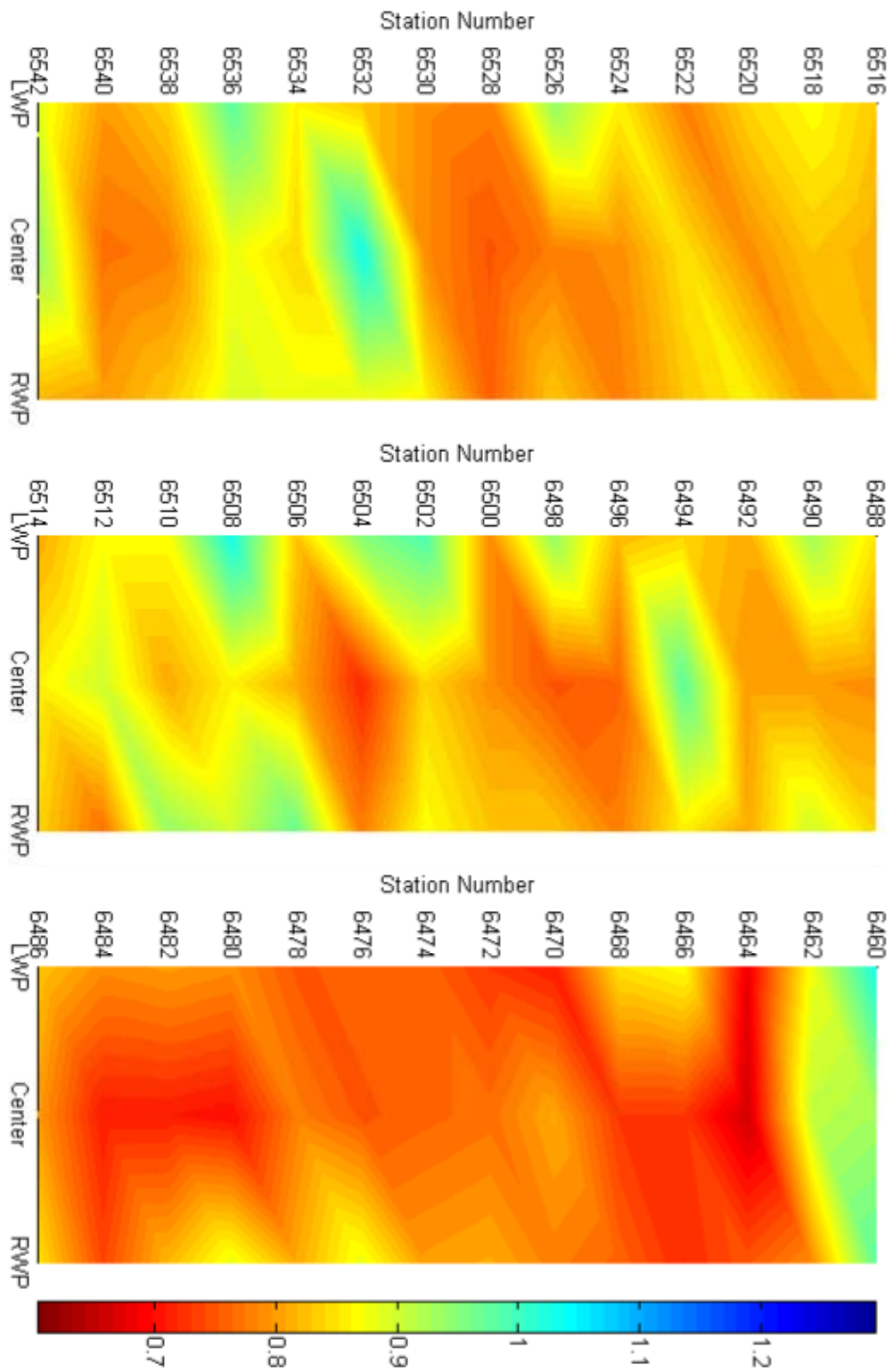


Figure G.2 – Contour Plots of Variation in Normalized Modulus (PSPA/Target Modulus) for Buckeye (Site 1)

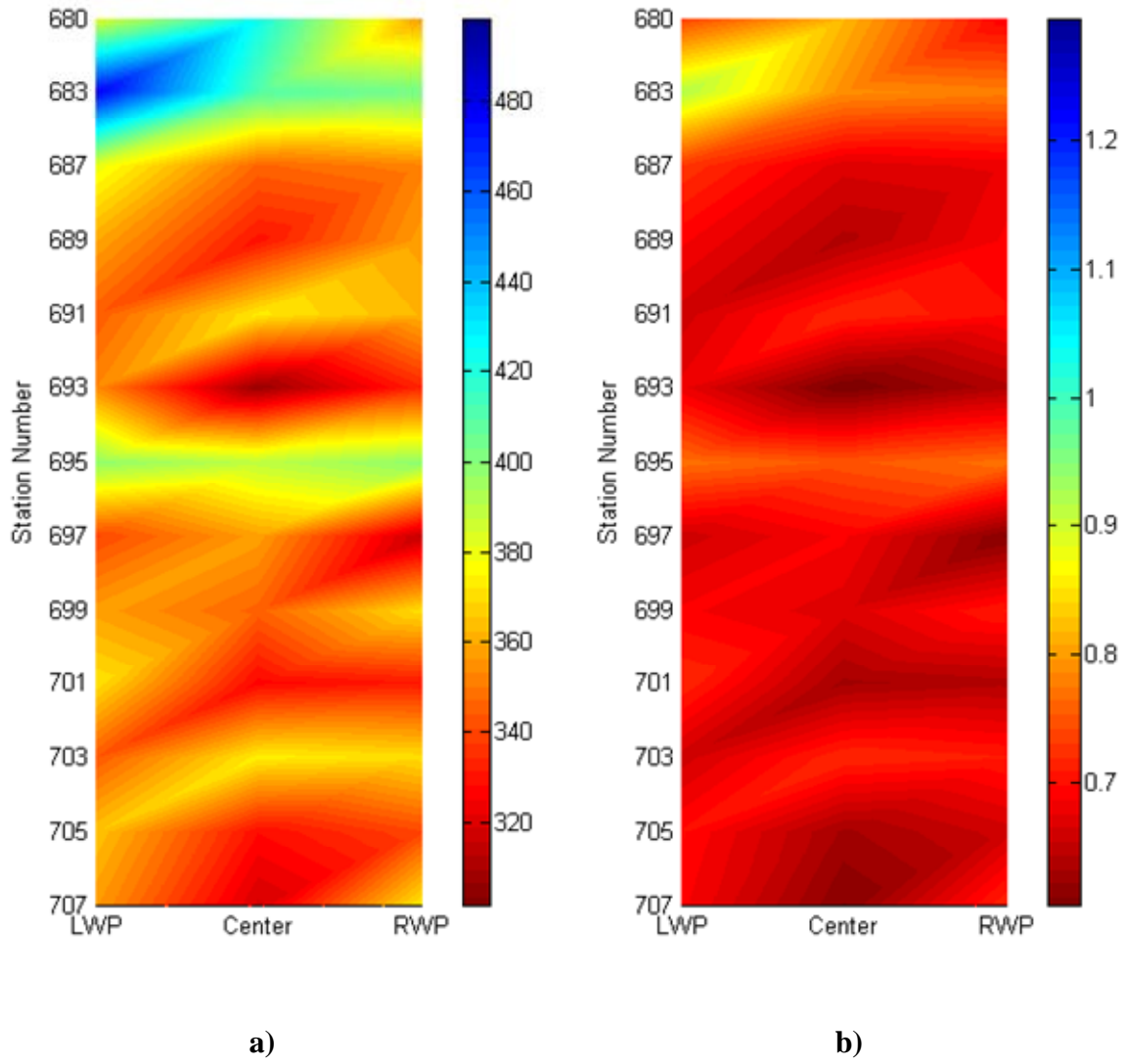


Figure G.3 – Contour Plots of Variation in Design Modulus with PSPA (a) and Normalized Modulus (b) for Show Low (Site 2)

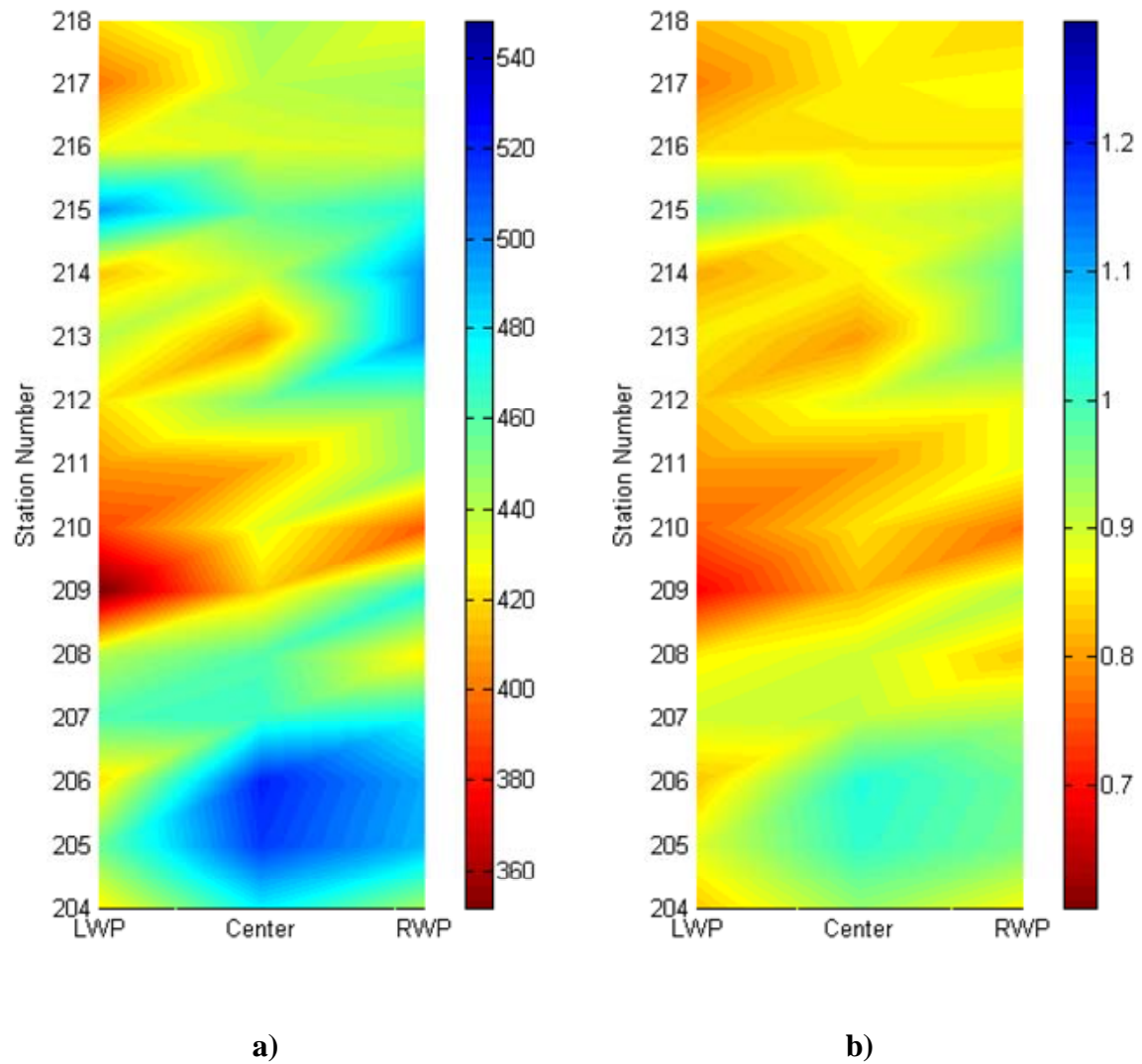


Figure G.4 – Contour Plots of Variation in Design Modulus with PSPA (a) and Normalized Modulus (b) for Holbrook (Site 3)

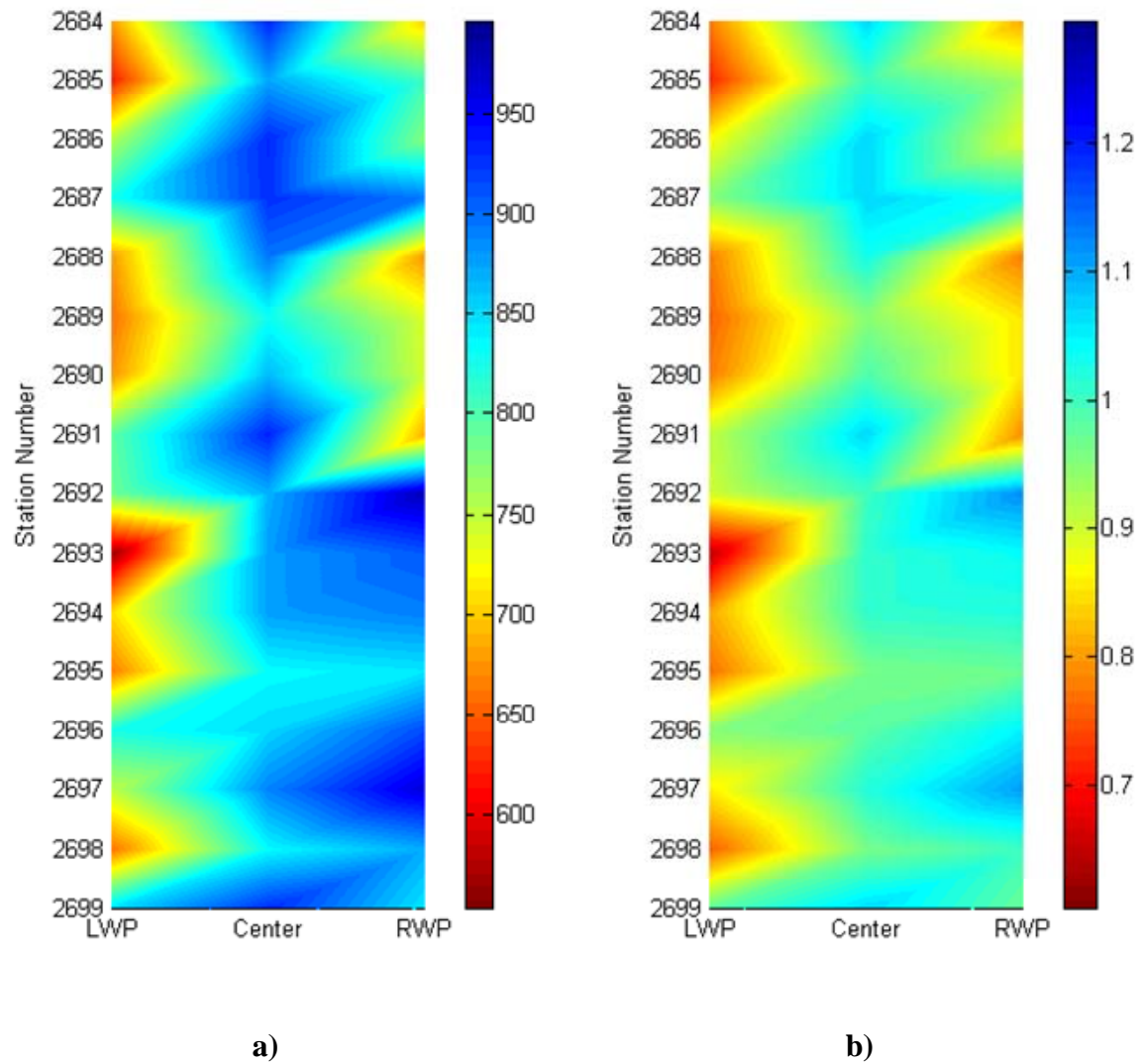


Figure G.5 – Contour Plots of Variation in Design Modulus with PSPA (a) and Normalized Modulus (b) for Burro Creek (Site 4)

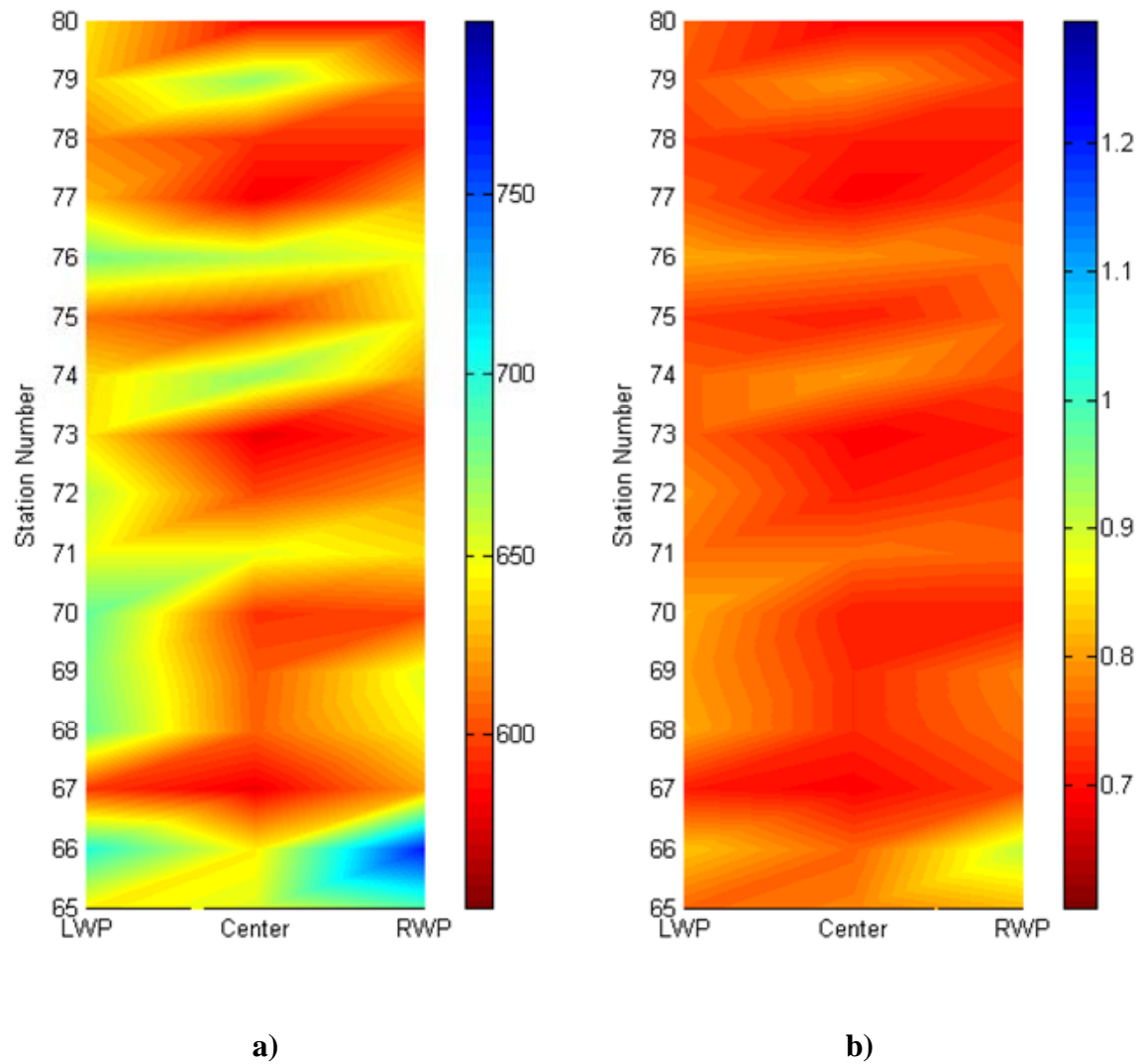


Figure G.6 – Contour Plots of Variation in Design Modulus with PSPA (a) and Normalized Modulus (b) for Cordes JCT (Site 5)

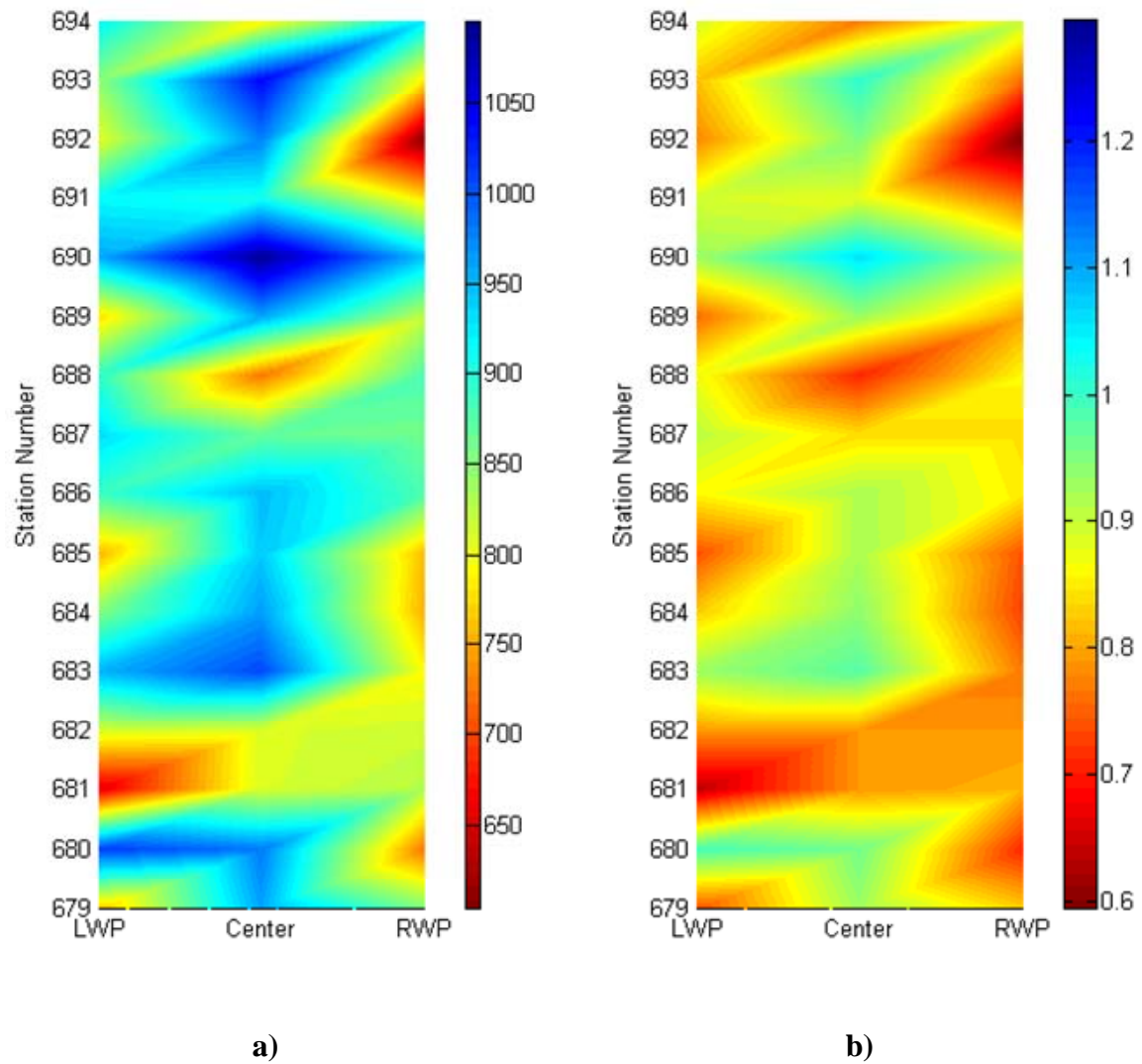


Figure G.7 – Contour Plots of Variation in Design Modulus with PSPA (a) and Normalized Modulus (b) for Roosevelt (Site 6)

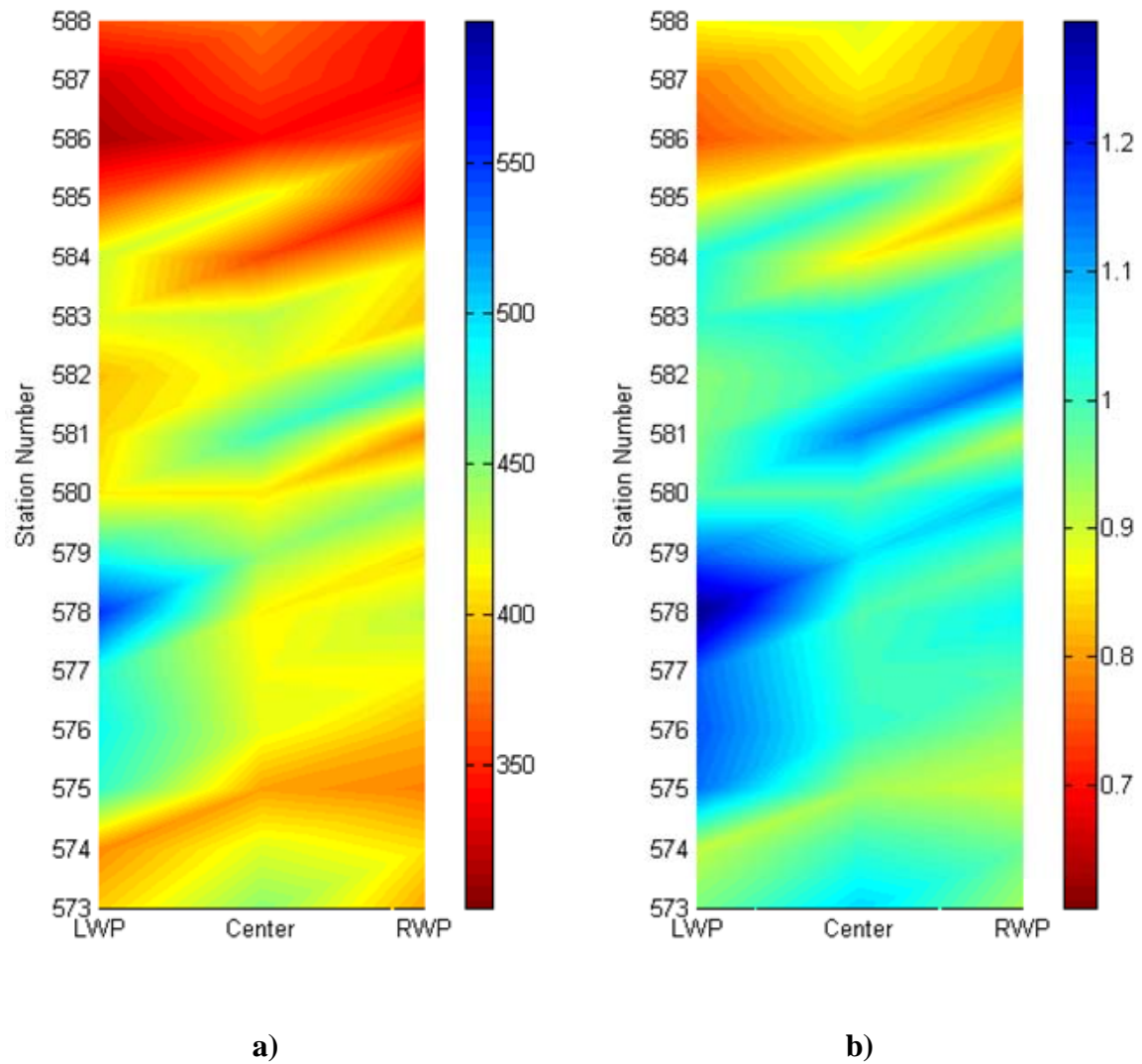


Figure G.8 – Contour Plots of Variation in Design Modulus with PSPA (a) and Normalized Modulus (b) for Safford (Site 7)

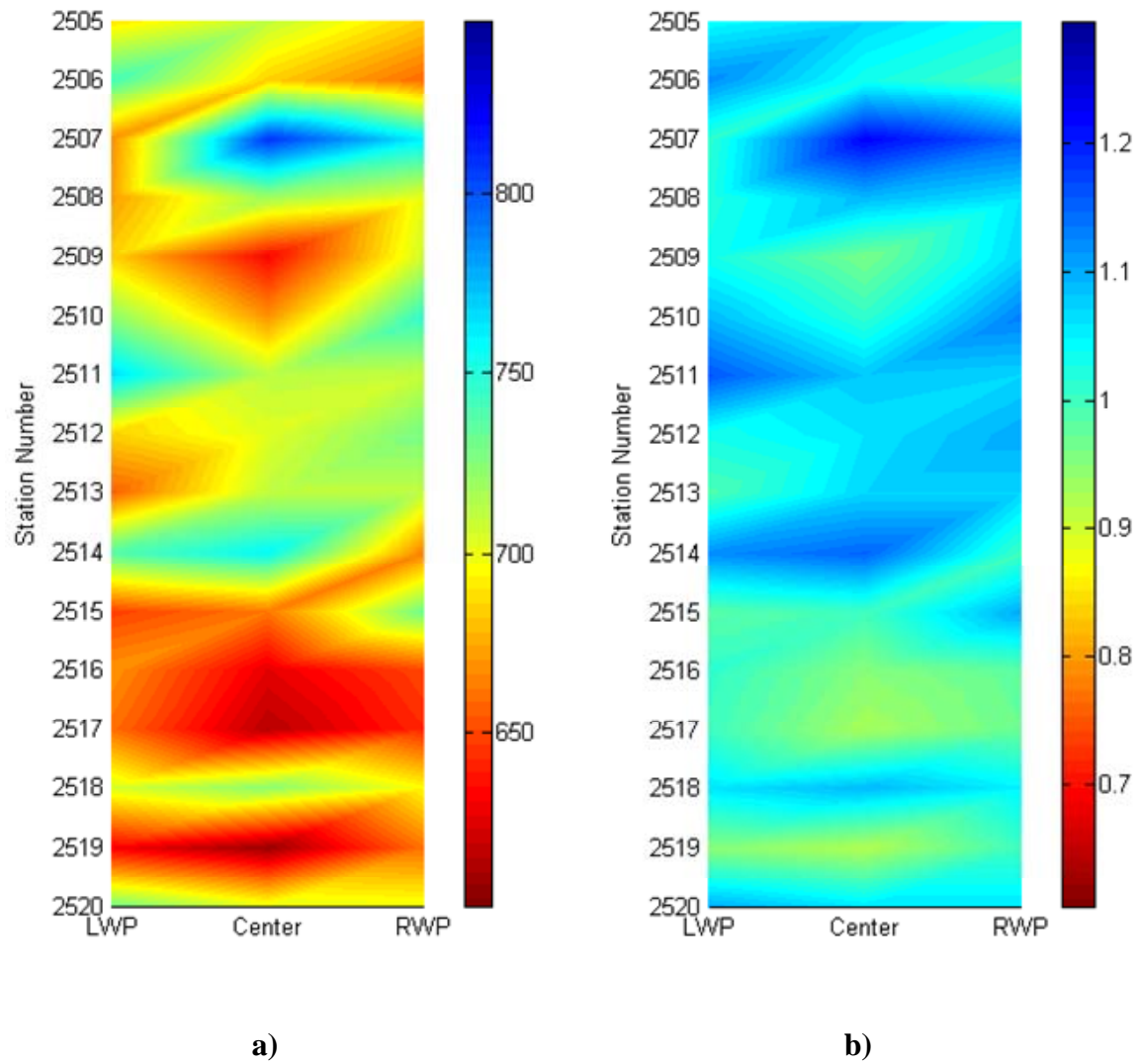


Figure G.9 – Contour Plots of Variation in Design Modulus with PSPA (a) and Normalized Modulus (b) for Holbrook B (Site 8)

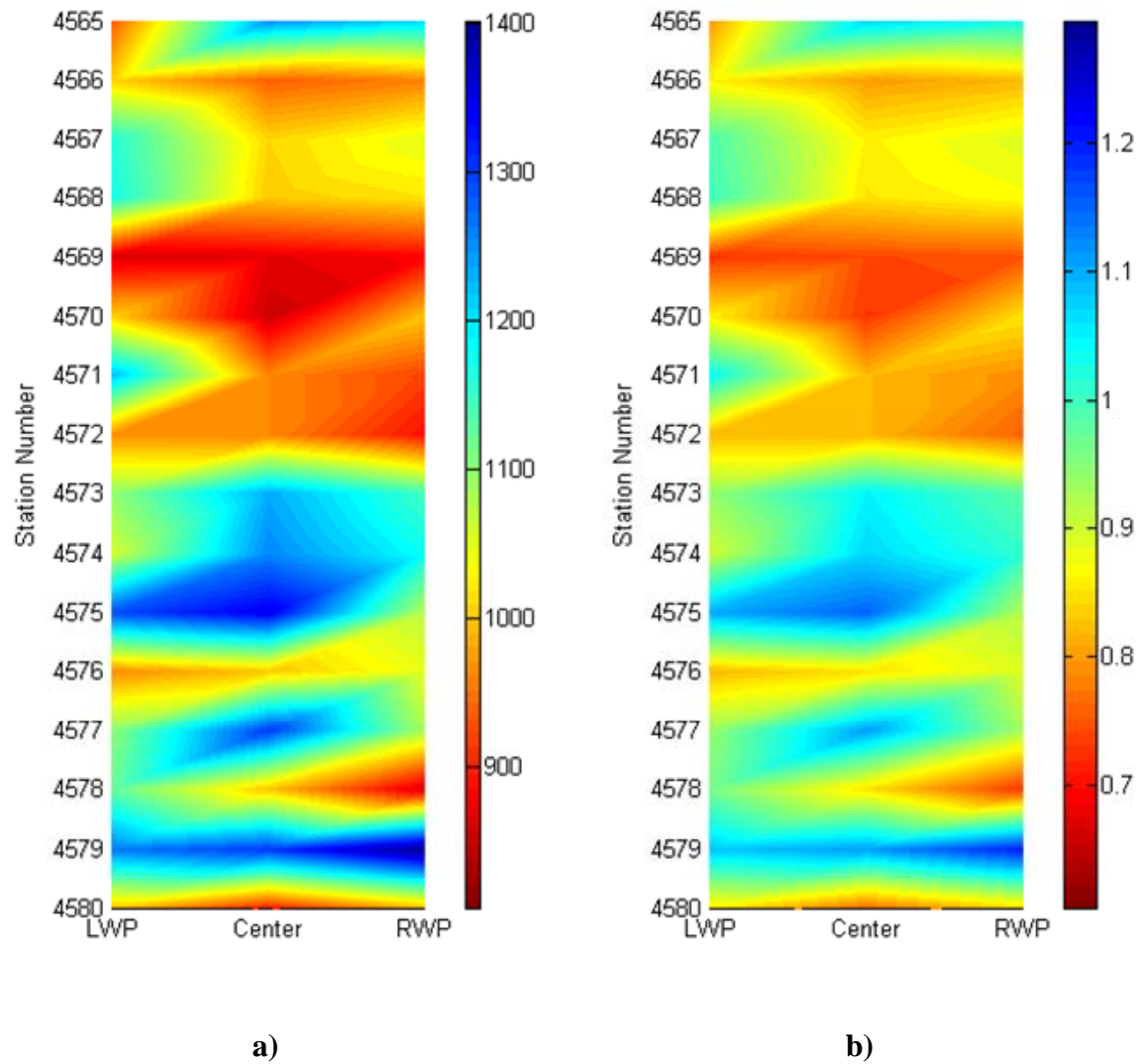


Figure G.10 – Contour Plots of Variation in Design Modulus with PSPA (a) and Normalized Modulus (b) for Tucson (Site 10)

APPENDIX H. MODULUS CONTROL CHARTS

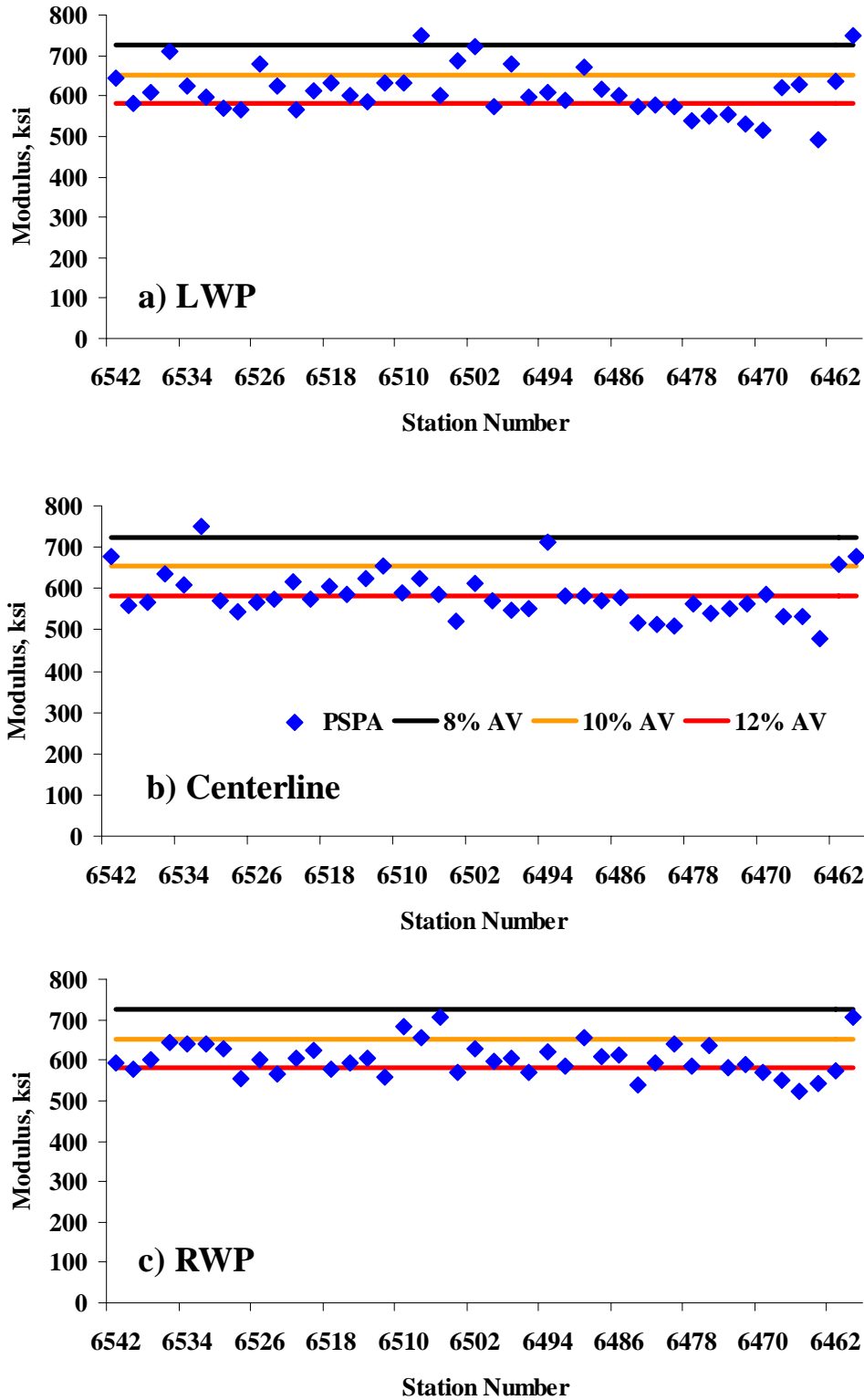


Figure H.1 – Modulus Control Charts from Buckeye (Site 1)

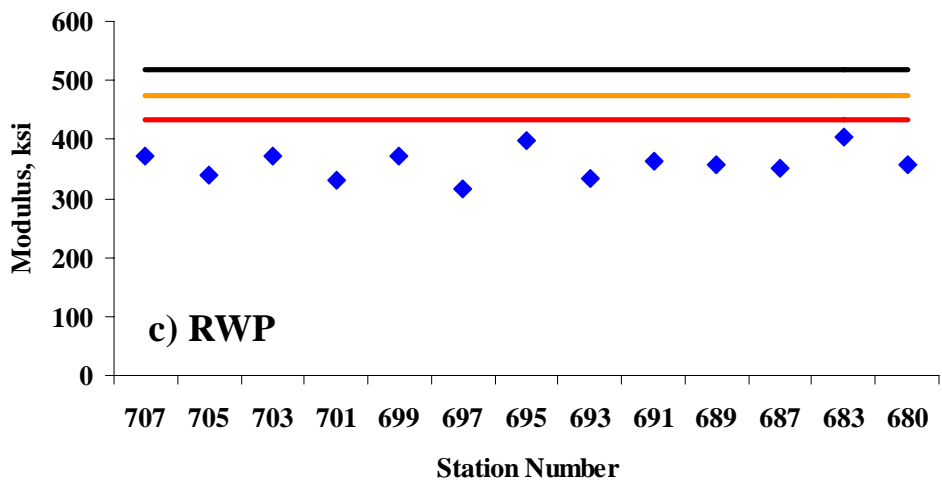
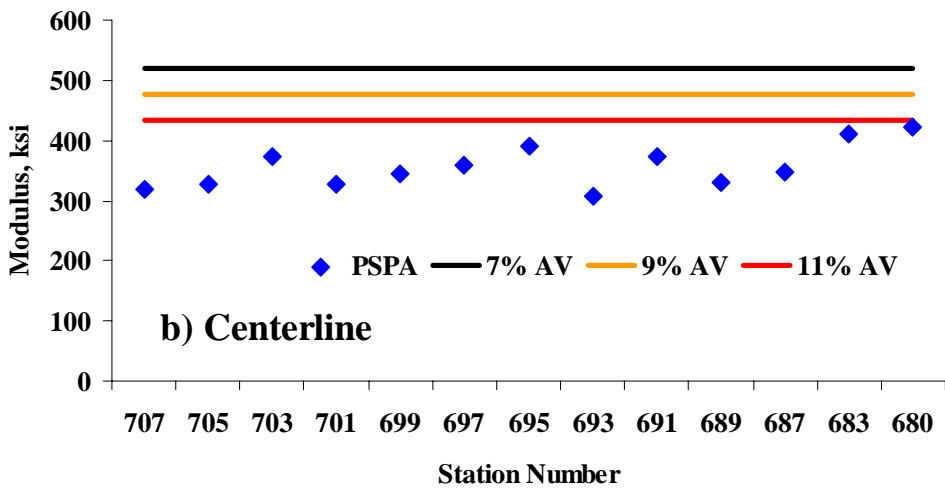
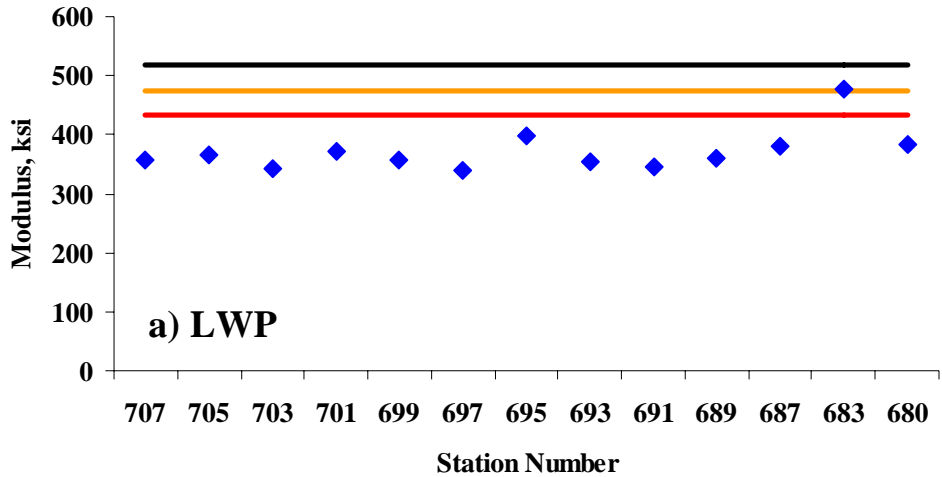


Figure H.2 – Modulus Control Charts from Show Low (Site 2)

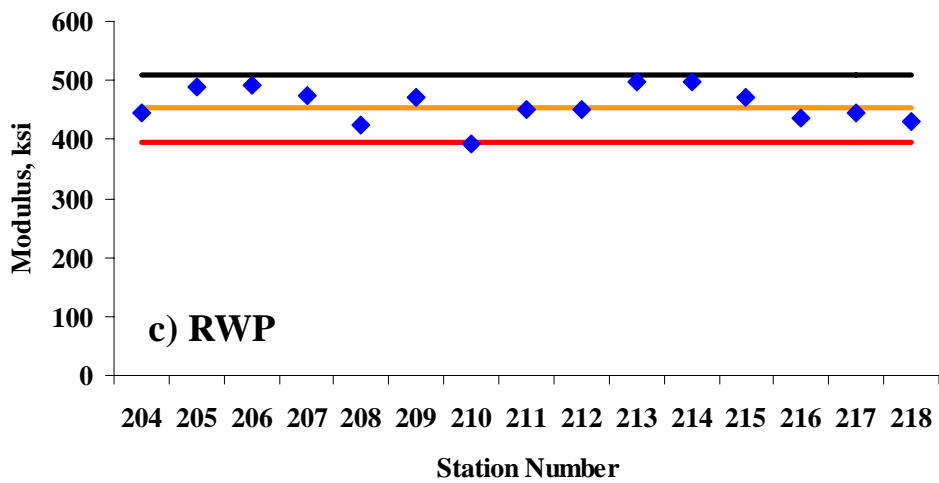
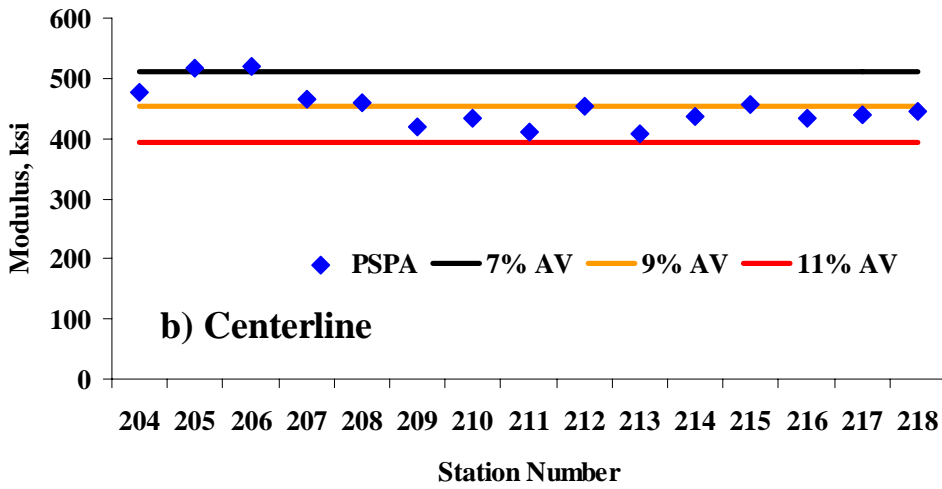
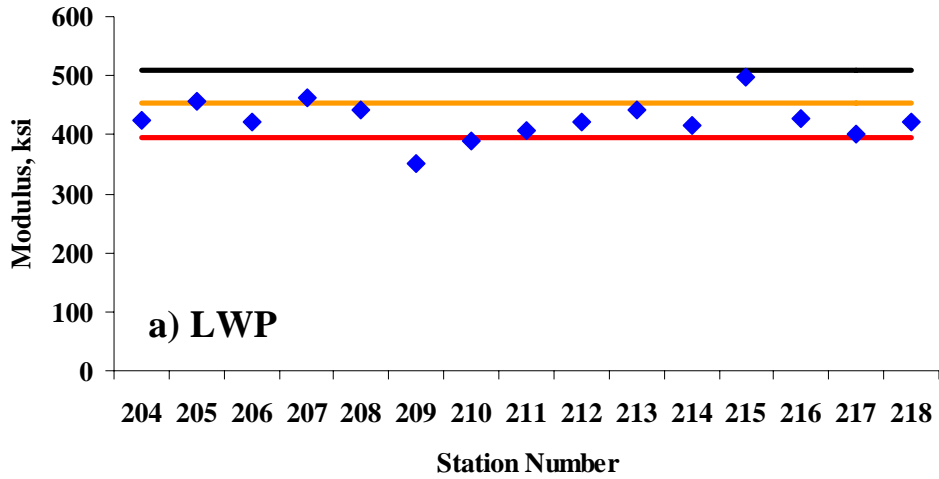


Figure H.3 – Modulus Control Charts from Holbrook (Site 3)

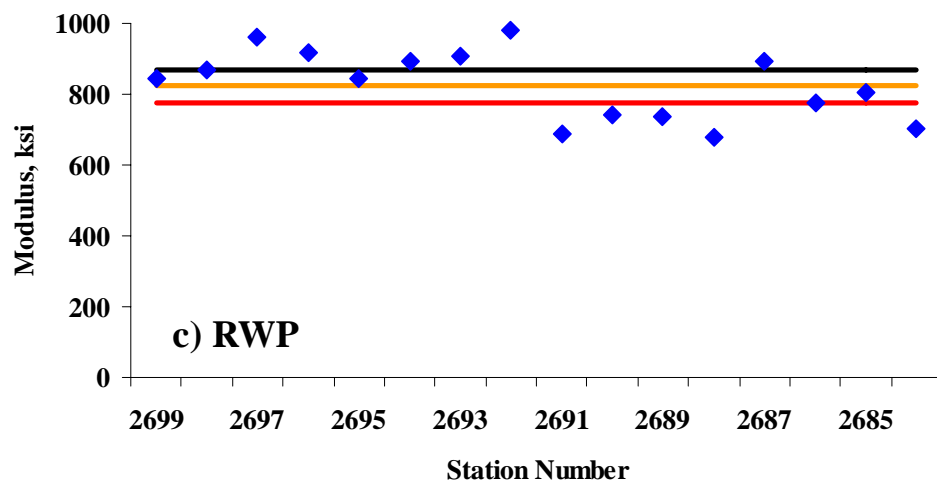
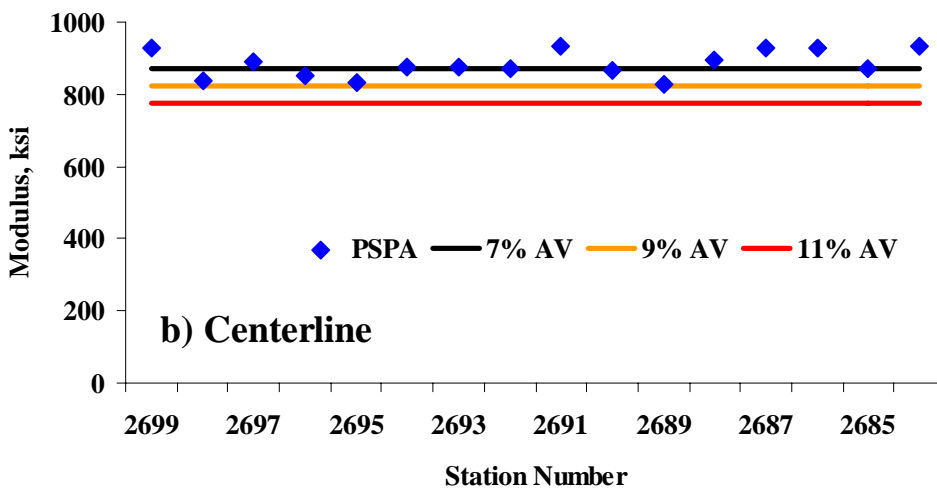
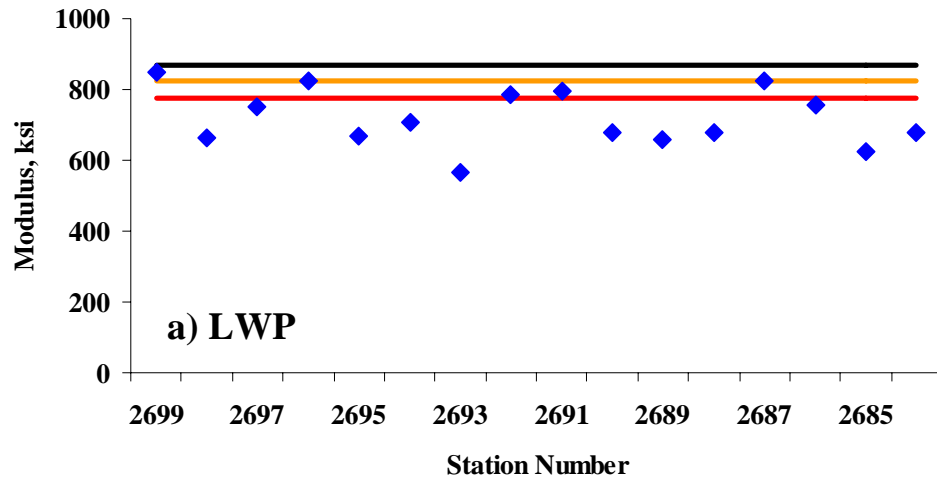


Figure H.4 – Modulus Control Charts from Burro Creek (Site 4)

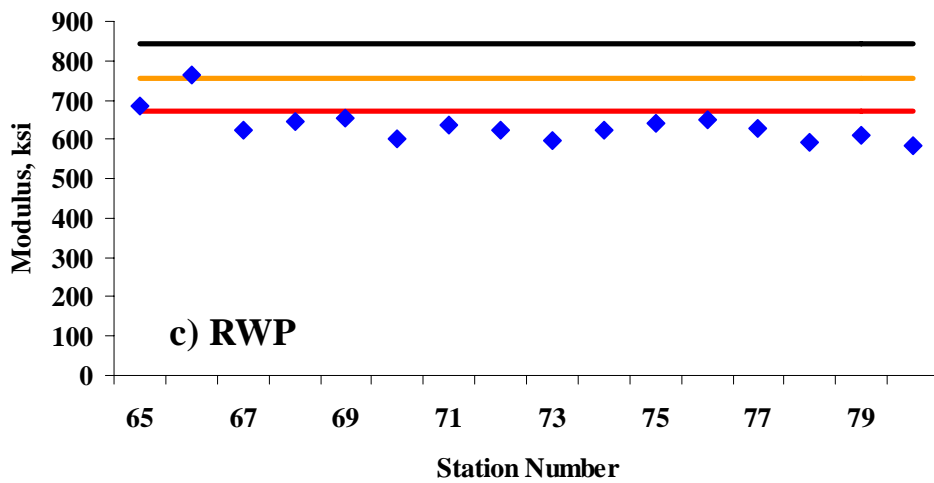
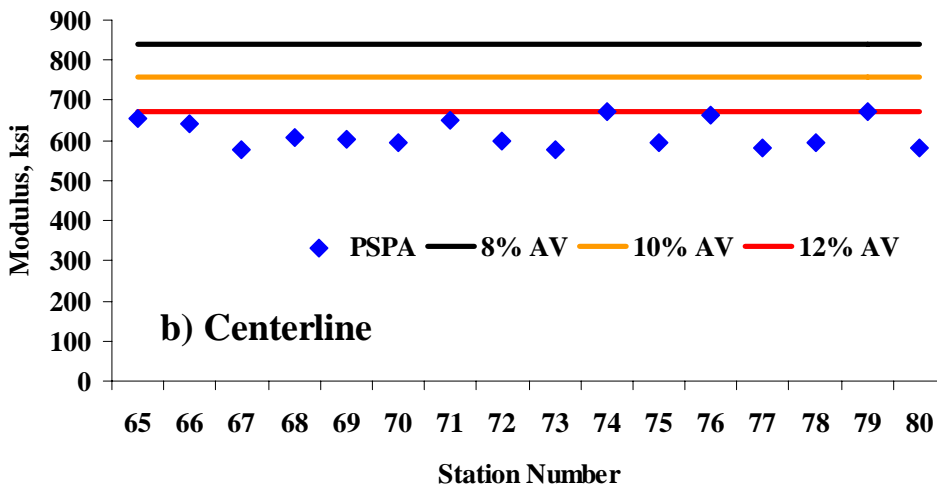
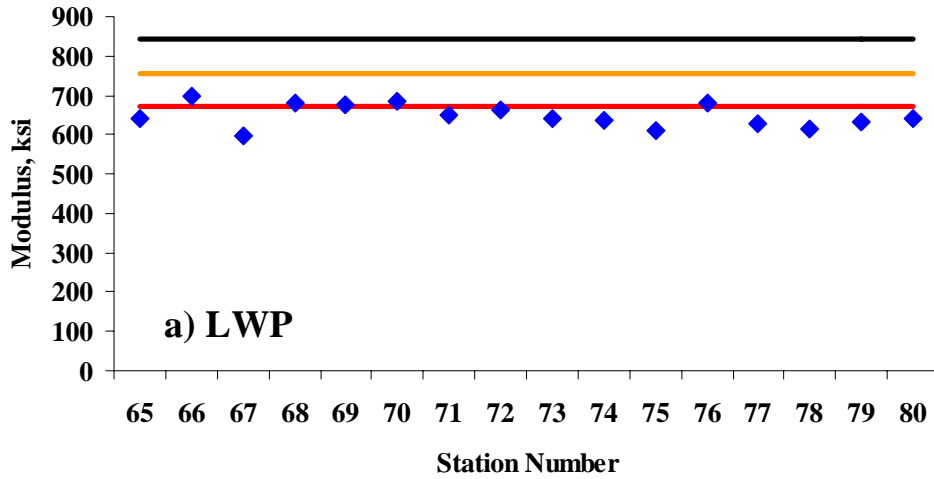


Figure H.5 – Modulus Control Charts from Cordes JCT (Site 5)

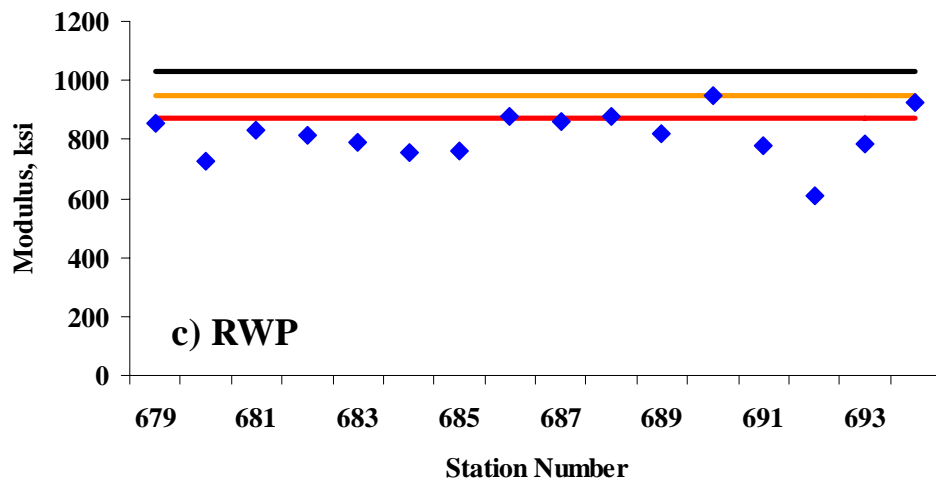
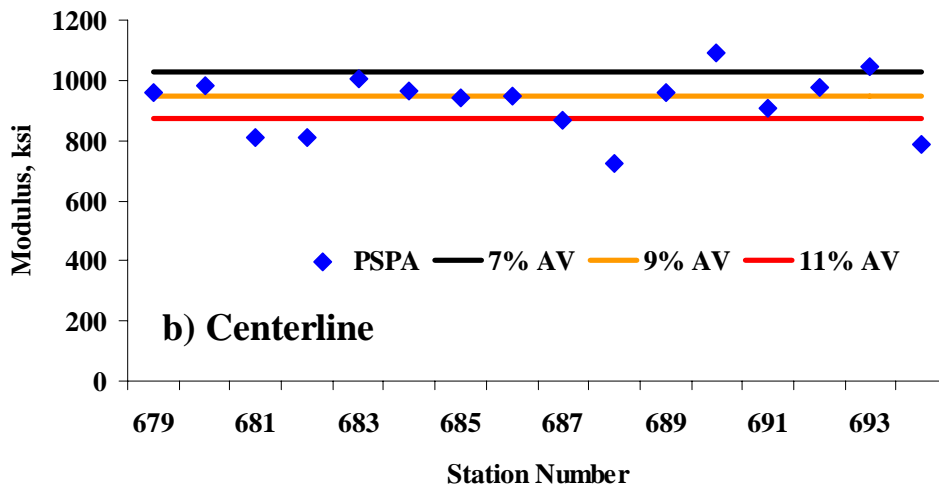
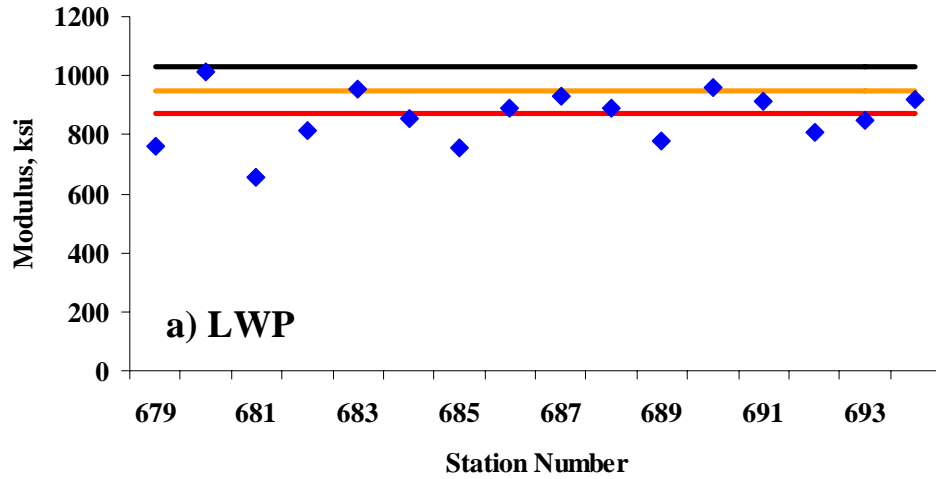


Figure H.6 – Modulus Control Charts from Roosevelt (Site 6)

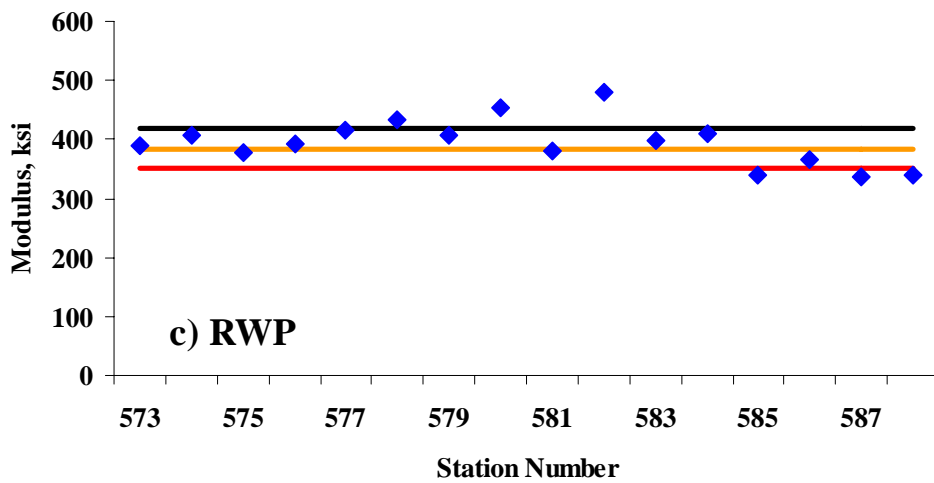
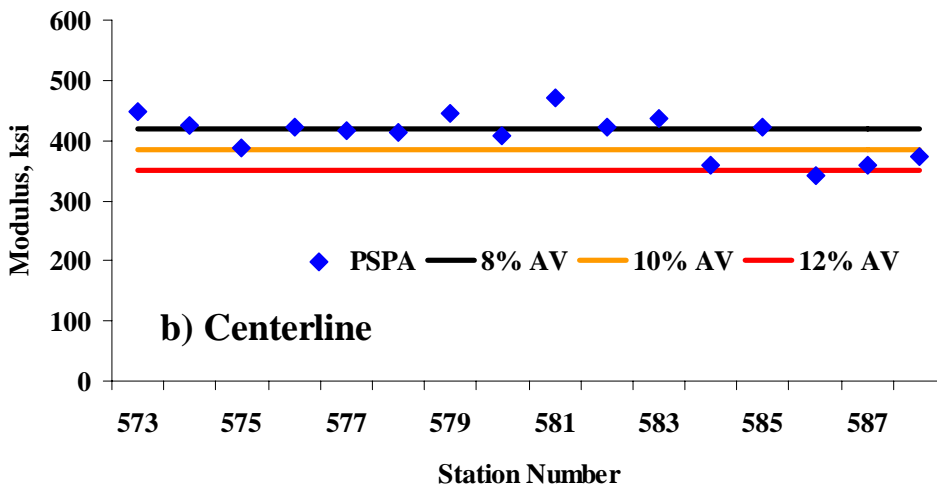
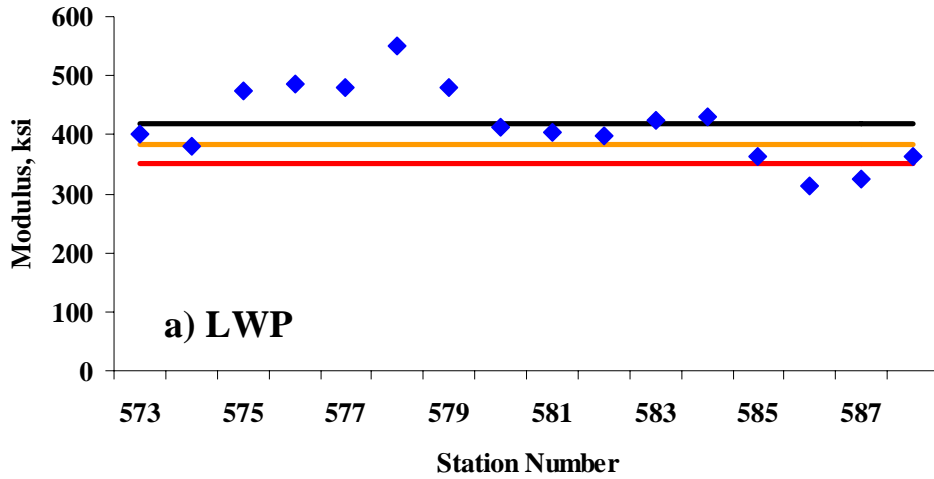


Figure H.7 – Modulus Control Charts from Safford (Site 7)

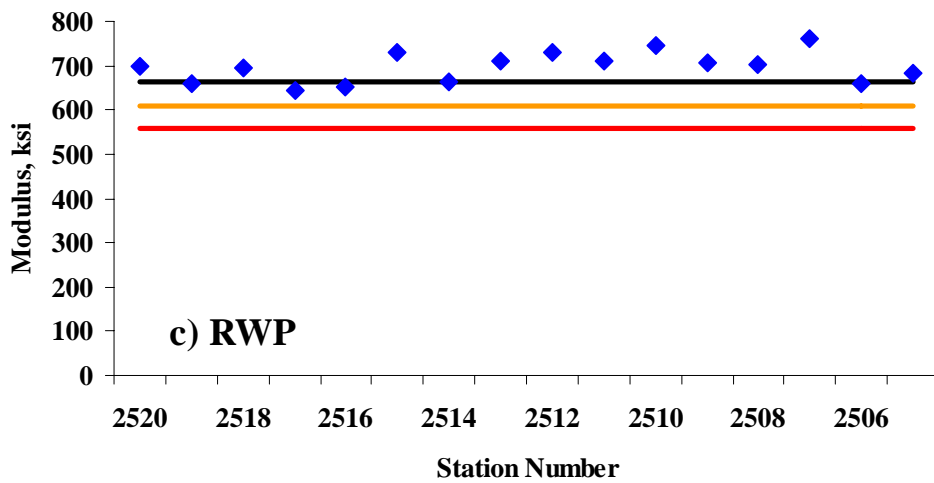
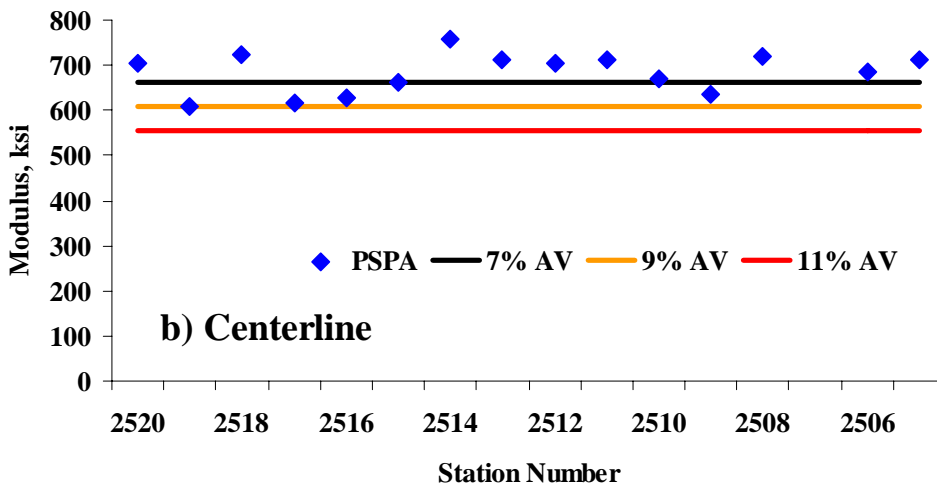
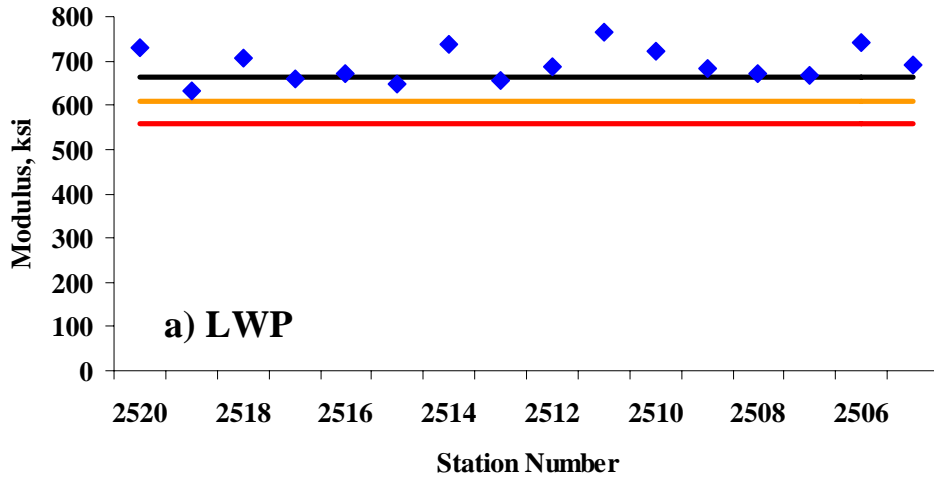


Figure H.8 – Modulus Control Charts from Holbrook B (Site 8)

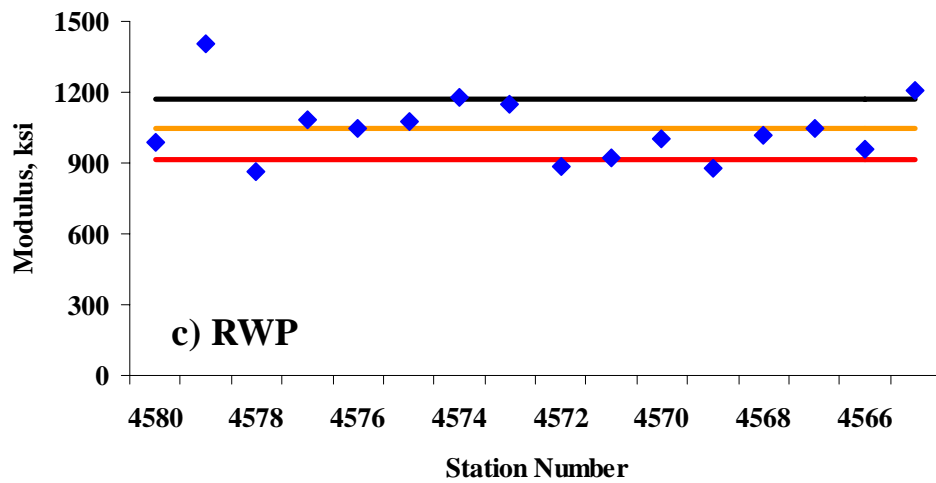
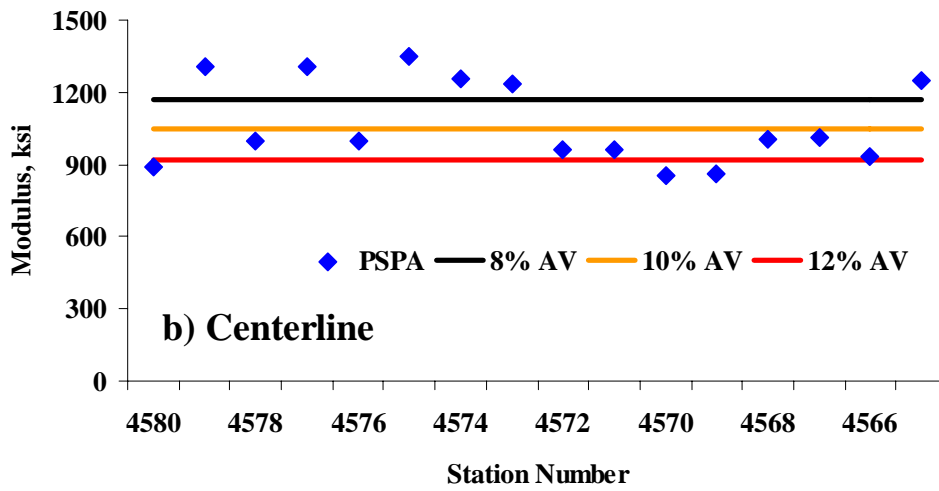
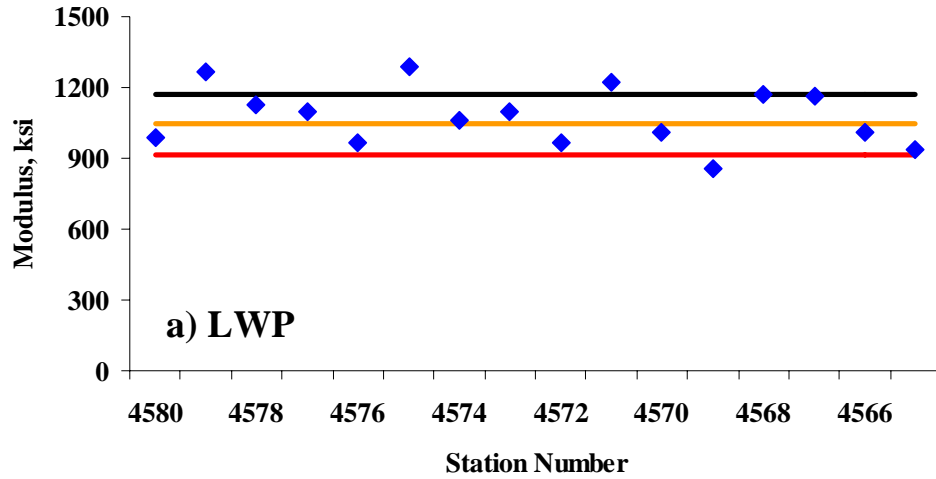


Figure H.9 – Modulus Control Charts from Tucson (Site 10)

APPENDIX I. CUMULATIVE DISTRIBUTION CHARTS

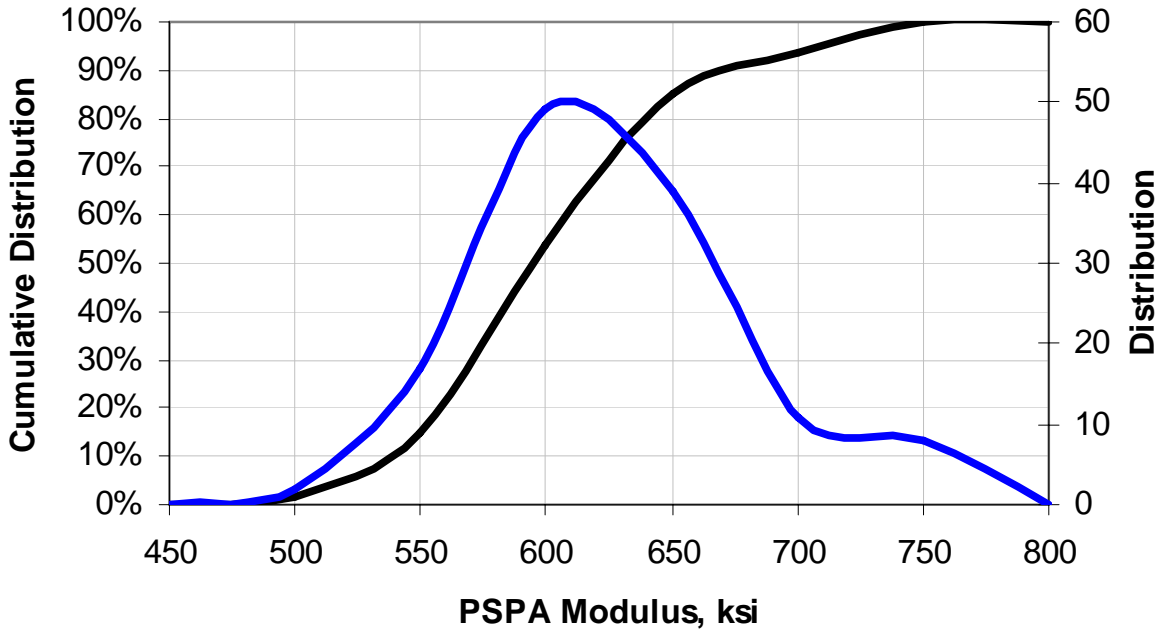


Figure I.1 – Distribution of Design Moduli for Buckeye (Site 1)

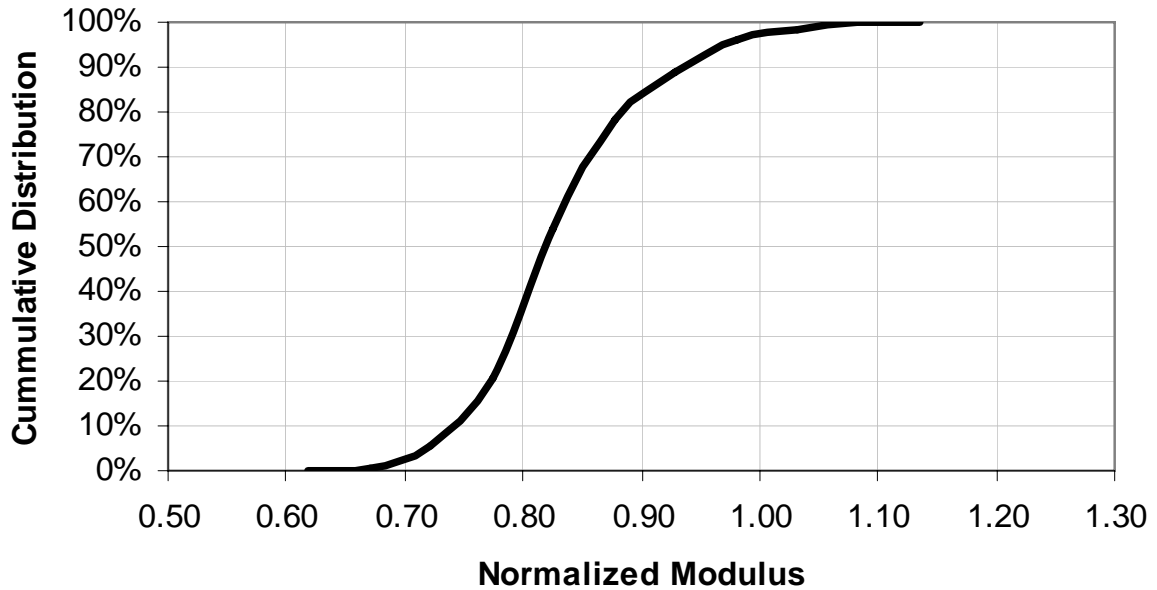


Figure I.2 – Distribution of Normalized Moduli (PSPA/Target Modulus) for Buckeye (Site 1)

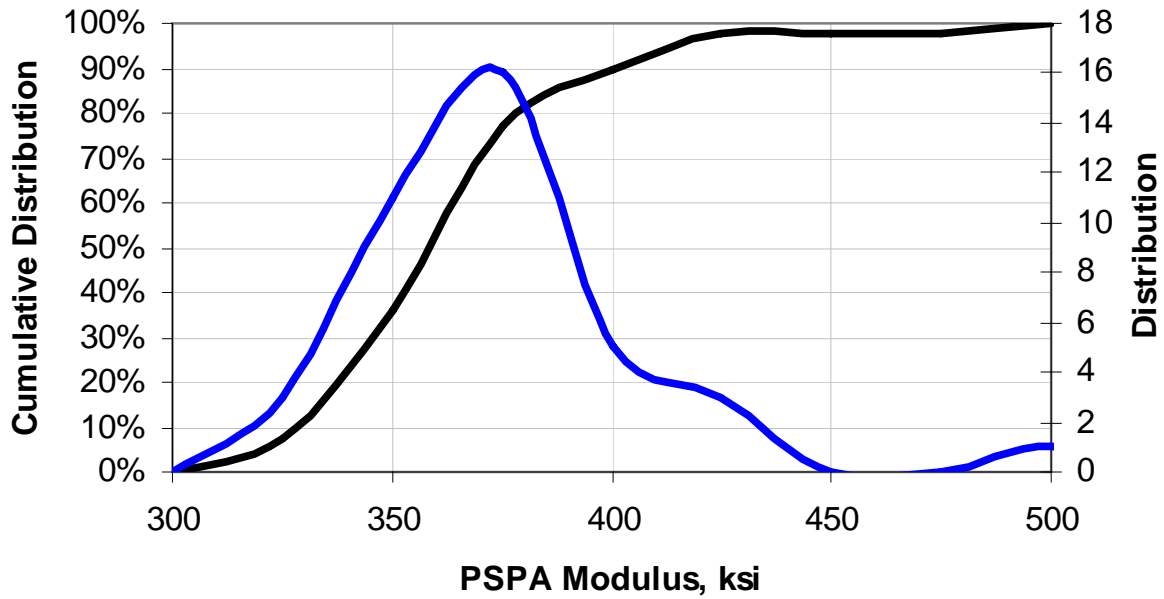


Figure I.3 – Distribution of Design Moduli for Show Low (Site 2)

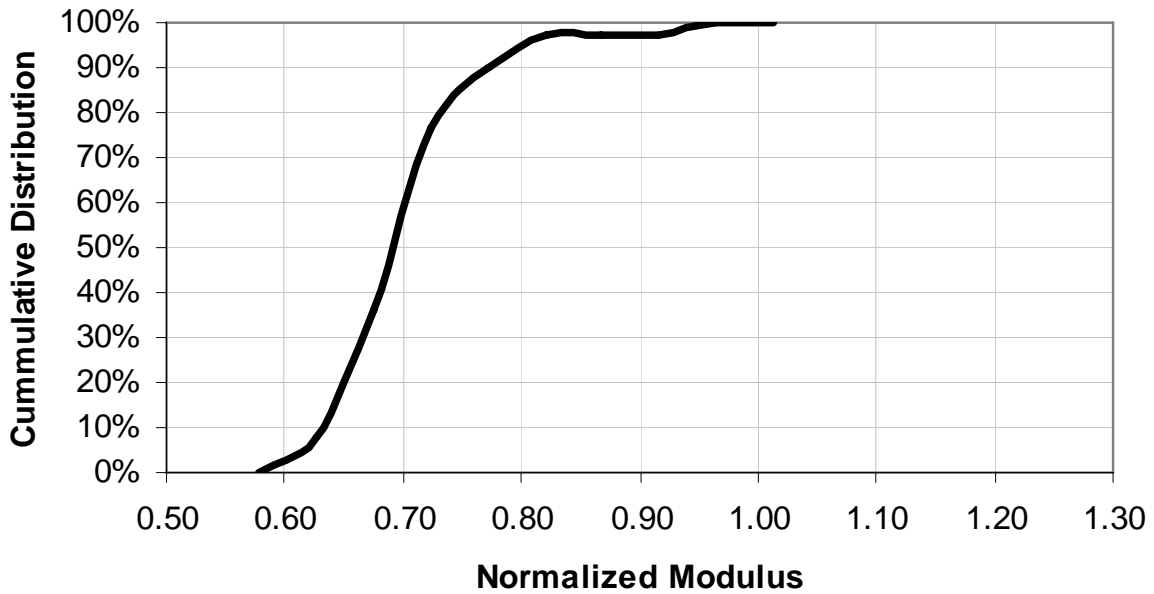


Figure I.4 – Distribution of Normalized Moduli (PSPA/Target Modulus) for Show Low (Site 2)

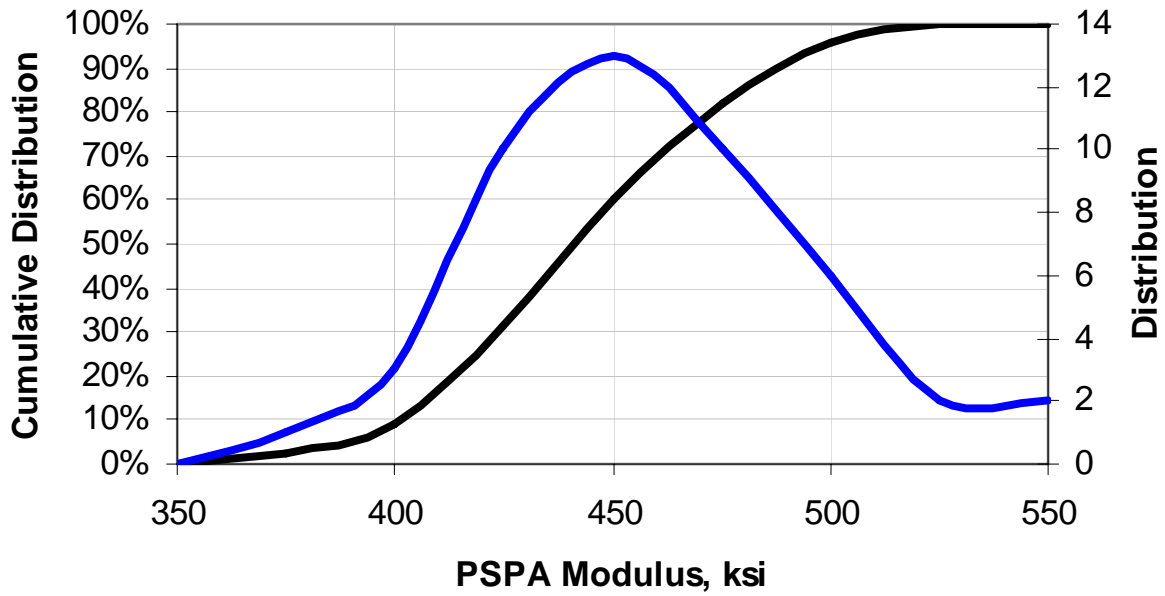


Figure I.5 – Distribution of Design Moduli for Holbrook (Site 3)

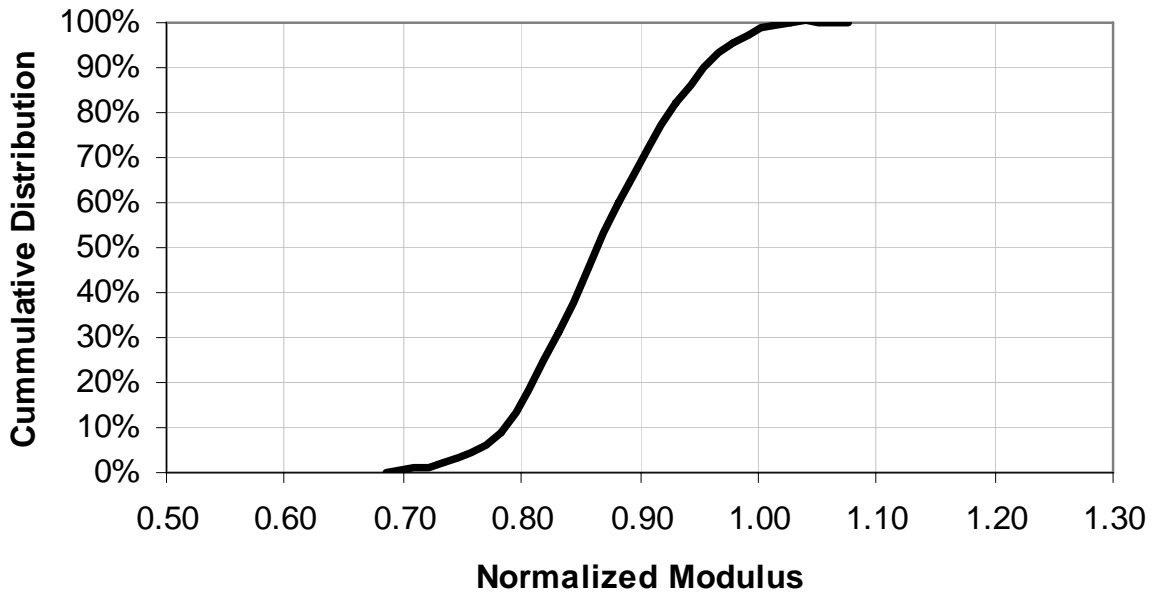


Figure I.6 – Distribution of Normalized Moduli (PSPA/Target Modulus) for Holbrook (Site 3)

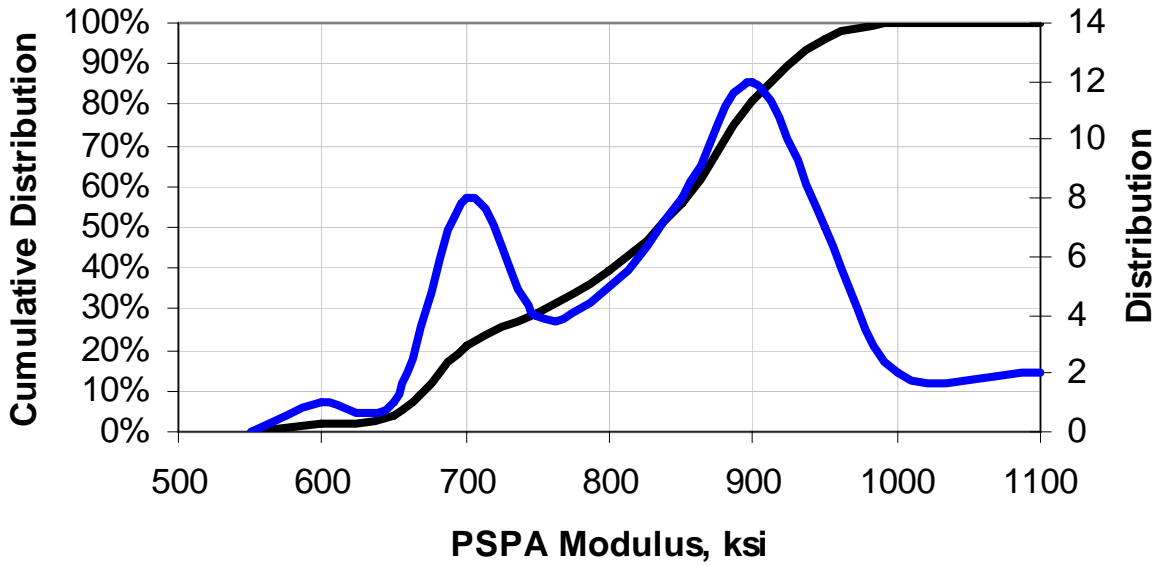


Figure I.7 – Distribution of Design Moduli for Burro Creek (Site 4)

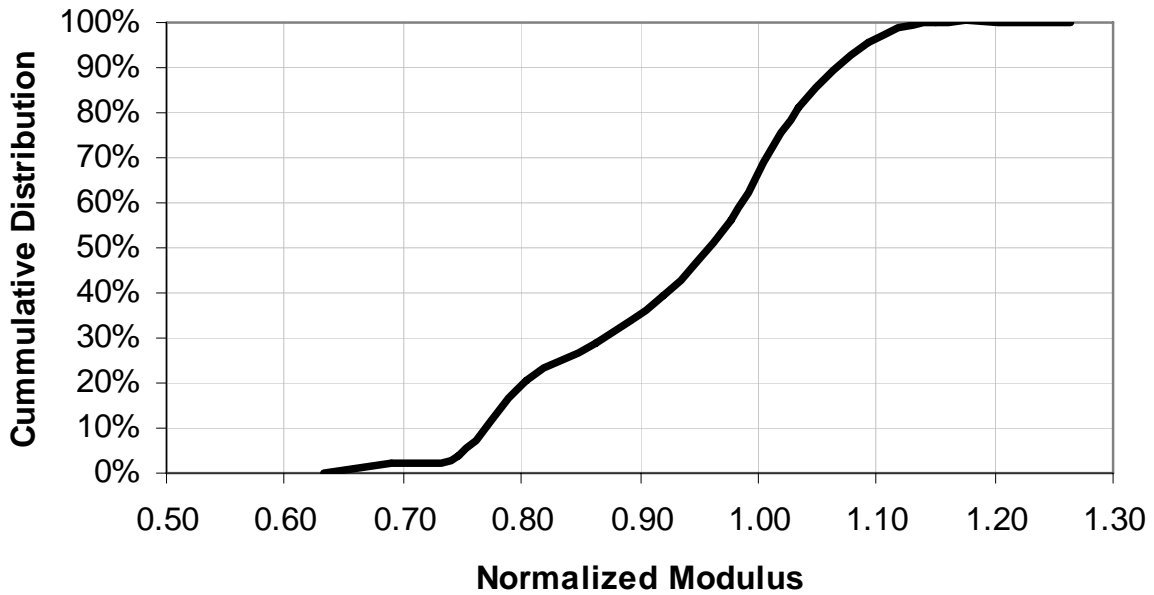


Figure I.8 – Distribution of Normalized Moduli (PSPA/Target Modulus) for Burro Creek (Site 4)

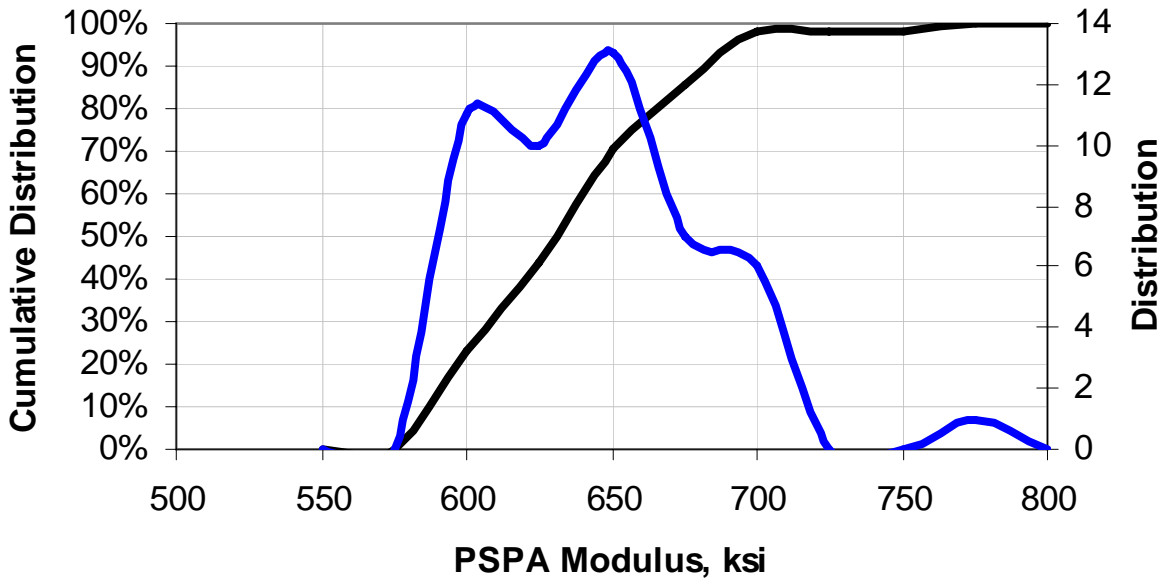


Figure I.9 – Distribution of Design Moduli for Cordes JCT (Site 5)

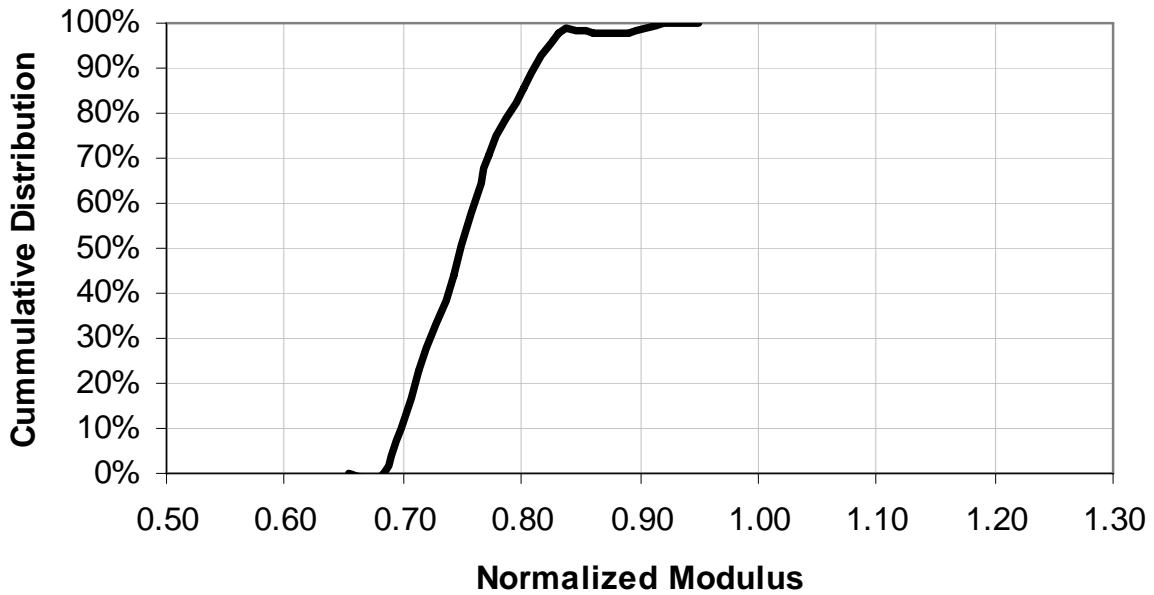


Figure I.10 – Distribution of Normalized Moduli (PSPA/Target Modulus) for Cordes JCT (Site 5)

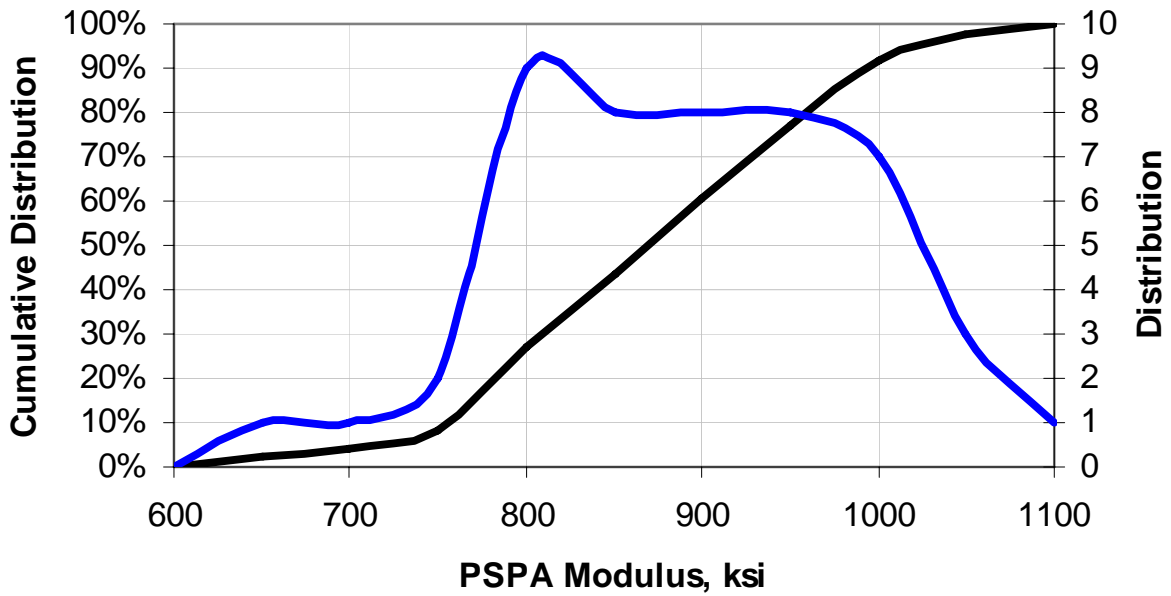


Figure I.11 – Distribution of Design Moduli for Roosevelt (Site 6)

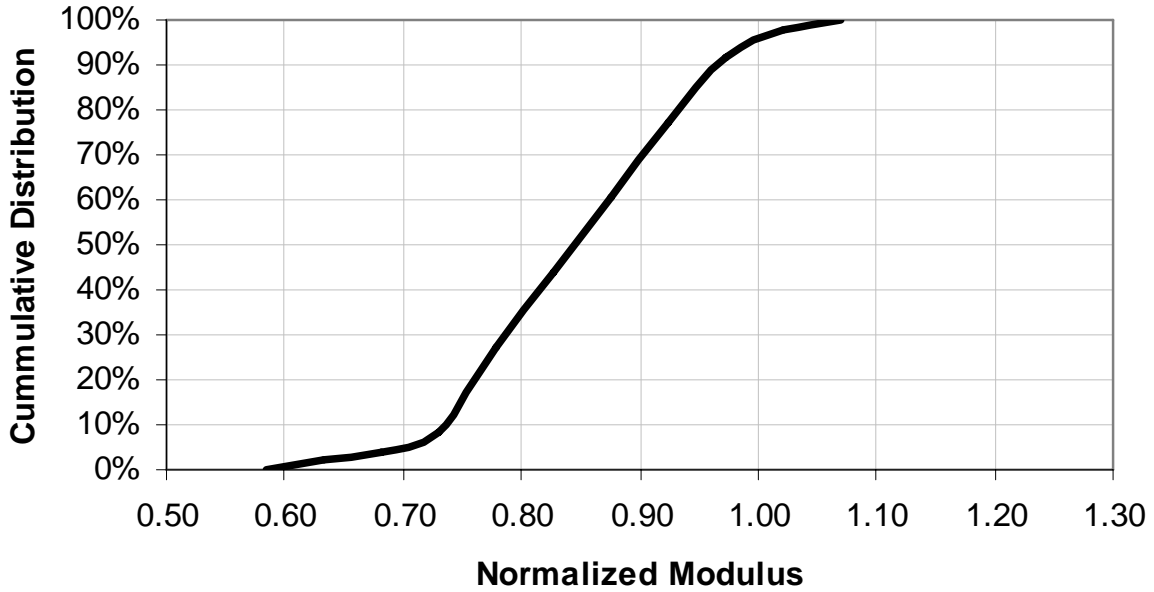


Figure I.12 – Distribution of Normalized Moduli (PSPA/Target Modulus) for Roosevelt (Site 6)

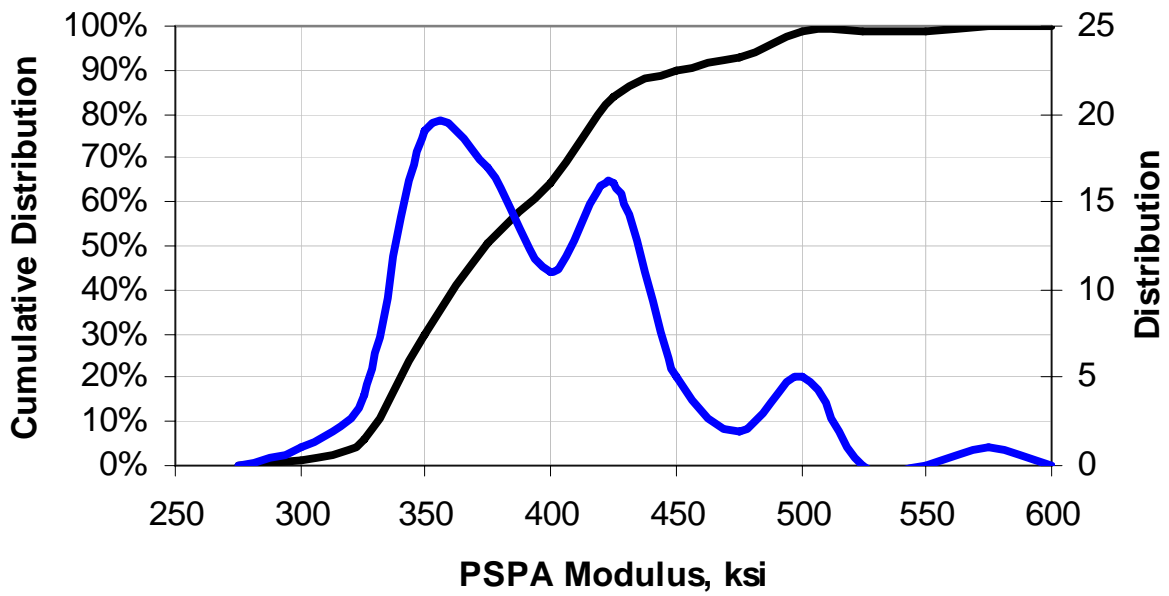


Figure I.13 – Distribution of Design Moduli for Safford (Site 7)

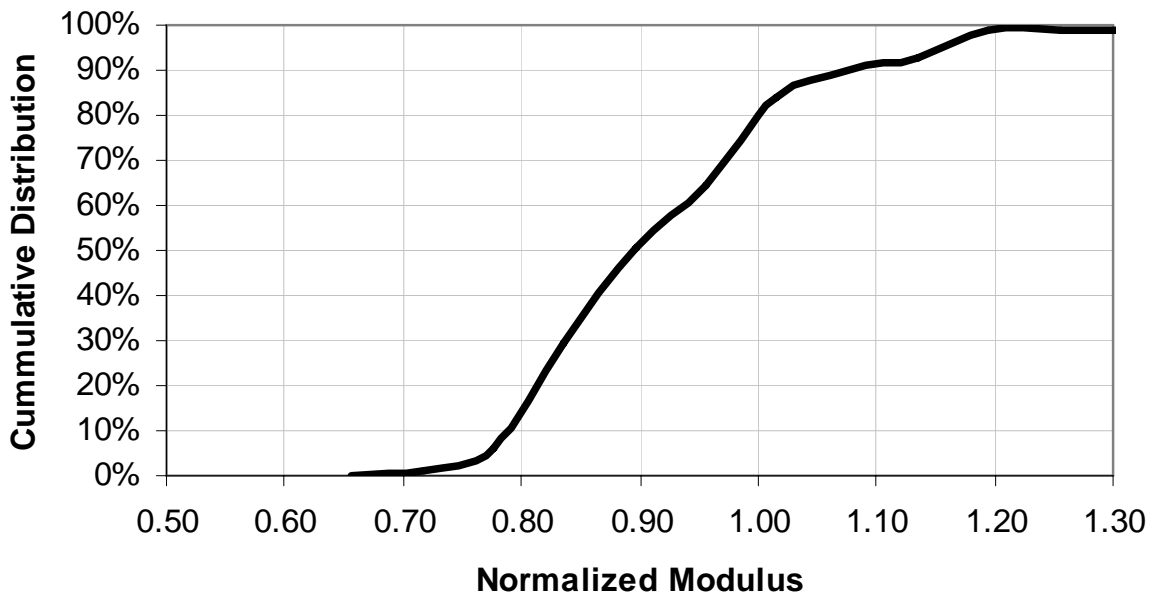


Figure I.14 – Distribution of Normalized Moduli (PSPA/Target Modulus) for Safford (Site 7)

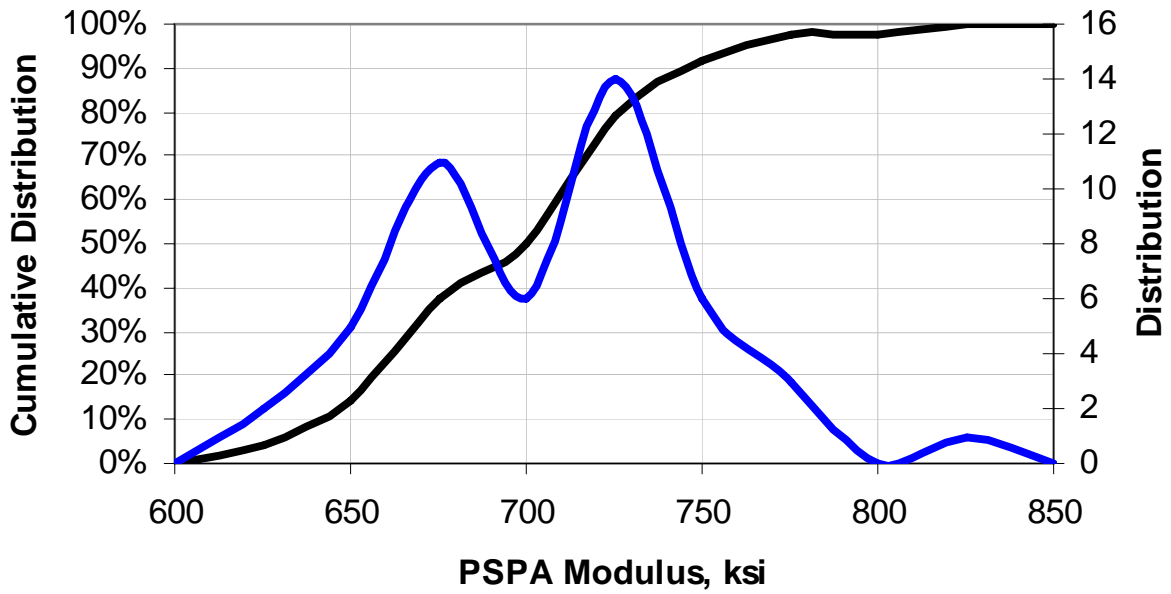


Figure I.15 – Distribution of Design Moduli for Holbrook B (Site 8)

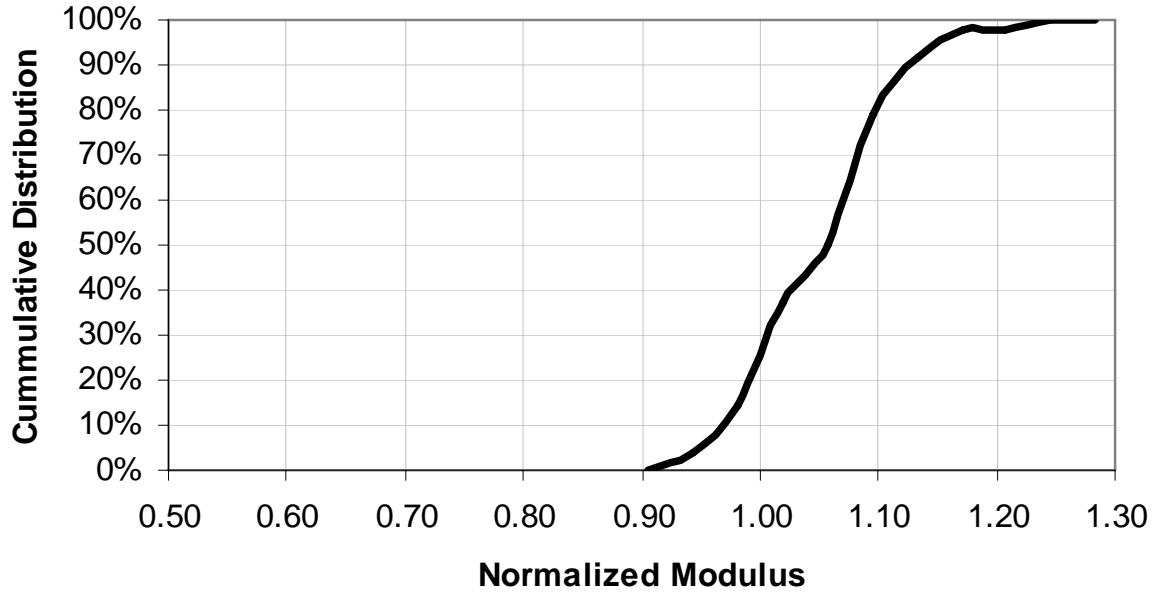


Figure I.16 – Distribution of Normalized Moduli (PSPA/Target Modulus) for Holbrook B (Site 8)

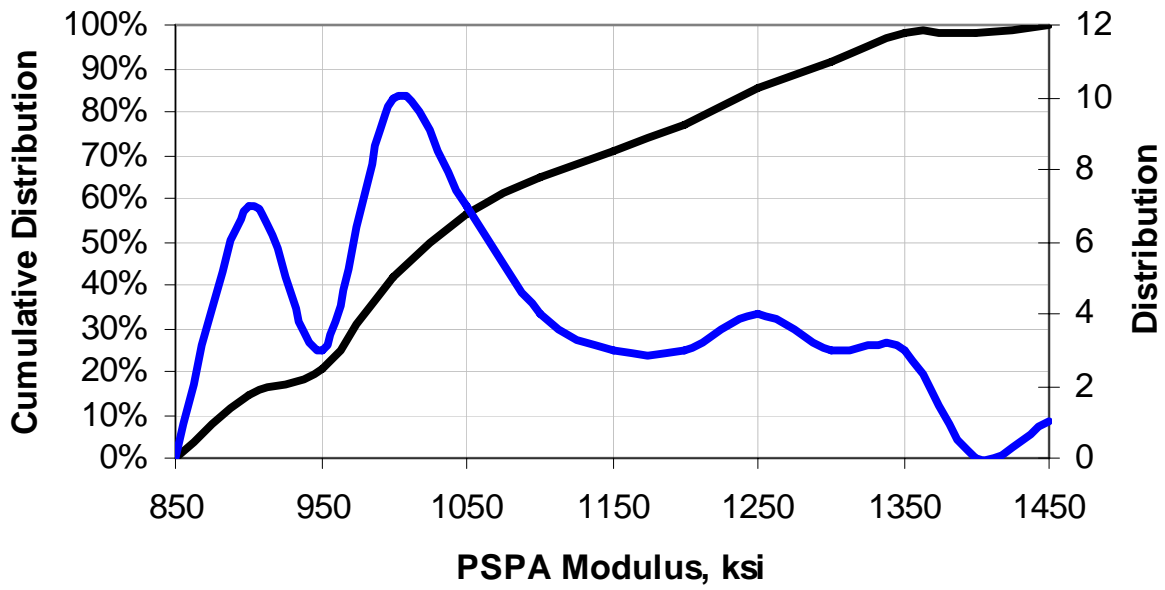


Figure I.17 – Distribution of Design Moduli for Tucson (Site 10)

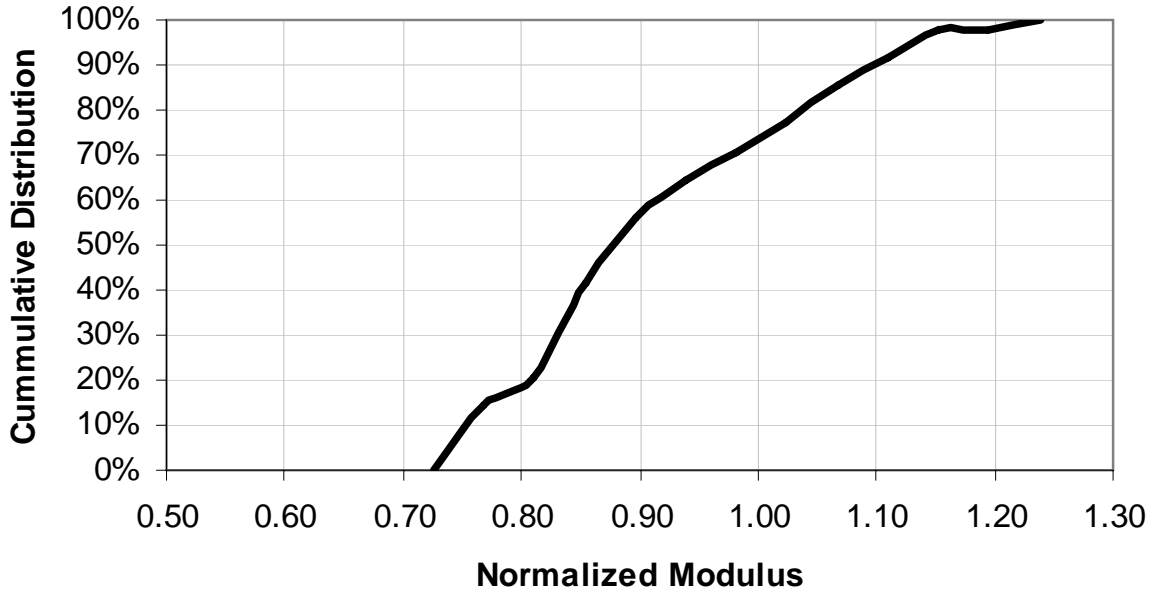


Figure I.18 – Distribution of Normalized Moduli (PSPA/Target Modulus) for Tucson (Site 10)

APPENDIX J. VALIDATION OF RESULTS

Table J.1 – Comparison of Moduli from PSPA and Lab Tests on Cores Extracted from Same Locations on Site 1

Core Number	Modulus, ksi	
	PSPA	Lab Test on Cores
1	711	783
2	635	704
3	675	695
4	671	742
5	823	724
6	693	690
7	628	628
8	710	620
9	667	651
10	639	605

Table J.2 – Comparison of Moduli from PSPA and Lab Tests on Cores Extracted from Same Locations on Site 2

Core Number	Modulus, ksi	
	PSPA	Lab Test on Cores
1	429	395
2	435	439
3	431	412
4	381	414
5	361	384
6	341	382
7	381	364
8	402	345
9	366	398
10	387	430

Table J.3 – Comparison of Moduli from PSPA and Lab Tests on Cores Extracted from Same Locations on Site 3

Core Number	Modulus, ksi	
	PSPA	Lab Test on Cores
1	451	456
2	393	401
3	458	456
4	478	460
5	456	464
6	487	496
7	458	428
8	--	445
9	--	459
10	--	462

Table J.4 – Comparison of Moduli from PSPA and Lab Tests on Cores Extracted from Same Locations on Site 4

Core Number	Modulus, ksi	
	PSPA	Lab Test on Cores
1	446	453
2	455	500
3	503	494
4	542	489
5	584	523
6	337	388
7	540	520
8	493	546
9	442	490
10	519	495

Table J.5 – Comparison of Moduli from PSPA and Lab Tests on Cores Extracted from Same Locations on Site 5

Core Number	Modulus, ksi	
	PSPA	Lab Test on Cores
1	--	442
2	412	453
3	425	462
4	433	399
5	417	399
6	427	421
7	457	432
8	396	406
9	389	446
10	--	457

Table J.6 – Comparison of Moduli from PSPA and Lab Tests on Cores Extracted from Same Locations on Site 6

Core Number	Modulus, ksi	
	PSPA	Lab Test on Cores
1	485	448
2	497	495
3	456	535
4	481	501
5	527	484
6	457	464
7	461	--
8	577	--
9	--	--
10	--	--

Table J.7 – Comparison of Moduli from PSPA and Lab Tests on Cores Extracted from Same Locations on Site 7

Core Number	Modulus, ksi	
	PSPA	Lab Test on Cores
1	292	287
2	316	366
3	356	365
4	357	347
5	343	370
6	319	340
7	346	368
8	287	354
9	275	291
10	338	314

Table J.8 – Comparison of Moduli from PSPA and Lab Tests on Cores Extracted from Same Locations on Site 8

Core Number	Modulus, ksi	
	PSPA	Lab Test on Cores
1	634	681
2	657	613
3	541	518
4	611	614
5	617	661
6	631	656
7	708	604
8	636	661
9	676	667
10	684	611

Table J.9 – Comparison of Moduli from PSPA and Lab Tests on Cores Extracted from Same Locations on Site 9

Core Number	Modulus, ksi	
	PSPA	Lab Test on Cores
1	550	650
2	465	516
3	568	650
4	549	534
5	Not Tested	627
6	763	721
7	662	568
8	657	678
9	660	643
10	698	650

Table J.10 – Comparison of Moduli from PSPA and Lab Tests on Cores Extracted from Same Locations on Site 10

Core Number	Modulus, ksi	
	PSPA	Lab Test on Cores
1	542	573
2	557	561
3	Not Tested	561
4	574	560
5	609	588
6	500	702
7	507	539
8	593	542
9	594	427
10	660	673

APPENDIX K. PAY FACTOR CALCULATIONS

Table K.1 – Pay Factor Calculations for Buckeye Site

Parameter	Avg.	Std. Dev.	COV	PT*	PF** (\$/ton)
3/8"	77.0	1.15	1.5%	100	\$0.00
#8	45.3	0.96	2.1%	100	\$0.00
#40	17.3	0.50	2.9%	100	\$0.00
#200	4.4	0.10	2.3%	100	\$0.00
% Asphalt	4.85	0.08	1.6%	100	\$0.00
% Voids	3.9	0.39	10.0%	76	-\$0.75
Unit Weight after Compaction (pcf)	140.9	1.16	0.8%	87	-\$0.25

* PT = total percentage of lot within limit

** PF = Pay factor

Table K.2 – Pay Factor Calculations for Show Low Site

Parameter	Avg.	Std. Dev.	COV	PT	PF (\$/ton)
3/8"	76.8	2.50	3.3%	100	\$0.00
#8	44.5	1.73	3.9%	98	\$0.00
#40	21.5	0.58	2.7%	100	\$0.00
#200	5.2	0.13	2.5%	100	\$0.00
% Asphalt	5.38	0.18	3.3%	91	\$0.00
% Voids	4.7	0.29	6.2%	100	\$1.00
Unit Weight after Compaction (pcf)	139.9	1.09	0.8%	100	\$1.00

Table K.3 – Pay Factor Calculations for Holbrook Site

Parameter	Avg.	Std. Dev.	COV	PT	PF (\$/ton)
3/8”	70.5	3.32	4.7%	100	\$0.00
#8	43.3	3.30	7.6%	73	-\$0.75
#40	24.8	1.71	6.9%	100	\$0.00
#200	5.0	0.38	7.6%	100	\$0.00
% Asphalt	4.84	0.17	3.5%	100	\$0.00
% Voids	4.8	0.34	7.1%	100	\$1.00
Unit Weight after Compaction (pcf)	150.0	1.30	0.9%	100	\$1.00

Table K.4 – Pay Factor Calculations for Burro Creek Site

Parameter	Avg.	Std. Dev.	COV	PT	PF (\$/ton)
3/8”	76.3	4.35	5.7%	2	-\$2.50
#8	36.3	0.96	2.6%	0	-\$2.50
#40	16.0	0.00	0.0%	100	\$0.00
#200	6.1	0.18	3.0%	100	\$0.00
% Asphalt	4.91	0.42	8.6%	65	-\$1.00
% Voids	4.6	0.74	16.1%	100	\$1.00
Unit Weight after Compaction (pcf)	145.2	1.08	0.7%	100	\$1.00

Table K.5 – Pay Factor Calculations for Cordes JCT Site

Parameter	Avg.	Std. Dev.	COV	PT	PF (\$/ton)
3/8”	74.8	2.06	2.8%	100	\$0.00
#8	37.5	2.38	6.3%	71	-\$0.75
#40	10.3	0.96	9.3%	100	\$0.00
#200	4.9	0.68	13.9%	100	\$0.00
% Asphalt	5.61	0.13	2.3%	100	\$0.00
% Voids	5.7	0.65	11.4%	100	\$1.00
Unit Weight after Compaction (pcf)	140.9	1.39	1.0%	69	-\$1.30

Table K.6 – Pay Factor Calculations for Roosevelt Site

Parameter	Avg.	Std. Dev.	COV	PT	PF (\$/ton)
3/8”	71.8	2.22	3.1%	100	\$0.00
#8	32.3	1.26	3.9%	100	\$0.00
#40	19.3	0.50	2.6%	100	\$0.00
#200	4.7	0.35	7.4%	100	\$0.00
% Asphalt	5.09	0.15	2.9%	74	-\$0.75
% Voids	2.6	0.22	8.5%	0	-\$2.50
Unit Weight after Compaction (pcf)	145.2	1.13	0.8%	100	\$1.00

Table K.7 – Pay Factor Calculations for Safford Site

Parameter	Avg.	Std. Dev.	COV	PT	PF (\$/ton)
3/8”	72.0	0.82	1.1%	100	\$0.00
#8	40.3	1.26	3.1%	100	\$0.00
#40	12.5	0.58	4.6%	100	\$0.00
#200	3.9	0.34	8.7%	100	\$0.00
% Asphalt	5.60	0.11	2.0%	100	\$0.00
% Voids	5.9	0.34	5.8%	100	\$1.00
Unit Weight after Compaction (pcf)	136.4	1.96	1.4%	98	\$0.50

Table K.8 – Pay Factor Calculations for Holbrook (B) Site

Parameter	Avg.	Std. Dev.	COV	PT	PF (\$/ton)
3/8”	72.5	3.32	4.6%	85	\$0.00
#8	32.3	1.50	4.6%	100	\$0.00
#40	16.8	0.50	3.0%	100	\$0.00
#200	4.3	0.15	3.5%	100	\$0.00
% Asphalt	5.12	0.13	2.5%	100	\$0.00
% Voids	4.8	0.56	11.7%	100	\$1.00
Unit Weight after Compaction (pcf)	149.3	1.41	0.9%	100	\$1.00

Table K.9 – Pay Factor Calculations for Payson Site

Parameter	Avg.	Std. Dev.	COV	PT	PF (\$/ton)
3/8”	71.3	4.86	6.8%	52	-\$2.50
#8	39.8	4.35	10.9%	56	-\$2.00
#40	20.8	2.63	12.6%	73	-\$0.75
#200	4.7	0.68	14.5%	100	\$0.00
% Asphalt	5.19	0.26	5.0%	87	\$0.00
% Voids	4.2	0.89	21.2%	99	\$0.50
Unit Weight after Compaction (pcf)	141.5	2.29	1.6%	92	\$0.00

Table K.10 – Pay Factor Calculations for Tucson Site

Parameter	Avg.	Std. Dev.	COV	PT	PF (\$/ton)
3/8”	71.3	0.96	1.3%	100	\$0.00
#8	45.5	1.00	2.2%	100	\$0.00
#40	16.5	0.58	3.5%	100	\$0.00
#200	4.2	0.24	5.7%	100	\$0.00
% Asphalt	5.41	0.18	3.3%	100	\$0.00
% Voids	5.4	0.29	5.4%	100	\$1.00
Unit Weight after Compaction (pcf)	140.5	1.54	1.1%	99	\$0.50

APPENDIX L. VARIATION IN LAB SEISMIC MODULUS WITH AIR VOIDS

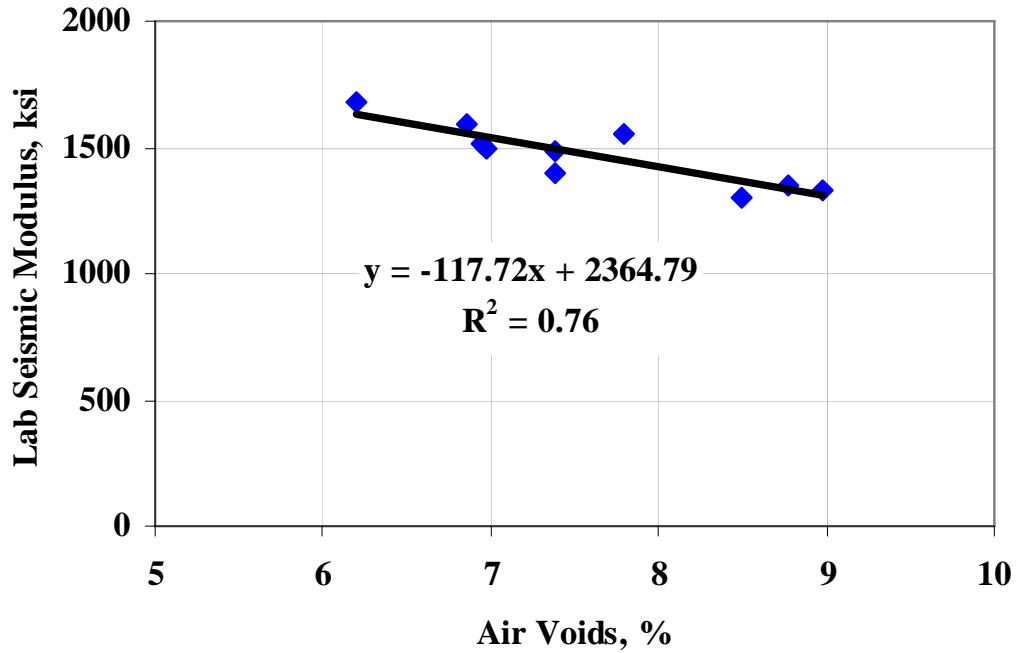


Figure L.1 – Variation in Lab Seismic Modulus with Air Voids at Core Locations from Buckeye (Site 1)

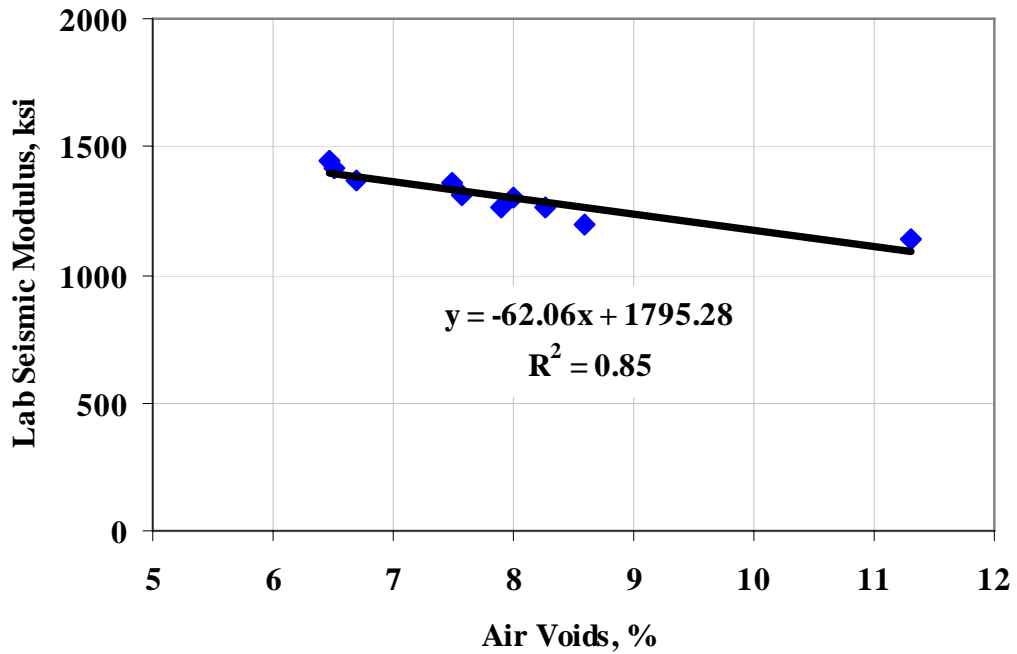


Figure L.2 – Variation in Lab Seismic Modulus with Air Voids at Core Locations from Show Low (Site 2)

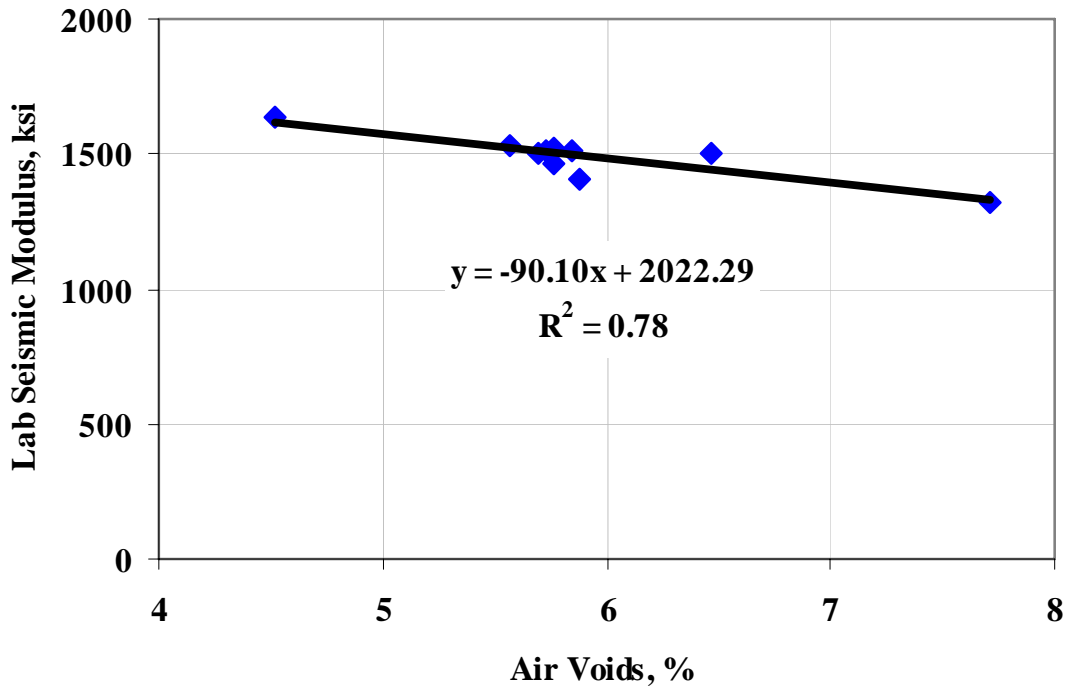


Figure L.3 – Variation in Lab Seismic Modulus with Air Voids at Core Locations from Holbrook (Site 3)

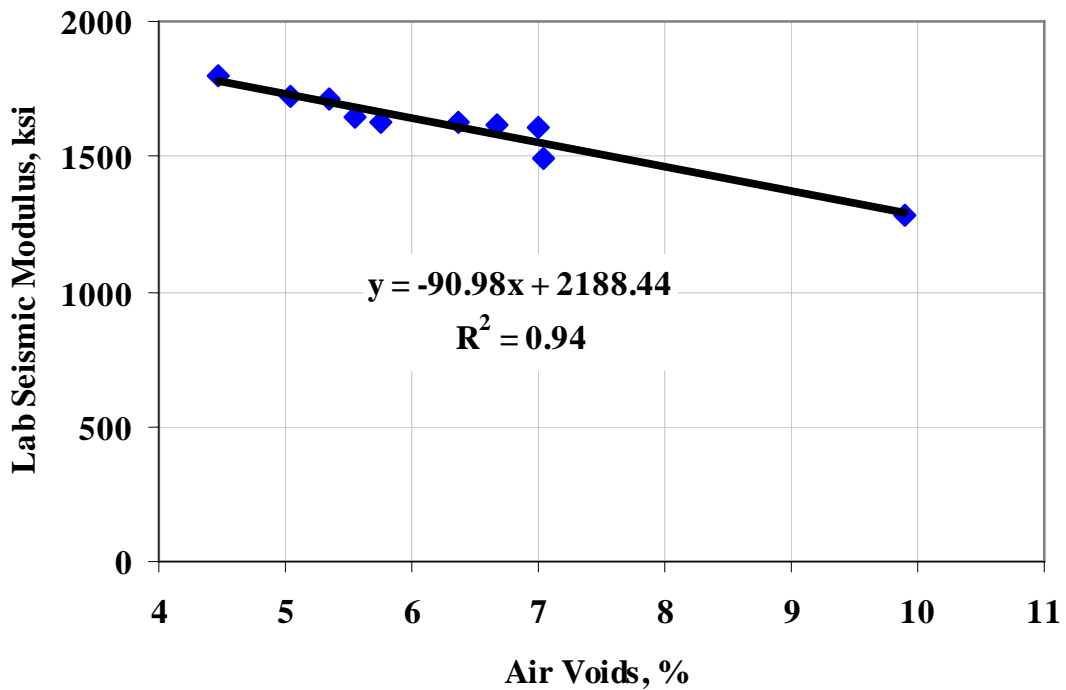


Figure L.4 – Variation in Lab Seismic Modulus with Air Voids at Core Locations from Burro Creek (Site 4)

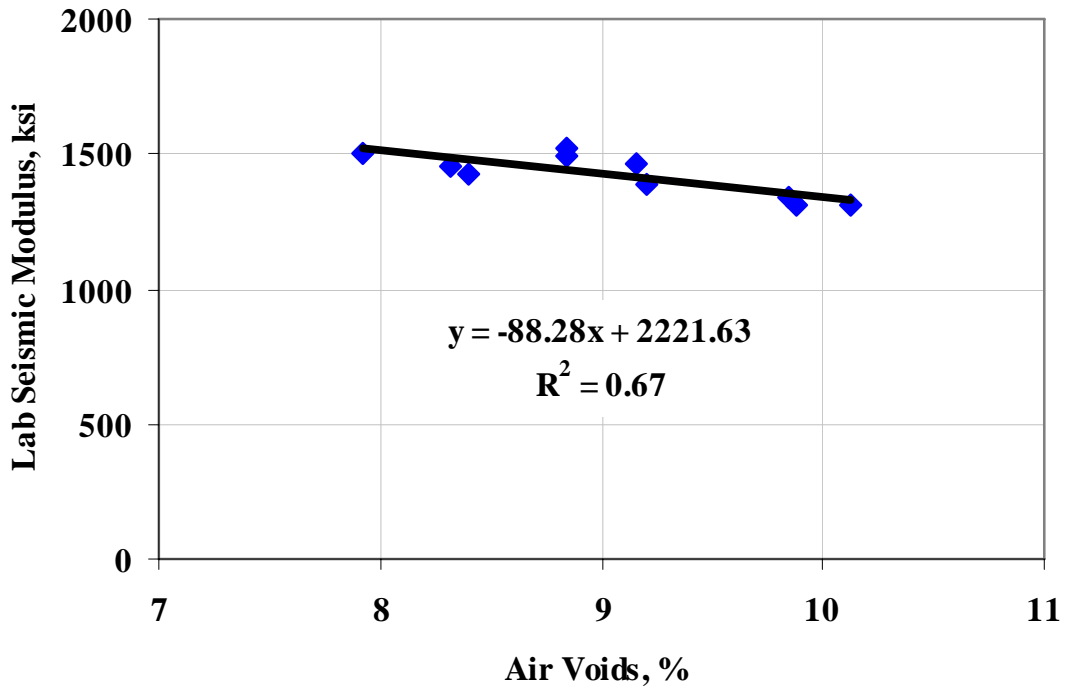


Figure L.5 – Variation in Lab Seismic Modulus with Air Voids at Core Locations from Cordes JCT (Site 5)

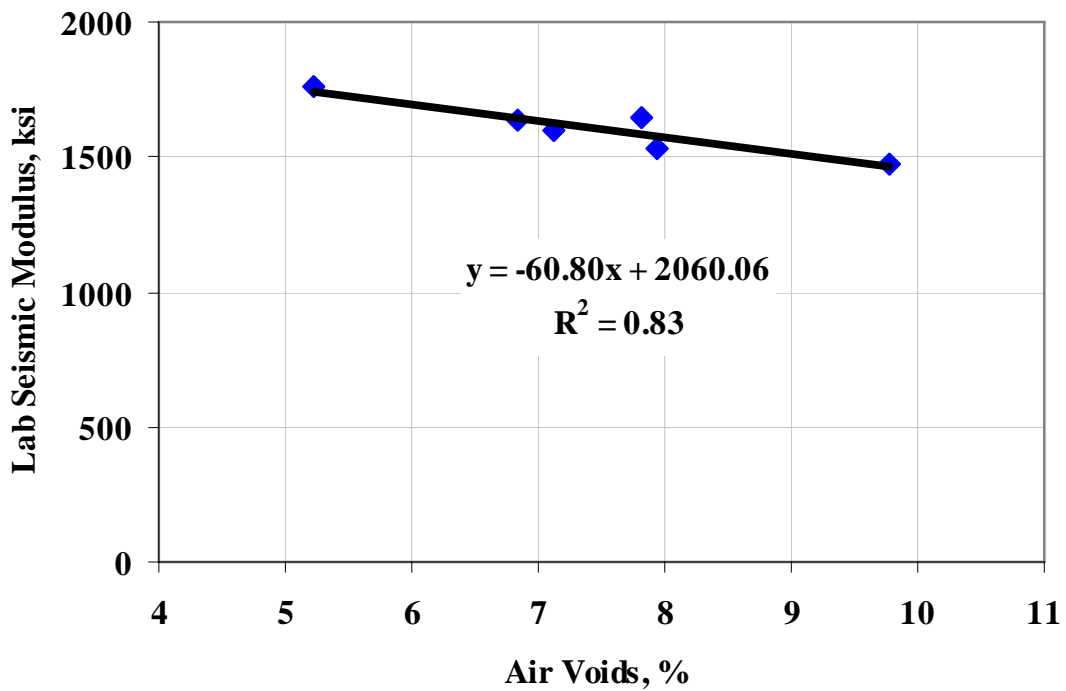


Figure L.6 – Variation in Lab Seismic Modulus with Air Voids at Core Locations from Roosevelt (Site 6)

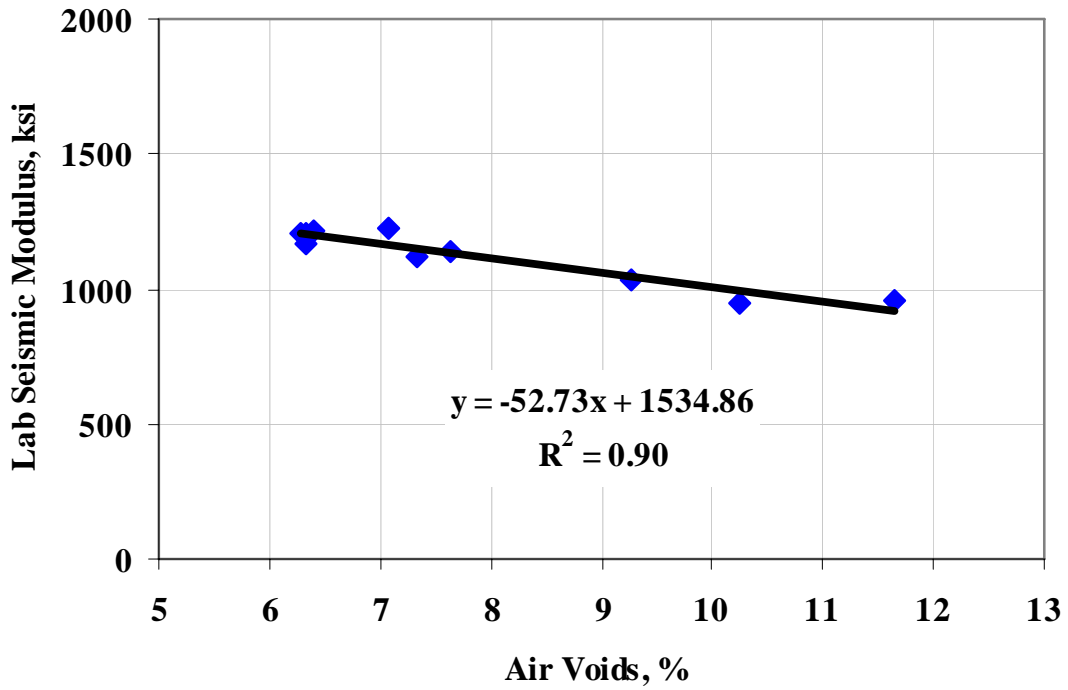


Figure L.7 – Variation in Lab Seismic Modulus with Air Voids at Core Locations from Safford (Site 7)

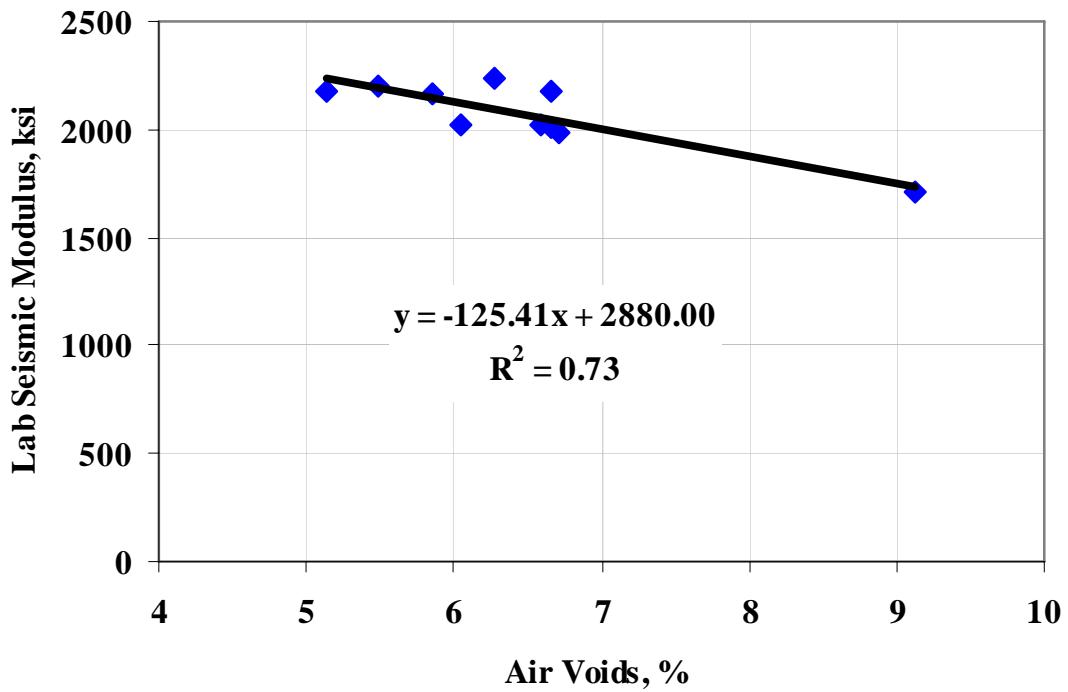


Figure L.8 – Variation in Lab Seismic Modulus with Air Voids at Core Locations from Holbrook (Site 8)

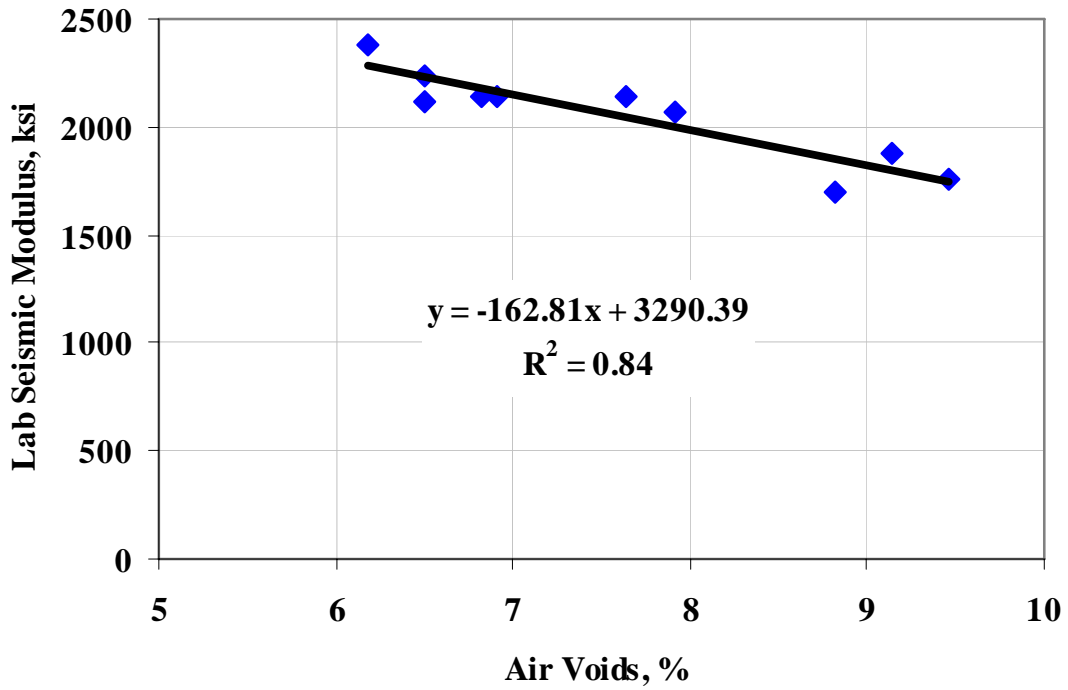


Figure L.9 – Variation in Lab Seismic Modulus with Air Voids at Core Locations from Payson (Site 9)

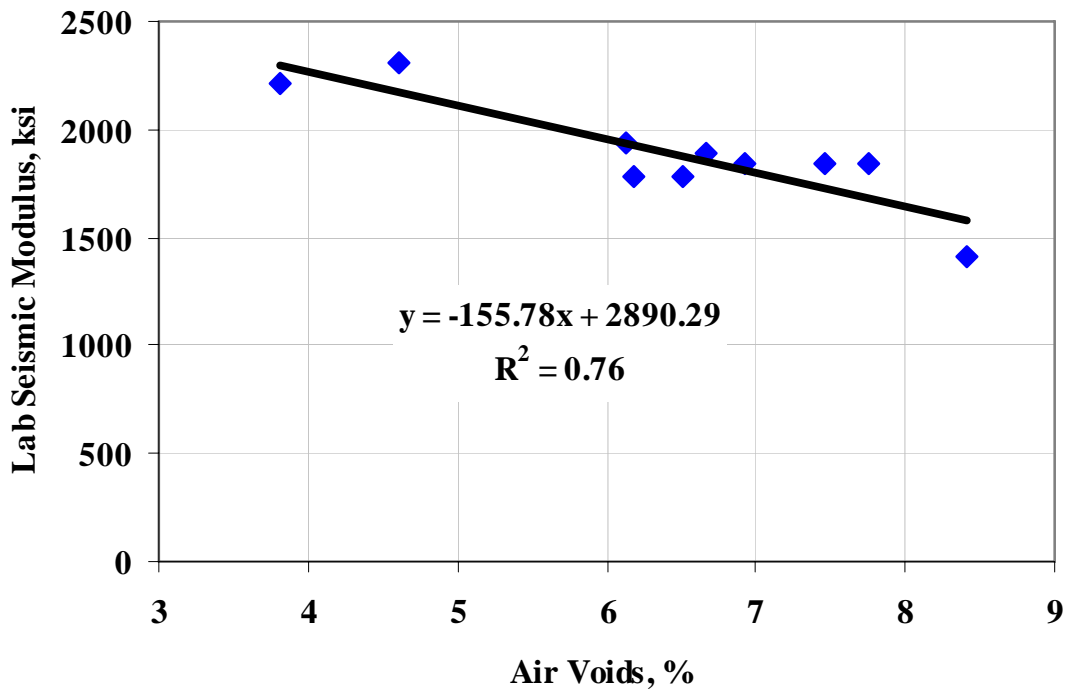


Figure L.10 – Variation in Lab Seismic Modulus with Air Voids at Core Locations from Tucson (Site 10)

APPENDIX M. MONTE CARLO SIMULATION RESULTS

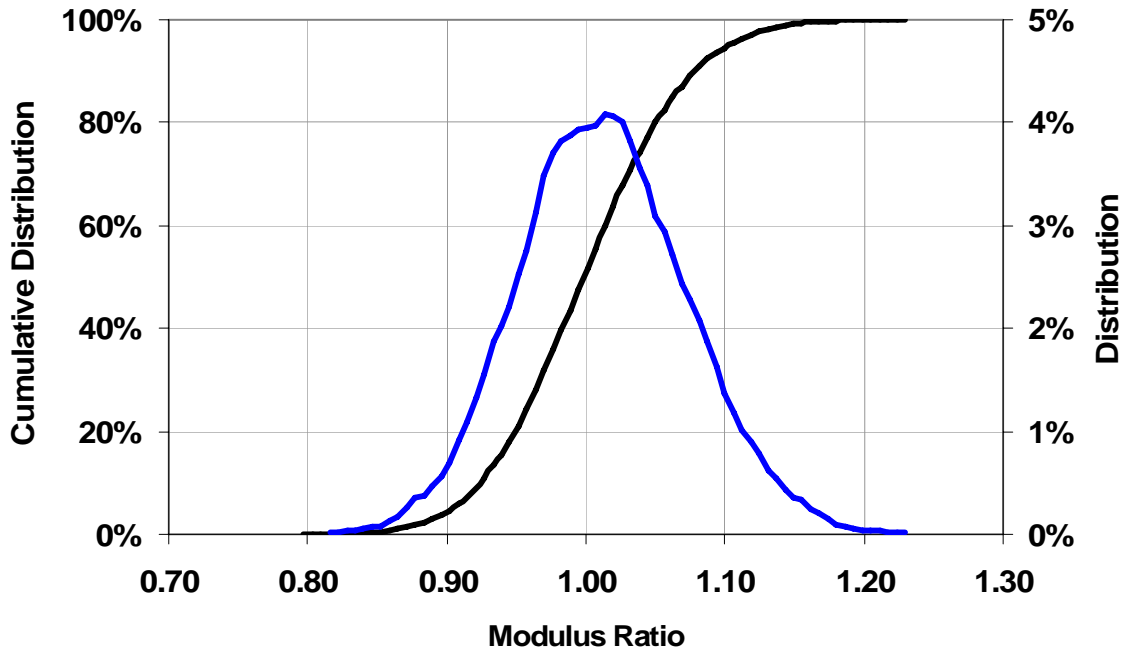


Figure M.1 – Distribution of Moduli due to Change in Gradation and Asphalt Content of Mixes for Buckeye (Site 1)

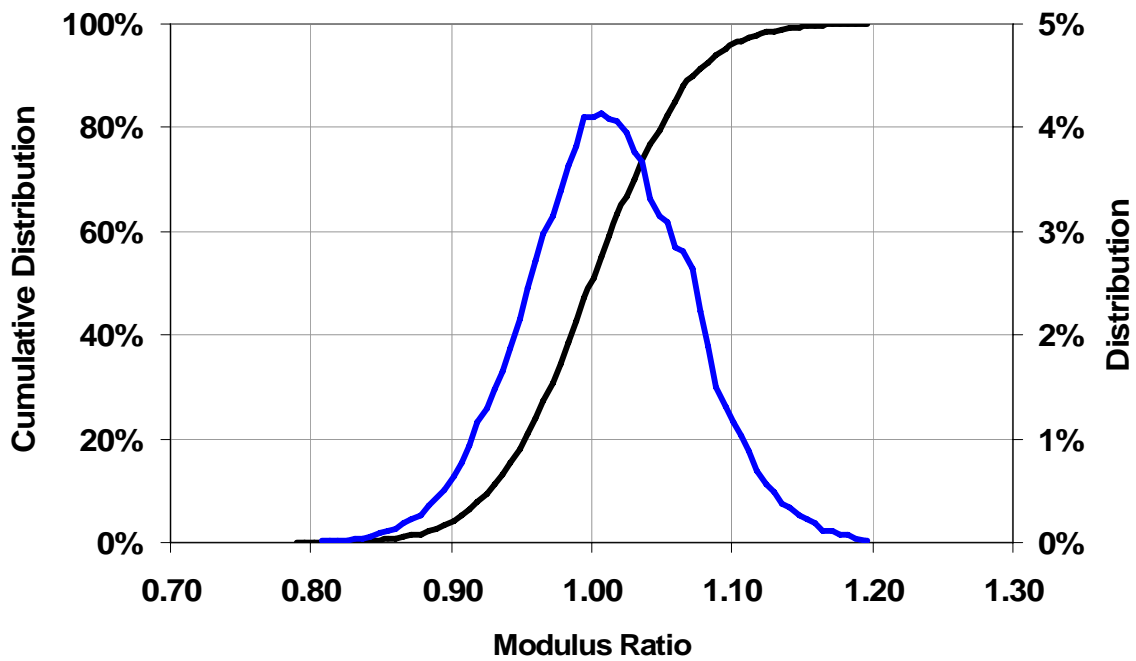


Figure M.2 – Distribution of Moduli due to Change in Gradation and Asphalt Content of Mixes for Show Low (Site 2)

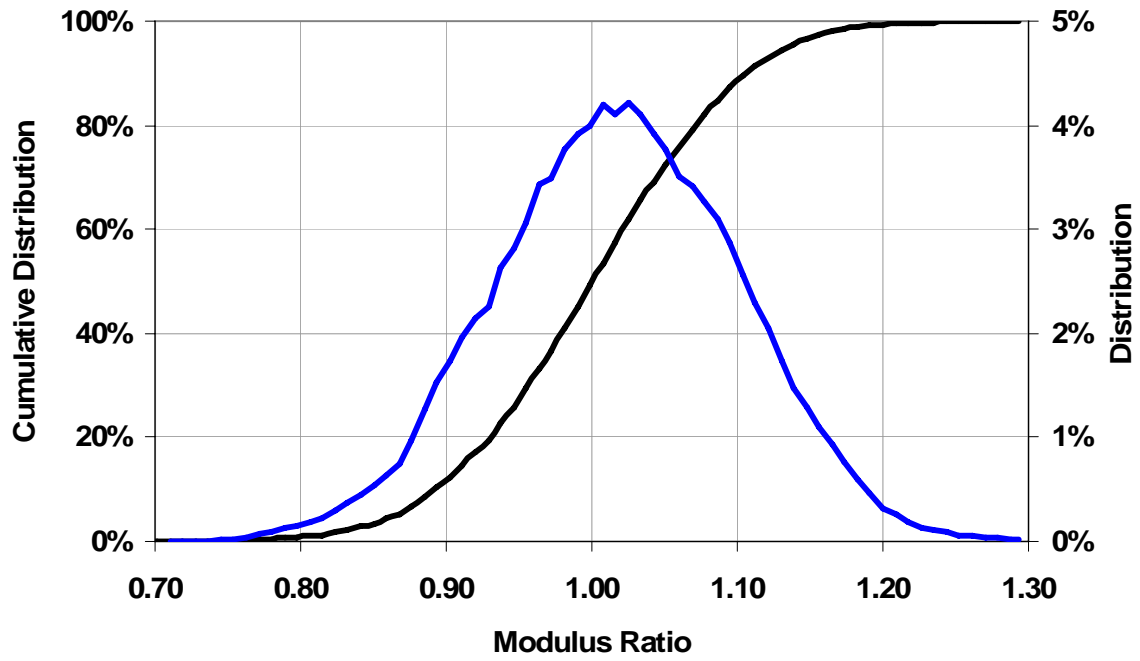


Figure M.3 – Distribution of Moduli due to Change in Gradation and Asphalt Content of Mixes for Holbrook (Site 3)

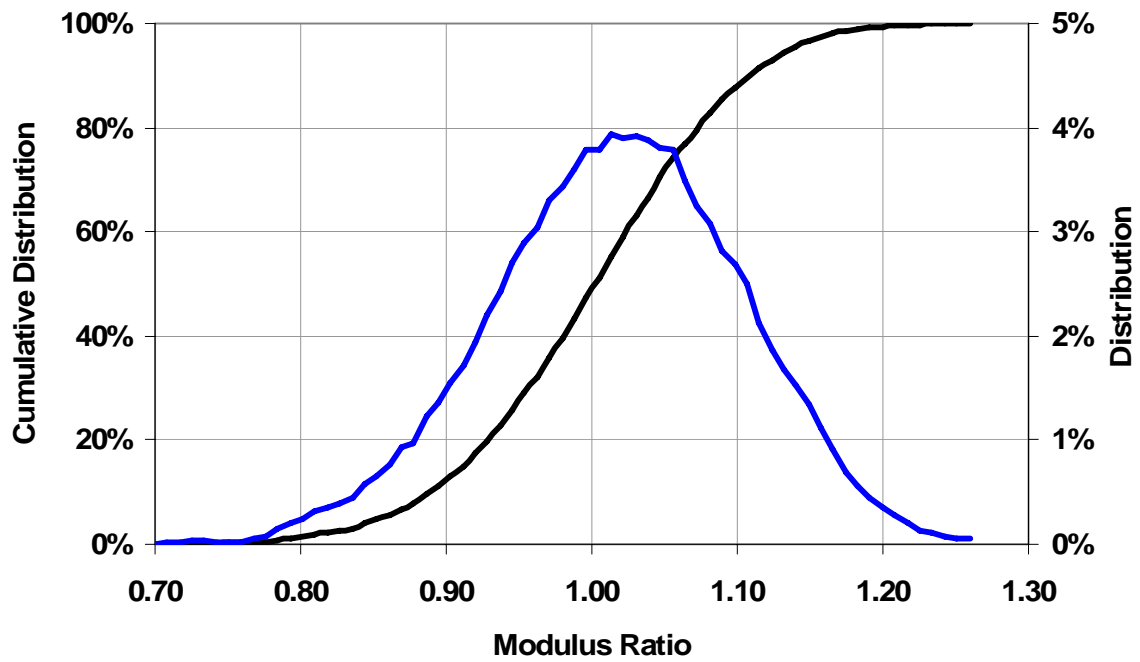


Figure M.4 – Distribution of Moduli due to Change in Gradation and Asphalt Content of Mixes for Burro Creek (Site 4)

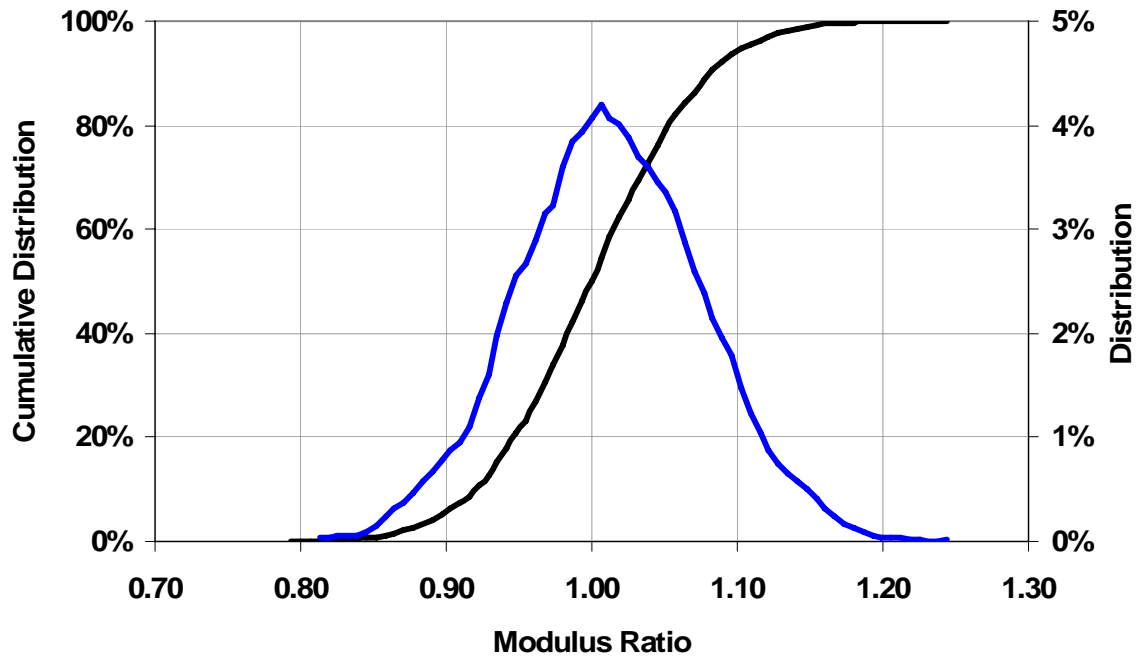


Figure M.5 – Distribution of Moduli due to Change in Gradation and Asphalt Content of Mixes for Cordes JCT (Site 5)

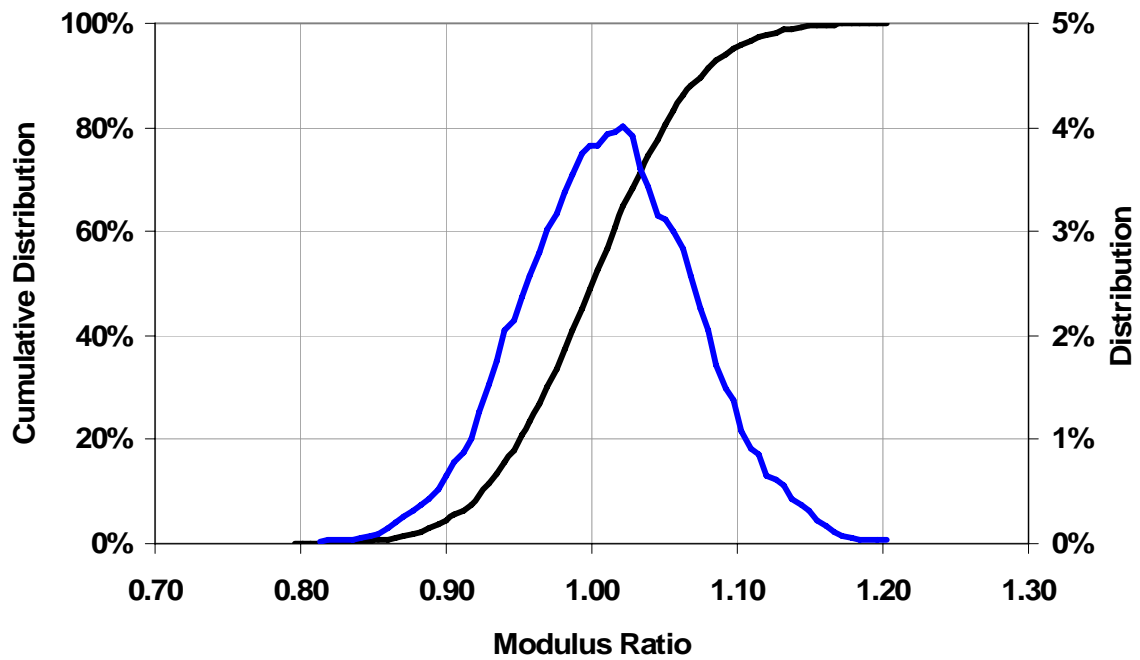


Figure M.6 – Distribution of Moduli due to Change in Gradation and Asphalt Content of Mixes for Roosevelt (Site 6)

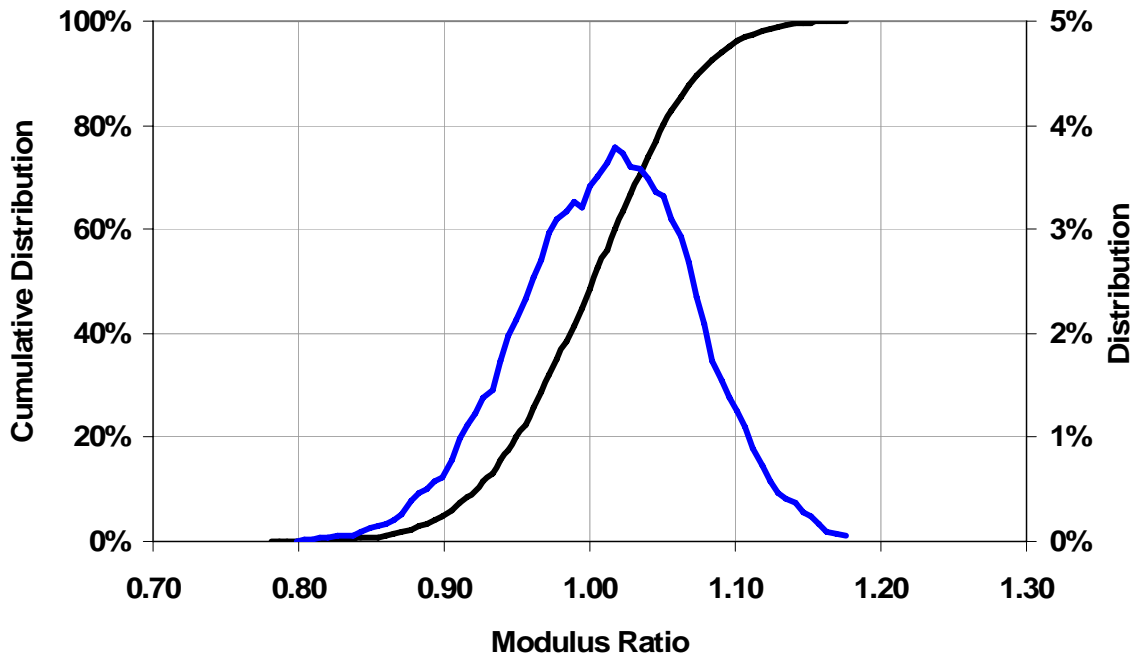


Figure M.7 – Distribution of Moduli due to Change in Gradation and Asphalt Content of Mixes for Safford (Site 7)

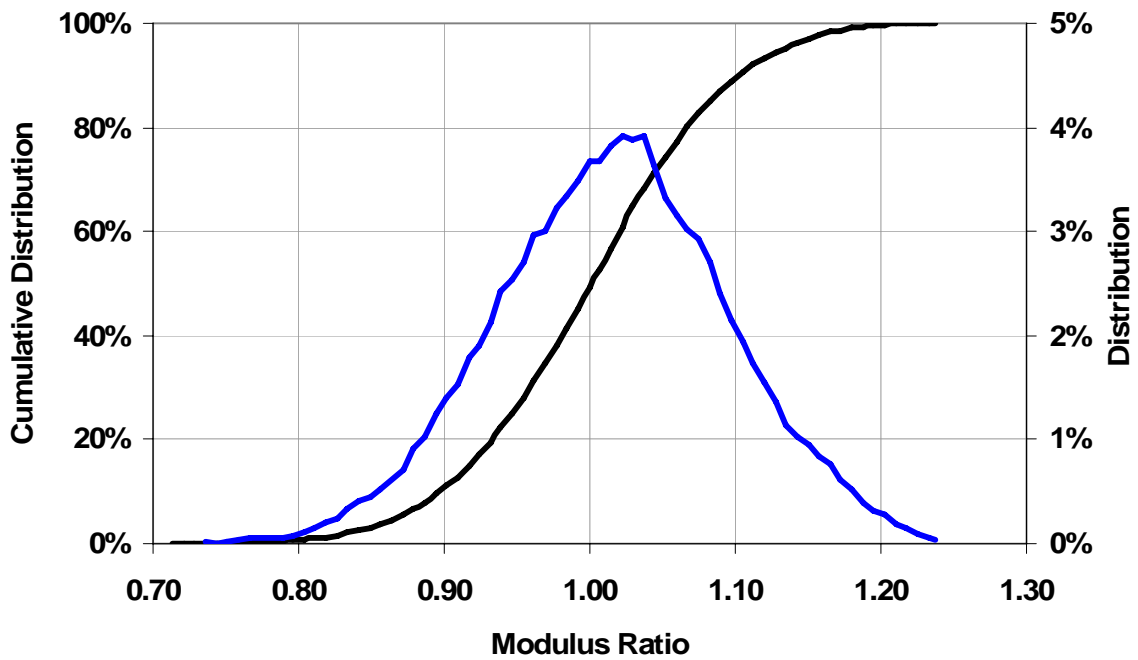


Figure M.8 – Distribution of Moduli due to Change in Gradation and Asphalt Content of Mixes for Holbrook B (Site 8)

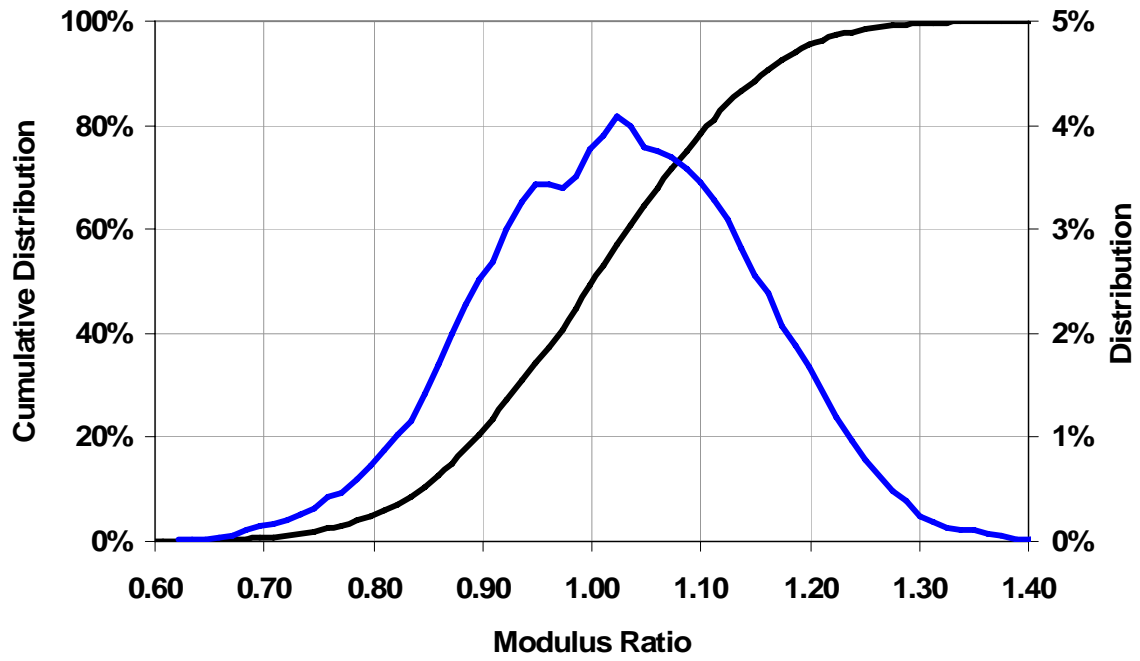


Figure M.9 – Distribution of Moduli due to Change in Gradation and Asphalt Content of Mixes for Payson (Site 9)

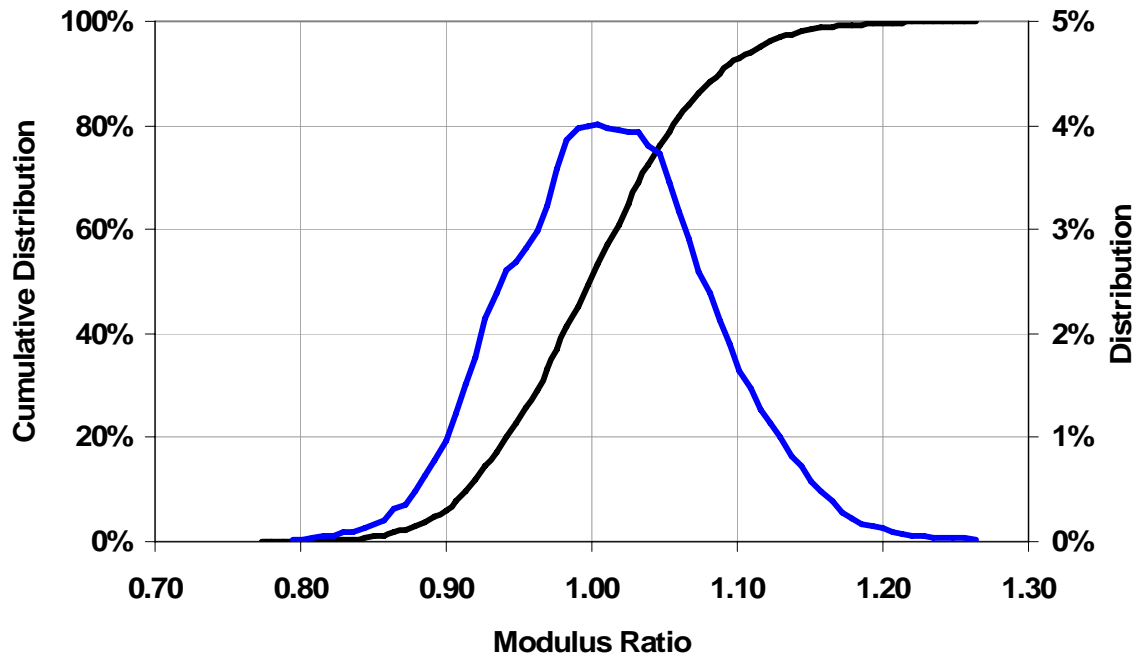


Figure M.10 – Distribution of Moduli due to Change in Gradation and Asphalt Content of Mixes for Tucson (Site 10)

APPENDIX N. PHOTO ALBUM



Figure N.1 – View of Site 1



Figure N.2 – ADOT Personnel Collecting Loose Samples on Site 1



Figure N.3 – Surface Temperature at Time of Collection on Site 1



Figure N.4 – PSPA Collecting Information on Site 1



Figure N.5 – PSPA Collecting on Core Location at Site 1



Figure N.6 – View of Site 2

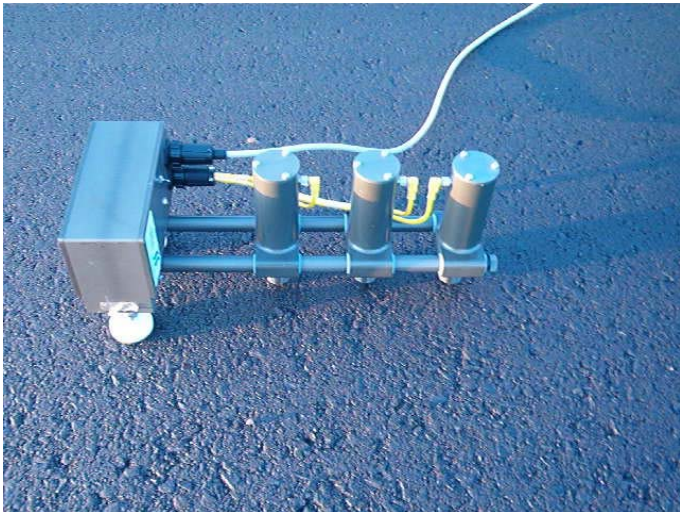


Figure N.7 – Detail of Site 2



Figure N.8 – PSPA Collecting on Site 2



Figure N.9 – View of Site 3

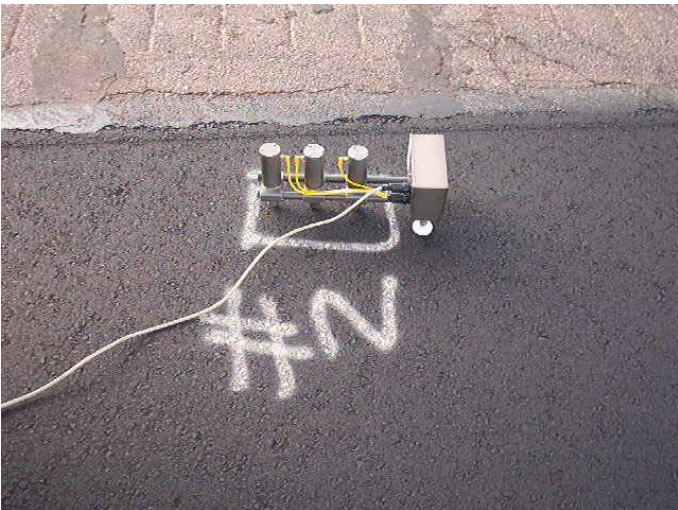


Figure N.10 – PSPA Testing on Core Location at Site 3



Figure N.11 – Construction Operations at Site 3



Figure N.12 – View of Site 4



Figure N.13 – PSPA Collecting on Core Location of Site 4



Figure N.14 – Segregated Area on Site 4



Figure N.15 – PSPA Testing at Site 5

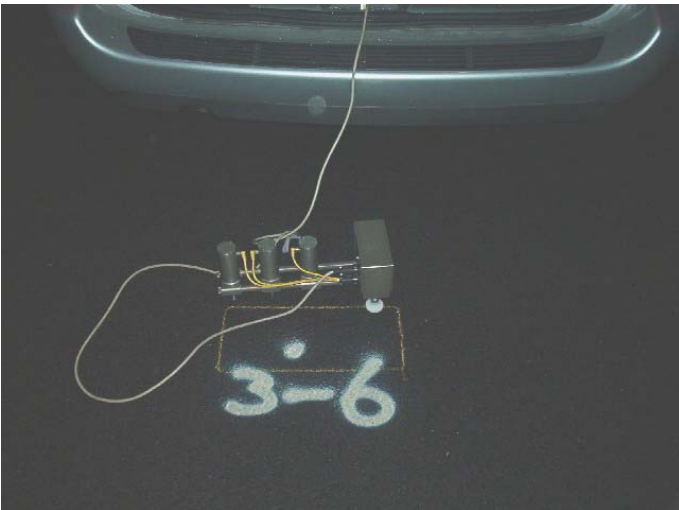


Figure N.16 – PSPA Collecting Data on Core Location of Site 5



Figure N.17 – View of Site 6



Figure N.18 – PSPA Testing on Site 6



Figure N.19 – PSPA Collecting Data on Core Location of Site 6



Figure N.20 – View of Site 7

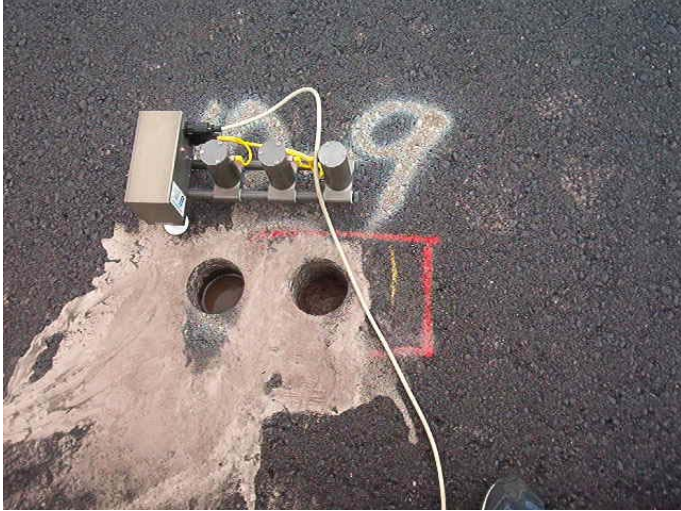


Figure N.21 – PSPA Testing on Core Location of Site 7



Figure N.22 – View of Site 8



Figure N.23 – PSPA Testing on Core Location of Site 8



Figure N.24 – View of Site 9



Figure N.25 – Nuclear Density Gage Testing on Site 9



Figure N.26 – Coring at Site 9



Figure N.27 – Pavement Construction of Site 10



Figure N.28 – ADOT Staff Gathering Loose Samples on Site 10



Figure N.29 – PSPA Testing on Core Location of Site 10